Synthesis of organocatalysts immobilized on temperature-responsive polymers for application in micellar catalysis

Dissertation

zur Erlangung des akademischen Grades

Doktor rerum naturalium

(Dr. rer. nat)

vorgelegt

der Fakultät für Naturwissenschaften

der Universität Paderborn

von

Xiaoqian Yu, M. Sc.

geboren am 10. September 1987 in Weifang (China)

Gutachter:	Prof. Dr. Dirk Kuckling
	Prof. Dr. Claudia Schmidt

Eingereicht am:	06.08.2018
Tag der Verteidigung:	18.09.2018

Experience is what you get when you don't get what you want

(Dan Stanfort)

Die vorgeliegende Arbeit wurde in dem Zeitraum vom 15. April 2014 bis 06. August 2018 an der Fakultät für Naturwissenschaften der Universität Paderborn am Lehrstuhl für Organische und Makromolekulare Chemie unter Betreuung von Herrn Prof. Dr. Dirk Kuckling angefertigt.

Abstract

The term "organocatalyst" describes a class of small organic molecules used to catalyze many organic transformations including the synthesis of chiral molecules within asymmetric reactions. Compared to catalysts based on metal complexes, the use of organocatalysts holds several advantages, such as insensitive experimental conditions, easy preparation and high sustainability.

In this work, the L-proline based organocatalysts immobilized on temperature-responsive polymer carrier were prepared and applied to the asymmetric aldol reaction between *para*-nitrobenzaldehyde (*p*-NBA) and cyclohexanone (CH) in water. The carrier consists of a block copolymer comprising a permanently hydrophilic block and a temperature-sensitive block containing the immobilized organocatalyst. By changing the solution temperature, the hydrophilicity of the temperature-sensitive block can be affected, thereby switching the activity of the immobilized catalyst. Compared to the unsupported catalyst under the same reaction conditions, the immobilized catalyst displayed a higher catalyst activity as well as a better recovery of the supported catalyst and its re-use in consecutive reaction cycles without loss of activity.

The block copolymers were synthesized via RAFT polymerization. The temperature-sensitive poly(*N*-isopropyl acrylamide) (PNIPAAm) block contained azlactone moieties allowing a post-polymerization attachment of the organocatalyst. The structure of the permanently hydrophilic block was varied from poly(ethylene glycol) (PEG) to poly(*N,N*-dimethylacrylamide) (PDMAA) and poly(2,3-dihydroxypropyl acrylate) (PDHPA). Different amino-functionalized L-proline and L-prolineamide derivatives were immobilized by post-polymerization attachment, yielding polymer chains with 2 – 5 mol% immobilized organocatalyst. The asymmetric aldol reaction between *p*-NBA and CH in aqueous medium was used as model reaction to evaluate the activity and selectivity of the immobilized organocatalysts.

Abstract

The resulting homo-and block copolymers were characterized by NMR-spectroscopy, size exclusion chromatography (SEC) and ESI-TOF-mass spectrometry. For the temperature-induced aggregation behavior of different amphiphilic block copolymers, dynamic light scattering was used to determine the phase transition temperature (T_{cr}) as well as the hydrodynamic diameter (D_h) of the aggregates above low critical solution temperature (LCST). The catalytic activity and selectivity of the polymeric L-proline/L-prolineamide catalysts were investigated by the NMR-spectroscopy and HPLC.

Kurzzusammenfassung

Unter dem Begriff "Organokatalysator" wird eine Klasse von kleinen organischen Molekülen zusammengefasst, die zur Katalyse vieler organischer Umwandlungen verwendet werden einschließlich der Synthese von chiralen Molekülen bei asymmetrischen Reaktionen. Verglichen mit Katalysatoren auf Basis von einen der Metallkomplexen birgt die Verwendung von Organokatalysatoren verschiedene Vorteile, wie z.B. robuste Reaktionsbedingungen, einfache Herstellung und Handhabbarkeit und hohe Nachhaltigkeit.

In dieser Arbeit wurden polymere Trägermaterialien für die Anbindung von L-Prolin basierten Organokatalysatoren hergestellt. Die immobilisierten Katalysatoren werden in der asymmetrischen Aldolreaktion zwischen *para*-Nitrobenzaldehyd (*p*-NBA) und Cyclohexanon in Wasser eingesetzt. Das Trägermaterial bestand aus einem Blockcopolymere mit einem permanent hydrophilen und einem Temperaturen-sensitiven Block, welcher den immobilisierten Organokatalysator enthielt. Durch Veränderung der Temperatur in der Polymerlösung kann die Hydrophilie des Temperature-sensitiven Blocks verändert werden, sodass die Aktivität des immobilisierten Katalysators gesteuert werden kann. Im Vergleich zum freien Organokatalysator unter den gleichen Reaktionsbedingungen zeigte der immobilisierte Katalysator eine bessere Aktivität. Zudem konnte der immobilisierte Organokatalysator nach der Reaktion leicht zurückgewonnen und anschließend in weiteren Reaktionscyclen ohne Verlust der Aktivität wiederverwendet werden.

Die Blockcopolymere wurde über RAFT-Polymerisation synthetisiert. Der Temperatur-sensitive PNIPAAm Block enthält Azlactone-Gruppen, die eine polymeranaloge Anbindung des Organokatalysators erlaubten. Die Struktur des permanent hydrophilen Blocks wurde von Poly(ethylenglycol) (PEG) über Poly(*N*,*N*-dimethylacrylamid) (PDMAA) bis hin zu Poly(2,3-dihydroxypropylacrylat) (PDHPA) variiert. Die Immobilisierung des Organokatalysators auf Basis von L-Prolin bzw. Prolinamid wurde durch nukleophile Ringöffnungsreaktion über die

Azlacton-Gruppe erreicht, wodurch Polymerketten mit 2-5 mol% immobilisiertem Organokatalysator erhalten wurden. Die asymmetrische Aldolreaktion zwischen *para*-Nitrobenzaldehyd (*p*-NBA) und Cyclohexanon in wässrigem Medium wurde als Modellreaktion zur Evaluierung der Aktivität und Selektivität der immobilisierten Organokatalysatoren verwendet.

Die resultierenden Homo- und Blockcopolymere wurden durch NMR-Spektroskopie, Größenausschlusschromatographie (SEC) und ESI-ToF-Massenspektrometrie charakterisiert. Das temperatur-induzierte Aggregationsverhalten verschiedener amphiphiler Blockcopolymere wurde mittels dynamischer Lichtstreuung die Phasenübergangstemperatur (T_{cr}) sowie der hydrodynamische Durchmesser (D_h) der Aggregate bestimmt. Die katalytische Aktivität und Selektivität des immobilisierten L-Prolin bzw. L-Prolinamid-Katalysators wurde durch NMR-Spektroskopie und HPLC untersucht.

Inhalt

1. Introduction

1.1 Problem

In organic chemistry the development of catalysts is an incredibly popular topic of academic and industrial research. The use of organic components to accelerate chemical reactions is well known for more than a century. It took until the later 1990s this type of the catalyst to become widely accepted as an important branch of enantioselective synthesis.[1] In 2000, when List et al. reported the proline-catalyzed direct intermolecular asymmetric aldol reaction, the great potential of this class of catalysts for the direct asymmetric reaction was realized.[2] Proline as the only natural amino acid with a secondary amine functionality that can promote many reactions such as aldol reaction, Mannich reaction[3] and others attracted the most attention in the research of organocatalyst.[4] On the other hand the immobilization and recycling of proline was proposed at the same time based on several reasons: Firstly, in terms of "green chemistry" the re-use of catalyst is of high value, especially from economic, environmental and scientific perspective. Moreover, organocatalyst immobilization allows the reaction to be conducted in a wide range of solvents, depending on the solubility of the carrier materials. It was shown that catalyst immobilization may enhance the reactivity and stereoselectivity of the catalyst compared to general reaction conditions.[5] In addition, catalyst activity can be tuned by employing specific supporting materials, e.g. stimuli-responsive polymer supports.[6] In respective literature, general approaches for immobilization were classified as: 1) covalently supported catalysts, which are covalently bound to the support (e.g. polymer, particle); 2) non-covalently supported catalysts, which are fixed through physical effect, such as adsorption or electrostatic interaction (e.g. ionic liquid modified silica gel, polyelectrolytes); 3) biphasic catalysis, where the reaction occurs at the interface between two immiscible phase.[5]

Micellar catalysis system have been attracting considerable attention for 50 years, because it represents an improvement of the biphasic catalysis concept, solving the problem of catalytic

transformations between organic and aqueous phases.[7] In nature, many biochemical processes take place in this isolated hydrophobic micro heterogenous system. This system combines the advantages of both homogeneous and heterogeneous catalysis, thereby offering the possibility of an efficient, selective multiphase catalysis in water.[8] Moreover, catalysis in micellar or micellar analogous structures offers even more advantages such as simplified product work-up, easy separation, and reuse of catalyst. These reactors attract great interest in the immobilization of catalysts especially from the industrial point of view.[9–11]

## 1.2 Objective and scope of the present work

The aim of this work is the design, synthesis and application of temperature sensitive organocatalytic nanoreactors for organocatalytic conversions in aqueous medium. Synthetic smart block copolymers were used as supporting material for the L-proline and L-proline-derivates, in order to conduct an efficient organocatalytic reaction within micellar aggregates formed by temperature-induced aggregation of the block copolymers. When the temperature of the reaction system exceeds a critical value, the smart block copolymers assemble into polymeric micelles containing the immobilized proline-moiety as well as the substrates inside their hydrophobic core. Spatial proximity of catalyst and substrate will increase catalyst efficiency. After the organocatalytic reaction, the nanoreactors are disassembled by decreasing temperature thus leading to phase separation of catalyst and product, enabling easy product work-up and catalyst recycling. Immobilization of L-proline on polymeric supports is known from literature.[12–14]

In this present work, a new strategy for the immobilization of proline derivatives was performed by post-polymerization attachment via through a ring opening reaction with azlactone moieties. First of all, linear smart block copolymers containing azlactone moieties within the temperature-responsive block were prepared by RAFT polymerization. The structure of the permanently hydrophilic block was varied from poly (ethylene glycol) (PEG), poly(N,N-dimethylacrylamide) (PDMAA) and poly (2,3-dihydroxypropyl acrylate) (PDHPA).

Post-polymerization attachment of the L-proline derivates to the smart block copolymer afforded the targeted polymer structure. Temperature-induced self-assembly behavior of the functionalized block copolymers was studied in aqueous solution. Finally, these functionalized block copolymers were used to form nanoreactors, in which aldol reactions were conducted (Figure 1). The efficiency of different immobilized L-proline derivates was investigated.

The RAFT polymerization process as well as the obtained homo- and block copolymers were characterized by NMR spectroscopy, size exclusion chromatography (SEC) and electrospray ionization time-of-flight mass spectrometry (ESI-Tof-MS). The temperature-induced aggregation of the block copolymers was investigated by dynamic light scattering (DLS). The catalytic activity and selectivity of the polymer supported L-proline/L-Prolineamide catalysts was examined by NMR spectroscopy and HPLC.
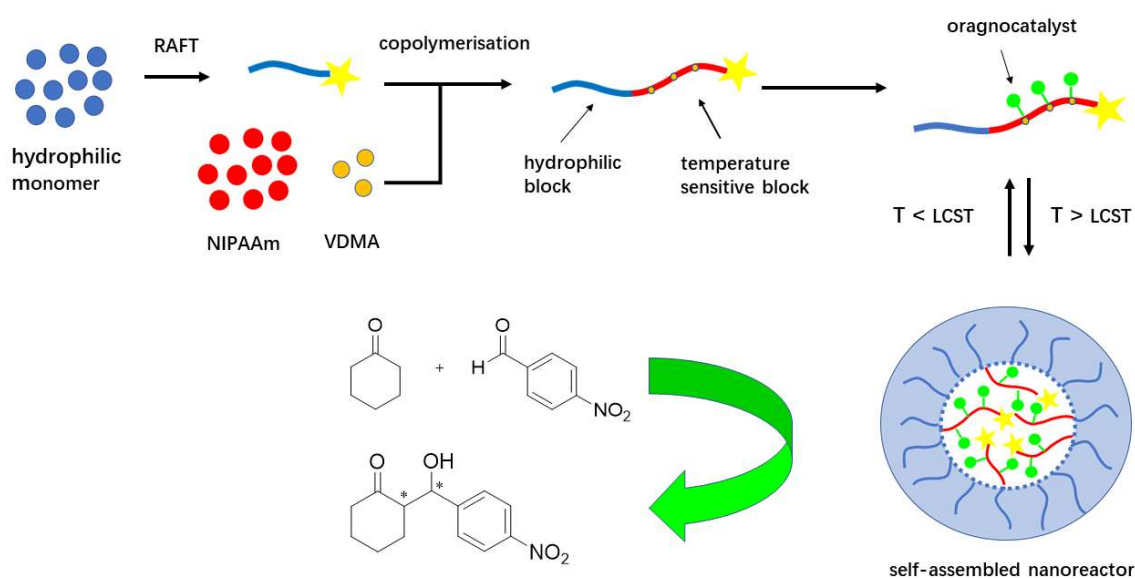

Figure 1. Synthesis of the temperature responsive block copolymers as organocatalyst support and their application as self-assembled nanoreactor for organocatalytic reaction in water.

2. Theoretical background

2.1 Stimuli responsive block copolymers

Stimuli responsive polymers, also known as "smart polymers", are able to respond to slight changes in the external environment such as temperature, pH, light and electric field.[15] The most important feature of this kind of polymers is the reversibility of the process, so that the polymer will return to its initial state when the external stimuli disappears. In analogy to biopolymers such as proteins and nucleic acids, smart polymer as synthetic materials are capable of interacting with their surrounding environment, thus representing one of the most exciting and emerging research areas for the application in pharmacy and biotechnology, e.g. as controlled drug-delivery and release systems, biosensors and biocatalysts.[16,17] The external stimuli can be classified into physical stimuli (temperature, radiation, ionic strength or electric field), chemical stimuli (pH, redox, solvent) and biological stimuli (enzyme specific molecules) (Figure 2).
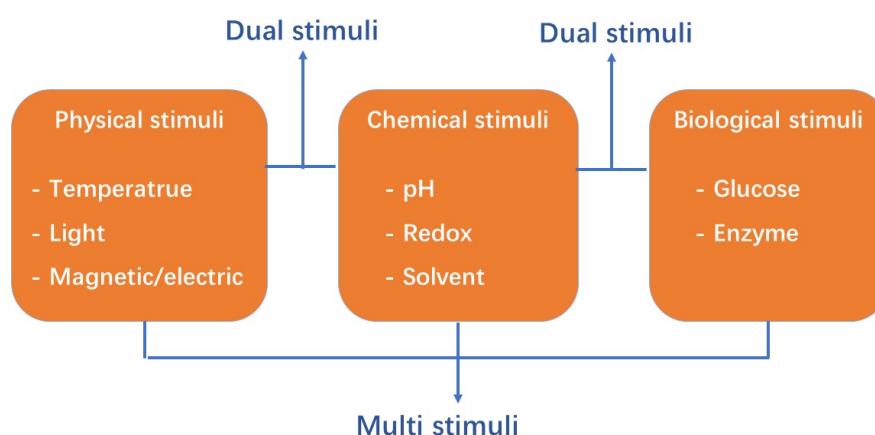

Figure 2. Classification of external stimuli.

The "response" of the polymer can occur in different ways. Typical responses can be the change of the polymers physical properties such as chain dimension/size, secondary structure, solubility or the degree of intermolecular association (Figure 3). Many physical or chemical

factors can cause destruction and reconstruction of secondary structure forces (e.g. hydrogen bonding, hydrophobic effects, electrostatic interactions, etc.) and result in a change of polymer chain behavior in solution.[18] The application of the stimuli-responsive polymers was extended to two-dimensional (2D) (film) and three-dimensional (3D) systems including polymeric solutions, nanoparticles (micelles, vesicles, core-shell particles), thin film, cross-linked polymer gels as well as polymeric networks.[19]
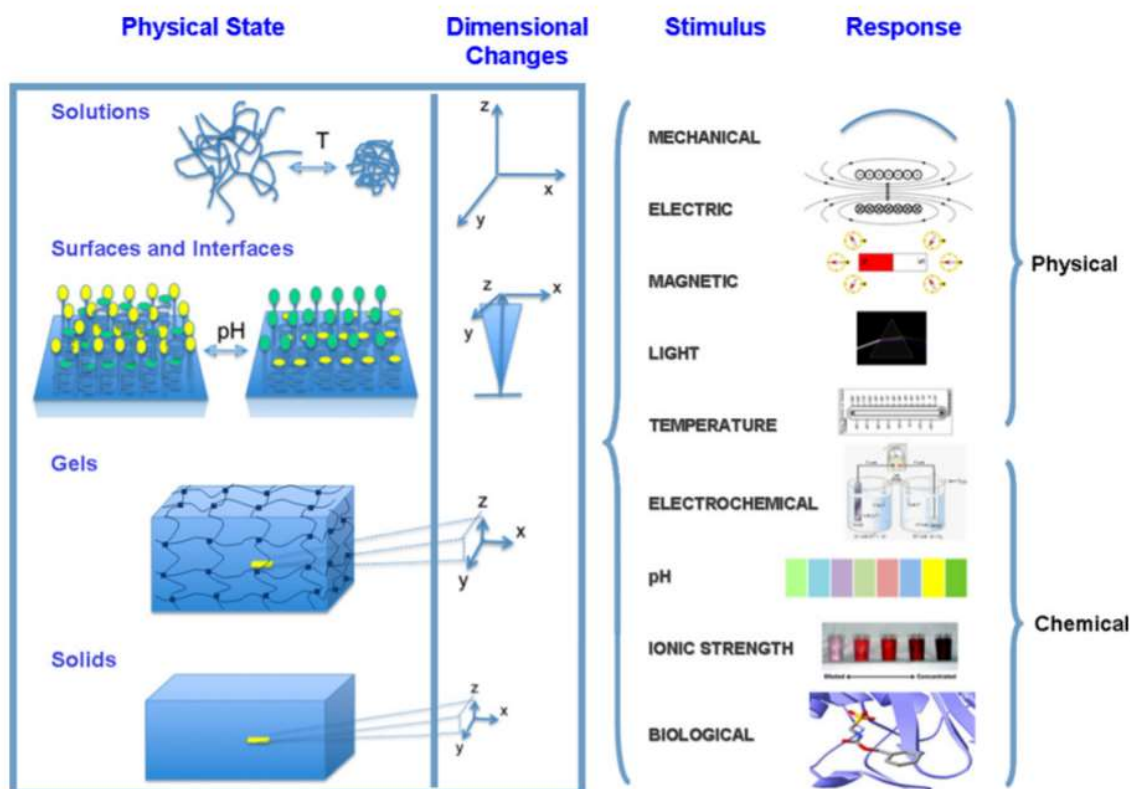
Figure 3. Schematic representation of dimensional changes in polymeric solutions, at surfaces and interfaces, in polymeric gels, and polymer solids resulting from physical or chemical stimuli.[20] Reprinted from [20] with permission from Elsevier Copyright (2018)

The most widely used class of responsive polymers are temperature-sensitive polymers because temperature is an easily controllable parameter in the polymer system. Since the first report by Scarpa et al. in 1967, the development of the thermoresponsive system contributes to the development of the functional polymers.[21] The most common applications of temperature-sensitive polymers is based on their reversible phase transition in solution below or above a demixing temperature.[22] The phase transition arises from a coil-to-globule phase transition of the polymer chains at the critical phase transition temperature, which was also

called as a critical solution temperature (T_{cr}). If the phase transition occurs above the critical temperature, this polymer is referred to as lower critical solution temperature (LCST) polymer. In contrast, polymers showing an upper critical solution temperature (UCST) behavior, will precipitate from the aqueous solution below critical solution temperature. As shown in Figure 4, LCST or UCST investigated a minimum or maximum of transition curve. LCST polymers in solution adopt an expanded coil conformation to form a one phase system at low temperature. When the temperature increases above the LCST, a phase separation can be observed because of chain collapse forming a compact globuli. In literature, this coil-to-globuli transition of aqueous solutions of poly(*N*-isopropylacrylamide) was evidenced e.g. by light scattering[23] as well as FT-IR spectroscopy[24]. For UCST polymers an inverse behavior is observed in the phase diagram.
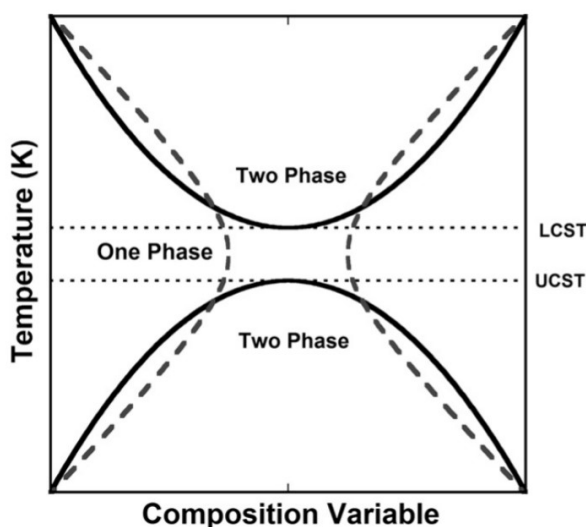
Figure 4. UCST and LCST type phase diagrams.[25] Reprinted from [25] with permission from Elsevier Copyright (2018)

Depending on the hydrophilic/lipophilic-balance in chemical structure, a number of temperature-sensitive polymers with significantly different transition temperatures have been reported: poly(*N*-isopropylacrylamide) (PNIPAAm, 32 °C), poly(*N,N*-propyl acrylamide) (PNNPAAm, 10 °C),[26] poly(*N*-cyclopropyl acrylamide) (PNCPAm, 53 °C),[27] poly(*N*-vinyl-*n*-butylamide) (PNVBA, 32 °C),[28] poly(*N*-vinylcaprolactam) (PVCL, 32 °C).[29] As mentioned above, the PNIPAAm homopolymer exhibits a critical temperature in the range of 32 °C - 34 °C, which

lies close to body temperature and make this polymer particularly suitable for biomedical applications.[30]
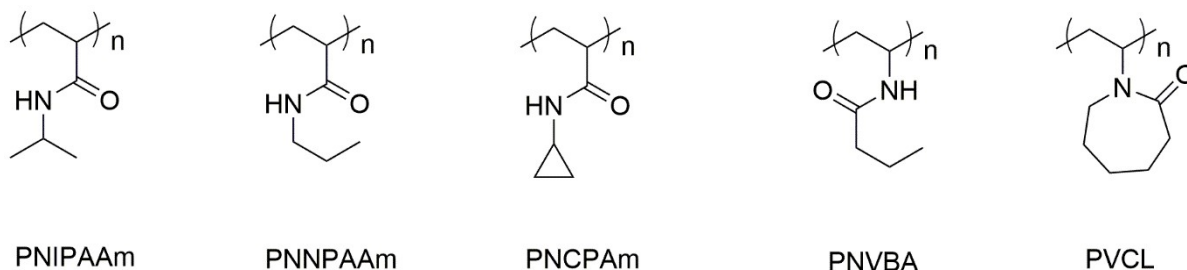
Figure 5. Typical chemical structures of thermosensitive homopolymers.[22]

The polymeric materials can also be potentially employed as carriers for therapeutics or biomolecules. The term "polymer therapeutics" has been coined including polymeric drugs,[31] polymer–drug conjugates,[32] polymer–protein conjugates[33] and polymeric micelles to which drug is covalently bound.[34,35] Amphiphilic block copolymers with temperature-responsive properties are widely investigated in triggered self-assembled systems for drug delivery. One benefit is the control and adjustment of micelle size between 20 and 100 nm, so that the therapeutic drug can be selectively addressed to tumor cells.[36–38] Self-assembled nanoreactors of amphiphilic block copolymers are also very interesting for catalysis, which will be discussed in detail in chapter 2.4.

The synthesis of block copolymers with defined structure can be carried out by using many different techniques, including ionic (cationic, anionic),[39] reversible deactivation radical (ATRP, NMRP, RAFT) polymerization techniques[40–42] and ring opening metathesis (ROMP)[43]. Generally, the strategy for block copolymer synthesis for the block copolymer mainly includes: (1) the sequential chain extension with addition of monomers via "living"/controlled polymerization techniques and (2) coupling reactions exploiting the active chain ends of different chain segments.[44]

2.2 Reversible deactivation radical polymerization (RDRP)

Living polymerization is one of the most important characteristices for the synthesis of defined polymers via an anionic,[45] cationic or ring-opening mechanism[46] in the absence of irreversible chain transfer and chain termination. The "living" character of the polymerization allows the preparation of a series polymers with different architectures e.g. block copolymers and star polymers.[44] Due to the high purity requirements of ionic polymerization techniques, advanced reversible deactivation radical polymerization (RDRP) techniques have been developed, which can also be used to synthesize block copolymers with a defined average molar mass and low dispersity. In contrast to traditional living polymerization techniques, many new materials can be obtained by RDRP under mild reaction conditions, allowing the synthesis of a broad range of functional materials.[47] Control of the RDRP systems relies on a dynamic balance between activation/deactivation processes or a reversible chain exchange process (as shown in Figure 6), thus leading to a consistent chain growth. Bimolecular termination steps, such as recombination and disproportionation are minimized by decreasing radical concentration or by establishing stable radical intermediates.[48]
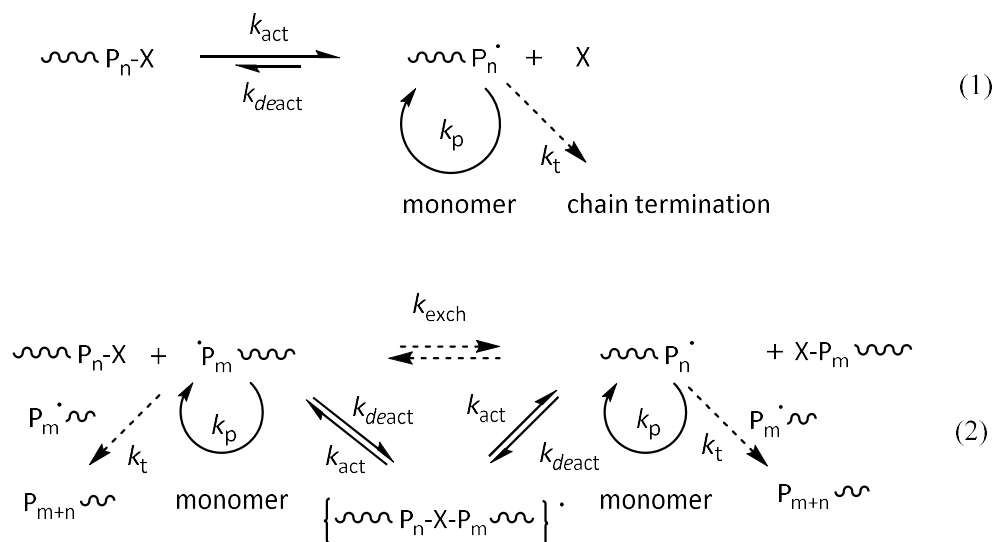
Figure 6. General mechanisms of CRP with the (1) activation/deactivation process and (2) reversible chain exchange process.[49]

The following features can be observed if the RDRP proceeds in controlled manner: 1) First-

order kinetics regarding monomer consumption indicated a constant radical concentration. 2) RDRP allows pre-determinable degrees of polymerization and a consistent chain growth proved by a direct proportionality between the number average molar mass (M_n) and monomer consumption. 3) The synthesized polymers exhibit a narrow mole mass distribution (Đ ≤ 1.2), whose dispersity should decrease with increasing degree of polymerization. 4) the end of the polymer chain remains a reactive group, which can either be extended in the sequential addition of another monomer or can be used as a macroinitiator in a separate reaction.[50] Moreover, the active end group allows the construction of complex structures via post-polymerization modification. Based on the mechanisms of the polymerization process, the controlled radical polymerization can be classified into the following three fundamental techniques.[50–52]

1) Atom transfer radical polymerization (ATRP)

2) Nitroxide-mediated radical polymerization (NMRP)

3) Reversible addition-fragmentation chain transfer polymerization (RAFT)

2.2.1 Atom transfer radical polymerization (ATRP)

The ATRP is considered the most effective method of controlled radical polymerization which was developed by Krzysztof Matyjaszewski in 1995.[49] It has been widely used to synthesize many well-defined (co)polymers with predetermined molar mass, narrow molar mass distributions and improved chain-end functionality.[53–56] Compared to living polymerization techniques (e.g. ionic polymerization) ATRP, as a radical process, is more tolerant to a wide range of functional groups and reaction conditions. Therefore, a variety of monomers including styrenes, (meth)acrylates, (meth)acrylamides, and acrylonitrile could be successfully polymerized using ATRP, thereby allowing the straightforward introduction of functional groups into the polymer structure.[57–59]

$$R-X \; + \; Mt^n-Y/Ligand \xrightleftharpoons[k_{deact}]{k_{act}} \quad R^\bullet \; + \; X-Mt^{n+1}-Y/Ligand$$
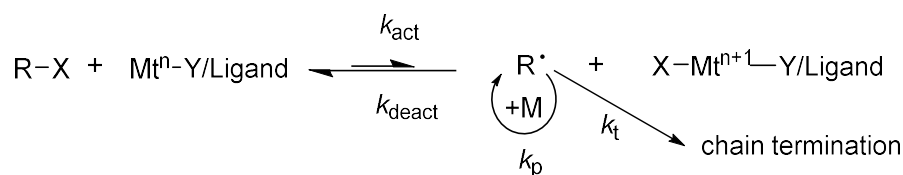
Figure 7. Schematic mechanism of transition-metal-catalyzed ATRP. [50]

The general mechanisms for ATRP involving transition metal catalysis is shown in Figure 7. The control of ATRP polymerization is based on a reversible transfer of halogen atoms between a transition-metal complex and the growing polymer chain. ATRP initiator react with the transition metal complex Mt^n-Y/Ligand in the lower oxidation state to yield a radical R• and the oxidized halogenated metal complex X-Mt^{n+1}-Y/Ligand. For the reversible step the complex can transfer the halogen atom back to the radical forming the alkyl halide as a dormant species and the reduced transition metal complex. Radical R• reacts with the monomer for chain propagation with a rate constant k_p which is similar to a conventional radical polymerization. Undesired bimolecular termination reactions (k_t) e.g. disproportion and combination cannot be ignored during the polymerization process. However, in a well-controlled ATRP only a small amount of dead polymer chains was observed during the polymerization and the control of the polymerization was achieved by fast initiation and rapid reversible deactivation (k_{deact}) that decrease the stationary concentration of growing radicals. Thereby the contribution of termination reactions is minimized and the resulting polymer will be determined by a narrow molar mass distribution.[50] The rate constants for the reversible atom transfer k_{act} and k_{deact} were closely related to halogenated ATRP initiator as well as the transition metal complex. As introduced previously, the synthesis of well-defined polymers with low dispersity requires a fast initiation. A variety of initiators such as alkyl halides R-X (X = Cl, Br),[60,61] α-haloesters,[62,63] and sulfonyl halides[64] with easily homolytically cleavable carbon-halogen bonds have been used successfully in ATRP. The rate of homolytic cleavage of the alkyl halides increases in the series R-I <R-Br <R-Cl. Therefore, initiators containing chlorine or bromine atoms (Figure 8) are optimal for ATRP. The use of alkyl iodides is unusual because the C-I bond is photosensitive and react with the transition metal to form thermodynamically unstable complexes (e.g. CuI_2)

which cannot be isolated in the reaction mixture. On the other hand, the R-I bond may also show heterolytically cleavage, thus leading to a loss of control over the ATRP process.[65]

Transition metal complexes are perhaps the key components of ATRP and the selected transition metal must have at least two oxidation states in order to be able to undergo one-electron transfer reactions. Transition metals in groups 6-11, e.g. Mo (V),[66] Cu (I),[49] Fe (II)[67] and Re (V)[68] were often reported in ATRP. However, the metal salts mostly have poor solubility in the organic medium. For this reason, the metals must complexe with ligands. Depending on the ligand used, a certain redox potential and thus a certain equilibrium position arises. The adjustment of the equilibrium must be proceeded much faster than the chain growth. A series of nitrogen ligands (Figure 8) was synthesized, which are particularly suitable for the ATRP with copper salts. In contrast to the nitrogen-based ligands, sulfur, oxygen, or phosphorus ligands are less effective or have unfavorable binding constants. For this reason, the choice of ligands strongly affects the catalytic activity and selectivity. For a successful ATRP, other factors such as solvent and temperature should also be considered.

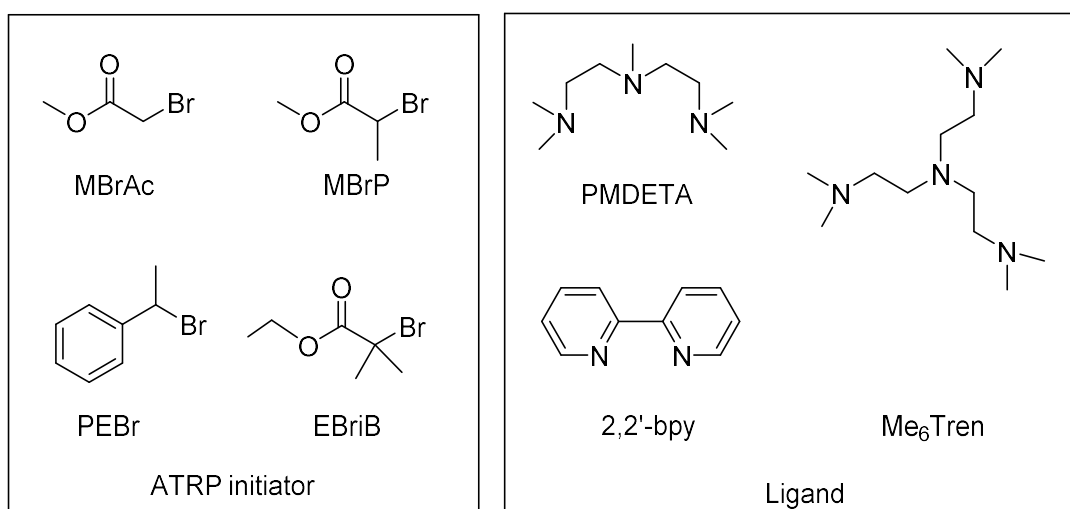

Figure 8. Typical ARTP initiators and ligands.[50]

2.2.2 Nitroxide-mediated radical polymerization (NMRP)

Another controlled radical polymerization process known as alkoxyamine/nitroxide-mediated radical polymerization (NMRP) is based on a reversible termination of the growing polymer chain with persistent radicals.[69,70] In the first experiments 2,2,6,6-tetramethylpiperidine-1-oxyl

(TEMPO) was used to mediate the polymerization of styrene at high reaction temperatures (T > 100 °C) yielding polymers with a relatively narrow molar mass distributions showing dispersities from 1.26 to 1.50.[71] The optimization of the polymerization process could be achieved by the addition of various additives as well as the design of the new alkoxyamines/nitroxides.[72–74] In the NMRP mechanism, the alkoxyamines are used as initiators/regulators. Due to the thermal instability, the C-ON bond of alkoxyamines decomposes at high temperatures and initiate the polymerization. The active polymer chain grows through addition with monomers. Depending on temperature, the equilibrium between dormant and active species is shifted to the polymeric alkoxyamines so that the concentration of free radicals is low during the polymerization. As a result, the probability of irreversible termination such as combination and disproportionation significantly decreases, meanwhile the degree of polymerization increases linearly with monomer conversion, as expected for a consistent chain growth (Figure 9).
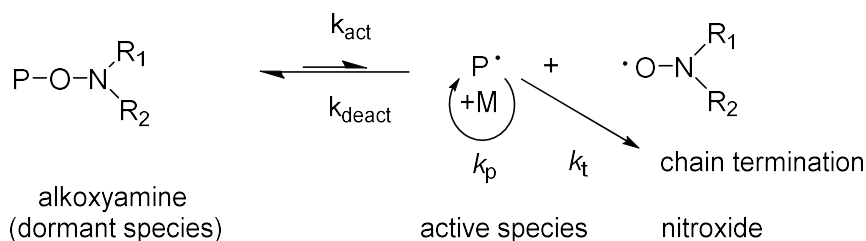
Figure 9. Schematic mechanism of Nitroxide-mediated radical polymerization.[48]

Apart from (1) (TEMPO), many other nitroxides for NMRP were developed, to improve control over the polymerization and to extend applicability of NMRP from styrene derivatives to a broader range of monomers (Figure 10).[75] In 1993, Georges and co-workers were the first to investigate the polymerization of styrene using TEMPO as nitroxide and benzoyl peroxide (BPO).[71] Thermal initiators such as azo-bis (isobutyronitrile) (AIBN) or dibenzoylperoxid (BPO) are required to start polymerization. The alkoxyamine is formed in-situ during the polymerization. Such systems are known as bimolecular initiator systems and possess a better control of the polymerization with a narrow molar mass distribution.[76,77]
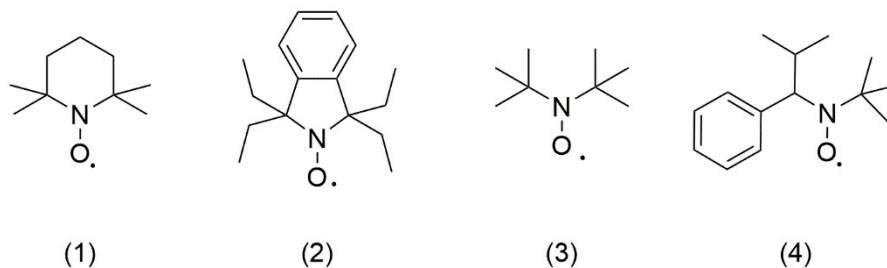
Figure 10. Chemical structure of typical nitroxides[78]

Craig Hawker described the first unimolecular NMRP system in 1994.[79] The nitroxide radical can be obtained by homolytic thermal decomposition of low molecular alkoxylamines. Because of the 1:1 stoichiometry between the persistent radical and the initiator radical, the targeted average molar mass can be adjusted directly by the ratio of alkoxyamine to monomer.
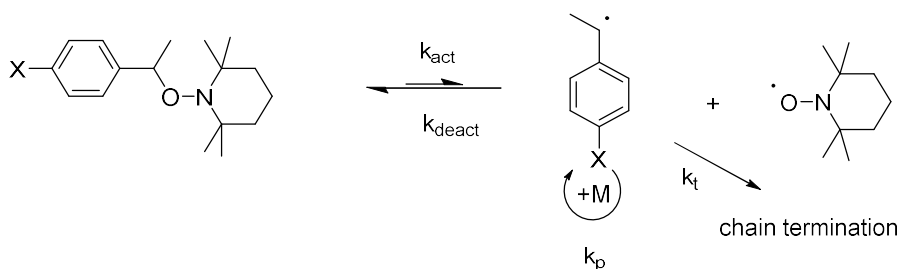
Figure 11. Nitroxide-mediated polymerization of styrene with a TEMPO-based alkoxyamine as initiator.[79]

2.2.3 Reversible addition-fragmentation chain transfer polymerization (RAFT)

The radical addition-fragmentation process was first proposed in organic synthesis in the early 1980s.[80] Reversible addition-fragmentation chain transfer polymerization, which shows the properties of controlled polymerization, was first developed by an Australian Commonwealth Scientific and Research Organization (CSIRO) team in 1998.[80] Compared to other controlled radical polymerization techniques such as NMRP, which has been exploited extensively for the synthesis of styrenic and acrylic polymers and which is only applicable to a restricted range of monomers, RAFT process was proved to be more robust and versatile for the synthesis of functional polymers. The majority of monomers including acrylates, acrylamides and methacrylates could be polymerized by RAFT under mild conditions. The control of polymerization could be achieved by the selection of appropriate RAFT agent for the respective

monomer and the reaction conditions.[81,82] As shown in Figure 12 the mechanism of RAFT polymerization includes a reversible or degenerate chain transfer process to control the polymerization. After initiation by conventional initiators (AIBN or BPO), the growing polymer chain is added to the C=S double bond of the transfer reagent to form an "inactive" intermediate. Upon fragmentation, these dormant species disintegrate by β-cleavage splitting off a radical R · capable of initiating a new polymer chain. For an ideal RAFT polymerization the RAFT agent should behave as a transfer agent and the transfer equilibrium between active and dormant species is crucial for polymerization control. An effective process in RAFT requires a higher rate of the addition/fragmentation steps compared to the propagation steps. As a consequence only a few monomer units are added per activation cycle and therefore, all the macromolecular chains show a similar polymerization degree at each time of polymerization. Therefore, the chain transfer agent determines polymers as the α- and ω- end group functionality of the majority of the macromolecular chains.[83]
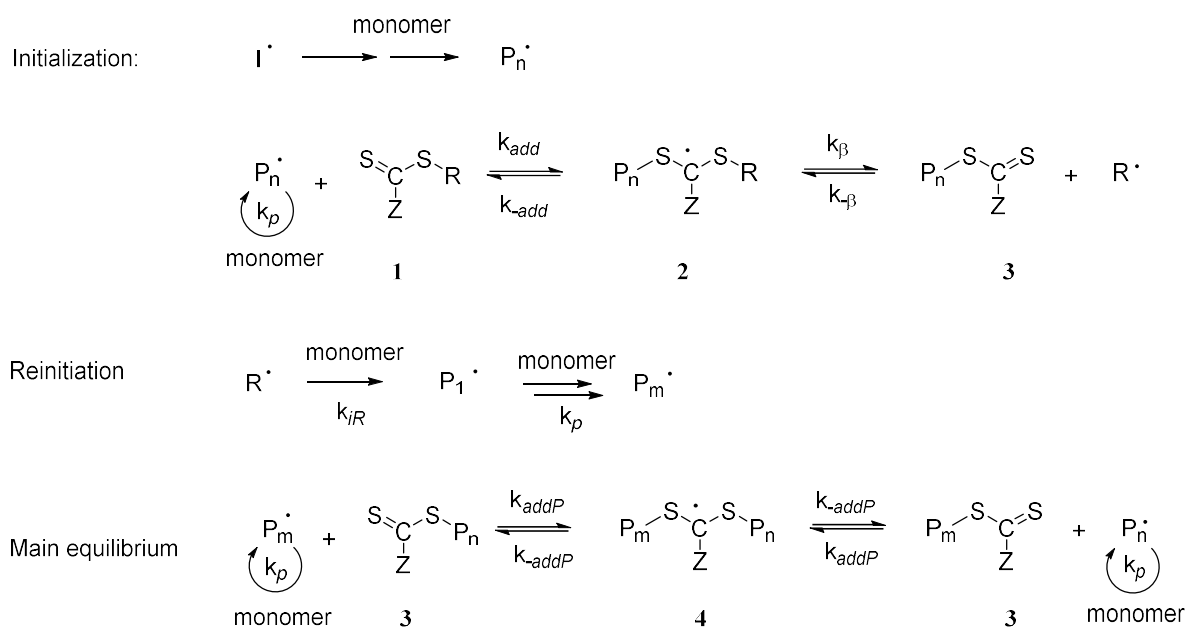
**Figure 12.** Schematic mechanism of the RAFT polymerization.[82]

As mentioned above, the most striking advantage of RAFT process is the high compatibility with a broad range of monomers. Based on their reactivity monomers can be classified into two general classes: The "more activated" monomers (MAM) are the monomers which have their vinyl group conjugated to an aromatic ring (e.g. styrene), a carbonyl group (e.g. methyl

acrylate, acrylamide), or a nitrile (e.g. acrylonitrile). The "less activated" monomers (LAM) are those, whose double bond is adjacent to saturated carbon atoms or to oxygen-, nitrogen-, halogen-, sulfur-atom with free electron pairs (e.g. vinyl acetate, *N*-vinylpyrrolidone, vinyl chloride, 1-alkenes). The successful control of the polymerization process is achieved by careful selection of R and Z groups determining the reactivity of the chain transfer agent (CTA): The Z group of the corresponding CTA has an influence on the reactivity of C=S bond toward radical addition as well as the stability of the intermediate radicals during the polymerization. As shown in Figure 13, the addition rates of different radicals to the C=S bond decrease from left to right. Therefore, the most reactive RAFT agents include trithiocarbonates (Z = *S*-alkyl) and dithiobenzoates (Z = Ph), which are often employed to control the polymerization of MAMs. Since propagating radicals with a MAM as terminal unit are less reactive in radical addition, reactive Z groups are required to prepare low dispersity polymers. On the other hand, propagating radicals with a LAM as terminal unit are highly reactive in radical addition but poor in homolytic cleavage. RAFT agents such as xanthates (Z = O - alkyl) or dithiocarbamate (Z = N-alkyl) was employed in order to promote propagation and intermediate fragmentation.[83]
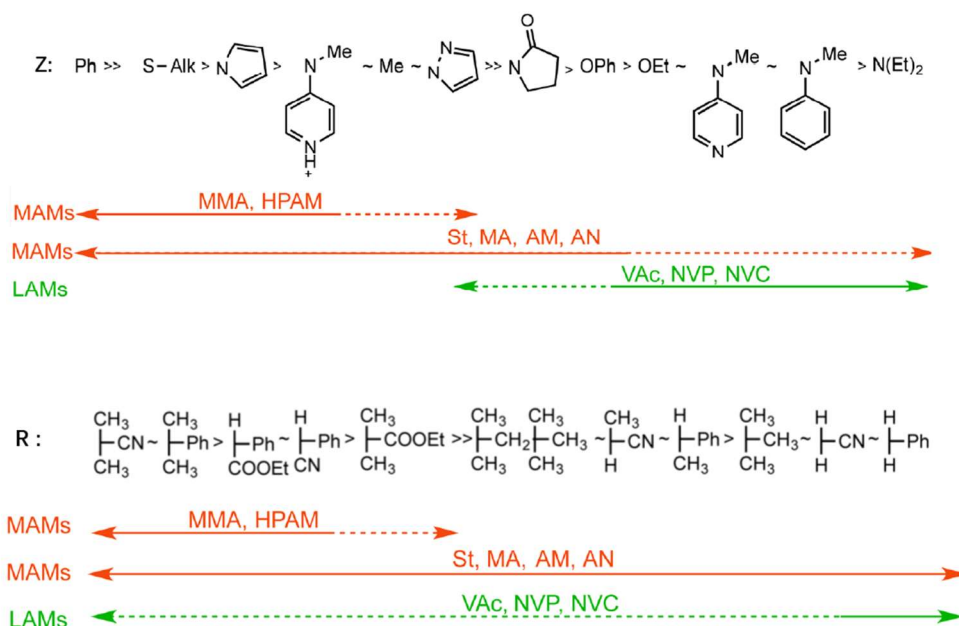
Figure 13. Guidelines for the selection of Z and R groups of RAFT agents (ZC(=S)SR) for different monomers.[81,83,84] Reprinted with permission from (Perrier, S. 50th Anniversary Perspective: RAFT Polymerization—A User Guide. Macromolecules 2017, 50, 7433–7447). Copyright (2018) American Chemical Society.

The nature of R group determines fragmentation and reinitiation rate constants. In the guidelines (Figure 13) for selection of a proper R group, the transfer coefficients decrease from left to right. For the optimal control of the RAFT polymerization, the R group must be a good homolytic leaving group and the R group must be able to efficiently reinitiate propagation, thus making sure that all chains were initiated at the same time in order to obtain a narrow molar mass distribution. Furthermore, the synthesis of block copolymer is also appreciably affected by the R group. In general, the synthesis of a block copolymer PMAM-*b*-PLAM, PMAMs should be prepared first and used as macro-CTA for the attachment of the PLAM block, since PLAM are relatively poor homolytic leaving groups. For the synthesis of the PLAM-*b*-PMAM, an alternative approach was proposed to control the polymerization of the monomers with different reactivity by using "universal" or "switchable" RAFT agents.[85,86] The reactivity of the designed CTA can be modulated by external conditions. As a successful example *N*-(4-pyridinyl)-*N*-methyldithiocarbamates used as a pH-switchable RAFT agent provide excellent control over the polymerization of both MAMs and LAMs under different pH conditions: The neutral CTA offer a low reactivity promoting the control of the polymerization of LAMs. After addition of a strong acid or a nonprotic Lewis acids, the protonation of the pyridine ring favors control of the MAMs polymerization (Figure 14). Using this method, the synthesis of block copolymers PMAM-*b*-PLAM with narrow molar mass distributions was successfully achieved by adjusting RAFT agent reactivity after synthesis of the first block.
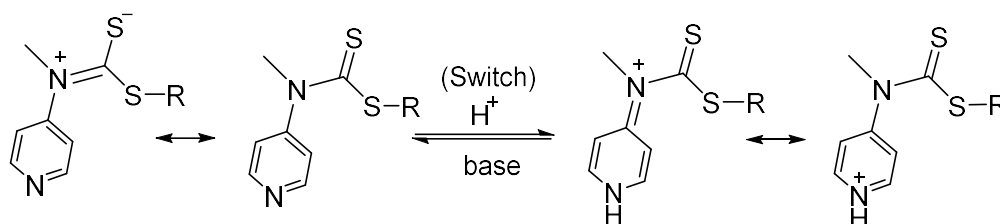
Figure 14. *N*-(4-Pyridinyl)-*N*-methyldithiocarbamate as switchable RAFT agent.[87]

End group modification is highlighted as further feature of RAFT synthesized polymers, showing an increasing number of respective publications.[88] Polymers possessing a thiocarbonylthio functionality at the ω-end can be utilized to post-polymerization. As shown in Figure 15, a detailed description of the distinct ω-end group modification involving different

types of reaction were investigated. First of all, the hydrolysis or aminolysis reaction of thiocarbonylthio group is one of the most widely reported method to obtain thiol end groups.[89] Kim et al. synthesized thiocarbonylthio end-capped polystyrene derivates via RAFT. Subsequent aminolysis of the terminal dithioester afforded secondary thiol end group. This end group was used to covalently attach the polymer to gold nanoparticles.[90] Thermolysis was proved to be efficient in cleaving thiocarbonylthio compounds via Chugaev elimination reaction.[91] The resulting polymer exhibits an unsaturated chain end, which can be used for further modification. The thermal stability of end groups is related to both the type of polymer and the chemical structure of the Z group of the RAFT-CTA. Therefore, different RAFT-synthesized polymers required different temperatures for thermal decomposition of the end group. Thermolysis of polystyrene was carried out at 210-250 °C to cleave the *S*-butyl trithiocarbonate, obtaining a colorless product.[92] In contrast, thermal degradation of poly(*n*-butyl acrylate) usually occurs at significantly higher temperatures of more than 300 °C.[93] Radical-induced transformations of the thiocarbonylthio end groups were achieved by the radical addition of the radical to the C=S bond. This strategy was proved as a versatile route for both end-group removal and alternative chain end functionalization.[94] For this process, radicals were generated in situ using thermal initiators (e.g. AIBN), redox-initiator systems similar to ATRP or photo initiator. Thus, various end groups could be introduced into the polymer.[95] An alternative modification of RAFT end groups was achieved using the electron deficiency of thiocarbonylthio groups as dienophiles in reversible hetero-Diels–Alder reactions. As described, this method was successfully used to synthesize poly(styrene) (PS) star polymers with up to 4 arms with high conversions and high selectivity.[96] With respect to the broad applicability, the combination of RAFT chemistry and hetero-Diels-Alder (HDA) cycloaddition was considered as convenient conjugation tool in the range of complex macromolecular designs.[97, 98]

A lot of work was focused on the synthesis of homo- and copolymers based on PNIPAAm via RAFT polymerization. In 2004, Convertine et al. reported the successful synthesis of PNIPAAm homopolymer using a trithiocarbonate RAFT-CTA (2-dodecylsulfanylthiocarbonylsulfanyl-2-

methylpropionic acid) and 2,2' azobis(4-methoxy-2,4-dimethylvaleronitrile) in DMF. The kinetic studies showed all the characteristics of a controlled or "living" polymerization.[99] In addition, numbers of publications dealing with the topic temperature-sensitive multi-block copolymer was published and a series of well-defined PNIPAAm-containing block copolymers were successfully prepared via RAFT polymerization with the appropriate choice of both a suitable RAFT chain transfer agent (CTA) and initiating species.[100–102]
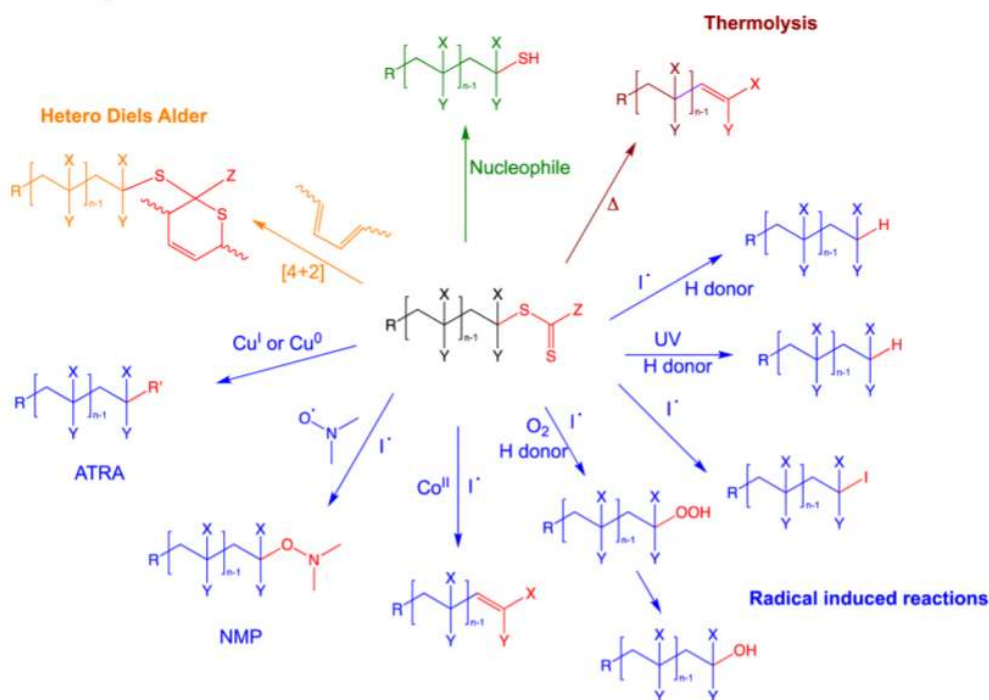
Figure 15. Different strategies of thiocarbonylthio end-group modification.[83] Reprinted with permission from (Perrier, S. 50th Anniversary Perspective: RAFT Polymerization—A User Guide. Macromolecules 2017, 50, 7433–7447). Copyright (2018) American Chemical Society.

2.3 Post-polymerization modification using azlactone moieties

Macromolecular materials functionalized with chemically reactive groups have attracted great interest in polymer chemistry. Numbers of functional polymers based on different kinds of reactive monomers such as active esters,[103,104] azlactones,[105] epoxides,[106] isocyanates[107] and anhydrides[108] were investigated and applied in versatile applications.[104,109,110] Azlactone-functionalized polymers have attracted increasing attention in the past decade as a very promising category of functional materials. With respect to the development of azlactone

chemistry and its application in technology, a significant contribution, especially from industrial point of view, over 100 patents have been made by the groups at 3M, Polaroid, and Rohm GmbH.[111] Due to the high reactivity of azlactones, a rapid, atom-economic ring opening reaction occurs under relatively mild conditions, providing an efficient and facile approach of post polymerization modification.[112,113] Compared to other types of the reactive polymers (e.g. activated esters containing pentafluorophenyl groups), azlactone moiety offer a higher stability against hydrolysis, thus nucleophilic ring opening of azlactone carbon conducted even in aqueous solutions (Figure 16).[114] Moreover, many of the azlactone-functionalized polymers show good solubility in different organic solvents. Azlactone chemistry can be extended to various kinds of supporting materials (e.g. hydrophilic, hydrophobic, proteins and other biomacromolecules).[112] In the report by zhu et al., poly(2-vinyl-4,4-dimethylazlactone) (PVDMA) was used as a reactive platform to design the PVDMA-derived (co)polymers with LCST or UCST behavior in aqueous solution.[105] The different thermoresponsive behavior as implemented by varying the composition of the side-chain with zwitterionic sulfobetaine, intermediately polar tetrahydrofurfuryl and hydrophobic benzyl functionalities.
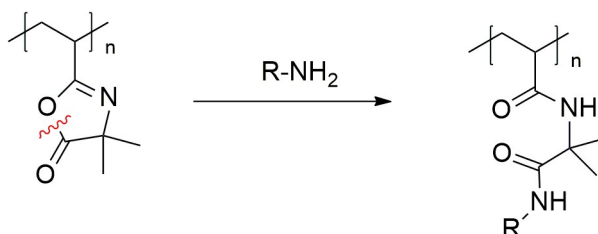
Figure 16. Post polymerization modification of PVDMA with a nucleophilic species to yield a poly(acrylamide) type polymer.[115]

Figure 16 shows the post-polymerization modification of a primary amine with the azlactone group of PVDMA. With the nucleophilic attack at the carbonyl group (e.g., by primary amines, hydroxyl groups, or thiol groups), a ring-opening reaction takes place to form the corresponding modified polymer with the former nucleophile attached to the side chain. The ring-opening process was observed to be slightly exothermic when primary amines and thiolates were employed as nucleophiles in the absence of a catalyst. However, for the reaction

with alcohols, either acid or base was required as catalyst to perform the reaction. Applying strong acids, the azlactone group displays a high reactivity towards side reactions e.g. Michael addition. For this reason, cyclic amines like 1,8-diazabicyclo [5.4.0] undec-7-ene (DBU) were usually used as the catalyst for the ring-opening reaction with alcohols. The early synthesized azlactone-functionalized polymers were prepared by conventional free radical polymerization.[112] The development of new polymerization techniques such as RDRP made it possible to achieve well-defined functional polymers. Tully et al. were one of the first to apply nitroxide-mediated mediated polymerization (NMRP) to azlactone monomer and the polymerization displayed high conversions as well as the control over the molar mass.[116] Fontaine and coworkers reported the synthesis of PVDMA using copper-mediated atom transfer radical polymerization (ATRP) in both solution and on surface of solid polymer supports.[117,118] The controlled polymerization of VDMA was carried out to obtain macroinitiators used for the chain extension yielding statistical and block copolymers with styrene and methyl acrylate using CuBr/Me$_6$TREN as catalyst complex. The molar mass distribution of the obtained copolymers showed a good control over the number average molar mass as well as low dispersities. Polymerization of VDMA using RAFT was firstly investigated by Schilli et al.[119] A series of temperature- and pH-sensitive polymers consisting of short blocks of reactive monomers were synthesized via RAFT. The thiol-terminated polymers were used for polymer-protein conjugation. For the controlled polymerization of the VDMA in this paper, 2-cyanoisopropyl dithiobenzoate (CPDB) was used as chain transfer agent with AIBN as initiator. Over 64 % conversion was achieved and polymer with a low dispersity (Đ = 1.09) were obtained. In 2011, Levere et al. reported stable azlactone-functionalized nanoparticles prepared from thermoresponsive amphiphilic block copolymers.[120] In this study, RAFT polymerization was applied to synthesize block copolymers containing a PNIPAAm thermoresponsive block and a hydrophilic statistic block based on DMAA and VDMA (Figure 17). PVDMA displayed high reactivity towards diamine in a ring-opening reaction to form stable core-shell particles in aqueous solution. The DLS analysis of the resulting crosslinked particles showed a hydrodynamic diameter of 29 nm at 25 °C, which was stable at different

concentrations, temperatures and pH value.
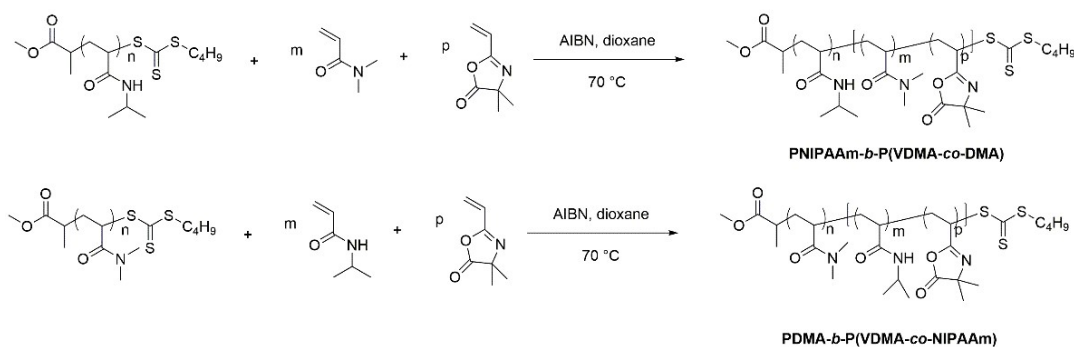
Figure 17. Synthesis of PNIPAM-*b*-P(VDMA-*co*-DMAA) and PDMAA-*b*-P(VDMA-*co*-NIPAAm) copolymers by RAFT polymerization.[120]

## 2.4 Temperature sensitive polymer supports for organocatalysts

Organocatalysis has been accepted as a new and immature field of enantioselective synthesis for the last 30 years.[121] The use of small organic molecules as catalyst being generally unsensitive to oxygen and water and requiring mild reaction conditions, holds serveral economic, environmental and scientific benefits.[2,122] However, for a long time, organocatalyst were to be considered as low-valued substrates for immobilization.[1,4] With the development of sophisticated organocatalysts and the increased awareness of sustainability situation emerged. The use of polymer supports for catalyst does not only improve the handling of the catalyst but also directly affect both activity and selectivity of the catalyst.[123,124] Moreover, immobilization of organocatalysts on the stimuli responsive polymer carriers allows the reuse and recovery of catalyst by simply altering ambient conditions. This could be of high value from the perspective of green chemistry.

In 2000 List et al. reported the first proline-catalyzed direct asymmetric aldol reaction, which followed the seminal Hajos-Parrish-Eder-Sauer-Wiechert reaction.[2] Until now proline and various proline analogs were regarded as the most successful organocatalysts for enamine-type reactions.[125,126] Proline as a simple amino acid with a secondary amine functionality has a higher pK_a value and reacts as a nucleophile with carbonyl groups to form iminium ions or enamines (Figure 18). Both enantiomers of proline were applied as catalysts for a variety of

21

reactions.[2,127–129] Although proline itself can be considered as an inexpensive catalyst, for many reactions high catalyst loadings of 10 mol% or more are needed. Removal of the proline catalyst after the reaction is often quite challenging. Reduced catalyst loadings can be achieved by more active proline derivatives, e.g. substituted proline amides. These derivatives are usually obtained by multiple step synthesis. Therefore, easy catalyst separation and catalyst recycling gained increased attention. In 1985, Kondo et al. reported the first type of polymer-supported proline.[130] In the past decades many researchers focused on the immobilization and recycling of proline on polymeric carriers like linear and cross-linked polymers, dendrimers and polymeric capsules.[13,124,131–135] Numerous reviews are available summarizing the efforts on both soluble and insoluble polymer supports for proline.[5,121,136–139] Recently, the use of stimuli-responsive supports for proline gained more and more attention, since they do not only offer the possibility of easy catalyst separation but also of reversibly tuning of catalyst activity by external stimuli.
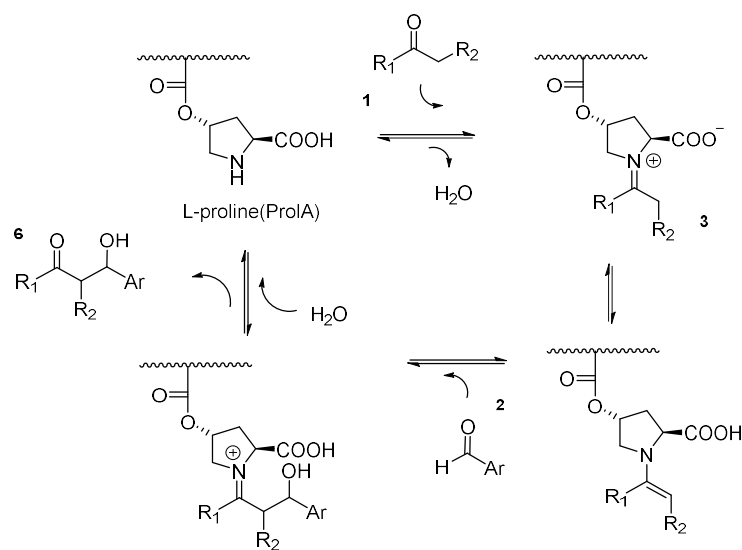
Figure 18. Proposed mechanism for the proline-catalyzed intermolecular aldol reaction cycle.[125] (Adapted from [125] with permission from Elsevier Copyright (2018))

Hu et al. reported the synthesis of hairy particles with immobilized proline catalyst in the corona. The particle core consisted of poly(methacrylic acid) crosslinked by ethylene glycol dimethacrylate. Hairy structure was achieved by modification of the particle surface with dithiobenzoate, and subsequent surface-initiated RAFT copolymerization. Particles with three

different kinds of grafted copolymers were synthesized: (1) the brushes consisted of a terpolymer of NIPAAm, styrene and *O*-acrylic hydroxyproline, (2) the copolymer brushes only contained NIPAAm and *O*-acrylic hydroxyproline units, (3) the copolymer brushes comprised of styrene and *O*-acrylic hydroxyproline units. The catalytic activity of the immobilized proline catalyst was investigated using the Aldol reaction of *p*-nitrobenzaldehyde (*p*-NBA) and cyclohexanone (CH) at different temperatures. Hairy particle (1) containing both hydrophobic and hydrophilic moieties showed excellent catalytic activity and stereoselectivity with over 80 % conversion at all temperatures. The other hairy particles (2) and (3) exhibited far less catalytic activity and stereoselectivity. These results proved that high substrate affinity and high stereoselectivity require hydrophilic and hydrophobic domains surrounding the catalyst. Catalyst separation could be realized by simple centrifugation. The immobilized catalyst could be reused in several cycles with only minimal loss of activity, still showing exceptionally high stereoselectivity.

In the period of 2011-2015, the research group of O´Reilly published a series of papers describing the use of the polymer-supported proline as highly efficient catalysts for aldol and acylation reactions.[137,140–142] In 2014, O´Reilly and coworkers reported the synthesis of recyclable L-proline nanoreactors with temperature-tuned activity based on core-shell nanogels.[142] Two distinct core-shell-type nanoreactors were synthesized and compared with respect to their catalytic activity. The first one represented core-shell (CS) nanogels based on a proline-containing core and a thermoresponsive cross-linked PNIPAAm shell (Figure 19). It was synthesized via a seeded precipitation polymerization process. The second one, also comparing a proline-containing core but a cross-linked PNIPAAm shell (GS) with a declining gradient in cross-linking density in the outer corona. These GS microgels were obtained by a one-pot-two-step reaction. A thin cross-linked PNIPAAm shell was first formed on hydrophobic seeds and in the second step NIPAAm monomer was added without additional cross-linker.

The catalytic efficiency of L-proline immobilized in the two-distinct core-shell nanogels was evaluated and compared using the asymmetric aldol reaction between CH and *p*-NBA in water at three different temperatures and 2 mol% catalyst loading. As shown, the hydrodynamic

diameter (D_h) of both nanogels was greatly affected by temperature. The thermo-responsive behavior of PNIPAAm results in a decrease of the hydrodynamic nanogel diameter from 133 nm to 30 nm (for CS) at elevated temperatures. At lower temperatures, GS proved a better catalytic activity than the corresponding CS nanogel. With increasing temperature, the CS nanogels showed an Arrhenius-type temperature depended behavior with an increase in catalytic activity from 40 % at 4 °C to 88 % at 40 °C. The increased catalytic activity was supposed to be caused by the increased hydrophobicity of the shell leading to a higher substrate affinity. On the contrary, a drop of conversion to 28 % was observed for the GS nanogel at 40 °C, which was attributed to the collapse of less cross-linked polymers in the outer shell corona, thus blocking the access to the catalytic core. However, both nanogel systems gave excellent steroselectivities in the asymmetric aldol reaction in water, and they could be reused with minimal loss of catalytic efficiency for the first 4 cycles.
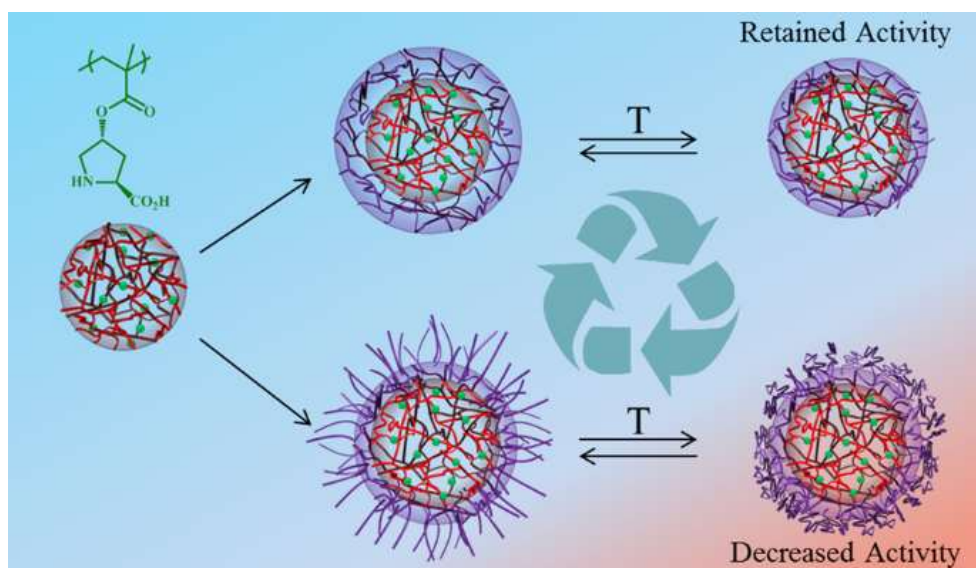
Figure 19. Temperature-tuned activity of proline immobilized in core-shell nanogel (CS) and core gradient shell (GS) nanogels.[142] Reprinted with permission from (A. Lu, D. Moatsou, I. Hands-Portman, D. A. Longbottom, R. K. O'Reilly, ACS Macro Lett. **2014**, 3, 1235). Copyright (2018) American Chemical Society.

Nanoreactors can also be formed by temperature-induced aggregation of smart polymers in aqueous solutions. The polymer aggregates are capable of solubilizing hydrophobic substrates within their core. The high substrate concentration within the aggregates can be utilized to conduct a chemical reaction in presence of an immobilized catalyst. In contrast to microgels, nanoreactors based on polymer aggregates are more flexible, thereby allowing easy substrate

uptake before the reaction and product release after the reaction is finished. O´Reilly and coworker recently reported on L-proline immobilized on a thermoresponsive block copolymer and its use for micellar catalysis of a direct asymmetric aldol reaction in water.[14] The block copolymer was synthesized by RAFT polymerization and comprised a permanently hydrophilic block PDMAA and a thermoresponsive block (poly(*N*-isopropylacrylamide)-*co*-butylacrylate-*co*-N-*tert*-butoxycarbonyl-*O*-acryloyl-*trans*-4-hydroxy-L-proline) (Figure 20).
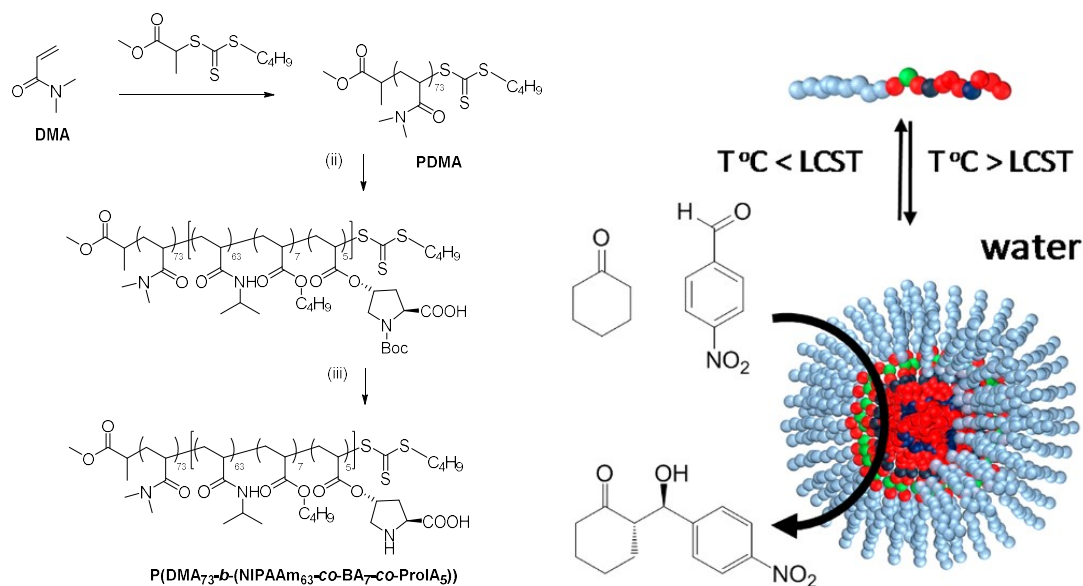
Figure 20.: RAFT block copolymerization affording a temperature-sensitive block copolymer with immobilized L-proline moieties (left), temperature-induced aggregation of the block copolymers and micellar catalysis of a direct asymmetric aldol reaction in water.[14] Reprinted with permission from (H. A. Zayas, A. Lu, D. Valade, F. Amir, Z. Jia, R. K. O'Reilly, M. J. Monteiro, ACS Macro Lett. **2013**, 2, 327). Copyright (2018) American Chemical Society.

The block copolymer exhibited a phase transition temperature of approximately 35 °C, above which micelles with a hydrodynamic diameter of 15-20 nm were formed. The immobilized L-proline catalyst was located in the hydrophobic PNIPAAm core. The direct asymmetric aldol reaction between CH and *p*-NBA was carried out using the supported L-proline catalyst at different temperatures ranging from 25 °C to 50 °C. Increased reaction rates were found if the aldol reaction was conducted at temperatures above the phase transition temperature. Thus, aggregate formation enhanced the solubility of the substrates and led to a close spatial proximity of substrate and catalyst. After the reaction, catalyst separation and recovery was achieved by precipitation and centrifugation. However, reuse of the immobilized catalyst revealed a constant decline in catalyst activity with each cycle.

3. Experimental section

3.1 Reagents and solvents

Table 1. Summary of solvents

Solvent	Supplier	Purity	Note
1,4-Dioxane	Grüssing	> 99.5 % (p.a.)	dried over 4 Å molecular
2-Propanol	Carl Roth	≥ 99.9 % (HPLC)	For HPLC
Acetone	Grüssing	> 99.5 % (p.a.)	-
Chloroform	Grüssing	> 99 % (p.a.)	-
Chloroform-d_1	Deutero	99.7 D%	-
Dichloromethane	Stomeier Chemie	techn.	-
Diethyl ether	Hanke+Seidel	techn.	-
DMSO-d_6	Deutero	99.5 D%	-
Ethyl acetate	-	-	-
Water	-	-	Tri distillations
Methanol	Grüssing	> 99.5 % (p.a.)	-
n-Hexane	Carl Roth	≥ 99 % (HPLC)	For HPLC
n-Hexane	DHC Solvent Chemie	techn.	
N,N-Dimethylacet-amide	Acros Organics	99.5 %	For GPC
Tetrahydrofuran	Grüssing	> 99.5 % (p.a.)	For GPC
Tetrahydrofuran	BASF	techn.	-

Table 2. Summary of regeants

Regent	Supplier	Purity	Note
1,2-Diaminoethane	Acros Organics	> 99 %	-
1-Dodecanethiol	Alfa Aesar	98 %	-

3. Experimental section

1-Hydroxybenzotriazole hydrate	GL Biochem (Shanghai)	-	-
2,2'-Azobis(2-methylpropio-nitrile)	Fluka	98 %	recrystallized from methanol
2-Aminoisobutyric Acid	TCI EUROPE	> 98 %	-
3,5-Di-tert-4-butylhydroxy-toluene	Fluka	>99 %	-
4-(Dimethylamino)pyridine	Fluka	> 99 %	recrystallized from toluene
4,4'-Azobis(4-cyanovaleric acid)	Sigmal-aldrich	> 75 %	-
Acryloyl chloride	Alfa Aesar	96 %	stab. with 400 ppm phenothiazine
Benzaldehyde	TCI EUROPE	98 %	-
Boc-glycine	TCI	-	-
Carbon disulfide	Sigma-Aldrich	≥ 99.9 %	-
Cbz-glycine	TCI EUROPE	> 98 %	-
Citric acid	Normapur	-	-
Copper (I) chloride	Sigmal-Aldrich	≥ 97.0 %	recrystallized from acetic acid
Cyclohexanone	Acros Organics	99.8 %	-
D,L-2-Amino-propanol	Alfa Aaesar	> 98%	-
Di-tert-butyl dicarbonate	Acros Organics	97%	-
Ethyl chloroformate	Sigmal-Aldrich	97%	-
Fmoc-glycine	TCI EUROPE	> 98 %	-
Glycerol	Carl Roth	> 98 %	water free
Hydrochloric acid	Sigmal-Aldrich	37 %	-
Hydrochloric acid solution	Alfa aesar	99 %	4M in 1,4-Dioxane
Hydrobromic acid solution	Sigmal-Aldrich	-	33 wt.% in acetic acid
Iodine	Abcr	99 %	-
L-Leucine	Avocado	99 %	-

L-proline	TCI EUROPE	>99 %	-
L-(+)-Leucinol	TCI EUROPE	>96 %	-
N,N'-Diisopropylcarbo-diimide	Arcos organic	99 %	-
N,N-Diisopropylethylamine	Alfa Aesar	99 %	-
N,N-Dimethylacrylamide	Sigma-Aldrich	99 %	stab. with 400 ppm (MEHQ), distillation under argon
N-Ethyl-*N'*-(3-dimethyl-aminopropyl) carbo-diimide hydrochloride	adcr	98 %	-
N-Isopropylacrylamide	TCI EUROPE	> 98 %	stab. with 400 ppm (MEHQ), recrystallized from n-hexane
Palladium on carbon	Acros Organics	-	10 % w/w palladium content
p-Nitrobenzaldehyde	Merck	≥ 98.0 %	-
Phenylmagnesium bromide solution	Sigmal-Aldrich	-	3.0 M in diethyl ether
p-Toluenesulfonic acid monohydrate	Sigmal-aldrich	98.5 %	-
Sodium carbonate	Normapur	-	-
Sodium chloride	Normapur	-	-
Sodium hydride	Sigmal-Aldrich	60 %	dispersion in mineral oil
Sodium hydrogen carbonate	Normapur	-	-
Sodium hydroxide	Normapur	-	-
tert-Butanol	Acros Organics	99.5 %	-
trans-4-Hydroxy-L-proline	TCI EUROPE	>99 %	-
Triethylamine	Acros Organics	99 %	-
Triethylsilane	TCI EUROPE	>98 %	-
Trifluoroacetic acid	TCI EUROPE	99+ %	-
4-Benzyloxybenzaldehyde	TCI EUROPE	-	-

2-Phenylglycinol	TCI EUROPE	>98 %	-
D-Valinol	TCI EUROPE	>98 %	-
Ethylamine	J. T. Baker	-	30 % in water
Tricaprylmethylammonium chloride (Aliquat 336)	Alfa Aersa	-	-
Poly (ethylene glycol) Mono-methylether (M_n=5000 g/mol)	Sigmal-aldrich	-	-

3.2 Characterization methods

Nuclear Magnetic Resonance (NMR) spectroscopy

The ^{1}H-NMR spectra and ^{13}C-NMR spectra were recorded on a BRUKER Avance 500 instrument in deuterated solvents at 500 MHz and 125 MHz, respectively. The chemical shifts δ in ppm are referenced to the respective solvent residual peak with $CHCl_3$ δ =7.26 ppm and DMSO δ =2.50 ppm). As solvents Chloroform-d (CDCl$_3$-*d*, 99.8 D%), dimethylsulfoxide-d$_6$ (DMSO-*d$_6$*, 99.5 D%) were used for NMR measurements. Data were obtained and processed using MestReNova Software (Version: 6.0.2-5475, Mestrelab Research Chemistry Software Solutions).

Attenuated Total Reflection-Fourier Transformation Infrared (ATR-FTIR) spectroscopy

IR spectra of the protected and unprotected block copolymers were recorded with a Bruker VERTEX 70 FT-IR spectrometer (Bruker Optik, Ettlingen, Germany). Samples were measured in the wavelength region of 4000 cm^{-1} to 400 cm^{-1}. Data were obtained and processed using OriginPro 2017 Software (Version: 94E, OriginLab Corporation)

Size-Exclusion Chromatography (SEC)

Polymers were characterized by two different SEC systems:

The first SEC system was running on THF as eluent. Two PSS-SDV columns (PSS, Mainz, 10^5 Å and 10^3 Å porosity with 5 µm particle size) were applied to separate the polymers at room temperature. Fractions were detected using a Knauer Smartline 2300 refractive index detector. The flow rate was set to 1.0 mL/min and narrowly distributed PMMA standards were used for calibration.

The second system was using N, N-dimethyl acetamide (DMAc) as eluent. Polymer separation was performed using 3 PSS-GRAM columns (10^4, 10^3, and 10^2 Å porosity, 10 µm particle size) at a temperature of 50 °C. The flow rate was set to 0.5 mL/ min. Fractions was detected by a Waters RI 2410 detector. Molar mass distribution was calculated based on a calibration with narrowly distribution PMMA standards.

For both systems data acquisition was accomplished using a PSS Universal Data center UDCS10. Data evaluation was performed using PSS WinGPC Unity software.

Ultraviolet-visible light (UV-VIS) spectroscopy

To analyze the UV-VIS absorption of thiocarbonyl end groups before and after aminolysis, UV-VIS absorption spectra were recorded with a "Specord-50 plus"-UV-VIS spectrophotometer from Analytik Jena at 250-800 nm using a concentration of sample 1 mg/mL in methanol.

Dynamic light Scattering (DLS)

To analyze the temperature-induced aggregation behavior of the amphiphilic block copolymers, dynamic light scattering (DLS) measurements were performed with a Malvern Instruments Zetasizer Nano at the scattering angle of 173°. The temperature trend measurements were recorded from 20 °C to 60 °C with an equilibration time of three minutes. Before the measurement, all samples were dissolved in water with the concentration 0.5

mg/mL overnight and then filtered through Millipore membranes with pore sizes of 0.45 μm.

High Performance Liquid Chromatography (HPLC)

The HPLC measurements were performed with Merck Hitachi D-Line 7000 system equipped with a diode array ultra-violet detector at 254 nm. Samples separation was achieved using Chiralpak AD-H columns (from J. T. Baker B. V. at 25 °C) and the flow rate was set to 0.8 mL/min using 2-propanol and *n*-hexane (20/80) as eluent.

Electrospray-Ionization-Time-of-Flight Mass Spectrometry (ESI-Tof-MS)

ESI-MS spectra were recorded on a SYNAPT G2 HDMS from Waters. Sodium iodide was added for ion formation. The PSKA samples were dissolved in THF (2 g/L) and then mixed with NaI solution (2 g/L in water/isopropanol 1:1) and acetonitrile in a ratio of 5:5:990. The spectra after ion mobility separation were exported for the analysis. To assign the chain end groups, the program Polymerix software from Sierra Analytics was used. To illustrate the appropriate composition, the individual components as α- and ω-end groups, repeat unit, charge states, and counterions have to be taken into account. Series with a relative intensity >10 % have been assigned.

The mass spectrometric parameters read as following: Capillary voltage: 2.5 kV; sampling cone voltage: 160 V; extraction cone voltage: 2.0 V; cone gas flow: 30 L/h; source temperature: 120 °C; desolvation gas flow: 600 L/h; desolvation temperature: 350 °C; helium cell gas flow: 180 mL/min; IMS gas flow: 90 mL/min; IMS wave velocity: 700 m/s; IMS wave height: 40 V.

3.3 Synthesis of low molecular weight compounds and block copolymers

3.3.1 Synthesis of L-proline and L-prolinamide derivates

Synthesis of di-tert-butyl (2S,4R)-4-hydroxypyrrolidine-1,2-dicarboxylate (2)
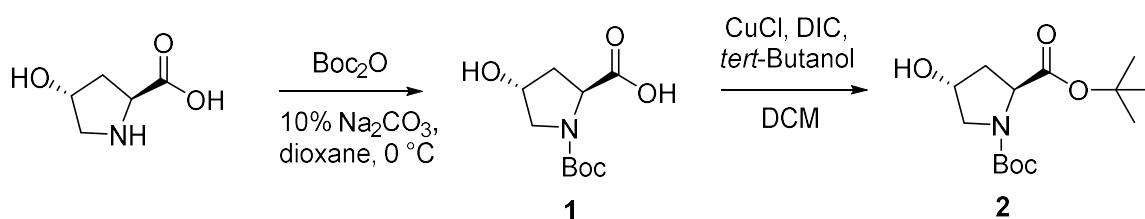
Di-*tert*-butyl (2S,4R)-4-hydroxypyrrolidine-1,2-dicarboxylate was prepared by the method described by J. Pícha et al.[143]

Trans-4-hydroxy-L-proline (4.0 g, 30.5 mmol) was dissolved in 10 % aqueous solution of Na_2CO_3 (40 mL) at 0 °C. Di-*tert*-butyl dicarbonate (1.2 equiv., 8.0 g, 36.6 mmol) in 1,4-dioxane (25 mL) was then added slowly to this solution and the reaction mixture were stirred overnight at room temperature. After the reaction was completed (TLC test), the solution was acidified to pH = 4 with saturated citric acid and the mixture was extracted with ethyl acetate (3 × 100 mL each, 5 × 50 mL). The combined organic phases were dried over $MgSO_4$ and the solvent was then removed by rotary evaporation. 4.916 g crude product (1) (70 %) was observed as viscous colorless oil and no further purification was needed for the next step.

Diisopropylcarbodiimide (DIC, 2 equiv., 14.6 mL, 86 mmol) and CuCl (0.02 equiv., 0.042 g, 0.43 mmol) were added to *tert*-butanol (9.5 mL, 100 mmol) and the mixture was stirred at room temperature for 12 hours to form of *O-tert*-butyl-*N*, *N'*-diisopropylisourea (about 2 equiv., 122 mmol). A solution of crude product (1) (4.916 g, 21 mmol) in dichloromethane (50 mL) was added to the reaction mixture under cooling with ice bath and then heated to reflux for a further 1 day. A third equivalent of *O-tert*-butyl-*N*, *N'*-diisopropylisourea (43 mmol) was added and the reaction was heated for another day. After the reaction was finished, the precipitate

was filtered off and the solvents were then removed by rotary evaporation. The Residual crude product was dissolved in toluene (200 mL) and the resulting dispersion was filtered off. The resulting bright green solution was concentrated in vacuo and the crude product was purified by column chromatography (*n*-hexane/EtOAc, 50:50, R_f = 0.47) yielding 4.504 g (51 %).

Characterization:

(2S, 4R)-1-(tert-butoxycarbonyl)-4-hydroxypyrrolidine-2-carboxylic acid (1)
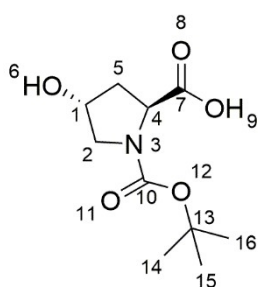
^{1}H-NMR (500 MHz, CDCl$_3$-*d*):

δ (ppm) = 1.41 (m, 9H, 14, 15, 16-CH$_3$); 2.10-2.28 (m, 1H, 5-CH$_2$); 2.35 (s, 1H, 5-CH$_2$); 3.55 (m, 2H, 2-CH$_2$); 4.40-4.48 (m, 2H, 1-CH, 4-CH)

^{13}C-NMR (125 MHz, CDCl$_3$-*d*):

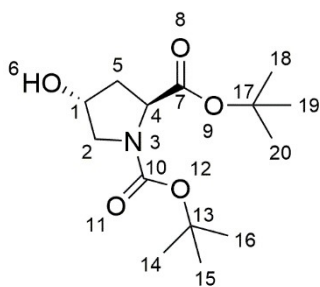δ (ppm) = 28.16 (14-16); 39.13 (5); 58.49 (2); 69.49 (4); 80.07 (1); 81.14 (13); 154.35 (10); 171.87 (7)

ESI-MS (m/z): $C_{10}H_{17}NO_5Na^+$ (mass found: 254.1013 Da, mass calc.: 254. 1004 Da)

Due to the proton exchange effect with solvents, the proton form OH- and COOH groups were not observed in the ^{1}H-NMR-spectrum.

Di-tert-butyl (2S, 4R)-4-hydroxypyrrolidine-1,2-dicarboxylate (2)
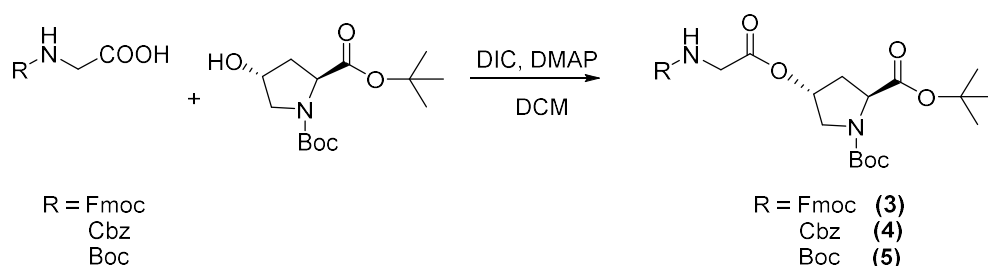

^{1}H-NMR (500 MHz, CDCl$_3$-d):

δ (ppm) = 1.45 (m, 18H, 14-20-CH$_3$); 1.86-2.28 (m, 2H, 5-CH$_2$); 3,36-3,67 (m, 2H, 2-CH$_2$); 4,26 (m, 1H, 1-CH); 4,46 (s, 1H, 4-CH)

^{13}C-NMR (125 MHz, CDCl$_3$-d):

δ (ppm) =28.08-28.45 (14-16, 18-20); 36.75 (5); 58.48 (2); 65.97 (4); 70.48 (1); 80.59 (17); 81.64 (13); 155.82 (10); 171.65 (7)

ESI-MS (m/z): C$_{14}$H$_{25}$NO$_5$Na$^+$ (mass found: 310.1638 Da, mass calc.: 310. 1630 Da)

Synthesis of L-proline derivatives with different protecting groups (3)-(5)

Protected L-proline was prepared by Steglich esterification described by B. Neises *et al*.[144]

Protected *trans*-4-hydroyl-L-proline (2) (1 g, 3.48 mmol), Cbz-glycine (0.728 g, 3.48 mmol), DIC (878 mg, 2 eq., 6.96 mmol) and a catalytic amount of *N*, *N*-dimethylaminopyridine (DMAP) were added to dichloromethane (30 mL) and the reaction mixture was stirred at room temperature overnight. Subsequently, the precipitate was filtered off and the solvents were then removed by rotary evaporation. The crude produce was purified by column
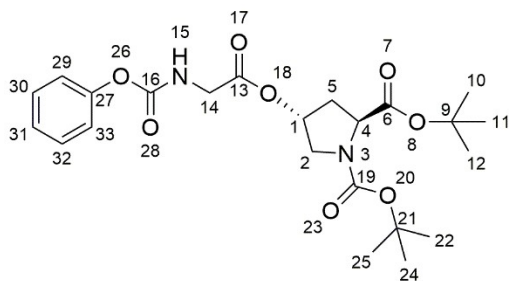
chromatography on silica (detail see in Table 3).

Table 3. Conversion of the protecting L-Proline derivates.

Entry	Protected group	Yield (g)	Conversion (%)	R_f
(3)	R = Fmoc	-	-	-
(4)	R = Cbz	1.93	84	0.31 (n-hexane/EtOAc, 70:30)
(5)	R = Boc	1.45	94	0.34 (n-hexane/EtOAc, 70:30)

Characterization:

<u>Di-tert-butyl (2S,4R)-4-((((benzyloxy)carbonyl)glycyl)oxy)pyrrolidine-1,2-dicarboxylate (4)</u>

^{1}H-NMR (500 MHz, CDCl$_3$-*d*):

δ (ppm) = 1.43 (m, 18H, 10-12, 22, 24, 25-CH$_3$); 2.01 - 2.28 (m, 2H, 5-CH$_2$); 3.33-3.65 (m, 2H, 2-CH$_2$); 3.83 (m, 2H, 14-CH$_2$); 4.20 (m, 1H, 4-CH); 5.30 (m, 1H, 1-CH); 7.34 (m, 5H, 29-33-CH)

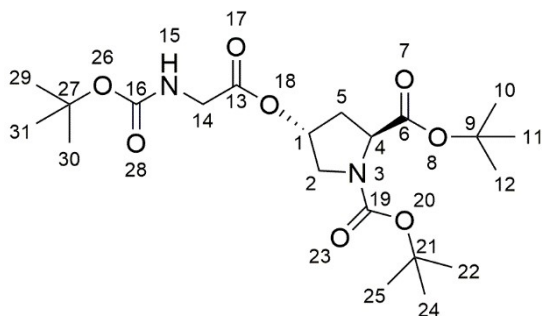**^{13}C-NMR (125 MHz, CDCl$_3$-*d*):**

δ (ppm) = 28.03 (10-12 and 22, 24, 25); 36.55 (5); 42.84 (14); 58.63 (2); 67.14 (4); 73.02 (1); 79.93 (21); 81.11 (9); 128.47 (arom.); 153.26 (27); 154.18 (16); 156.44 (19); 172.24 (6)

ESI-MS (m/z): $C_{24}H_{34}N_2O_8Na^+$ (mass found: 501.2216 Da, mass calc.: 501. 2213 Da)

The proton form NH- group was not observed in the ^{1}H-NMR-spectrum.

<u>Di-tert-butyl (2S,4R)-4-(((tert-butoxycarbonyl)glycyl)oxy)pyrrolidine-1,2-dicarboxylate (5)</u>

**^{1}H-NMR (500 MHz, CDCl$_3$-*d*):**

δ (ppm) =1.45 (m, 27H, 10-12, 22, 24, 25, 29-31-CH$_3$); 2.18 - 2.39 (m, 2H, 5-CH$_2$); 3.68 (m, 2H, 2-CH$_2$); 3.89 (m, 2H, 14-CH$_2$); 4.23 (m, 1H, 4-CH); 5.32 (m, 1H, 1-CH)

^{13}C-NMR (125 MHz, CDCl$_3$-*d*):

δ (ppm) = 28.08-28.45 (10-12 and 22, 24, 25, 29-31); 36.75 (5); 42.66 (14); 58.48 (2); 65.97 (4); 69.3 (1); 80.40 (21, 27); 81.64 (9); 153.94 (19); 155.54 (6); 170.95 (16), 171.5 (13)

ESI-MS (m/z): $C_{21}H_{36}N_2O_8Na^+$ (mass found: 467.2374 Da, mass calc.: 467. 2369 Da)

<u>Synthese von (2S, 4R)-4-(glycyloxy)pyrrolidine-2-carboxylic acid dihydrochloride (6)</u>
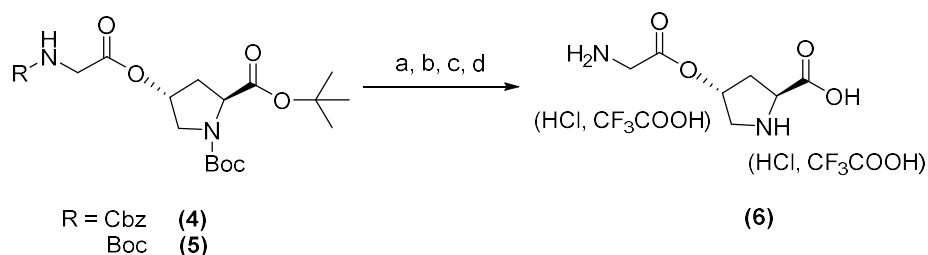
a. Deprotection of the benzyl carbamates group (Cbz) using Pd/C

Deprotection of the benzyloxycarbonyl group (Cbz) was carried out using the method described by P. K. Mandal *et al*.[145]

Compound 4 (0.433 g, 0. 90 mmol) and 50 mg Pd/C (10 %) were transformed to a 50-mL round bottom flask and mixed with MeOH (10 mL). Triethylsilan (10 eq., 1.43 mL, 9.0 mmol) was

added dropwise to the reaction mixture, thereby releasing CO_2 gas. The reaction mixture was stirred for 20 min at room temperature, the mixture was filtered off and the solvents were removed by rotary evaporation.

b. Deprotection of the benzyl carbamates group (Cbz) using HBr/HAc (33% wt)

Deprotection of the benzyloxycarbonyl group (Cbz) was prepared by the method described by D. Ben-Ishai *et al*. [146]

Compound 4 (0.669 g, 1.39 mmol) were transformed to a 50-mL round bottom flask under argon and mixed with diethyl ether (6 mL) at 0 °C. Hydrogen bromide solution (6 mL, 33 % wt in acetic acid) was added dropwise to the reaction mixture. With release of CO_2 gas, a white precipitate was observed. The reaction mixture was stirred for 20 min at room temperature, followed by filtration. The obtained solid was washed with diethyl ether and dried in vacuo.

c. Deprotection of the *tert*-butoxycarbonyl group (Boc) using TFA

Deprotection of the *tert*-butoxycarbonyl group was firstly deprotected with the presence of trifluoroacetic acid (TFA) was conducted according to literature.[147]

Compound 5 (0.5 g, 1.125 mmol) were transformed to a 50-mL round bottom flask under argon and mixed with chloroform (4 mL) at room temperature. TFA (2 mL) was added dropwise to the reaction mixture. With the release of CO_2 gas, the solution turns brown. The reaction mixture was stirred for 2 hours at room temperature. The resulting solution was concentrated in vacuo and the remaining product was observed as a brown viscous oil.

d. Deprotection of the *tert*-butoxycarbonyl group (Boc) using HCl/dioxane (4M)

Deprotection of the tert-butoxycarbonyl group (Boc) was carried out as described by G. Han et al.[148]

Compound 5 (0.5 g, 1.125 mmol) were transformed to a 50-mL round bottom flask under argon and mixed with $CHCl_3$ (5 mL) at room temperature. HCl/dioxane (5 mL, 4M in dioxane) was added dropwise to the reaction mixture. With release of CO_2 gas, a white precipitate was

observed. The reaction mixture was stirred overnight at room temperature. The white precipitate was filtered off and dissolved in methanol (10 mL). After drying in vacuo, the remaining crude was used directly for the next step without further purification.
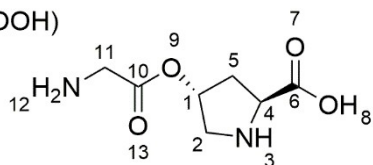
Table 4. Overview over deprotection mehtods for compounds 4 (R=Cbz) and 5 (R=Boc)

Method	Protective group	Deprotection reagent	Yied (g)	Conversion (%)
a	R = Cbz	Pd/C	-	-
b	R = Cbz	HBr/HAc (33 %wt)	-	-
c	R = Boc	TFA	0.092	26
d	R = Boc	HCl/dioxane	0.191	53

Characterization:

<u>(2S,4R)-4-(glycyloxy)pyrrolidine-2-carboxylic acid (6)</u>

^{1}H-NMR (500 MHz, DMSO-d_6):

δ (ppm) = 2.27-2.48 (m, 2H, 5-CH$_2$); 3.38 (dd, 2H, J = 4.4 Hz, 9.0 Hz, 2-CH$_2$); 3.8 (d, 2H, J = 5.7 Hz, 11-CH$_2$); 4.55 (dd, 1H, J = 7.7 Hz, 10.7 Hz, 4-CH); 5.43 (t, 1H, J = 4.3 Hz, 1-CH); 8.62 (b, 2H, 12-NH$_3$), 9.21 (b, 1H, 3-NH); 10.8 (b, 1H, 8-COOH)
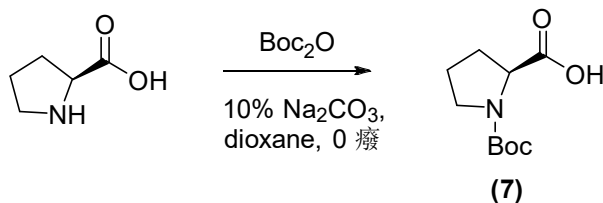
^{13}C-NMR (125 MHz, DMSO-d_6):

δ (ppm) = 34.33 (5); 50.45 (11); 57.68 (2); 66.62 (4); 74.48 (1); 166.33 (10); 169.96 (6)

ESI-MS (m/z): $C_7H_{14}ClN_2O_4^+$ (mass found: 224.0926 Da, mass calc.: 224. 0558 Da)

Synthesis of *N*-(*tert*-butoxycarbonyl)-L-proline (7)

The Boc protection of *L*-proline is analogous to the synthesis of (2S, 4R) -1- (*tert*-butoxycarbonyl) -4-hydroxypyrrolidine-2-carboxylic acid (1).

In a 250-mL flask with dropping funnel L-proline (5.0 g, 43, 4 mmol) was dissolved in 10 % aqueous solution of Na_2CO_3 (40 mL) at 0 °C. Di-*tert*-butyl dicarbonate (1.2 equiv., 11,37 g, 52,1 mmol) was dissolved in 1,4-dioxane (30 mL). This solution was slowly added to the reaction mixture, followed by stirring overnight at room temperature. After the reaction, the mixture was acidified to pH = 4 with saturated citric acid and the aqueous phase was extracted with ethyl acetate (3 × 200 mL and 5 × 100 mL). The collected organic phases were dried over $MgSO_4$ and the solvent was then removed by rotary evaporation. The crude product was observed as colorless viscous oil. 9.163 g (98 %)
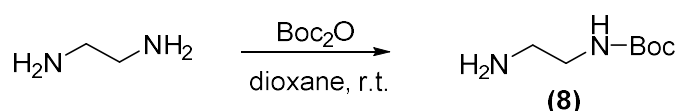
Characterization:
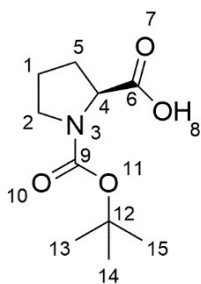
¹H-NMR (500 MHz, CDCl₃-*d*):

δ (ppm) = 1.48 (m, 9H, 13-15-CH₃); 1.88 (m, 2H,1-CH₂); 2.06 - 2.30 (m, 2H, 5-CH₂); 3.43 (m, 2H, 2-CH₂), 4.32 (m, 1H, 4-CH)

^{13}C-NMR (125 MHz, CDCl$_3$-*d*):

δ (ppm) = 24.46 (1); 28.82 (13-15); 30.99 (5); 47.21 (2); 59.38 (4); 81.80 (12); 157.05 (9); 174.45 (6).

ESI-MS (m/z): $C_7H_{12}N_2O_4H^+$ (mass found: 189.0878 Da, mass calc.: 189. 0831 Da)

Synthese von *tert*-butyl-*N*-(2-aminoethyl)-carbamat (8)

A 250 mL three-necked flask with drying tube and dropping funnel was charged with 1,2-diaminoethane (17 mL, 0.25 mol) and 1,4-dioxane (65 mL). A solution of di-*tert*-butyl decarbonate (7.35 g, 33.5 mol) in 1,4-dioxane (70 mL) was then added dropwise. The resulting white suspension was stirred for overnight at room temperature. The precipitate was filtered off and the solvents were then removed by rotary evaporation. The residual crude product was redispersed in deionized water (130 mL). After filtration, the aqueous phase was saturated with NaCl and extracted 5 times with dichloromethane (65 mL). The collected organic phases were dried over MgSO$_4$ and the solvent was removed under reduced pressure. The product was obtained as a light-yellow viscous oil. (3.426 g, 76 %)

Characterization:
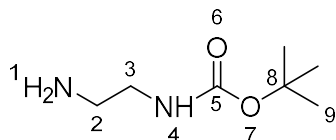
^{1}H-NMR (500 MHz, CDCl$_3$-*d*):

δ (ppm) = 1.29 (s, 9H, 9-CH$_3$); 1.38 (s, 2H, 1-NH$_2$); 2.64 (t, 2H, ^{3}J = 5.90 Hz, 2H, 2-CH$_2$); 3.01 (d, 2H, ^{3}J = 5.60 Hz, 3-CH$_2$); 5.31 (b, 1H, 4-NH)
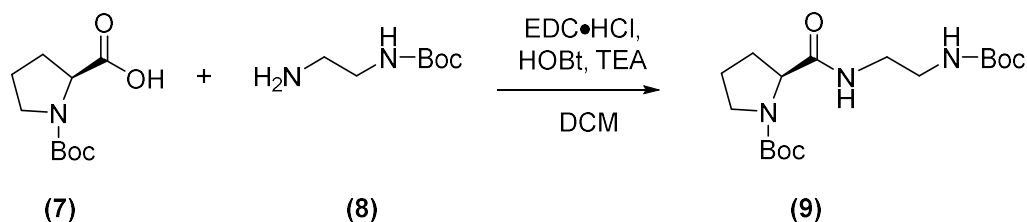
^{13}C-NMR (125 MHz, CDCl$_3$-*d*):

δ (ppm) = 28.27 (9); 41.91 (3), 43.24 (2), 78.82 (8), 156.26 (5)

## Synthesis of tert-butyl (S)-2-((2-((tert-butoxycarbonyl)amino)ethyl)carbamoyl) pyrrolidine-1-carboxylate (9)

(7)   (8)   (9)

The formation compound 9 was prepared by condensation of Boc-protected amine (8) with carboxylic acid (7) in the presence of *N*-(3-dimethylaminopropyl)-*N*'-ethylcarbodiimide hydrochloride (EDC·HCl) and 1-hydroxy-benzotriazole (HOBT).

N-Boc protected L-proline (7) (0.5 g, 2.32 mmol), EDC·HCl (0.479 mg, 1.07 eq., 2.5 mmol) and HOBt (0.355 mg, 2.32 mmol) were dissolved in dichloromethane (25 mL) and stirred for 10 min. After addition of triethylamine (1.8 eq., 0.58 mL, 4.18 mmol), *N*-Boc ethylenediamine (8) (0.372 g, 2.32 mmol) was added to the reaction mixture, followed by stirring at room temperature overnight. The solution was washed with water (50 mL), sat. NaHCO$_3$-solution (50 mL), sat. citric acid (50 mL) and brine (50 mL). The organic phase was dried over MgSO$_4$ and concentrated under reduced pressure yielding a solid product. (0.755 g, 91 %).

Characterization:
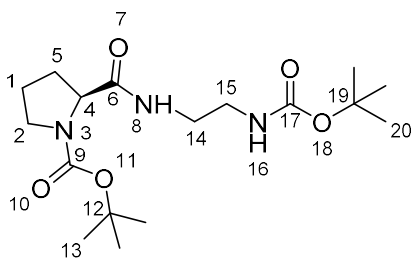
^{1}H-NMR (500 MHz, CDCl$_3$-*d*):

δ (ppm) = 1.43 – 1.46 (m, 18H, 13, 20-CH$_3$); 1.75-2.35 (b, 4H, 1, 5-CH$_2$); 3.15-3.55 (m, 6H, 2-
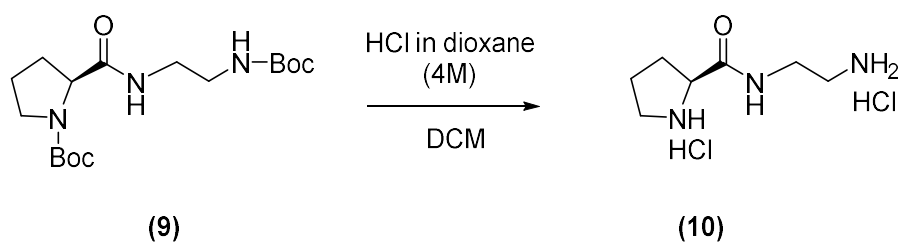
CH$_2$, 14-CH$_2$, 15-CH$_2$), 4.21 (s, 1H, 4-CH), 4.75-5.25 (b, 1H, 16-NH$_3$); 6,46-7,0 (b, 1H, 8-NH)

^{13}C-NMR (125 MHz, CDCl$_3$-*d*):

δ (ppm) = 23.65 (1); 28.4 (2, 13, 20); 29.7 (5); 40.2 (14); 42.4 (15); 60.5 (4); 80.0 (19); 80.6 (12); 156.0 (9); 156.6 (17); 172.8 (6)

**Synthesis of (S)-N-(2-aminoethyl) pyrrolidine-2-carboxamide dihydrochloride (10)**

(9)   (10)

The Boc group deprotection of compound 9 is analogous to the synthesis of compound 6 by the application of HCl/dioxane (4M).

Compound 9 (0.71 g, 1.6 mmol) were transformed to a 50-mL round bottom flask under argon and mixed with CHCl$_3$ (5 mL) at room temperature. HCl/dioxane (5 mL, 4M in dioxane) was added dropwise to the reaction mixture. With release of CO$_2$ gas, a white precipitate was observed. The reaction mixture was stirred overnight at room temperature. The white precipitate was filtered off and washed with cooled diethyl ether. After drying in vacuo, the remaining crude was used directly for the next step without further purification. (0.732 g, 57%)

Characterization:
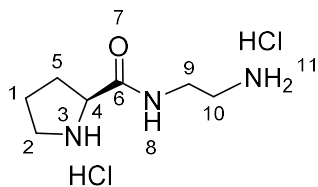
^{1}H-NMR (500 MHz, DMSO-*d$_6$*):

δ (ppm) = 1.89 (m, 3H, 1-CH$_2$, 5a-CH$_2$); 2.27 (m, 1H, 5b-CH$_2$); 2.91 (s, 2H, 10-CH$_2$); 3.19 (s, 2H, 9-CH$_2$); 3.45 (m, 1H, 2-CH$_2$); 4.17 (s, 1H, 4-CH); 8.27 (b, 2H, 11-NH$_3$); 8.61 (b, 1H, 8-NH), 9.05
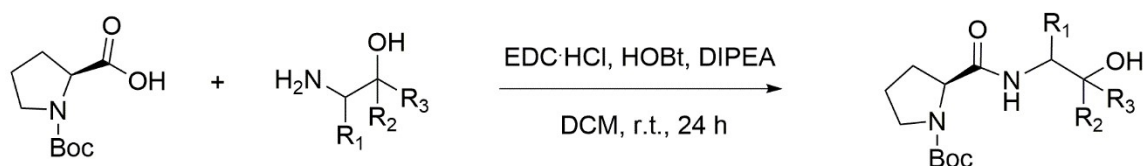
(b, 1H, 3-NH)

^{13}C-NMR (125 MHz, DMSO-d_6):

δ (ppm) = 23.69 (1); 29.27 (5); 37.0 (10); 37.8 (9); 45.53 (2); 59.07 (4); 168.6 (6)

ESI-MS (m/z): $C_7H_{15}N_3ONa^+$ (mass found: 180.1100 Da, mass cal. 180.1113 Da)

Synthesis of the prolinamide derivatives (16-20)

R$_1$= isobutyl, R$_2$,R$_3$= Phenyl (11)   R$_1$= isobutyl, R$_2$,R$_3$= Phenyl (16)
R$_1$= Phenyl, R$_2$,R$_3$= Phenyl (12)   R$_1$= Phenyl, R$_2$,R$_3$= Phenyl (17)
R$_1$= Phenyl, R$_2$,R$_3$= H (13)   R$_1$= Phenyl, R$_2$,R$_3$= H (18)
R$_1$= isopropyl, R$_2$,R$_3$= H (14)   R$_1$= isopropyl, R$_2$,R$_3$= H (19)
R$_1$= isobutyl, R$_2$,R$_3$= H (15)   R$_1$= isobutyl, R$_2$,R$_3$= H (20)

(7)

Synthesis of the prolinamide derivatives (16-20) using peptide coupling conditions is carried out analogously to the synthesis of compound 9.

N-Boc *L*-proline (7), EDC·HCl and HOBt were dissolved in dichloromethane (25 mL) and stirred for 10 min. After addition of DIPEA, alkanol amine was added to the reaction mixture, which was stirred at room temperature overnight. Afterwards, the reaction mixture was washed with water (50 mL), sat. NaHCO$_3$-solution (50 mL), sat. citric acid solution (50 mL) and brine (50 mL). The organic phase was dried over MgSO$_4$ and concentrated under reduced pressure. The crude product was purified by column chromatography.

3. Experimental section

Table 5. Synthesis results for compounds (16)-(20)

Entry	Product mass (g)	Yield (%)	Eluent for chromatography and R_f
(16)	1.03	63	-
(17)	2.25	65	-
(18)	4.28	71	EE, 0.41
(19)	0.86	62	-
(20)	3.43	78	EE/MeOH (10:1), 0.63

Characterization:

tert-butyl (S)-2-(((R)-1-hydroxy-4-methyl-1,1-diphenylpentan-2-yl)carbamoyl)pyrrolidine-1-carboxy- late (16)
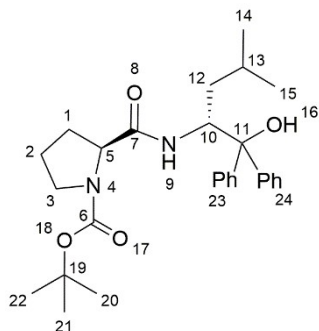
^{1}H-NMR (500 MHz, CDCl$_3$-_d_):

δ (ppm) = 0.89 (m, 6H, 14, 15-CH$_3$); 1.41 (m, 9H, 20-22-CH$_3$); 1.56 (b, 2H, 12-CH$_2$); 1.6-1.9 (m, 5H, 1, 2-CH$_2$, 13-CH); 3.16-3.37 (m, 2H, 3-CH$_2$); 4.07 (m, 1H, 10-CH); 4.7 (m, 1H, 5-CH); 7.1-7.6 (m, 10H, arom.)

^{13}C-NMR (125 MHz, CDCl$_3$-_d_):

δ (ppm) = 21.51 (14, 15); 24.08 (2); 25.05 (13); 28.44 (20-22); 38.0 (12); 47.02 (3); 56.3 (10); 81.03 (19); 125.7-128.5 (arom.); 145.27 (arom.); 156.3 (6); 173.1 (7).

tert-butyl (2S)-2-((2-hydroxy-1,2,2-triphenylethyl)carbamoyl)pyrrolidine-1-carboxylate (17)
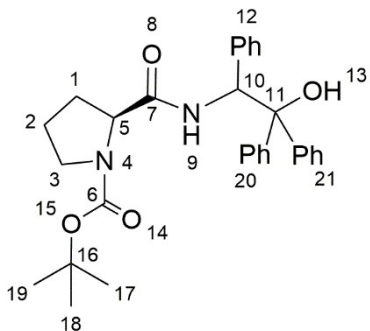
¹H-NMR (500 MHz, CDCl₃-_d_):

δ (ppm) = 1.44 (m, 9H, 17-19-CH₃); 1.5-2.3 (m, 4H, 1, 2-CH₂); 3.3-3.6 (m, 2H, 3-CH₂); 4.19 (m, 1H, 5-CH); 6.85 (m, 1H, 10-CH); 7.1-7.6 (m, 15H, arom. 10 and 11-CH)

¹³C-NMR (125 MHz, CDCl₃-_d_):

δ (ppm) = 23.89 (2); 28.34 (17-19); 30.94 (1); 46.24 (3); 59.30 (5); 72.56 (10); 79.70 (16); 89.21 (11); 125.9-128.3 (arom.); 142.67 (arom); 173.26 (7)

tert-butyl (2S)-2-((2-hydroxy-1-phenylethyl)carbamoyl)pyrrolidine-1-carboxylate (18)
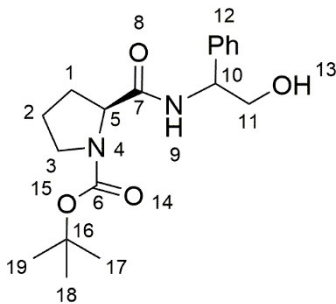
¹H-NMR (500 MHz, CDCl₃-_d_):

δ (ppm) = 1.46 (ms, 9H, 17-19-CH₃); 1.8-2.4 (m, 4H, 1, 2-CH₂); 3.27-3.54 (m, 2H, 3-CH₂); 4.33–4.18 (m, 1H, 5-CH); 3.76 (m, 2H, 11-CH₂); 5.07 (dt, J = 10.4 Hz, 5.31 Hz, 1H, 10-CH), 7.2-7.4 (m, 5H, arom. 10-CH)

¹³C-NMR (125 MHz, CDCl₃-_d_):

δ (ppm) = 23.63 (2); 28.48 (17-19); 29.1 (1); 47.34 (3); 56.40 (10);60.8 (5); 66.64 (11); 80.87

(16); 126.91, 128.89 and 138.99 (arom.); 153.2 (6); 173.4 (7)

tert-butyl (2S)-2-((1-hydroxy-3-methylbutan-2-yl)carbamoyl)pyrrolidine-1-carboxylate (19)
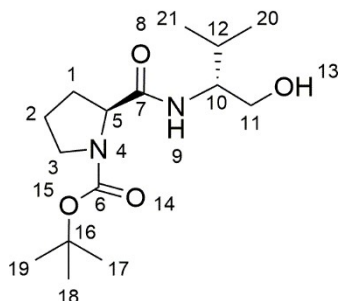
^{1}H-NMR (500 MHz, CDCl$_3$-*d*):

δ (ppm) = 0.94 (m, 6H, 20-21-CH$_3$); 1.45 (m, 9H, 17-19-CH$_3$); 1.7 -2.5 (m, 5H, 1-2-CH$_2$, 12-CH); 3.2-3.8 (m, 5H, 3, 11-CH$_2$, 10-CH); 4.0-4.4(m, 1H, 5-CH)

^{13}C-NMR (125 MHz, CDCl$_3$-*d*):

δ (ppm) = 18.6 (2); 19.7 (20, 21); 28.5 (17-19); 28.9 (1, 10, 12); 47.3 (3); 57.9 (9); 60.7 (7); 64.2 (11); 81.07 (16); 156.2 (6); 173.6 (7)

ESI-MS(m/z): $C_{15}H_{29}N_2O_4^+$, (mass found: 301.2772 Da, mass cal. 301.2122 Da)

tert-butyl (S)-2-(((R)-1-hydroxy-4-methylpentan-2-yl)carbamoyl)pyrrolidine-1-carboxylate (20)
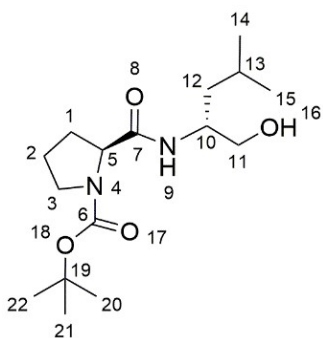
^{1}H-NMR (500 MHz, CDCl$_3$-*d*):

δ (ppm) = 0.91 (m, 6H, 14, 15-CH$_3$); 1.29-1.40 (m, 2H, 12-CH$_2$); 1.47 (m, 9H, 20-22-CH$_3$); 1.58

(m, 1H, 13-CH); 1.72-2.53 (m, 4H, 1 and 2-CH$_2$); 3.45 (m, 3H, 3-CH$_2$, 11a-CH), 3.68 (m, 1H, 11b-CH); 4.00 (b, 1H, 10-CH); 4.27 (b, 1H, 5-CH)

^{13}C-NMR (125 MHz, CDCl$_3$-*d*):

δ (ppm) = 22.13(14, 15), 23.23(13), 25.04 (2), 28.32 (20-22), 29.4 (1); 40.15 (12), 47.32 (3), 50.59 (10), 60.62 (11), 66.49 (5), 80.92 (19), 156.31 (6), 173.12 (7)

ESI-MS(m/z): C$_{16}$H$_{30}$N$_2$ONa$^+$ (mass found: 337.2114 Da, mass cal. 337.2103 Da)

<u>Synthesis of prolinamide-derivate (21)-(25)</u>
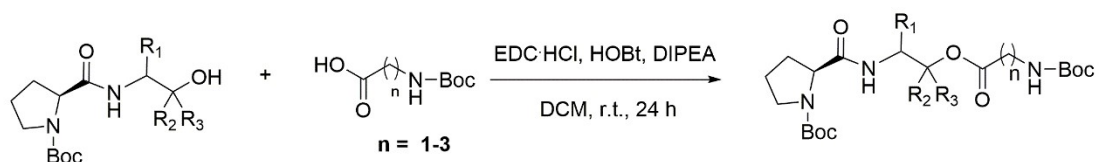
R$_1$= isobutyl, R$_2$,R$_3$= Phenyl (16)
R$_1$= Phenyl, R$_2$,R$_3$= Phenyl (17)
R$_1$= Phenyl, R$_2$,R$_3$= H (18)
R$_1$= isopropyl, R$_2$,R$_3$= H (19)
R$_1$= isobutyl, R$_2$,R$_3$= H (20)

R$_1$= isobutyl, R$_2$,R$_3$= Phenyl, n=3, (21)
R$_1$= Phenyl, R$_2$,R$_3$= Phenyl, n=3 (22)
R$_1$= Phenyl, R$_2$,R$_3$= H, n=3 (23)
R$_1$= isopropyl, R$_2$,R$_3$= H, n=3 (24)
R$_1$= isobutyl, R$_2$,R$_3$= H, n=1 (25)

Chain-extended prolinamide derivatives 21-25 were synthesized analogously to the synthesis of prolinamide derivates 16-20.

N-Boc protected L-proline (7), EDC·HCl and HOBt were dissolved in dichloromethane (25 mL) and stirred for 10 min. After addition of DIPEA, the Boc-protected amino acid was added to the reaction mixture, which was stirred at room temperature overnight. Subsequently, the reaction mixture was washed with water (50 mL), sat. NaHCO$_3$-solution (50 mL), sat. citric acid solution (50 mL) and brine (50 mL). The organic phase was dried over MgSO$_4$. Concentrated under reduced pressure. The crude product was purified by column chromatography.

3. Experimental section

Table 6. Synthesis results for compounds (21)-(25).

Entry	Product mass (g)	Yield (%)	Eluent for chromatograph and R_f
(21)	-	-	-
(22)	-	-	-
(23)	-		-
(24)	1.15	90	EE/hexane (1:1), 0.41
(25)	4.51	89	EE/hexane (1:1), 0.51

Characterization:

tert-butyl (2S)-2-((1-((4-((tert-butoxycarbonyl)amino)butanoyl)oxy)-3-methylbutan-2-yl) carbamoyl) pyrrolidine-1-carboxylate (24)
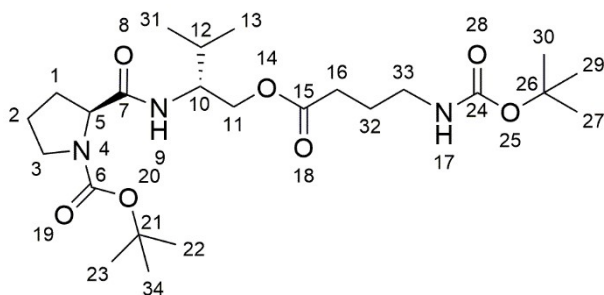
^{1}H-NMR (500 MHz, CDCl$_3$-_d_):

δ (ppm) = 0.88 (m, 6H, 13, 31-CH$_3$); 1.44 (m, 18H, 22, 23, 34, 27, 29, 30-CH$_3$); 1.65-1.96 (m, 6H, 1, 2, 32-CH$_2$); 2.33 (m, 2H, 16-CH$_2$); 3.15 (m, 2H, 33-CH$_2$); 3.41 (b, 2H, 3-CH$_2$); 3.9-4.3 (m, 4H, 5-CH, 10-CH, 11-CH$_2$)

^{13}C-NMR (125 MHz, CDCl$_3$-_d_):

δ (ppm) = 19.54 (13); 25.32 (2); 28.56 (22, 23, 34, 27, 29, 30); 29.55 (1); 29.82 (12); 31.36 (16); 39.84 (33); 47.30 (3); 60.58 (10); 64.86 (11); 80.60 (21, 26); 156.20 (6); 173.16 (7)

ESI-MS (m/z): C$_{23}$H$_{41}$N$_3$O$_7$Na$^+$ (mass found: 494.2853 Da, mass cal. 494.2842 Da)

tert-butyl (S)-2-(((R)-1-(((tert-butoxycarbonyl)glycyl)oxy)-4-methylpentan-2-yl) carbamoyl) pyrrolidine-1-carboxylate (25)
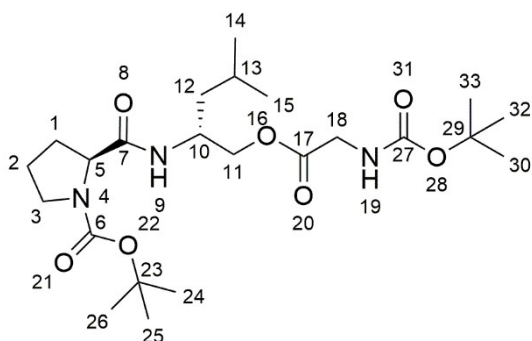
^{1}H-NMR (500 MHz, CDCl$_3$-*d*):

δ (ppm) = 0.90 (m, 6H*, * 14, 15-CH$_3$); 1.42 – 1.28 (m, 2H, 12-CH$_2$); 1.46 (d, 18H, 24-26, 30, 32, 33-CH$_3$); 1.88-2,50 (m, 4H, 1, 2-CH$_2$); 3.39 (b, 2H, 3-CH$_2$); 3.91 (s, 2H, 18-CH$_2$); 4.01 – 4.15 (m, 1 H, 10-CH); 4.18 (m, 1H, 12a-CH$_2$); 4.24 (b, 2H, 5-CH, 12b-CH$_2$)

^{13}C-NMR (125 MHz, CDCl$_3$-*d*):

δ (ppm) = 22.3 (14, 15); 23.4 (13); 25.2 (32); 28.7 (24-26, 30, 32, 33); 29.4 (1); 40.6 (12); 42.7 (18); 46.75 (10); 47.5 (3); 66.49 (5), 67.4 (11); 80.6 (21, 26); 153.4 (23, 29); 156.2 (27); 170.8 (7)

ESI-MS (m/z): C$_{23}$H$_{41}$N$_3$O$_7$Na$^+$ (mass found: 494.2853 Da, mass cal. 494.2842 Da)

Deprotection of the chain-extended Prolinamide derivatives (27)
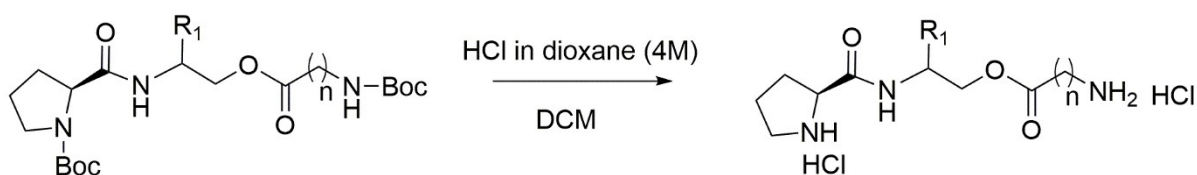
R$_1$= isopropyl, R$_2$,R$_3$= H, n = 3, (24)
R$_1$= isobutyl, R$_2$,R$_3$= H, n = 1, (25)

R$_1$= isopropyl, R$_2$,R$_3$= H, n = 3, (26)
R$_1$= isobutyl, R$_2$,R$_3$= H, n = 1, (27)

The Boc group deprotection of compound (24) and (25) was carried out analogously to the synthesis of compound (6) using HCl/dioxane (4M).

Compound 25 (1.4 g, 2.97 mmol) were transformed to a 50-mL round bottom flask under argon

and mixed with $CHCl_3$ (9 mL) at room temperature. HCl/dioxane (9 mL, 4M in dioxane) was added dropwise to the reaction mixture. With release of CO_2 gas, a white precipitate was observed. The reaction mixture was stirred overnight at room temperature. The white precipitate was filtered off and washed with cooled diethyl ether. After drying in vacuo, the remaining crude was used directly for the next step without further purification.

Table 7. Synthesis results for compounds (21)-(25)

Entry	Product mass (g)	yield (%)
(26)	-	-
(27)	0.99	97

Characterization:

(R)-4-methyl-2-((S)-pyrrolidine-2-carboxamido) pentyl glycinate dihydrochloride (27)
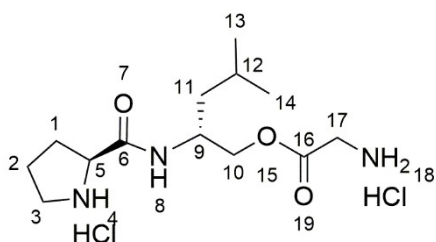
^{1}H-NMR-Spektrum (500 MHz, DMSO-d_6):

δ (ppm) = 0.83 (m, 6H, 13, 14-CH_3); 1.31-1.51 (m, 2H, 11-CH_2); 1.61 (m, 1H, 12-CH); 1.7-2.32 (m, 4H, 2-CH_2, 1-CH_2); 3.1-3.27 (m, 2H, 3-CH_2); 3.3-3.5 (b, 1H, 5-CH_2); 3.78 (b, 2H, 17-CH_2); 3.9-4.3 (m, 3H, 9-CH, 10-CH_2)

^{13}C-NMR (125 MHz, DMSO-d_6):

δ (ppm)= 23.10 (13, 14); 23.65 (12); 24.18 (2); 30.04 (1); 4.13 (7); 45.64 (3); 49.67 (9); 63.57 (5); 66.96 (10); 167.34 (16); 168.07 (6)

ESI-MS (m/z): $C_{13}H_{26}N_3O_3^+$ (mass found: 272.1995 Da, mass cal. 272.1974 Da)

3.3.2 Synthesis of RAFT chain transfer agents

Synthesis of 2-(Dodecylthiocarbonothioylthio)-2-methylpropionic acid (DMP) (28)

The RAFT agent 2-(Dodecylthiocarbonothioylthio)-2-methylpropionic acid (DMP) was synthesized according to a literature procedure from Lai et. al..[149]
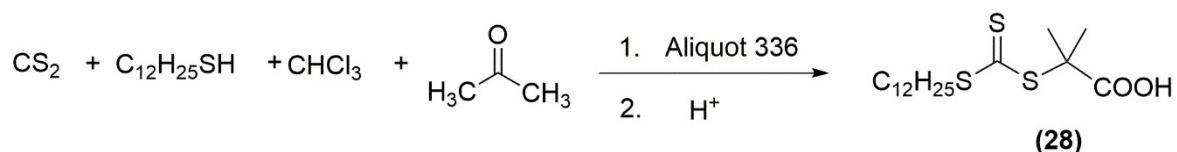
Under an nitrogen atmosphere 1-dodecanethiol (4.8 mL, 20 mmol), acetone (12.11 mL) and aliquat 336 (tricaprylylmethylammonium chloride) (0.37 mL, 0.80 mmol) were mixed in a 100-mL Schlenk flask and cooled to 10 °C. Sodium hydroxide solution (1.1 mL, 50 wt%) was slowly added dropwise over 20 minutes, a white solid precipitated and the suspension was stirred for additional 15 minutes under ice cooling before a solution of carbon disulfide (1.2 mL, 0.02 mol) in acetone (2.52 mL) was added dropwise over 20 minutes. A white precipitate dissolved and the color of the reaction mixture turned red. After stirring for 10 minutes under ice cooling, 2.4 mL of chloroform was added in one portion and finally a further of the 50 wt% sodium hydroxide solution (5.25 mL) were added dropwise over 30 minutes. The ice bath was removed and the reaction mixture was stirred overnight at room temperature. Water (30 mL) and of conc. HCl (5 mL) were slowly added to acidify the reaction mixture. The mixture was purged with nitrogen to help to evaporate the remaining acetone. The yellow precipitate was filtered and dissolved in 2-propanol (50 mL). The insoluble by-product was removed by filtration and the solvents were removed under reduced pressure. The crude product was recrystallized from *n*-hexane. (3.16 g, 8.6 mmol, 43%)

Characterization:
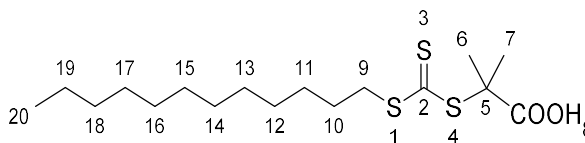
^{1}H-NMR-Spektrum (500 MHz, CDCl$_3$-*d*):

δ (ppm) = 0.88 (t; 3H; J = 7.0 Hz, 20-CH$_3$), 1.25-1.38 (m; 18H; 11-19-CH$_2$), 1.67 (m; 2H; 10-CH$_2$), 1.72 (s; 6H; 6, 7-CH$_3$), 3.28 (t; 2H; 9-CH$_2$)

^{13}C-NMR-Spektrum (125 MHz, CDCl$_3$-*d*):

δ (ppm) = 14.1 (20), 22.7 (19), 25.2 (6,7), 27.8 – 29.6 (10-18), 31.91 (10), 37.1 (9), 55.6 (5), 178.4 (8)

Synthesis of 4-cyano-4-(((dodecylthio)carbonothioyl)thio)pentanoic acid (31) and 2-cyano-2-propyl dodecyl trithiocarbonate (32)
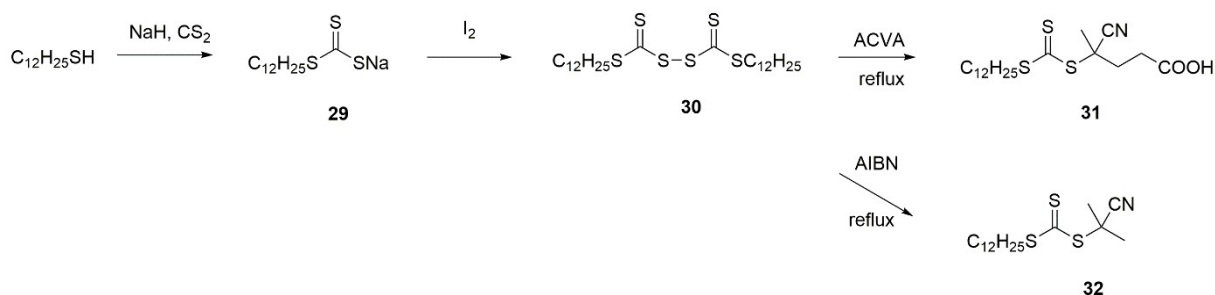
The RAFT agents 4-cyano-4-(((dodecylthio)carbonothioyl)thio)pentanoic acid (31) and 2-cyano-2-propyl dodecyl trithiocarbonate were synthesized according to literature. [150,84]

In a stirred suspension of sodium hydride (60% in oil, 3.15 g, 79 mmol) in diethyl ether (150 mL) with ice bath, 1-dodecylthiol (15.4 g, 76 mmol) was added slowly. The reaction mixture was stirred at 0 °C for one hour, thereby observing the release of hydrogen. After the addition of carbon disulfide (6.0 g, 79 mmol) a thick yellow precipitate of sodium S-dodecyltrithiocarbonate (**29**) was obtained. The crude product was collected by filtration used in the next step without purification.

Iodine (6.3 g, 25 mmol) was added stepwise wise to a suspension of sodium dodecyl

trithiocarbonate (14.6 g, 49 mmol) in diethyl ether (100 mL). The resultant mixture was then stirred at room temperature for 1 h. Afterwards the white sodium iodide precipitate was removed by filtration. The yellow-brown filtrate was washed with conc. aqueous sodium thiosulfate, to remove excess iodine. The organic phase was dried over sodium sulfate. Subsequently, the solvent was removed under reduced pressure, yielding 12.6 g crude product (**30**). (22.8 mmol, 93 %)

As solution of 4,4′-azobis(4-cyanovaleric acid) (ACVA) (4.20 g, 15 mmol) and bis-(dodecylsulfanylthiocarbonyl) disulfide (**30**) (5.54 g, 10 mmol) in ethyl acetate (100 mL) was heated at reflux for 18 h. After removal of the volatiles under reduced pressure, the crude product was washed with water (6*200 mL). Afterwards, recrystallizing from *n*-hexane 4-cyano-4-(dodecylsulfanyl-thiocarbonyl)sulfanyl pentanoic acid (**31**) as a pale yellow solid (6.96 g, 8.3 mmol, 83 %).

For the synthesis of 4-cyano-4-(((dodecylthio)carbonothioyl)thio)pentanoic acid (**32**), a solution of AIBN (1.0 g, 0.006 mol) and bis(dodecylsulfanylthiocarbonyl) disulfide (2.2 g, 0.004 mol) in ethyl acetate (25 mL) was heated to reflux for 18 h. After the reaction, the solvent was removed under reduced pressure and *n*-hexane was added to precipitate the unreacted AIBN and tetramethylsuccinodinitrile. The crude product was purified by column chromatography with *n*-hexane/ethyl acetate (95/5) as eluent. Produce 2-cyanopropan-2-yl dodecyl trithiocarbonate (**32**) was obtained as a pale-yellow oil (1.65 g, 60 % yield), which solidified when stored in the freezer (-15 °C) but remelted at room temperature.

Characterization:

Sodium Dodecylcarbonotrithioate (29)
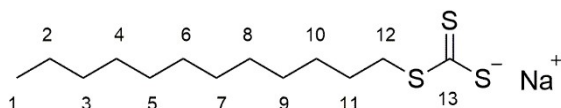
^{1}H-NMR-Spektrum (500 MHz, DMSO-d_6):

δ (ppm) = 0.85 (t; 3H; J = 7.0 Hz; 1-CH₃); 1.17-1.35 (m; 18H; 2-10-CH₂); 1.50 (m; 2H; 11-CH₂);

2.98 (m; 2H; 12-CH_2)

^{13}C-NMR-Spektrum (125 MHz, DMSO-d_6):

δ (ppm) = 14.1 (1); 22.27 (2); 28.7 – 29.1 (3-10); 31.3 (11), 39.1 (12)

Bis(dodecylsulfanylthiocarbonyl) disulfide (30)
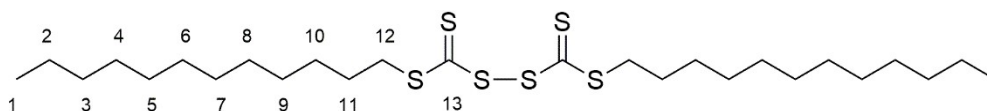
^{1}H-NMR-Spektrum (500 MHz, CDCl$_3$-d):

δ (ppm) = 0.88 (t; 6H; J = 7.0 Hz; 1-CH_3); 1.20-1.33 (s; 32H; 2-9-CH_2);1.40 (m; 4H; 10-CH_2); 1,70 (m; 4H; 11-CH_2); 3.30 (m; 4H; 12-CH_2).

^{13}C-NMR-Spektrum (125 MHz, CDCl$_3$-d):

δ (ppm) = 13.9 (1); 22.5(2); 27.2 – 29.5 (3-10); 31.8 (11); 38.2-39.6 (12).

4-cyano-4-(((dodecylthio)carbonothioyl) thio)pentanoic acid (31)
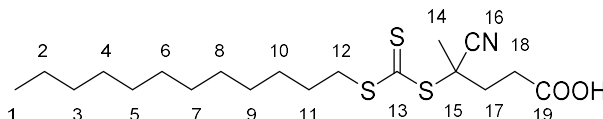
^{1}H-NMR-Spektrum (500 MHz, CDCl$_3$-d):

δ (ppm) = 0.88 (t; 6H; J = 7.0 Hz; 1-CH_3); 1.20-1.33 (s; 16H; 2-9-CH_2); 1.35 -1.44 (m; 2H; 10-CH_2); 1.70 (dt; 2H; J= 7.4 Hz, J=15.0 Hz; 11-CH_2); 1.89 (s; 3H; 14-CH_3); 2.47 (m; 1H, 18a-CH_2); 2.54 (m; 1H, 18b-CH_2); 2.50 (m; 2H; 17-CH_2); 3.30 (m; 2H; 12-CH_2)

^{13}C-NMR-Spektrum (125 MHz, CDCl$_3$-d):

δ (ppm) = 14.5 (1); 23.08 (14); 28.0 (2); 27.2 – 30.0 (3-10, 18); 32.3 (11, 17); 34.0 (12); 37.5 (15); 119.3 (16); 176.0 (19); 217.2 (13)

4-(((dodecylthio)carbonothioyl)thio)-4-methylpentanoic acid (32)
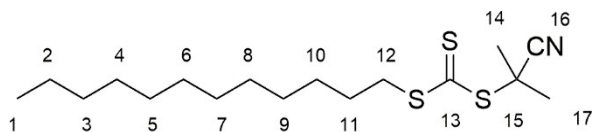
^{1}H-NMR-Spektrum (500 MHz, CDCl$_3$-*d*):

δ (ppm) = 0.88 (t; 6H; J = 7.0 Hz; 1-CH$_3$); 1.21-1.35(s; 16H; 2-9-CH$_2$); 1.39 (m; 2H; 10-CH$_2$); 1,70 (m; 2H; 11-CH$_2$); 1.89 (s; 3H; 14, 17-CH$_3$); 3.33 (m; 2H; 12-CH$_2$)

^{13}C-NMR-Spektrum (125 MHz, CDCl$_3$-*d*):

δ (ppm) = 14.5 (1); 23.08 (14); 27.5 (2); 28.1 – 30.0 (3-10); 34.0 (12); 32.3 (11, 17); 37.3 (15); 120.8 (16); 217.2 (13)

3.3.3 Monomer synthesis

Synthesis of (2,2-dimethyl-1,3-dioxolan-4-yl)methyl acrylate (SKA) (33)

The synthesis of 2,2-dimethyl-1,3-dioxolan-4-yl-methyl acrylate (solketal acrylate) was carried out by a two-stage reaction. In the first step, isopropylidene glycerol was prepared by the reaction of glycerol with acetone, and the resulting isopropylidene glycerol reacts further with acryloyl chloride.[151,152]
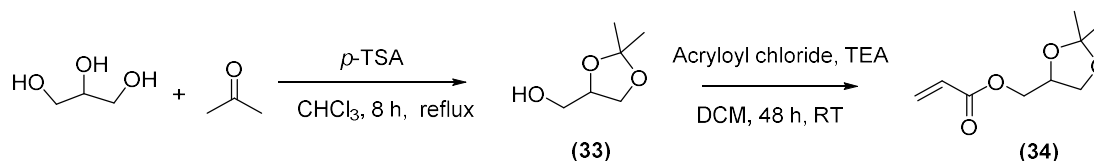
To a mixture of acetone (60 g, 1.03 mol) and glycerol (50 g, 0.54 mol) in chloroform (160 mL) *p*-toluenesulfonic acid monohydrate (2.28 g, 12 mmol) was added under stirring. The reaction mixture was refluxed for 8 h using a water separator. About 9 mL of water could be collected during the reaction. After cooling to room temperature, sodium carbonate was added to the reaction mixture, was subsequently stirred overnight at room temperature. After filtration of

the precipitate, the solvent was under reduced pressure to obtain 69.93 g isopropylidene glycerol (**33**) as viscous liquid (98%).

To a 1-L three-necked flask with dropping funnel was set under a nitrogen atmosphere. Afterwards 60 g (0.47 mol) of isopropylidene glycerol were added to a solution of triethylamine (65 mL, 0.47 mol) in dichloromethane (550 mL) and the mixture was cooled to 0 °C. (34 mL, 0.42 mol) of acryloyl chloride dissolved in dichloromethane (90 mL) were added dropwise to the reaction mixture within 30 minutes. The reaction mixture was stirred at room temperature for 48 hours. The precipitate was filtered and the solution was washed three times with distilled water (100 mL for each). The organic phase was dried over magnesium sulfate. Afterwards, dichloromethane was evaporated under reduced pressure. The product (**34**), was obtained as colorless liquid after distillation under fine vacuum. (61 °C at 0.035 mbar, 73.5 g, 0.4 mol, 87 %)

Characterization:

Isopropylidene glycerol (33)
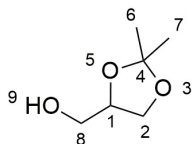
^{1}H-NMR (500 MHz, CDCl$_3$-*d*):

δ (ppm) = 1.36 (s, 3H, 6-CH$_3$); 1.42 (s , 3H, 7-CH$_3$); 2.11 (s, 1H, 9-OH); 3.58 (m, 1H, 8a-CH$_2$,); 3.71 (dd, H$_{8a}$, J$_{8a-8b}$ = 11.6 Hz, J$_{8a-1}$ = 4,0 Hz, 1H, 8b-CH$_2$); 3.77 (dd, H$_{2a}$, J$_{2a-2b}$ = 8.2 Hz, J$_{2a-1}$ = 6.5 Hz, 1H, 2a-CH$_2$,); 4.02 (dd, *H$_{2b}$*, J$_{2b-2a}$ = 8.2 Hz, J$_{2b-1}$ = 6.6 Hz, 1H, 2b-CH$_2$); 4.22 (m, 1H, 1-CH)

^{13}C-NMR (125 MHz, CDCl$_3$-*d*):

δ (ppm) = 25.22 (6); 26.64 (7); 62.99 (8); 65.78 (2); 77.33 (1); 109.35 (4)

3. Experimental section

(2,2-dimethyl-1,3-dioxolan-4-yl) methyl acrylate (SKA) (34)
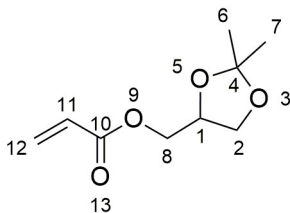
^{1}H-NMR-Spektrum (500 MHz, CDCl$_3$-*d*):

δ (ppm) = 1.36 (s, 3H, 6-CH$_3$); 1.42 (s, 3H, 7-CH$_3$); 3.76 (dd, H$_{8a}$, J$_{8a-8b}$ = 11.6 Hz, J$_{8a-1}$ = 4.0 Hz, 1H, 8b-CH$_2$); 4.08 (dd, H$_{8b}$, J$_{8a-8b}$ = 8.5 Hz, J$_{8b-1}$ = 6.5 Hz, 1H, 8b-CH$_2$); 4.18 (d, H$_{2a}$, J$_{2a-1}$ = 5.8 Hz, 1H, 2a-CH$_2$); 4.23 (d, H$_{2b}$, J$_{2b-1}$ = 4.7 Hz, 1H, 2b-CH$_2$); 4.30-4.40 (m, 1H, 1-CH); 5.85 (dd, H$_{trans}$, J$_{trans-gem}$ = 10.5 Hz, J$_{trans-cis}$ = 1.3 Hz, 1H, 12-CH$_2$); 6.14 (dd, H$_{gem}$, J$_{gem-cis}$ = 17.3 Hz, J$_{gem-trans}$ = 10.4 Hz, 1H, 11-CH); 6.43 (dd, 1H, J$_{gem-cis}$ = 17.3 Hz, J$_{trans-cis}$ = 1.3 Hz, 12-CH$_2$)

^{13}C-NMR-Spektrum (125 MHz, CDCl$_3$-*d*):

δ (ppm) = 25.24 (6); 26.67 (7); 64.76 (2); 65.72 (8); 66.36 (2); 73.62 (1); 109.86 (4); 127.99 (11); 131.31 (12); 165.87 (10)

Synthesis of 2,3-dihydroxypropyl acrylate (35)
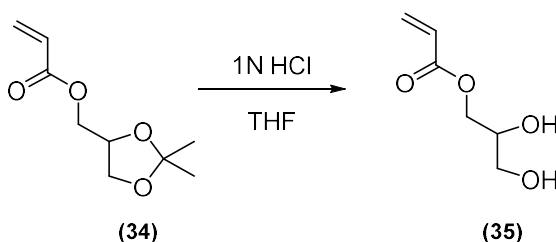
The hydrolysis of (2,2-dimethyl-1,3-dioxolan-4-yl) methyl acrylate (SKA) to 2,3-dihydroxypropyl acrylate (DHPA) was carried out using of HCl as catalyst.

In a 50-mL round-bottom flask SKA (4.312 g, 23 mmol) and 5 mg hydroquinone were dissolved in THF (10 mL). HCl solution (10 mL, 1N) was then slowly dropped into reaction mixture and stirred continuously at room temperature. TLC was used to detect the conversion of the reactants (ethyl acetate as eluent, R$_f$ = 0.38). The resulting clear solution was concentrated

under reduced pressure and the remaining liquid was extracted with ethyl acetate (3×30 mL). The combined organic phases were dried over $MgSO_4$ and the solvent was removed under reduced pressure to give the product (**35**) as a colorless liquid. (2.32 g, 15.87 mmol, 69 %)

Characterization:
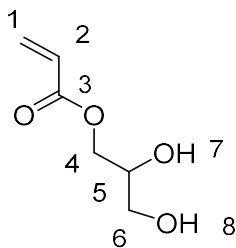
^{1}H-NMR-Spektrum (500 MHz, DMSO-d_6):

δ (ppm) = 3.38 (m, 2H, 6-CH$_2$); 3.76 (m, 1H, 5-CH); 4.02 (ddd, J = 13.5 Hz, J = 7.6 Hz, J = 4.3 Hz, 1H, 4b-CH$_2$); 4.15 (dd, J = 11.2 Hz, J = 4.1 Hz, 1H, 4a-CH$_2$); 4.63 (t, J = 5.7 Hz, 1H, 8-OH); 4.9 (d, J = 5.3 Hz, 1H, 7-OH); 5.85 (dd, H$_{trans}$, J$_{trans-gem}$ = 10.5, J$_{trans-cis}$ = 1.3 Hz, 1H, 1-CH$_2$); 6.14 (dd, H$_{gem}$, J$_{gem-cis}$ = 17.3 Hz, J$_{gem-trans}$ = 10.4 Hz, 1H, 2-CH); 6.43 (dd, 1H, J$_{gem-cis}$ = 17.3 Hz, J$_{trans-cis}$ = 1.3 Hz, 1-CH$_2$); 5.78 - 6.03 (m, 1H, 1a-CH$_2$); 6.15 - 6.23 (m, 1H, 2-CH); 6.28 – 6.40 (m, 1H, 1b-CH$_2$)

^{13}C-NMR-Spektrum (125 MHz, DMSO-d_6):

δ (ppm) = 60.19 (6); 66.35 (4); 69.75 (5); 128.52 (2); 131.78 (1); 166.01 (3)

Synthesis of 2-vinyl-4,4-dimethylazlacton (VDM) (37)

The synthesis of VDM involves a two-step reaction. *N*-acryloyl-2-methylalanine is first obtained by reaction of acrylic acid chloride with 2-methylalanine. The ring closure reaction is then followed by the presence of ethyl chloroformate and triethylamine.[120]

(36)   (37)

58
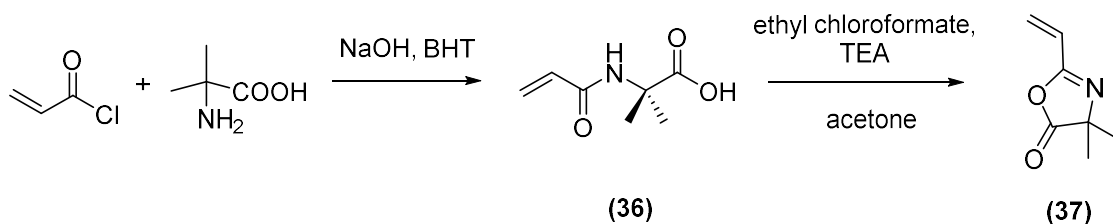
A solution of sodium hydroxide (1.77 g, 44.2 mmol) in water (4.4 mL) was cooled to 0 °C. 2-methylalanine (2 g, 19.4 mmol) and 2,6-di-*tert*-butyl-*p*-cresol (BHT) (2 mg, 9.07 × 10^{-3} mmol) were then slowly added. After complete dissolution, acryloyl chloride (2 g, 22.1 mmol) were added dropwise, and the reaction mixture was then stirred at 0 °C for 3 hours. A white precipitate was observed after addition of concentrated hydrochloric acid (2.3 mL). The solid was collected by filtration and recrystallized from a mixture of ethanol/water (v/v = 1/1). After drying under a fine vacuum, 1.25 g of product was obtained as a white crystalline solid (**36**) (7.89 mmol, 40.7 %).

N-acryloyl-2-methylalanine (0.4 g, 2.54 mmol) and triethylamine (0.38 g, 3.75 mmol) were dissolved in acetone (10 mL). The reaction mixture was then cooled to 0 °C and ethyl chloroformate (0.28 g, 2.5 mmol) was added. The reaction mixture was stirred at 0 °C for 3 hours. The solution was filtered off and the white precipitate was washed with acetone. The solvent of the filtrate was removed under reduced pressure and the residue was distilled under fine vacuum. A colorless liquid was obtained as a product (**37**) (0.22 g, 1.62 mmol, 64 %).

Characterization:

__N-Acryloyl-2-methylalanin (36)__
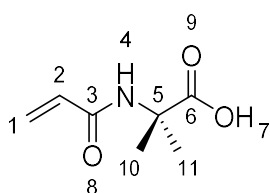
^{1}H-NMR-Spektrum (500 MHz, DMSO-d_6):

δ (ppm) = 1.36 (s, 6H, 10, 11-CH$_3$); 5.57 (dd, H$_{trans}$, J$_{trans-gem}$ = 10.2 Hz, J$_{trans-cis}$ = 2,2 Hz, 1H, 1-CH$_2$); 6.06 (dd, H$_{cis}$, J$_{cis-gem}$ = 17.1 Hz, J$_{cis-trans}$ = 2.2 Hz, 1H, 1-CH$_2$); 6.25 (dd, H$_{gem}$, J$_{gem-trans}$ = 10.2 Hz, J$_{gem-cis}$ = 17.1 Hz, 1H, 2-CH); 8.29 (s, 1 H, 4-NH); 12.20 (s, 1 H, 7-COOH).

^{13}C-NMR-Spektrum (125 MHz, DMSO-d_6):

δ (ppm) = 25.02(10, 11); 55.03 (5); 125.28 (1), 131,77 (2), 163.93 (3); 175.38 (6)

2-Vinyl-4, 4-dimethylazlacton (VDMA) (37)
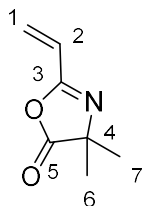
^{1}H-NMR -Spektrum (500 MHz, CDCl$_3$-*d*)

δ (ppm) = 1.45 (d, J = 2.2 Hz, 6H, 6, 7-CH$_3$); 5.92 (dd, H$_{trans}$, J$_{trans\text{-}gem}$ = 10.2, J$_{trans\text{-}cis}$ = 1.7 Hz, 1H, 1- CH$_2$); 6.22 (dd, H$_{cis}$, J$_{cis\text{-}gem}$ = 17.6 Hz, J$_{cis\text{-}trans}$ = 1.7 Hz, 1H, 1-CH$_2$); 6.28 (dd, H$_{gem}$, J$_{gem\text{-}cis}$ = 17.6 Hz, J$_{gem\text{-}trans}$ = 10.2 Hz, 1H, 2-CH)

^{13}C-NMR -Spektrum (125 MHz, CDCl$_3$-*d*)

δ (ppm) = 24.50 (6, 7); 64.61 (4); 123.88 (1); 128.81 (2); 158.92 (3); 180.53 (5).

Synthese von *N*-(1-hydroxypropan-2-yl)acrylamide (HIPAAm)[153] (38)

(38)
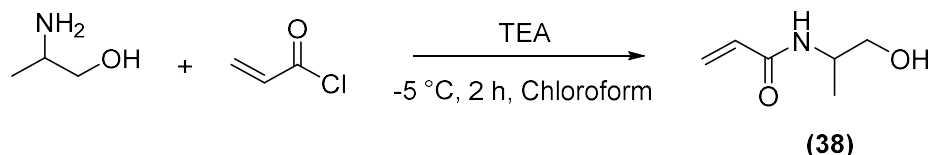
In a 100 mL three-necked round-bottom flask with dropping funnel and internal thermometer D,L-2-amino-propanol (5.62 g, 75 mmol) and triethylamine (7.58 g, 75 mmol) were dissolved in dry chloroform (30 mL) under a nitrogen atmosphere for 20 min. The reaction mixture was then cooled to -5 °C and acryloyl chloride (6.75 g, 75 mmol) was added dropwise. After stirring for 2 hours at -5 °C, the solvent was removed and the residue was dissolved in 2-propanol (100 mL). The reaction mixture was stored at -20 °C for 24 hours to precipitate the triethylamine hydrochloride salt. The precipitate was filtered off and was removed under reduced pressure. The pure product was obtained as a colorless viscous liquid after purification by column chromatography with ethyl acetate as an eluent (6 g, 46.5 mmol, 62%).

Characterization:
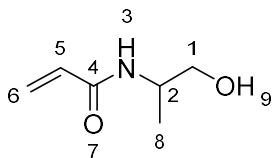
^{1}H-NMR-Spektrum (500 MHz, D$_2$O):

δ = 1.17 (m, 3H, 8-CH$_3$); 3.61 (m, 2H, 1-CH$_2$); 4.04 (m, 1H, 2-CH); 5.74 (d, H$_{trans}$, J$_{trans-gem}$ = 10.1 Hz, 1H, 6-CH$_2$); 6.17 (d, H$_{cis}$, J$_{cis-gem}$ = 17.6 Hz, 1H, 5-CH); 6.25 (dd, H$_{gem}$, J$_{gem-cis}$ = 17.1 Hz, J$_{gem-trans}$ = 10.1 Hz, 2H, 5-CH)

^{13}C-NMR-Spektrum (125 MHz, D$_2$O):

δ (ppm) = 17.2 (8); 53.3 (2); 64.61 (1); 128.81 (6); 132.4 (5); 167.5 (4)

3.3.4 Homo- and block copolymer synthesis via RAFT

Synthesis of PSKA and PSKA-*b*-PNIPAAm (40)
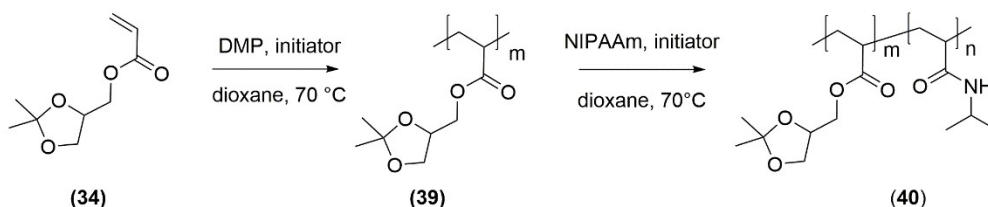
Subsequently SKA (1.0 g, 5.3 mmol), DMP (35 mg, 0.125 mmol), ACVA (7 mg, 0.025 mmol) (ratio 5:1) and 1,4-dioxane (7 mL) were placed in a schlenk tube, which was equipped with magnetic stirrer and septum. The reaction mixture was purged with argon for 20 min. The polymerization was initiated by placing the schlenk tube in an oil bath at 70 °C. For the kinetic study of the polymerization 0.1 mL solution were withdrawn with a deoxygenated syringe after certain time intervals. Each sample was frozen in liquid nitrogen to stop the polymerization process. 0.05 mL of the sample were analyzed by ^{1}H-NMR spectroscopy in order to determine the monomer conversion (conv.$_{NMR}$) and the other 0.05 mL were investigated by SEC. After 24 h reaction time the polymerization was stopped by freezing the reaction mixture in liquid

nitrogen. 1,4-dioxane was evaporated under reduced pressure and the residue was dissolved in THF. The polymer was precipitated in *n*-hexane (100 mL) at room temperature as sticky oil. To determine the yield of the polymer, *n*-hexane was decanted and the polymer was dissolved in diethyl ether and transferred into a small flask. Both solvents were evaporated.

AIBN

ACVA

CTA 1　　　　　　**CTA 2**　　　　　　**CTA 3**
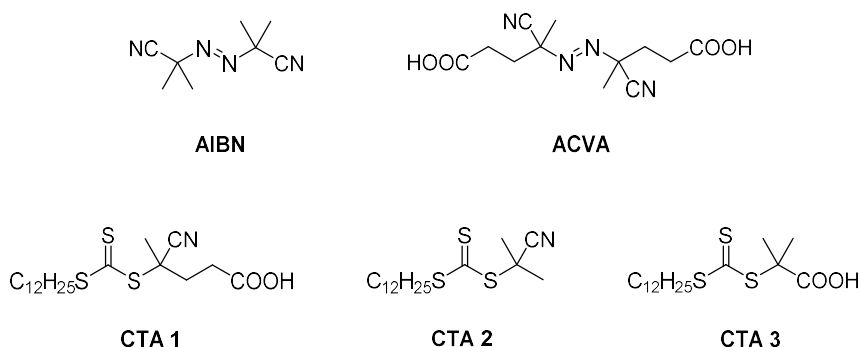
Figure 21. Chemical structure of the used RAFT-CTAs and initiators.

PSKA-macroinitiator (0.30 g, 1.6 mmol) (**39**), of NIPAAm (141.4 mg, 9.4 mmol), AIBN (1.0 mg, 0.006 mmol) and 1,4-dioxane (2 mL) with the ratio of [NIPAAm]/[PSKA-CTA]/[AIBN] = 40/1/0.15 were filled in a Schlenk tube equipped with magnetic stirrer and septum. The reaction mixture was purged with argon for 20 min and polymerization was started by placing the Schlenk tube in an oil bath at 70 °C. The polymerization was stopped after 100 min by freezing the reaction mixture with liquid nitrogen. The polymer was precipitated in *n*-hexane. After drying under vacuum overnight the block copolymer was received (0.26 g, 59 %).

Characterization:

PSKA (39)
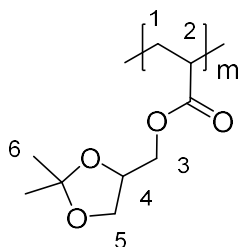
^{1}H-NMR -Spektrum (500 MHz, CDCl$_3$-*d*)

δ (ppm) = 1.33 (m, 6H, 6-CH$_3$); 1.54-2.44 (br, 3H, 1-CH$_2$, 2-CH); 3.77 (br, 1H, 3a-CH$_2$); 3.92 − 4.13 (br, 3H, 3b-CH$_2$, 5-CH$_2$); 4.22 (br, 1H, 4-CH)

GPC (Eluent: DMAc, PMMA- calibration): M_n = 5000 g/mol, Đ = 1.19

PSKA-*b*-PNIPAAm (40)

^{1} H-NMR -Spektrum (500 MHz, DMSO-d_6)

δ (ppm) = 1.05 (br, 6H, 10-CH_3); 1.33 (m, 6H, 6-CH_3); 1.54-2.44 (br, 3H, 1-CH_2, 2-CH, 7-CH_2, 8-CH); 3.68 (s, 1H, 9-CH); 3.86 (br, 1H, 3a-CH_2); 3.92 – 4.13 (br, 3H, 3b-CH_2); 4.23 (br, 1H, 4-CH)

GPC (Eluent: DMAc, PMMA- calibration): M_n = 10,800 g/mol, Đ = 1.21

Deproctection of PSKA-*b*-PNIPAAm to PDHPA-*b*-PNIPAAm (41)
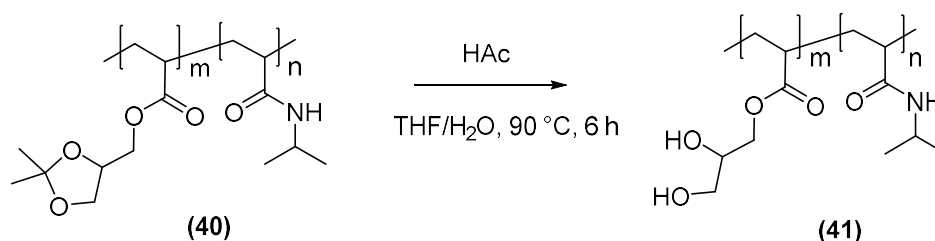
1 g of PSKA-*b*-PNIPAAm was dissolved in a mixture of glacial acetic acid (15 mL) and THF (10 mL). The solution was heated to reflux for 6 h. During heating deionized water (50 mL) were added in portions to the reaction mixture. The acetic acid was then removed under reduced pressure and the residue was purified by dialysis in water at room temperature (Spectra Por® 6 Dialysis Membrane MWCO 1000). Polymers were obtained after freeze-drying as white powder.

Characterization:
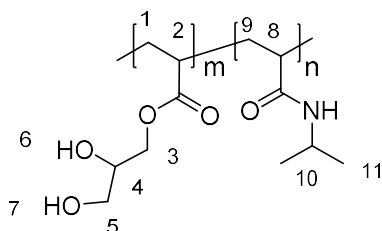
^{1}H-NMR -Spektrum (500 MHz, DMSO-d_6)

δ (ppm) = 1.06 (br, 6H, 11-CH$_3$); 1.16-2.40 (br, 4H, 1-CH$_2$, 2-CH, 9-CH$_2$, 8-CH); 3.38 (br, 2H, 5-CH$_2$); 3.67 (br, 1H, 10-CH); 3.74-3.96 (br, 2H, 3-CH$_2$); 4.03 (br, 1H, 4-CH); 4.61 (br, 1H, 7-OH); 4.81 (br, 1H, 6-OH)

GPC (Eluent: DMAc, PMMA- calibration): M_n = 13,000 g/mol, Đ = 1.22

Synthesis of PSKA-*b*-P(NIPAAm-*co*-VDMA) block copolymers (42)
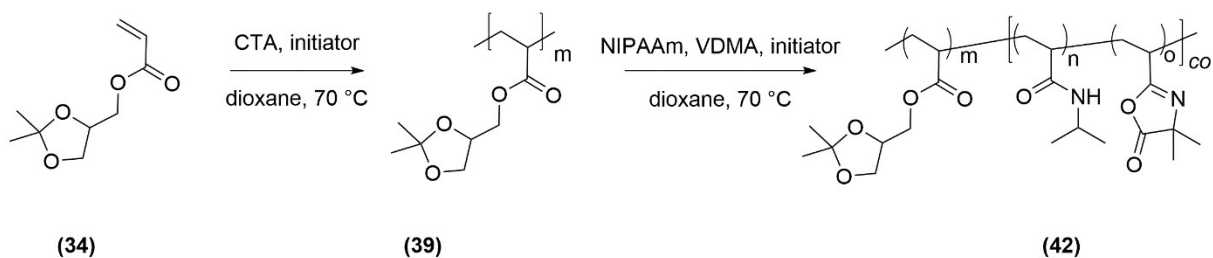
A schlenk tube with septum and magnetic stirrer was charged with SKA (2.997 g, 16.1 mmol), DMP (117 mg, 0.322 mmol), AIBN (5 mg, 0.0322 mmol) and solvent dioxane (5.3 mL) in the ratio of [SKA]$_0$/[CTA]$_0$/[AIBN]$_0$ =50/1/0.1. The resulting reaction mixture was purged with N$_2$ for 20 minutes, before the schlenk tube was immersed into an oil bath at 70 °C. After 24 h, the polymerization was stopped by cooling of the reaction mixture with liquid nitrogen. Dioxane was removed under reduced pressure and the polymer was isolated by precipitation in *n*-hexane at room temperature. The PSKA was obtained as a sticky oil and used for the copolymerization as a macro RAFT agent.

For the copolymerization, the previously obtained RAFT agent (0.35 g) von last step, NIPAAm (1.5 g, 13.2 mmol), VDMA (0.15 g, 1.07 mmol) and AIBN (5.28 mg, 0.0322 mmol) were dissolved in dioxane (5 mL). Before the schlenk tube was immersed into the oil bath, the reaction mixture was purged with N$_2$ for 20 minutes. The polymerization proceeded at 70 °C for 24 h. Afterwards the reaction was stopped by cooling the reaction mixture with liquid nitrogen. Dioxane was removed under reduced pressure and the polymer was isolated by a series of precipitations in cold diethyl ether. The block copolymer was obtained as light-yellow powder after drying in vacuo.

Characterization:
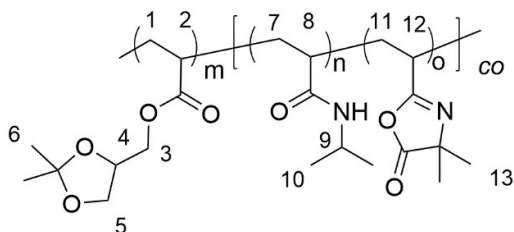
^{1}H-NMR -Spektrum (500 MHz, CDCl$_3$-*d*)

δ (ppm) = 1.13 (br, 6H$_{PSKA}$, 10-CH$_3$); 1.39 (br, 6H$_{PNIPAAm}$, 6-CH$_3$); 1.57-2.49 (br, 3H$_{PSKA}$, 3H$_{PNIPAAm}$, 3H$_{VDMA}$, 1-CH$_2$, 2-CH, 7-CH$_2$, 8-CH, 11-CH$_2$, 12-CH); 3.88 (br, 1H, 9-CH); 3.88 – 4.18 (br, 3H, 3b-CH$_2$, 5-CH$_2$); 4.23 – 4.34 (br, 1H, 4-CH)

GPC (Eluent: THF, PMMA- calibration): M_n = 14,400 g/mol, Đ = 1.22

Synthesis of PDHPA (43) and PDHPA-*b*-PNIPAAm (44)
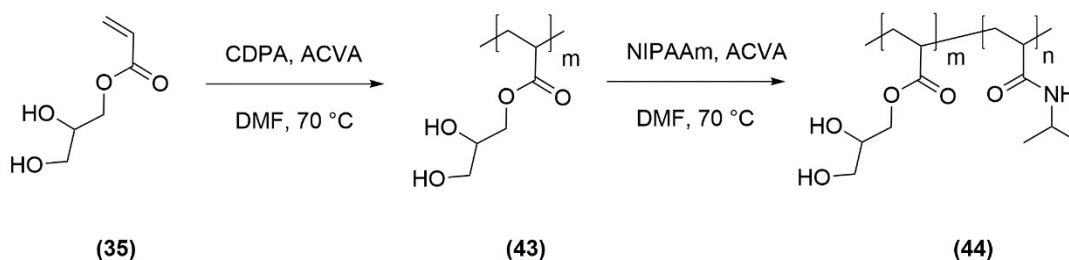
A schlenk tube with septum and magnetic stirrer was charged with DHPA (730 mg, 5 mmol), CDPA (50 mg, 0.125 mmol), ACVA (3.5 mg, 0.0125 mmol) and solvent DMF (2 mL) in the ratio of [DHPA]$_0$/[CTA-2]$_0$/[ACVA]$_0$ =40/1/0.1. The resulting reaction mixture was purged with N$_2$ for 20 minutes, before the schlenk tube was immersed into an oil bath at 70 °C. After 24 h, the polymerization was stopped by rapid cooling of the reaction mixture with liquid nitrogen. DMF was removed under reduced pressure and the polymer was obtained as light-yellow oil and analyzed without further purification.

PDHPA (200 mg), NIPAAm (0.5 g, 4.42 mmol), ACVA (2 mg, 0.007 mmol) and solvent DMF (2 mL) were charged in a schlenk tube with septum and magnetic stirrer. The resulting reaction mixture was purged with N$_2$ for 20 minutes and the schlenk tube was immersed into an oil

bath at 70 °C to initiate the polymerization. After 24 h, the reaction was stopped by rapid cooling of the reaction mixture with liquid nitrogen. DMF was removed using under reduced pressure and the polymer was precipitated in cold diethyl ether.

Characterization:

PDHPA (43)
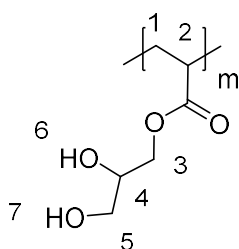
^{1}H-NMR -Spektrum (500 MHz, DMSO-d_6)

δ (ppm) = 1.30-2.45 (br, 3H, 1-CH$_2$, 2-CH); 3.38 (br, 2H, 5-CH$_2$); 3.69 (br, 1H, 4-CH); 4.86 (br, 1H, 3b-CH$_2$); 4.06 (br, 1H, 4a-CH$_2$); 4.60 (br, 1H, 7-OH); 4.79 (br, 1H, 6-OH)

GPC (Eluent: DMAc, PMMA- calibration): M$_n$ = 13,000 g/mol, Đ = 9

PDHPA-b-PNIPAAm (44)
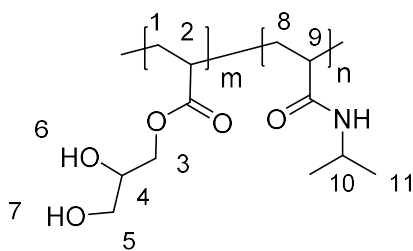
^{1}H-NMR -Spektrum (500 MHz, DMSO-d_6)

δ (ppm) = 1.06 (br, 6H, 11-CH$_3$); 1.18-2.43 (br, 4H, 1-CH$_2$, 2-CH, 7-CH$_2$, 8-CH); 3.33 (br, 2H, 5-CH$_2$); 3.69 (br, 1H, 10-CH); 3.89 (br, 2H, 3-CH$_2$); 4.06 (br, 1H, 4-CH); 4.61 (br, 1H, 7-OH); 4.80 (br, 1H, 6-OH)

GPC (Eluent: DMAc, PMMA- calibration): M$_n$ = 27,000 g/mol, Đ = 11.5

Synthesis of PHIPAAm (45) and PHIPAAm-*b*-PNIPAAm (46)
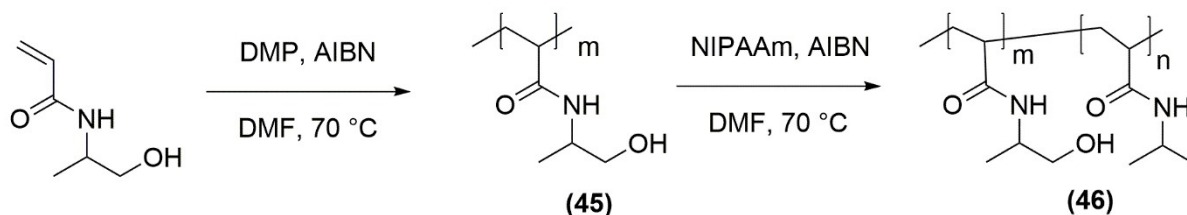
A schlenk tube with septum and magnetic stirrer was charged with HIPAAm (418 mg, 3.23 mmol), DMP (29 mg, 0.079 mmol), AIBN (1 mg, 0.0121 mmol) and solvent DMF (2 mL) in the ratio of $[HIPAAm]_0/[DMP]_0=40/1$. The resulting reaction mixture was purged with N_2 for 20 minutes, before the schlenk tube was immersed into an oil bath at 70 °C. After 24 h, the polymerization was stopped by rapid cooling of the reaction mixture with liquid nitrogen. DMF was removed under reduced pressure and the residual polymer was purified by dialysis against water at room temperature (Spectra Por® 6 Dialysis Membrane MWCO 1000). Polymers were obtained after freeze-drying as a white powder.

For the copolymerization, PHIPAAm-based macro-RAFT agent (0.2 g), NIPAAm (0.733 g, 6.48 mmol) and AIBN (5 mg, 0.0244 mmol) were dissolved in DMSO (2 mL) and the resulting mixture was purged with N_2 for 20 minutes. Polymerization was initiated by immersing the schlenk tube into the oil bath. The stirring proceeded continued overnight at 70 °C. The reaction was stopped by cooling the mixture with liquid nitrogen. DMSO was removed under reduced pressure.

Characterization:

PHIPAAm (45)
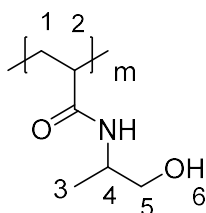
^{1}H-NMR -Spektrum (500 MHz, D$_2$O-d_2)

δ = 1.04 (br, 3H, 3-CH$_3$); 1.29 − 2.19 (br, 3H, 1-CH$_2$, 2-CH); 3.13 − 3.58 (br, 2H, 5-CH$_2$); 3.67 − 3.98 (br, 1H, 4-CH)

GPC (Eluent: DMAc, PMMA- calibration): M$_n$ = 7,500 g/mol, Đ = 1.94

PHIPAAm-b-PNIPAAm (46)
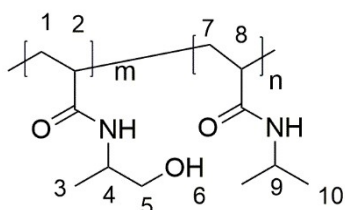
^{1}H-NMR -Spektrum (500 MHz, DMSO-d_6)

δ = 0.88 − 1.82 (br, 3H$_{HIPAAm}$, 6H$_{PNIPAAm}$, 3-CH$_3$, 10-CH$_3$); 1.29 − 2.19 (br, 3H$_{PHIPAAm}$, 3H$_{PNIPAAm}$, 1-CH$_2$, 2-CH, 7-CH$_2$, 8-CH); 3.13 − 3.58 (br, 2H, 5-CH$_2$); 3.66 − 4.01 (br, 2H, 4-CH, 9-CH)

GPC (Eluent: DMAc, PMMA- calibration): M$_n$ = 47,000 g/mol, Đ = 3.58

Synthesis of PDMAA (47) and PDMAA-b-PNIPAAm (48)
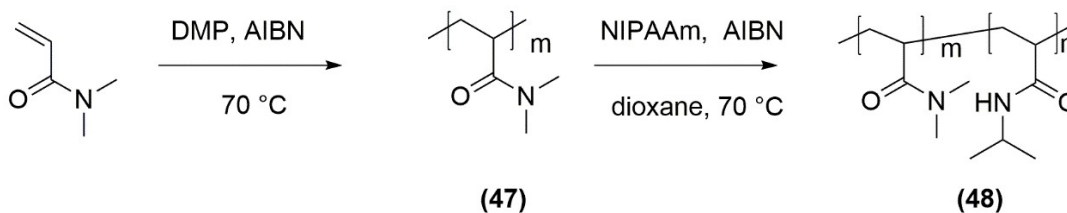
To a schlenk tube with septum and magnetic stirrer, DMAA (2.5 mL, 24.3 mmol), DMP (178 mg, 0.487 mmol), AIBN (4 mg, 0.0487 mmol) were added in the ratio of [DMAA]$_0$/[CTA]$_0$/[AIBN]$_0$ = 50/1/0.1. The resulting reaction mixture was purged with N$_2$ for 20 minutes, before the schlenk tube was immersed into an oil bath. The polymerization proceeded overnight at 70 °C. The reaction stopped by rapid cooling of the mixture with liquid nitrogen. The yellow solid reaction mixture was dissolved in THF (2 mL) and purified by precipitations in cold diethyl ether. After

drying under fine vacuum, the residual PDMAA was obtained as a light-yellow powder.

For the copolymerization, the PDMAA-based macro-RAFT agent (0.5 g), NIPAAm (0.569 g, 5.03 mmol) and AIBN (1 mg, 0.0121 mmol) were dissolved in dioxane (5 mL) and the resulting mixture was purged with N_2 for 20 minutes. Polymerization was initiated by placing the schlenk tube in the oil bath. The reaction proceeded overnight at 70 °C. The polymerization was stopped by cooling the reaction mixture with liquid nitrogen. Dioxane was removed under reduced pressure and the polymer was purified by a series of precipitations in cold diethyl ether and *n*-hexane. The block copolymer was obtained as yellow powder after drying under fine vacuum.

Characterization:

PDMAA (47)
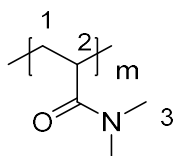
^{1}H-NMR -Spektrum (500 MHz, CDCl$_3$-*d*)

δ (ppm) = 1.07 − 2.68 (br, 3H, 1-CH$_2$, 2-CH); 2.72 − 3.15 (br, 6H, 3-CH$_3$)

GPC (Eluent: THF, PMMA- calibration): M_n = 4,500 g/mol, Đ = 1.15

PDMAA-*b*-PNIPAAm (48)
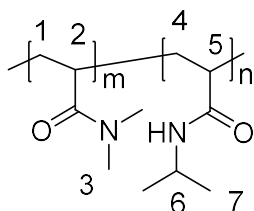
^{1}H-NMR-Spektrum (500 MHz, CDCl$_3$-*d*)

δ (ppm) = 1.07 (br, 6H, 7-CH$_3$); 1.41 − 1.95 (br, 3H$_{PDMAA}$, 3H$_{PNIPAAm}$, 1-CH$_2$, 2-CH, 4-CH$_2$, 5-CH);

2.83 (br, 6H, 3-CH₃); 3.95 (br, 1H, 6-CH)

GPC (Eluent: THF, PMMA- calibration): M_n = 6,500 g/mol, Đ = 1.18

Synthesis of PDMAA-*b*-P(NIPAAm-*co*-VDMA) (49)

(47)   (49)
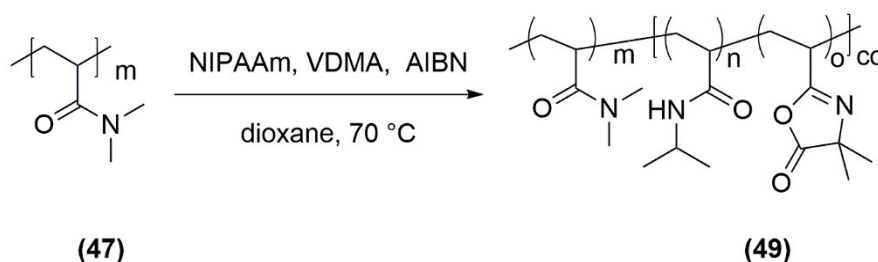
For the synthesis of copolymer PDMAA-*b*-P(NIPAAm-*co*-VDMA), PDMAA-based macro-RAFT agent (0.5 g), NIPAAm (0.25 g, 2.21 mmol), VDMA (0.025 g, 0.18 mmol) and AIBN (1 mg, 0.0121 mmol) were dissolved in dioxane (5 mL) in a schlenk tube with septum and magnetic stirrer. The mixture was purged with N₂ for 20 minutes and stirred over night at 70 °C. The polymerization was stopped by freezing the reaction mixture with liquid nitrogen. The polymer was purified by 2 times precipitation in cold diethyl ether and drying under fine vacuum.

Characterization:
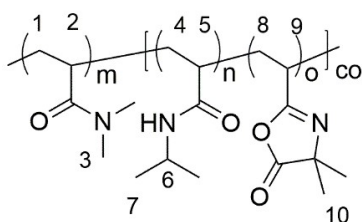
¹H-NMR -Spektrum (500 MHz, CDCl₃-*d*)

δ (ppm) = 1.14 (br, 6H, 7-CH₃); 1.43 – 2.35 (br, 3H_PDMAA, 3H_PNIPAAm, 3H_PVDMA, 1-CH₂, 2-CH, 4-CH₂, 5-CH, 8-CH₂, 9-CH); 2.90 (br, 6H, 3-CH₃); 4.00 (br, 1H, 6-CH)

GPC (Eluent: THF, PMMA-calibration): M_n = 7,200 g/mol, Đ = 1.27

Synthesis of poly(ethylene glycol) methyl ether (4-cyano-4-pentanoate dodecyltrithio-carbonate) (macro-RAFT agent) (50)
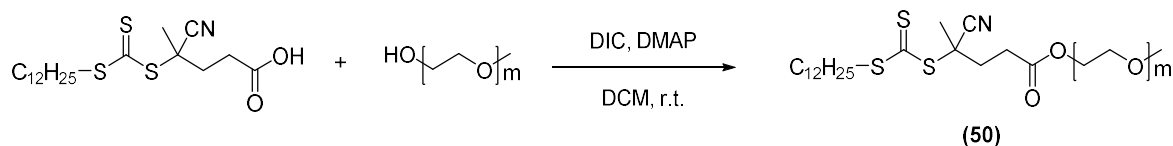
Macro-RAFT-agent poly(ethylene glycol) methyl ether (4-cyano-4-pentanoate dodecyltrithio-carbonate) (**50**) was synthesized analogously to the peptide coupling of prolinamide in the presence of DIC/DMAP.

Poly(ethylene glycol)methyl ehter (4 g, 0.8 mmol, M_n=5000 g/mol), CDPA (2.018 g, 5 mmol) and DMAP (97 mg, 0.8 mmol) were dissolved in water-free DCM (40 mL). The solution of DIC (631 mg, 5 mmol) in DCM (20 mL) was added dropwise to the reaction mixture at 0 °C. The stirring was continued for 24 h at room temperature. Subsequently, the reaction mixture was washed with brine (50 mL) and water and dried over $MgSO_4$. The PEG-based macro-RAFT-agent was precipitated 3 times in cold diethyl ether and dried under fine vacuum.

Characterization:
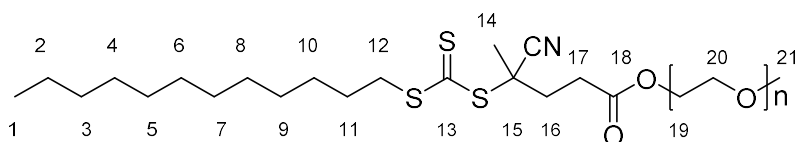
^{1}H-NMR-Spektrum (500 MHz, CDCl$_3$-*d*):

δ (ppm) = 0.88 (t, 6H, J = 7.0 Hz; 1-CH$_3$); 1.26 (br, 16H, 2-9-CH$_2$); 1.38 (d, 2H, J = 7.8 Hz 10-CH$_2$); 1.69 (dt, 2H; J= 7.4 Hz, J=14.9 Hz, 11-CH$_2$); 1.87 (s, 3H, 14-CH$_3$); 2.37 (m, 1H, 17a-CH$_2$); 2.52 (m, 1H, 17b-CH$_2$); 2.65 (m, 2H, 16-CH$_2$); 3.32 (m, 2H, 12-CH$_2$); 3.37 (s, 3H, 21-CH$_3$); 3.46-3.83 (br, 4H, 19, 20-PEG-CH$_2$); 4.25 (m, 2H, 19-CH$_2$)

GPC (Eluent: THF, PMMA- calibration): M_n = 8,900 g/mol, Đ = 1.05

Synthesis of PEG-*b*-PNIPAAm block copolymers (51)
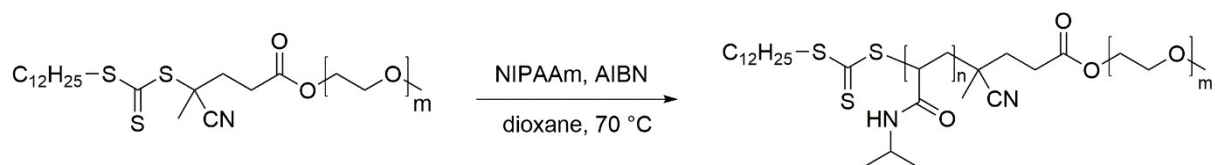
A schlenk tube with septum and magnetic stirrer was charged with the PEG-based macro-RAFT-agent (0.25 g, 0.045 mmol), AIBN (1 mg, 0.0121 mmol), NIPAAm (1.07 g, 9.47 mmol) and dioxane (5.3 mL) in the ratio of $[NIPAAm]_0/[PEG\text{-}CDPA]_0 = 226/1$. The resulting reaction mixture was purged with N_2 for 20 minutes and then the schlenk tube was immersed into an oil bath at 70 °C to start the polymerization. After 24 h, the polymerization was stopped by rapid cooling of the reaction mixture with liquid nitrogen. Dioxane was removed under reduced pressure and the polymer was purified by precipitation in cold diethyl ether and subsequent drying under fine vacuo.

Characterization:
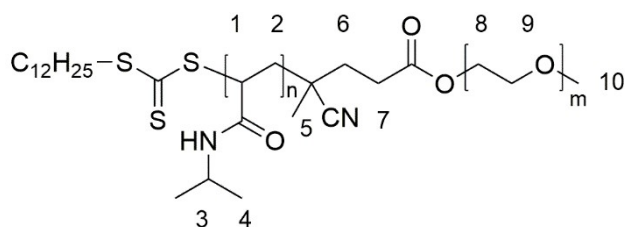
^{1}H-NMR -Spektrum (500 MHz, CDCl$_3$-*d*)

δ (ppm) = 0.98 – 1.23 (br, 6H$_{PNIPAAm}$, 4-CH$_3$); 1.46 – 2.40 (br, 3H, 1-CH$_2$, 2-CH); 3.63 (br, 4H, 8-CH$_2$, 9-CH$_2$); 4.0 (b, 1H, 3-CH)

GPC (Eluent: THF, PMMA- calibration): $M_n = 25,900$ g/mol, $Đ = 1.31$

Synthesis of PEG-*b*-P(NIPAAm-*co*-VDMA) block copolymers (52)
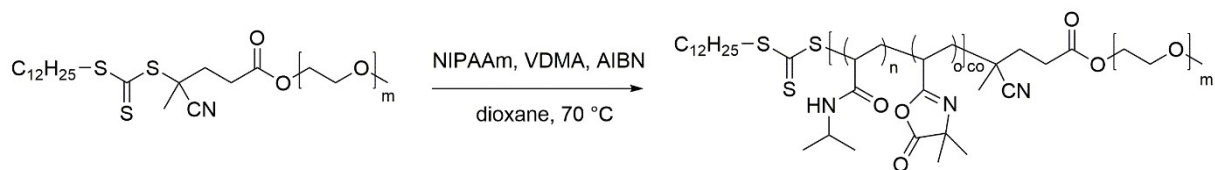
A schlenk tube with septum and magnetic stirrer was charged with PEG-based macro-RAFT-agent (0.25 g, 0.045 mmol), AIBN (1 mg, 0.0121 mmol), NIPAAm (2.14 g, 18.94 mmol), VDMA (138 mg, 1 mmol) and dioxane (5.3 mL) in the ratio of $[\text{NIPAAm}]_0/[\text{VDMA}]_0/[\text{PEG-CDPA}]_0 = 420/20/1$. The reaction mixture was purged with N_2 for 20 minutes and subsequently, the schlenk tube was immersed into an oil bath at 70 °C to start the copolymerization. After 24 h, the reaction was stopped by rapid cooling of the reaction mixture with liquid nitrogen. Dioxane was removed under reduced pressure and the polymer was purified by a series of precipitations in cold diethyl ether and dried under fine vacuum.

Characterization:
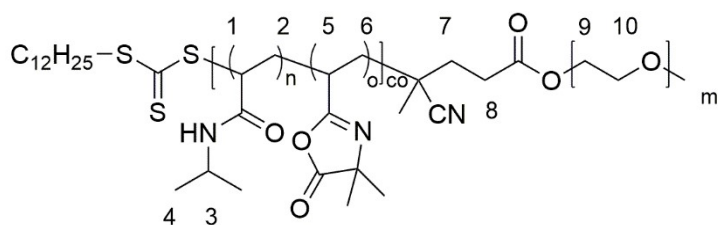
^{1}H-NMR -Spektrum (500 MHz, CDCl$_3$-*d*)

δ (ppm) = 0.98 – 1.23 (br, 6H$_{PNIPAAm}$, 4-CH$_3$); 1.46 – 2.40 (m, 3H$_{PNIPAAm}$, 3H$_{VDMA}$, 2-CH$_2$, 1-CH, 6-CH$_2$, 5-CH); 3.63 (br, 4H, 9-CH$_2$,10-CH$_2$O); 4.0 (br, 1H, 3-CH)

GPC (Eluent: THF, PMMA- calibration):   M$_n$ = 39,700 g/mol, *Đ* = 1.43

3.3.5 Post-polymerization attachment of L-proline and L-prolinamide derivatives[111]
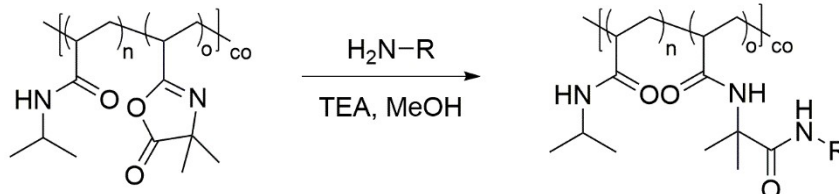
In a 25-mL round bottom flask 0.5 g VDMA-containing amphiphilic block polymer (5 mol% VDMA) and 2 eq. of the primary amine R-NH$_2$ were dissolved in MeOH (10 mL). TEA (0.3 mL) was slowly added and the resulting reaction mixture was stirred continuously overnight at room temperature. After the reaction, the clear solution was diluted with deionized water (5 mL) and residual small molecules were removed by dialysis against water at room temperature (Spectra Por® 6 Dialysis Membrane MWCO 1000). Modified polymers were obtained as white powder after freeze-drying.
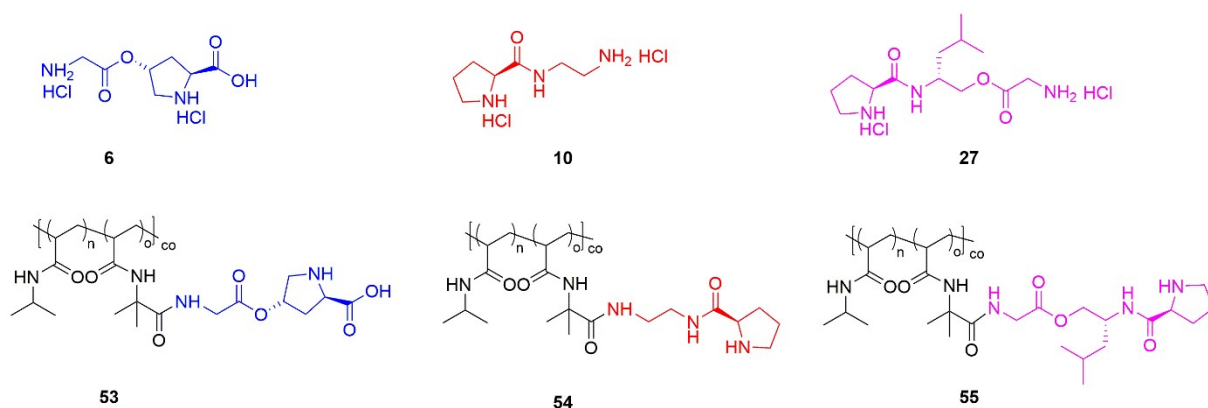
Figure 22. Chemical structures of the amino-modified L-proline and L-prolinamide organocatalysts and the chamical structrue of the modified xopoymers bearing the immobilized organocatalyst.

3.3.6 Aminolysis of the trithiocarbonate end groups

(48)

(56) R: isobutyronitrile
(57) R: isobutyric acid
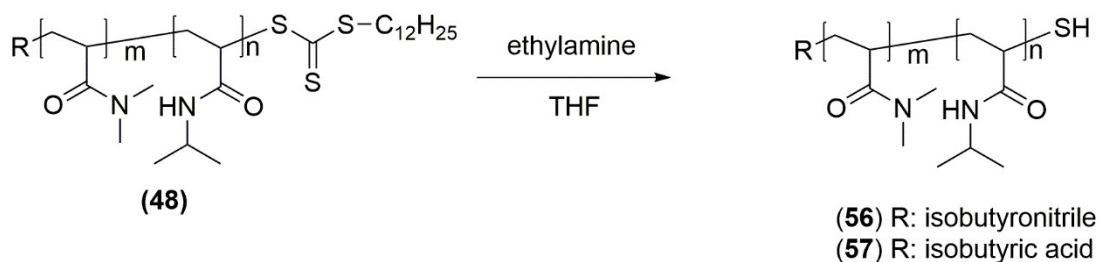
In a 50-mL round flask, 0.5 g block copolymer were dissolved in THF (12 mL). To the yellow solution, ethylamine solution (3 mL, 70 % in water) was added at room temperature. The stirring was continued for 2 hours, during which the solution turned colorless. After the reaction, polymers were precipitated 2 times in diethyl ether and dried under fine vacuum.

3.3.7 Temperature-dependent aggregation of the block copolymers

The amphiphilic block copolymers were dissolved in distil. water with a mass concentration of β = 0.5 mg/mL and the stirring of the polymer-solution was continued over night at room temperature. The resulting solution was filtered through a syringe PTFE-filter ($\varnothing$ = 0.45 µm) prior to be filled into a cuvette. The measurements for the temperature dependent solution behavior of the polymers were performed with the Zetasizer from Malvern Instruments and the particle size was determined as a function of the temperature, via dynamic light scattering (DLS). The measurements were carried out 3 times with increasing temperature from 20 °C to 65 °C.

3.3.8 Stereoselective synthesis

anti (58)   syn (59)
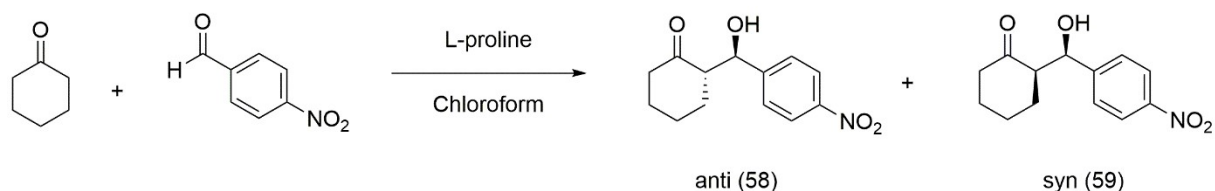
p-nitrobenzaldehyde (508 mg, 3.4 mmol), cyclohexanone (1.6 mL, 1.52 g, 15 mmol) and L-proline (40 mg, 0.34 mmol) were suspended in chloroform (30 mL). The resulting reaction

mixture was stirred overnight at room temperature. Afterwards, the solvent was removed under reduced pressure and the crude product was purified by column chromatography using *n*-Hexane: EtOAc (v:v = 60:40). (R$_{f1}$= 0.28, R$_{f2}$= 0.52)

Characterization:

(S)-2-((R)-hydroxy(4-nitrophenyl)methyl)cyclohexan-1-one (58)
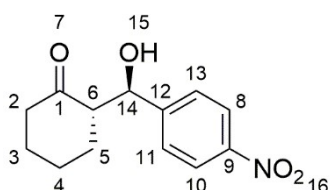
^{1}H-NMR (500 MHz, DMSO-*d$_6$*):

δ (ppm) = 1.46 – 1.86 (m, 6H, 3-CH$_2$, 4-CH$_2$, 5-CH$_2$); 2.22 – 2.38 (m, 2H, 2-CH$_2$); 2.62 – 2.76 (m, 1H, 6-CH); 5.22 (dd, ^{3}J$_{HH}$ = 7.1 Hz, ^{3}J$_{HH}$ = 4.5 Hz, 1H, 14-CH); 5.44 (d, ^{3}J$_{HH}$ = 4.8 Hz, 1H, 15-OH); 7.60 (d; ^{3}J$_{HH}$ = 9.8 Hz, 2H, 10-CH); 8.17 (d, ^{3}J$_{HH}$ = 8.8 Hz, 2H, 8-CH)

^{13}C-NMR (125 MHz, DMSO-*d$_6$*):

δ (ppm) = 23.6 (4); 25.9 (5); 26.6 (3); 40.2 (2); 41.6 (6); 70.4 (7); 123.0 (8); 127.4 (11); 146.3 (12); 153.1 (9); 210.0 (1)

Chirale HPLC: AD-H, *n*-Hexane:2-Propanol (80:20), 0.8 mL/min, λ = 254 nm, tR1 = 14.5 min, tR2 = 17.1 min

(R)-2-((R)-hydroxy(4-nitrophenyl)methyl)cyclohexan-1-one (59)
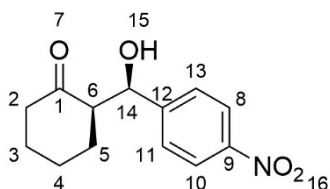
^{1}H-NMR (500 MHz, DMSO-*d$_6$*):

δ (ppm) = 1.48 – 1.93 (m, 6H, 3-CH$_2$, 4-CH$_2$, 5-CH$_2$); 2.29-2.41 (m, 2H, 2-CH$_2$); 2.67 – 2.78 (m, 1H, 6-CH); 5.09 (dd, ^{3}J$_{HH}$ = 6.8 Hz, ^{3}J$_{HH}$ = 4.7 Hz, 1H, 14-CH); 5.47 (d, ^{3}J$_{HH}$ = 4.5 Hz, 1H, 15-OH);

7.61 (d; $^3J_{HH}$ = 9.5 Hz, 2H, 10-CH); 8.17 (d, $^3J_{HH}$ = 8.3 Hz, 2H, 8-CH)

^{13}C-NMR (125 MHz, DMSO-d$_6$):

δ (ppm) = 23.3 (4); 27.4 (5); 29.6 (3); 40.0 (2); 40.1 (6); 70.5 (7); 123.0 (8); 128.1 (11); 146.6 (12); 151.6 (9); 210.7 (1)

Chirale HPLC: AD-H, n-Hexane:2-Propanol (80:20), 0.8 mL/min, λ = 254 nm, tR1 = 18.5 min, tR2 = 23.4 min

3.3.9 Micellar catalysis
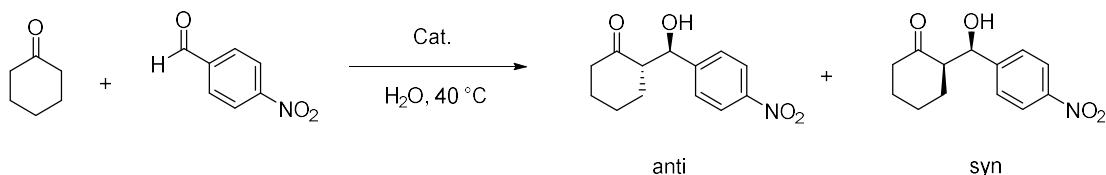
For micellar catalysis, 50 mg of proline-supported block copolymers, p-nitrobenzaldehyde (30 mg, 0.2 mmol), cyclohexanone (120 µL, 1.04 mmol) were suspended in deionized water (6 mL). The resulting reaction mixture was stirred continuously for 10 min at room temperature and subsequently immersed into an oil bath at 40 °C to start the catalytic reaction. For investigation of the reaction kinetics, samples of the reaction mixture were withdrawn after certain time intervals.

In addition, a recovery route was introduced by extract. After the reaction, the reaction mixture was diluted with water (10 mL) and extracted 3 times with diethyl ether. The organic phase was dried over MgSO$_4$ and the solvent was removed under reduced pressure Proline-supported block copolymers dissolved in aqueous phase, were obtained after freeze-drying and re-used in a consecutive reaction cycle up to 5 times.

4. Results and discussion

The overall objective of this work is to synthesize stimuli-responsive amphiphilic polymers bearing immobilized organocatalysts based on L-proline/L-prolinamide derivates. The amphiphilic polymers consisted of a temperature-sensitives PNIPAAm block with azlactone moieties. The chemical structure of the permanently hydrophilic block was varied from PDHPA and PDMAA to PEG. The three targeted copolymers PDHPA-*b*-P(NIPAAm-*co*-VDMA) (P1), PDMAA-*b*-P(NIPAAm-*co*-VDMA) (P2) and PEG-*b*-P(NIPAAm-*co*-VDMA) (P3) were prepared via RAFT polymerization. Immobilization of the organocatalyst was carried out by post-polymerization attachment via the azlactone moieties. To determine optimal conditions for the RAFT polymerization, different chain transfer agents (CTAs 1-3) and two different initiators were tested in detail especially for the RAFT polymerization of SKA. Due to the temperature-sensitive properties of the PNIPAAm block, a temperature-induced self-assembly of the copolymers in water occurs, what was determined by DLS measurements. The aggregation behavior of the copolymers in water was systematically investigated considering the block-length-ratio as well as the hydrophilic/lipophilic balance. Furthermore, the catalytic activity of the polymer-supported L-proline and L-prolinamide derivatives was tested in the direct asymmetric aldol reaction of with *p*-NBA and CH in water at different temperatures to investigate the influence of polymer aggregation on the catalyst activity.

4.1 Synthesis of the small molecular compounds

4.1.1 Synthesis of L-proline and L-prolinamide derivate

Proline as a simple amino acid with a secondary amine functionality belongs to the most successful organocatalysts for enamine-type reactions since the first proline-catalyzed direct asymmetric aldol reaction was reported in 2000.[2,4] In this work, the immobilization of L-proline and L-prolinamide organocatalysts is achieved via a the post-polymerization attachment: As

reported in literature, reactive azlactone-functionalized polymers can be readily modified after the polymerization, thereby utilizing a ring-opening reaction of the azlactone in presence of different types of nucleophilic species such as primary amines.[115,154] Therefore, proline or prolinamide derivatives containing primary amino groups need to be synthesized prior to the post-polymerization attachment (as shown in Figure 23).
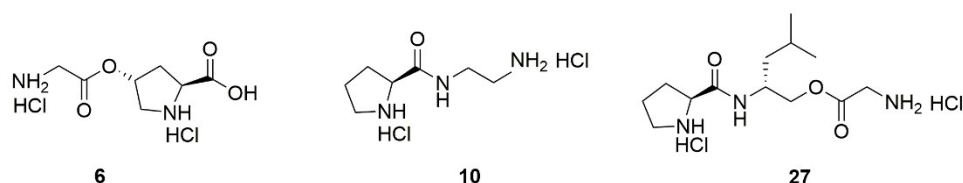
Figure 23. L-proline and L-prolinamide derivatives moieties for immobilization on azlactone-containing copolymers.

Synthesis of (2S,4R)-4-(glycyloxy)pyrrolidine-2-carboxylic acid dihydrochloride (6)
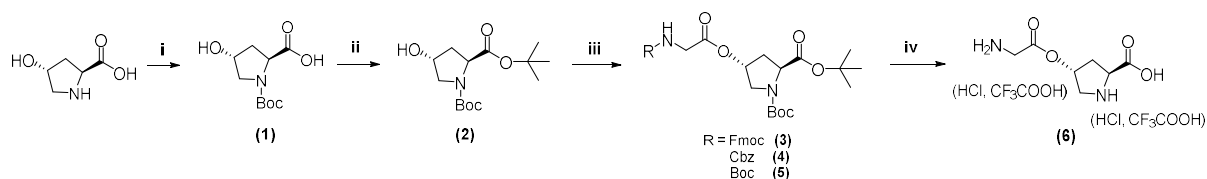
Figure 24. Synthesis of (2S, 4R)-4-(glycyloxy) pyrrolidine-2-carboxylic acid dihydrochloride: i) Boc$_2$O, 10% Na$_2$CO$_3$, H$_2$O-dioxane, rt, 1 d; ii) O-*tert*-butyl-*N,N*-diisopropylisourea, CH$_2$Cl$_2$, reflux, 2 d; iii) DIC, DMAP, DCM, protected glycine; iv) HCl in dioxane (4M), CHCl$_3$.

(2S,4R)-4-(glycyloxy) pyrrolidine-2-carboxylic acid dihydrochloride (**6**) was prepared starting from 4-hydroxy-L-proline. In the first two steps, both the amino and the carboxyl group were protected as *tert*-butyl-carbamate and *tert*-butyl ester. Subsequently, respectively Steglich esterification of the hydroxy group with *N*-protected glycine was carried out. For the construction of these polyfunctional molecules protection of the free-amino and carboxyl groups represents the most important issues in synthetic strategy. The choice of suitable protection groups should be associated with the following main characteristics: (1) it should easily reacted with the functional groups; (2) it should be stable under the reaction conditions; and (3) it should be selectively and rapidly removable at the end of the synthetic process.[155]

9-Fluorenylmethoxylcarbonyl (Fmoc)　　Benzyloxycarbonyl (Cbz)　　　*tert*-Butyloxycarbonyl (Boc)
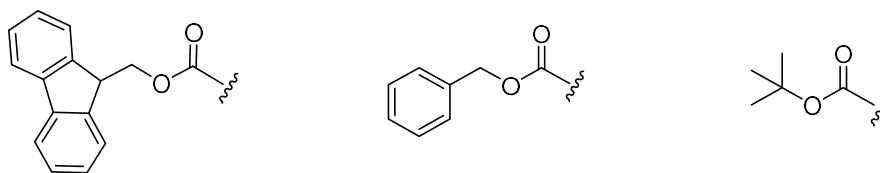
Figure 25. Chemical structures of the applied protecting groups.

With the method described by J. Pícha et al., di-*tert*-butyl (2*S*,4*R*)-4-hydroxypyrrolidine-1,2-dicarboxylate (**2**) was firstly successfully prepared yielding 51.4 % product after 2 steps.[143] In the next step, *N*-protected glycine was bound to the protected 4-L-hydroxy-proline via esterification reaction with the unprotected hydroxyl group. J. Li et al. reported the synthesis of a Merrifield resin-supported thiourea L-prolinamide organocatalyst derived in 2011.[156] In this paper, the immobilized Fmoc-protected L-proline turned out to be stable under acidic conditions in the presence of SOCl$_2$ and NH$_4$SCN. For the present working, esterification with Fmoc-protected glycine was carried out using Steglich conditions in the presence of DIC/DMAP and DMF as solvent. No expected product (**3**) could isolated after the reaction. Due to the use of a basic catalyst DMAP and relatively polar solvent DMF, the Fmoc-group was most likely removed during the esterification. Thus, intermolecular reactions between glycine molecules proceed much faster in the reaction mixture.[155]

In 1998, a DCC/DMAP-activated polycondensation of Cbz-protected 4-hydroxy-L-proline was reported.[157] After cleavage of the Cbz groups on the polyester backbone, the resulting poly(4-hydroxy-L-proline ester) was able to electrostatically complex with plasmid DNA. In this present work, Cbz-protected glycine was reacted with the hydroxyl group of *N*-Boc-4-hydroxy-L-proline under Steglich conditions with 80 % yield of product (**4**) purified by column chromatography on silica. At first, the cleavage of Cbz-group was attempted using HBr/acetic acid (33 %wt) at room temperature.[146] The deprotection with HBr/acetic acid resulted in an unexpected hydrolysis of the ester groups. Cbz deprotection was also performed by catalytic hydrogenation using a combination of triethylsilane and 10% Pd/C in CH$_3$OH at room temperature.[145] The desired product (**6**) could not be isolated, which might indicate that the ester groups were reductively cleaved as well. Therefore, the Cbz-groups seems to be

unsuitable, since deprotection require either acidic or reductive condition leading to unwanted side reactions.

In the paper by Putnam et al., *N*-Boc-4-hydroxy-L-proline was also investigated and used as a monomer for polycondensation.[157] In the present work using the DIC/DMAP method, di-tert-butyl (2S,4R)-4-(((*tert*-butoxycarbonyl)glycyl)oxy)pyrrolidine-1,2-dicarboxylate **(5)** was easily achieved. In comparison to the Cbz group, cleavage of Boc group can be conducted under milder reaction conditions by using HCl in dioxane (4M) at room temperature. Moreover, deprotection of both the amino acids the carboxyl group could be achieved in one step.[148] Cleavage of Boc-group was also attempted by using trifluoroacetic acid (TFA). Lower yields were observed because the deprotection employed under conditions known to hydrolyze ester bonds.

Synthesis of (*S*)-*N*-(2-aminoethyl) pyrrolidine-2-carboxamide dihydrochloride (10) and (*R*)-4-methyl-2-((*S*)-pyrrolidine-2-carboxamido) pentyl glycinate dihydrochloride (27)
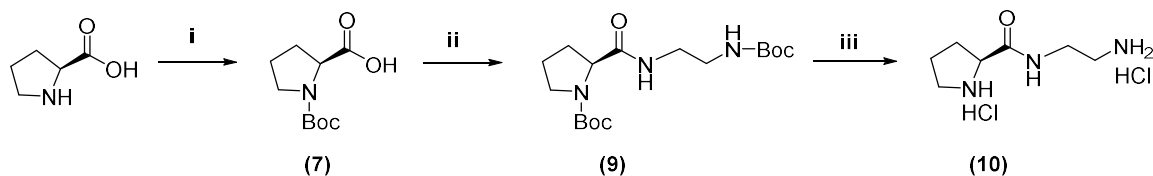
Figure 26. Synthesis of (*S*)-*N*-(2-aminoethyl)pyrrolidine-2-carboxamide dihydrochloride: i) Boc$_2$O, 10% Na$_2$CO$_3$ dioxane, 0 °C; ii) *N*-protected ethylene diamin, EDC·HCl, HOBt, TEA, CH$_2$Cl$_2$; iii) HCl in dioxane (4M), CHCl$_3$

The synthesis of L-prolinamide derivatives involves the amidation of *N*-Boc-protected L-proline with mono-Boc-protected ethylene diamine. As first, commercially available L-proline was protected with Boc$_2$O and the resulting *N*-Boc-L-proline was allowed to react with *tert*-butyl-*N*-(2-aminoethyl)-carbamat in present of EDC·HCl/HOBt. Since the by-product *N*,*N*'-diisopropylurea from DIC sporadically caused problem in the separation process, EDC·HCl was used as a water soluble carbodiimide condensing reagent. By-products could be easily removed by extraction with aqueous citric acid solution. After the *N*-Boc protecting group was removed with HCl in dioxane (4M), the desired (*S*)-*N*-(2-aminoethyl)pyrrolidine-2-carboxamide dihydrochloride was finally obtained and could be used for post-polymerization attachment to

the copolymer.
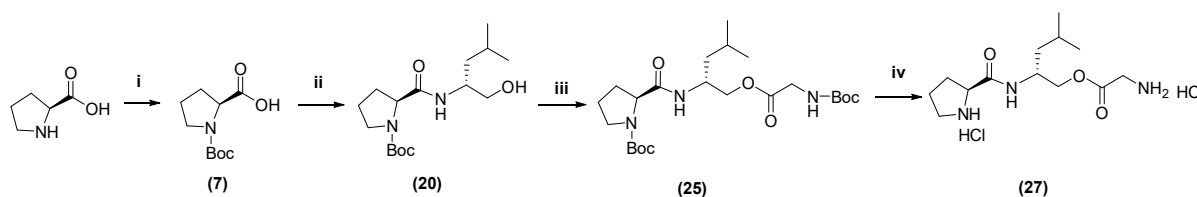
Figure 27. Synthesis of (*R*)-4-methyl-2-((*S*)-pyrrolidine-2-carboxamido) pentyl glycinate dihydrochloride: i) Boc₂O, 10% Na₂CO₃ dioxane, 0 °C; ii) aminoalcohol, EDC·HCl, HOBt, TEA, CH₂Cl₂; iii) Boc-glycine, EDC·HCl, HOBt, TEA, CH₂Cl₂; iv) HCl in dioxane (4M), CH₂Cl₂

The synthesis of (*R*)-4-methyl-2-((*S*)-pyrrolidine-2-carboxamido) pentyl glycinate dihydrochloride **(27)** was conducted in analogy to (*S*)-*N*-(2-aminoethyl)pyrrolidine-2-carboxamide dihydrochloride **(10)** using Steglich esterification.
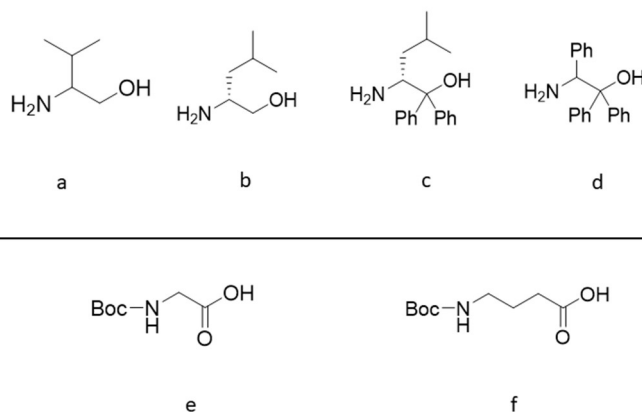
Figure 28. Chemical structures of the applied amino alcohol (a-d) and the *N*-Boc -amino acids (e, f)

The *N*-Boc-protected L-proline was reacted with different aminoalcohols **(a-d)** (Figure 28) using EDC·HCl/HOBt coupling and over 60 % yield were achieved after the reaction. The synthetic hydroxy-functionalized L-prolinamide was employed for a second peptide coupling reaction with *N*-Boc-glycine (e) and *N*-Boc-butanoic acid (d). As a result of steric hindrance of the phenyl rings, aminoalcohols **(c)** and **(d)** showed dramatically lower reactivity towards the esterification, and thus could not be coupled with the *N*-Boc amino acids. Subsequent, the cleavage of the Boc-groups was carried out by using HCl/dioxane (4M) at room temperature. The product resulting from coupling with *N*-Boc-butanoic acid was acid labile. Mass spectrometry results revealed an intramolecular nucleophilic attack by the deprotected primary amine group to the ester group, thereby producing five-membered lactams. In this

case, the desired free primary amino group was lost during the deprotection reaction. The product resulting from coupling with *N*-Boc-glycine exhibited a higher stability towards intramolecular transamination, because the resulting three-membered lactame would be instable. The successful cleavage of the Boc and *tert*-butyl groups was confirmed by the disappearance of the corresponding peaks in the ^{1}H-NMR spectrum and the molar mass was also proved by electrospray ionization (ESI) mass spectrometry.

4.1.2 Synthesis of RAFT chain transfer agent

Synthesis of 2-(dodecylthiocarbonothioylthio)-2-methylpropionic acid (DMP) (28)

Lai et al. presented a simple synthesis of the carboxylate-terminated trithiocarbonate DMP. This trithiocarbonate has an extremely high chain transfer efficiency and is well suited for the control of radical polymerizations. As reported, the most common solvents such as *tert*-butyl alcohol, acetone, toluene, xylene and DMF can be used in combination with DMP.[149]
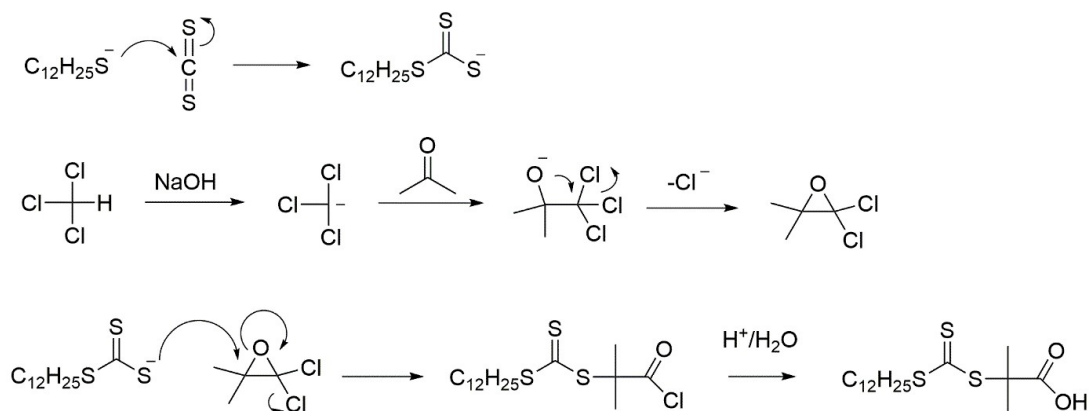
Figure 29. Mechanism of the DMP synthesis.[158]

The mechanism of the DMP synthesis follows a ketoform reaction involving the phase transfer catalyst Aliquot 336 under a nitrogen atmosphere.[158] The preparation of the dodecyl carbonotrithioate salt generally requires the use of a strong base like NaOH or NaH and the exothermic reaction proceeds fast. The product is formed by a nucleophilic attack of the thiolate at CS_2. In the presence of sodium hydroxide, chloroform is deprotonated and attacks the ketone to form an intermediate dichloroxirane. In the final step of the reaction, a ring-

opening reaction of the dichloro-epoxide occurs with the trithiocarbonate as nucleophile. After the addition of an acid, the dodecyl derivative CTA (DMP) is obtained as a stable product. The product was characterized by ^{1}H-NMR spectroscopy. The peaks of both methyl group at 1.73 ppm showed that the nucleophilic reaction of the trithiocarbonate was successful. After recrystallization from hexane, the yellow powder was obtained with a 67 % yield. Due to the good solubility of DMP in n-hexane, the product isolation from mixture was difficult. A better yield may be obtained by column chromatography using ethyl acetate and n-hexane as eluent.

Synthesis of 4-cyano-4-(((dodecylthio)carbonothioyl)thio)pentanoic acid (31) and 2-Cyano-2-propyl dodecyl trithiocarbonate (32)
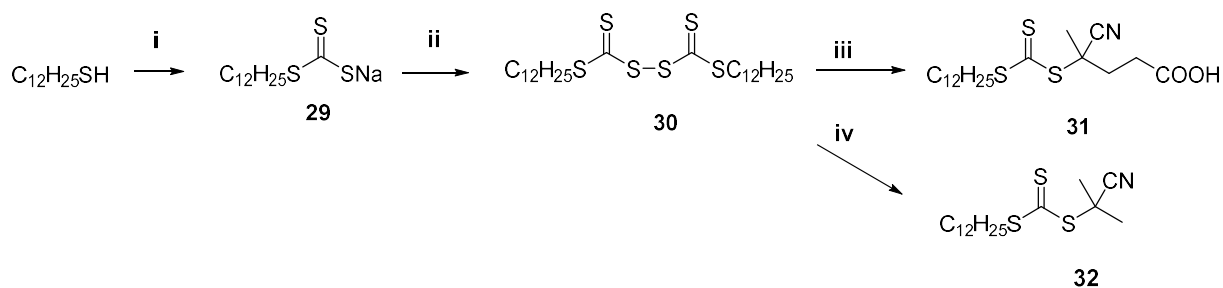
Figure 30. Synthesis of CDPA (**31**) and CPDT (**32**): i) NaH, diethyl ether, 0 °C; ii) I$_2$, diethyl ether, rt; iii) ACVA, ethyl acetate, reflux, 18 h; iv) AIBN, ethyl acetate, reflux, 18 h.

The synthesis of 4-cyano-4-(((dodecylthio)carbonothioyl)thio)pentanoic acid **(31)** and 2-cyano-2-propyl dodecyl trithiocarbonate **(32)** was achieved by radical-induced decomposition of bis(dodecylsulfanylthiocarbonyl) disulfide **(30).** In literature, this method was generally been applied to the synthesis of the most common forms of RAFT agents such as dithioesters, trithiocarbonates, xanthates and dithiocarbamates.[159,84] The bis(dodecylsulfanylthio-carbonyl) disulfide was generated by oxidation of sodium dodecyl carbonotrithioate **(29)** with solid iodine. After removal of the white sodium iodide, bis(dodecylsulfanylthiocarbonyl) disulfide was obtained in high yield. For the radical-induced decomposition, the thermal initiators AIBN and ACVA were used as radical source and heated under reflux for 18 h in presence of the disulfide **(30)**. After the reaction, byproducts from the azo-compound decomposition were isolated by silica gel column chromatography using ethyl acetate/n-hexane as eluent

(v/v=60/40). 4-Cyano-4-(((dodecylthio)carbonothioyl)thio)pentanoic acid (**31**) was dried under fine vacuum to give a yellow powder and 2-cyanopropyl-2-yl dodecyl carbonotrithioate (**32**) was collected as a yellow oil at room temperature.

4.1.3 Synthesis of monomers

Synthesis of hydrophilic monomers
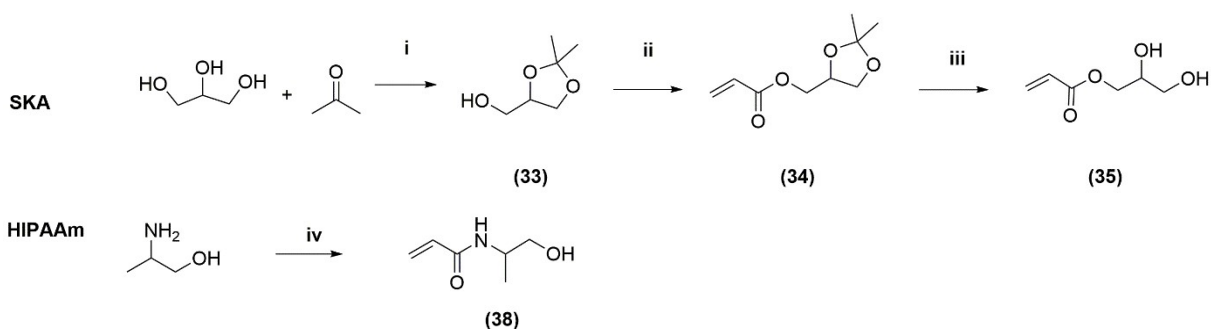
Figure 31. Synthesis of hydrophilic monomers SKA: i) p-TSA, CHCl$_3$, reflux, 8 h; ii) acryloyl chloride, TEA, CH$_2$Cl$_2$, r.t.; iii) DHPA: 1N HCl, THF, 2 h; iv) HIPAAm: acryloyl chloride, TEA, CH$_2$Cl$_2$, -5 °C, 2 h.

The synthesis of the solketal acrylate monomer (SKA) was performed via a two-step transformation using glycerol, acetone and acryloyl chloride. An isopropylidene glycerol (**33**) was first prepared under acid catalysis with glycine and acetone. For the second step, the free hydroxyl group reacted from acryloyl chloride in a highly exothermic esterification reaction. For this reason, the reaction mixture was cooled with ice bath and the acryloyl chloride was added dropwise. The crude product of the SKA was distilled under vacuum in the presence of hydroquinone, in order to avoid premature polymerization of the monomer under heating. Over 80 % yield were achieved after 2 steps, consistent with the literature.[160] The chemical structure was determined by ^{1}H-NMR spectroscopy with the three vinyl protons which are shifted between 5.5 and 6.5 ppm (Figure 32). Protons of the dioxolan ring shown typical signal splitting for cyclic systems. A further purification was achieved by flash chromatography on silica gel with ethyl acetate/n-hexane (3/7) as eluent, if necessary.

The hydrophilic monomer 2,3-dihydroxypropyl acrylate (DHPA) was successfully obtained by

acetal-group hydrolysis from solketal acrylate monomer. After the transformation, DHPA showed a poorly solubility in organic solvents. The successful cleavage of the both methyl groups were confirmed by the disappearance of the corresponding peaks in the ^{1}H-NMR spectrum at 1.42 ppm. Two new peaks at 4.6 ppm and 4.9 ppm emerged corresponding to the hydroxy-group (Figure 33).

Synthesis of *N*-(1-hydroxypropan-2-yl) acrylamide (HIPAAm) was carried out analogously to the SKA synthesis from D,L-2-aminopropanol in the presence of acryloyl chloride and triethylamine. The product was purified by column chromatography with ethyl acetate as eluent. Chemical structure was determined by ^{1}H-NMR spectroscopy with the three vinyl protons which are shifted between 5.75, 6.18 and 6.24 ppm (Figure 34).[153]
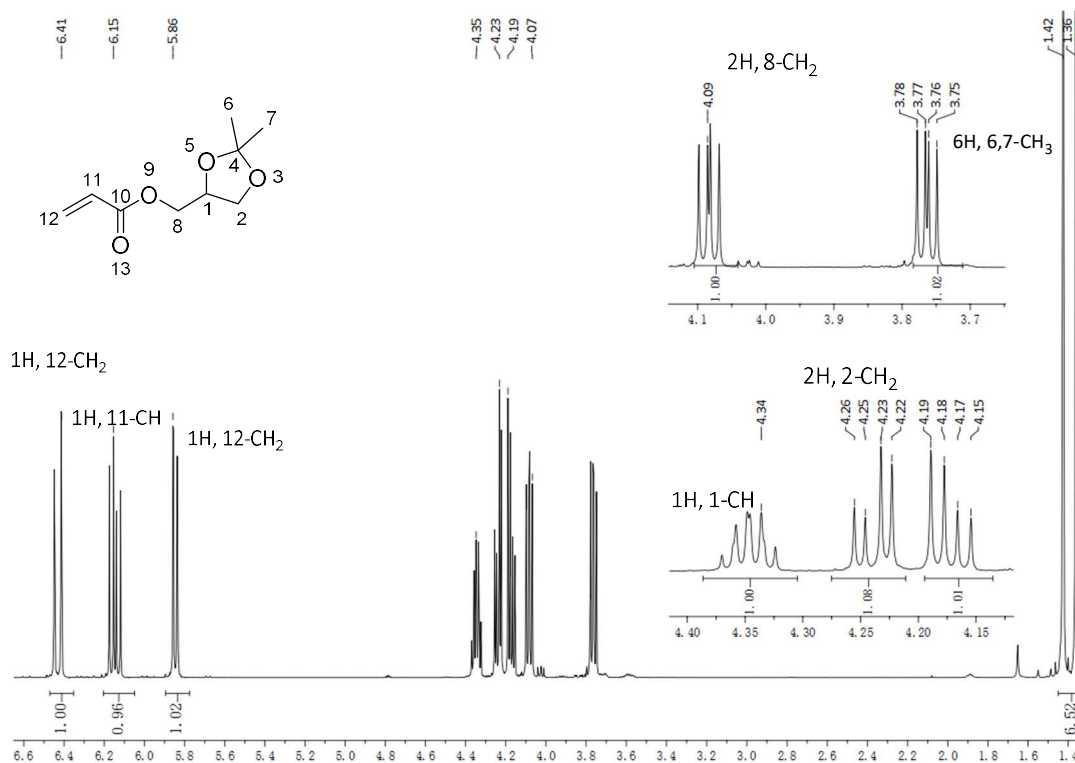
Figure 32. ^{1}H-NMR spectrum of SKA.
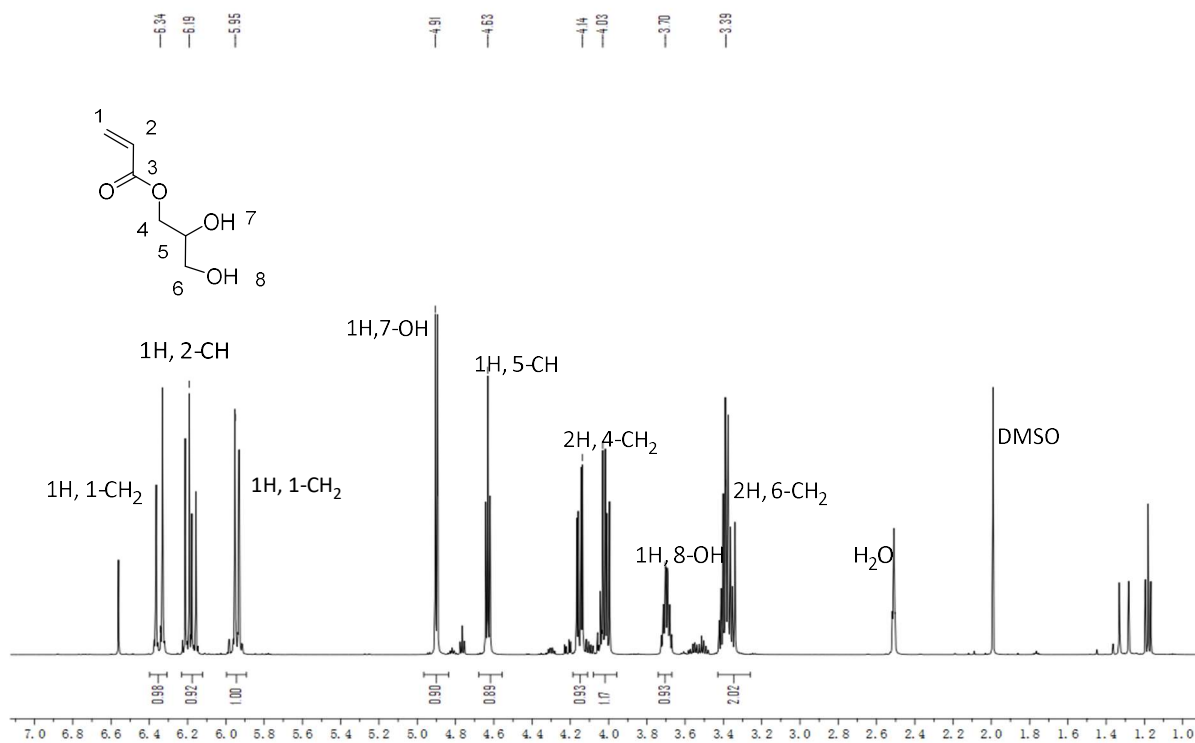
Figure 33. ^{1}H-NMR spectrum of DHPA
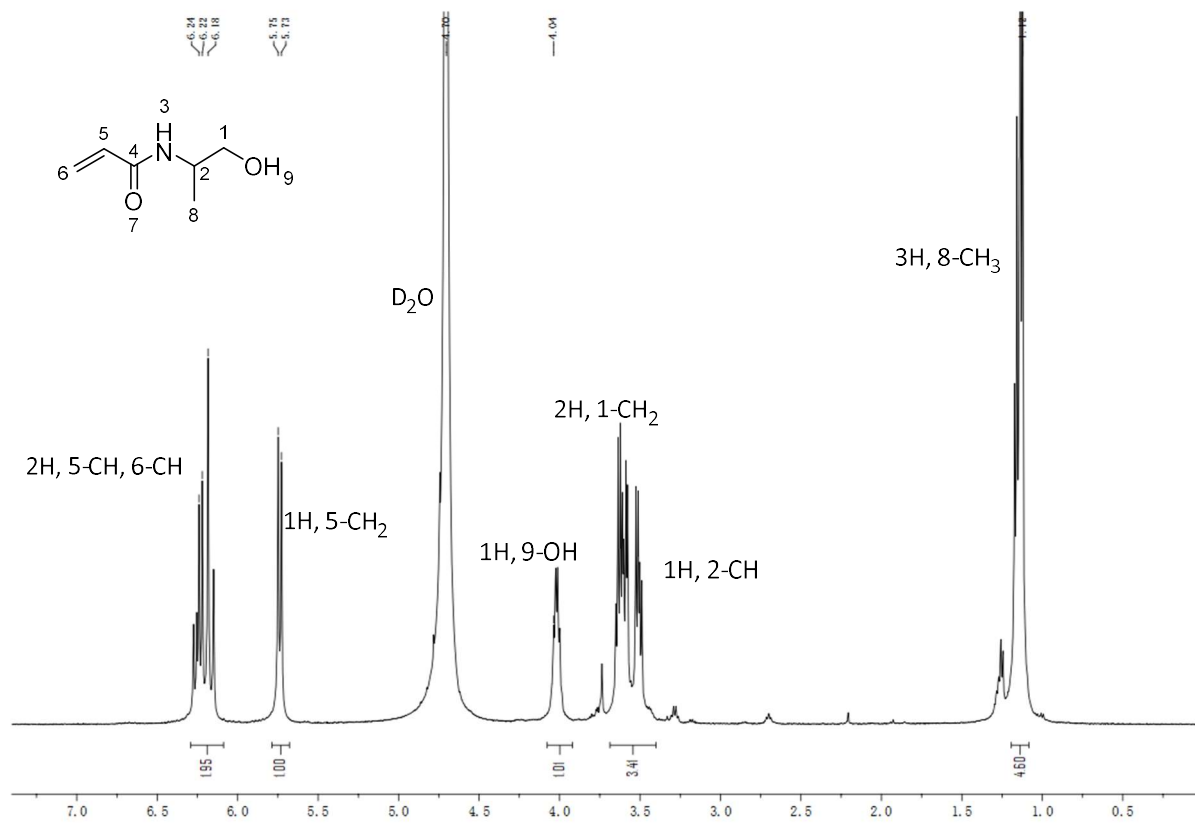
Figure 34. ^{1}H-NMR spectrum of HIPAAm.

Synthesis of 2-vinyl-4,4-dimethylazlacton (VDM) (37)
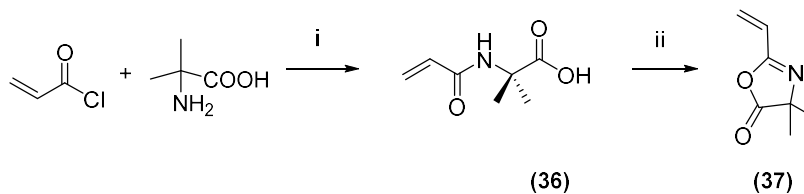
Figure 35. Synthesis of 2-vinyl-4,4-dimethylazlacton (VDM): i) NaOH, BHT, acryloyl chloride, H_2O, 0 °C, 3 h; ii) ethyl chloroformate, TEA, acetone, 0 °C, 3h.

The best-known synthesis of 2-vinyl-4,4-dimethyla-zlactone (VDMA) involves a two-step reaction that is depicted in Figure 36. *N*-Acryloyl-2-methylalanine is first obtained by the reaction between acryloyl chloride and 2-methylalanine in the presence of sodium hydroxide and 2,6-di-*tert*-butyl-*p*-cresol as a polymerization inhibitor. The crude produce was recrystallized from a mixture of ethanol and water with a ratio of 1/1 in volume. The ring-closure reaction proceeded by the addition of ethyl chloroformate and triethylamine.[120] the crude product was purified by distillation under fine vacuum. The product was obtained as a colorless oil. The chemical structure was determined by ^{1}H-NMR spectroscopy with the three vinyl protons which are shifted between 5.96, 6.23 and 6.27 ppm.

4.2 Synthesis of homo- and block copolymer via RAFT

4.2.1 Kinetic investigation of SKA polymerization and end-group functionality by Electrospray Ionization-Ion Mobility Separation-Time of Flight-Mass Spectrometry (ESI-IMS-ToF-MS)
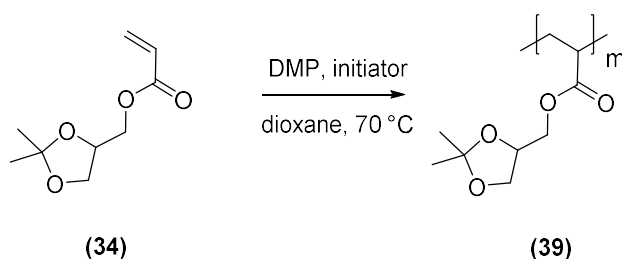
Figure 36. Polymerization of SKA via RAFT.
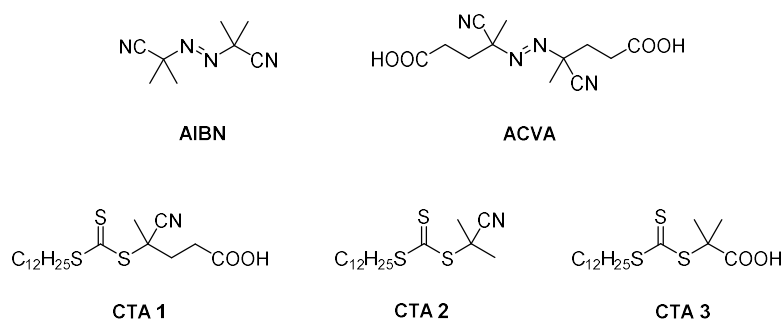
Figure 37. Chemical structures of initiators and RAFT chain transfer agents (CTA) used to synthesize PSKA.

Kinetic studies in this work were focused on the polymerization of SKA to investigate the effects of CTA, and polymerization time. Since only a few publications are currently available referring to the RAFT synthesis of PSKA, we looked for RAFT agents (**CTA 1–3**) to test their efficiency and find out the optimal polymerization conditions.[161–166] The proper selection of the RAFT agent for SKA polymerization is crucial to target well-defined polymers. Three trithiocarbonates were chosen as RAFT agents as they are more suitable for the solketal acrylate that belongs to "more active monomers" (MAMs).[82] In order to find optimal polymerization conditions, we varied also the polymerization time. Monomer conversions, average molar masses and dispersity values are summarized in Table 8.

4. Results and discussion

First experiments (data not shown) were performed with RAFT agents containing the same R leaving group (cyanopentanoic acid) and different Z groups. RAFT polymerization using the trithiocarbonate lead to a PSKA polymer with a lower dispersity value (Đ = 1.36) in comparison with the RAFT polymerization using the dithioesters (Đ = 1.45). It has been generally accepted that aryl derivatives as Z-groups could stabilize the intermediate radical and decrease fragmentation rate of the polymerization. In comparison, the polymerization with the trithiocarbonate is accompanied by the decrease of the dispersity, which is due to faster fragmentation and better equilibrium conditions.

Experiments were then performed with RAFT agents containing the same Z-group (dodecyltrithiocarbonate) but different R leaving groups (**CTA 1-3**, Figure 37). SKA conversion after 1.5 h reaction time with a methylpropionic acid leaving group was higher (77 %) in comparison with a SKA conversion of 20 and 16 % with a cyanoisopropyl and a cyanopentanoic acid leaving group, respectively (Samples PSKA 2-4, Table 8). This is probably due to a higher stability of methylpropanoic acid radicals. Since the propagating radicals of PSKA are primarily good leaving groups control over the polymerization was obtained.

On the other hand, the CTA/initiator ratio is also closely linked to the successful RAFT polymerization with respect to control of molar masses and dispersities. Higher CTA/initiator ratios lead to a better control of the polymerization process arising from a decrease of the number of available radicals for unfavorable side reactions, but often providing a longer polymerization time. First, experiments with a molar ratio of CTA/initiator = 1/0.2 (data not shown) were attempted. PSKA with higher dispersity values are obtained (Đ ≥ 1.3). This result is frequently observed for RAFT polymerization with higher applied initiator concentrations. It is most probably due to an irregular chain growth at relatively high conversion and thus the occurrence of unfavorable termination reactions. To obtain better control of the RAFT polymerization, the amount of initiator was then decreased to the ratio 1/0.15 (Table 8). Dispersity values vary between 1.02 and 1.20 even at high conversions. The lower concentration of the initiator decreases the formation of new radicals at the end of the polymerization (high conversions). Hence, less new chains were initiated and dispersities

remained nearly unaffected. Such result is in full conformity with the requirements of the controlled radical polymerization. Thereby, the polymerization of SKA with the ratio of CTA/initiator of 1/0.15 was successfully accomplished.

Table 8. Polymerization conditions and results for RAFT polymerization of SKA (solvent: 1,4-dioxane; 70 °C; $[SKA]_0/[CTA]_0/[I]_0 = 40/1/0.15$).

Sample	Initiator (I)	CTA	Time (h)	Conv.[a] (%)	$M_{n,NMR}$[b] (g/mol)	$M_{n,SEC}$[c] (g/mol)	$Đ_{SEC}$[c]	$M_{n,MS}$[d] (g/mol)	$Đ_{MS}$[d]
PSKA 1	ACVA	1	1.5	12.8	1,300	700	1.02	870	1.07
			2.0	12.3	1,300	800	1.02	910	1.07
			2.5	31.8	2,800	1,500	1.11	2,100	1.06
			3.0	65.8	5,300	3,100	1.14	3,200	1.07
			3.5	69.4	5,600	4,100	1.16	4,500	1.07
			4.0	80.4	6,400	4,600	1.18	4,500	1.07
PSKA 2	AIBN	1	1.5	15.8	1,600	800	1.04	850	1.08
			2.0	31.0	2,700	1,900	1.13	2,100	1.10
			2.5	53.8	4,400	3,400	1.14	4,000	1.06
			3.0	65.4	5,300	4,100	1.17	5,000	1.06
			3.5	69.7	5,600	4,400	1.18	5,400	1.07
			4.0	81.7	6,500	4,600	1.20	5,500	1.08
PSKA 3	AIBN	2	1.5	19.6	1,800	900	1.07	950	1.07
			2.0	48.5	4,000	2,700	1.13	3,000	1.07
			2.5	68.0	5,400	4,100	1.16	4,400	1.06
			3.0	78.5	6,200	4,600	1.18	5,200	1.07
			3.5	78.9	6,200	4,900	1.19	5,400	1.07
			4.0	86.0	6,800	5,700	1.12	5,500	1.07
PSKA 4	AIBN	3	1.5	77.0	6,100	4,400	1.17	5,800	1.08
			2.0	79.6	6,300	4,700	1.19	5,800	1.07
			2.5	80.8	6,400	4,800	1.22	5,400	1.10
			3.0	90.0	7,100	5,100	1.21	5,500	1.10
			3.5	91.1	7,200	5,400	1.18	5,800	1.10
			4.0	89.2	7,000	5,500	1.18	5,800	1.09

[a] Determined using ^{1}H-NMR spectroscopy

[b] The molecular weight was calculated from ^{1}H NMR data using the following equation: $M_{n,NMR} = [SKA]_0/[CTA]_0 * Conv._{SKA} * M_{SKA} + M_{CTA}$

[c] Determined by SEC in THF with PMMA standard calibration

[d] Determined by ESI-ToF-MS
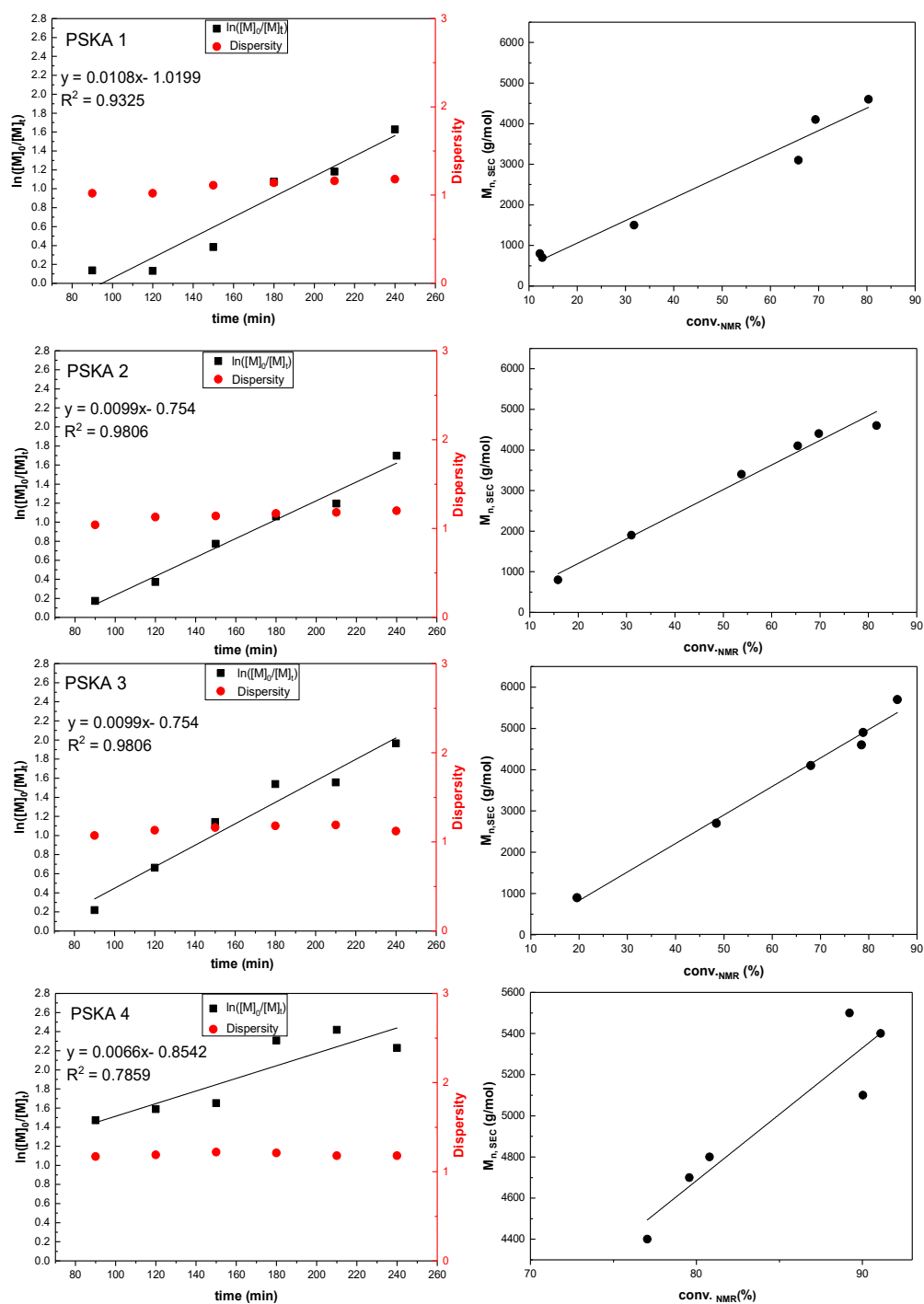
Figure 38. Kinetic data for the RAFT polymerization of SKA using different CTAs (PSKA 1-4). Left: plots of $\ln([M]_0/[M]_t)$ (■) and dispersity (●) versus polymerization time; right: plots of molar mass ($M_{n,SEC}$) versus conversion (conv.$_{NMR}$). Results of linear fits are given in the diagrams.[167] (Reprinted from [186] with permission from John Wiley and Sons (2018))

The molar masses increased linearly with conversion. Number average molar masses obtained by SEC analysis were comparable with the NMR results at the first 4 h of the polymerization (Figure 39) indicating that the end groups of the CTAs are present in the polymers. Kinetic data demonstrate the influence of R groups on the polymerization rate. For the used CTAs transfer coefficients of R groups decreased in the order: cyano isobutyl radical (CTA 2) > cyano proponic acid radical radical (CTA 1) > 2-carboxy-2-propyl radical (CTA 3).[82] Generally tertiary cyanoalkyl radicals (CTA 1 and CTA 2) gave a good control over the polymerization of "more activated" monomers such as methacrylamides.[81] Propagating radicals with a terminal SKA monomer are highly reactive in radical addition and could effectively be controlled with tertiary cyanoalkyl radicals whose reinitiation rate is a bit lower than for CTA 3. The retardation of the polymerization is especially pronounced in combination with an initiator that decomposes a bit slower (ACVA) as can be seen for PSKA 1. 2-carboxy-2-propyl radical (CTA 3) with a lower transfer coefficient, being as well a suitable radical leaving group with respect to the PSKA propagating radical, resulted hence in a significant acceleration of polymerization rate. Polymerization was finished after 1.5 h. Hence, kinetic data were collected for the first hour of polymerization (Table 9, Figure 39). Molar masses increased linearly with conversion while maintaining a low dispersity. With this study, it was possible to show that the four presented systems are suitable for the RAFT polymerization of SKA.

Table 9. Polymerization conditions and results for RAFT polymerization of SKA (solvent: 1,4-dioxane; 70 °C; $[SKA]_0/[CTA]_0/[I]_0$ 40/1/0.15) during the first hour of reaction.

Sample	CTA	Initiator (I)	Time (h)	Conv.[a] (%)	$M_{n, SEC}$[c] (g/mol)	$M_{n, NMR}$[b] (g/mol)	$Đ_{SEC}$[c]	$M_{n, MS}$[d] (g/mol)	$Đ_{MS}$[d]
PSKA 5	3	AIBN	0.25	24.8	1,700	2,200	1.14	2,700	1.07
			0.5	36.4	2,500	3,100	1.15	4,300	1.08
			0.75	46.7	3,500	3,800	1.16	4,500	1.07
			1.0	67.2	4,200	5,400	1.18	5,500	1.07

[a] Determined using ^{1}H-NMR spectroscopy

[b] The molecular weight was calculated from ^{1}H-NMR data using the following equation: $M_{n,NMR} = [SKA]_0/[CTA]_0 * Conv._{SKA} * M_{SKA} + M_{CTA}$

[c] Determined by SEC in THF with PMMA standard calibration

[d] Determined by ESI-ToF-MS
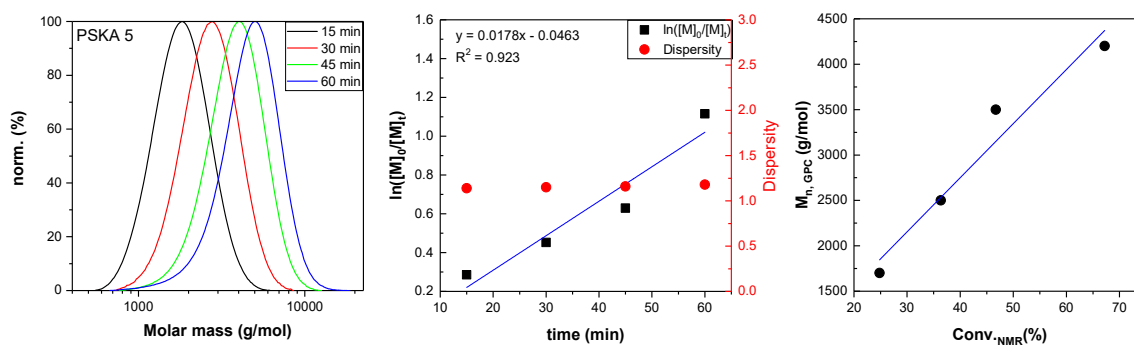
Figure 39. Kinetic data for the RAFT polymerization of SKA (PSKA 4) within 90 min. Left: plots of $\ln([M]_0/[M]_t)$ (■) and dispersity (●) versus polymerization time; right: plots of molar mass ($M_{n,SEC}$) versus conversion (conv.$_{NMR}$). Results of linear fits are given in the diagrams.[167] (Reprinted from [186] with permission from John Wiley and Sons (2018))

In order to investigate the livingness (chain end distributions) of the PSKA synthesized by RAFT polymerization in detail, ESI-IMS-ToF-MS was employed. For this study PSKA 3 was chosen since the structural complexity is lowest in this system (R group is identical with initiator fragment). Figure 41 shows a typical ESI-ToF-MS spectrum for PSKA obtained after 3 h of polymerization (PSKA 3, 79 % SKA conversion, Table 8). The signals in the area between 500-3,000 Da were continuously distributed and a pattern with a regular gap at a distance of 186.21 Da or one-half or one-third and even one-quarter of this value can be recognized, which results from the monomer SKA. However, the spectrum shows the overlap of signals reforming to differently charged species (+1, +2, +3 and +4), making it difficult to evaluate each pattern. A conclusive analysis of the series of original ESI measurement without the separation of charge states is quite complicated. Therefore, the coupling of the ESI with IMS is adaptable to simplify the mass spectrum (Figure 40).[168,169] First advantage of the ESI-IMS combination is the decrease of noise in the spectrum. By comparing the spectra without and with IMS, some other changes were visible as shown in Figure 41. Fundamentally, the measurement differs in the intensity of the signal. Due to the increased pressure in the IMS cell (4.26 mbar compared to 1.23×10^{-6} mbar in ToF unit) the transmittance of the ions is decreased. In the ESI-IMS-ToF-MS the visibility of the singly charged series is increased, while the other charge states seem to be suppressed, which again can be attributed to different transmittance of the ions. The

appearance of all series is maintained after IMS. After assigning the series in the separated spectra final molar mass calculations could be done from the ESI spectrum only.

A typical drift time spectrum of PSKA is shown in Figure 41. For species with the same charge state the collision cross section increases with increased molar mass. Hence, the drift time increase as well. Such series can be identified by a mostly linear correlation of signals. For a fixed m/z ratio species with larger collision cross section (CCS) have increased charge density. The effect of higher charge states on the CCS overrules the dimension dependence in the IMS experiment. Hence, high charged molecules show lower drift times.[170] The differences are usually so large that a series separation is possible; spectra of signals referring to charge state can be extracted. Clear distributions of PSKA species according to the shape and size of individual molecules up to quadruple charged ion peaks were visible. For instance, the series C with triply charged ion in the m/z range between 1,600 Da and 3,000 Da showing that the synthesized PSKA reaches molar masses up to 9,000 Da. This result is consistent with the SEC data (PSKA 3, polymerization 3 h, 79 % conversion, Table 8). Different signal correlations according to the charge states in drift time spectra could be identified and the corresponding MS spectra were extracted and used to further evaluate the chain end groups.
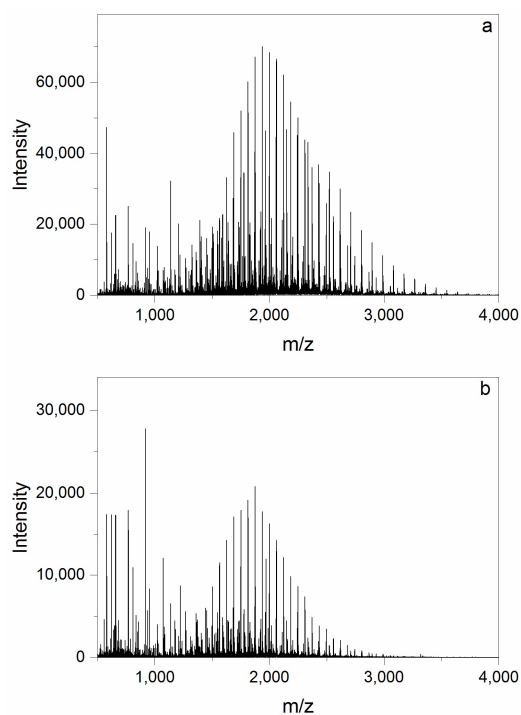
Figure 40. ESI-ToF-MS spectrum without IMS (a) and with IMS (b) of PSKA (PSKA 3, polymerization 3 h, 79 % SKA conversion, Table 8). (Reprinted from [186] with permission from John Wiley and Sons (2018))
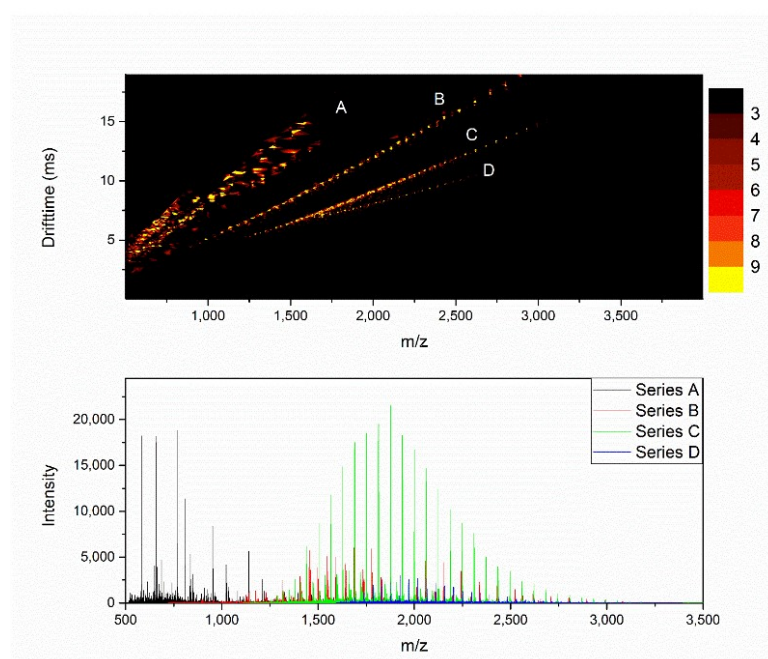
Figure 41. The upper diagram depicts the drift spectra after ion mobility separation of sample PSKA 3 (polymerization 3 h, 78 % conversion, Table 8), where the drift time is plotted versus the m/z-values. The lower diagram shows the raw ESI mass spectra of the same sample. (Series A: +1 charged species. B: +2 charged species, C: +3 charged species. and D: +4 charged species). (Reprinted from [186] with permission from John Wiley and Sons (2018))
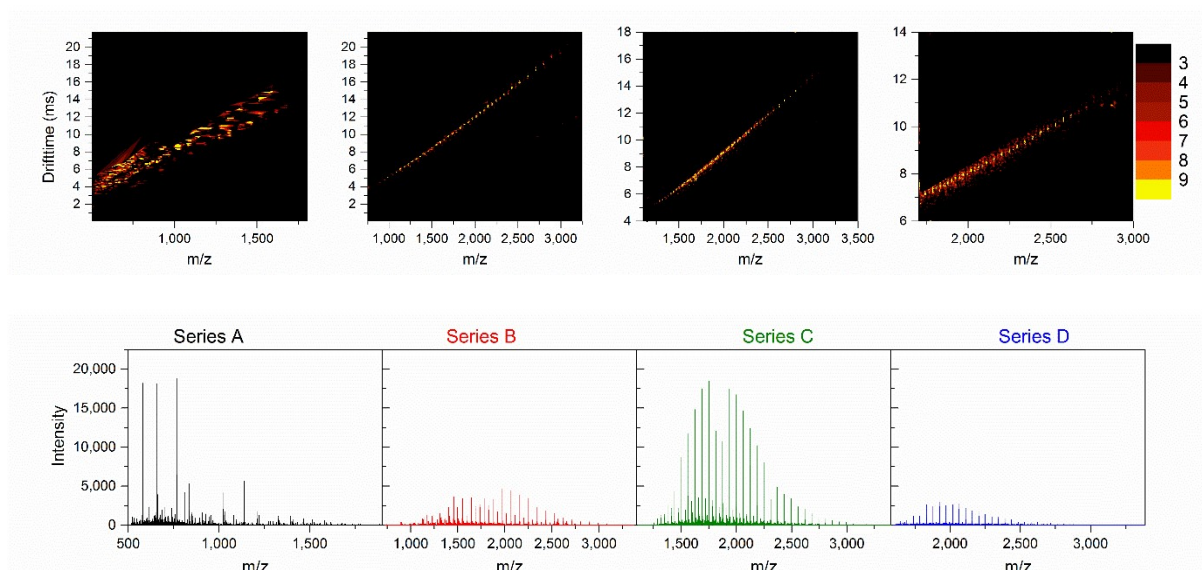
Figure 42. Separated series of the IMS-data for PSKA (sample PSKA 3, polymerization 3 h, 79 % conversion, Table 8), which are outlined in Figure 41, and the resulting simplified mass spectra. (Reprinted from [186] with permission from John Wiley and Sons (2018))

The control over the chain-end functionality is depended on the mechanism of the polymerization. The versatility of the RAFT process associated with different RAFT agents rely on the degenerative transfer allowing the control of chain-end functionalities. This means that the chain-end is constituted by the R-group as well as the Z-group from the RAFT agent. However, dead chains directly related to chain termination by disproportionation and combination cannot be avoided. Further, other side reactions might occur with prolonged reaction time. Based on the IMS technology all of the charged species could be separated (Figure 42). In the simplified mass spectra, species with different end groups were detected and summarized in Table 10. The singly charged species (+1) consisted of small molecules having molar masses below 2,000 g/mol. They can essentially be associated with PSKA dead chains with loss of the end groups. In all spectra the intended polymer structure (S1) can be found, whose intensity and spectral content increases with higher charge states. This series is started by the initiator or the R group of the RAFT-reagent, which both lead to the same α end group. Therefore, it can be assumed that all other series of this sample are related to dead chains. The intensity of triple charge species is significantly higher than for the other species; hence, they can be regarded as main species. The majority of peaks in this part contains both
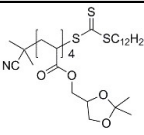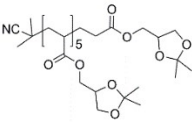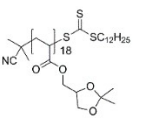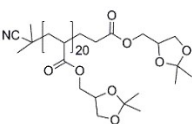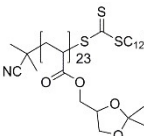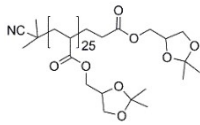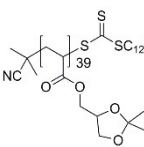
R and Z group (series S1) proving the controlled character of the polymerization. With an ongoing reaction, it can be observed that termination reactions become more prominent occurrence of series S2 and S3). While S3 could be assigned to the saturated termination product no meaningful assignment could be found for S2 (residue of end groups 78.01 g/mol). Their intensity increases in the lower mass range of the samples. These results are in accordance with the mechanism of RAFT polymerization. These indications could be obtained in all other samples as well. Especially in ranges of low molar masses a high number of different termination reactions are visible. After assigning all series the molar masses could be calculated. For PSKA 3 (polymerization 3 h, 79 % conversion, Table 8) M_n with IMS was 4,700 g/mol and without 5,200 g/mol. This deviation can be attributed to the decreased transmittance of the IMS especially for higher molar mass chains. All molar masses are hence calculated from ESI mass spectra without IMS. The results are in good agreement with the results obtained from SEC and NMR (Tables 8 and 9).
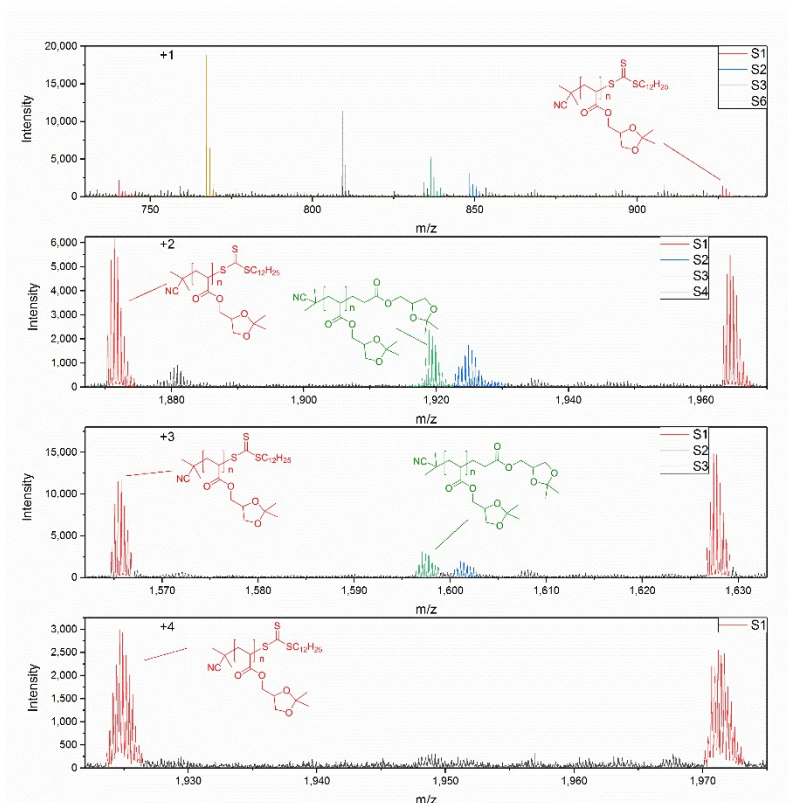
Figure 43. Except of ESI mass spectra of differently charged species agter extraction from IMS for PSKA 3 (polymerization 3 h, 79 % conversion, Table 8). (Reprinted from [186] with permission from John Wiley and Sons (2018))

4. Results and discussion

Table 10. End group analysis from ESI-IMS-ToF spectrum of PSKA 3 (polymerization 3 h, Table 8). (Reprinted from [186] with permission from John Wiley and Sons (2018))

	Series	Structure	Sum formula	m_{theo}/z [Da][a]	m_{exp}/z [Da]	Δm [ppm]
	S1		$C_{53}H_{87}O_{16}NS_3Na$	1112.509	1112.513	3.6
	S2		-	-	1034.652	
A / +1	S3		$C_{49}H_{77}O_{20}NNa$	1022.494	1022.503	8.8
	S5		-	-	1094.534	
	S6		-	-	953.436	
	S1		$C_{179}H_{283}O_{72}NS_3Na_2$	1870.374	1870.411	19.8
B / +2	S2		-	-	1922.919	
	S3		$C_{184}H_{286}O_{80}NNa_2$	1918.411	1918.398	-6.8
	S1		$C_{224}H_{353}O_{92}NS_3Na_3$	1564.728	1564.736	5.1
C / +3	S2		-	-	1600.423	
	S3		$C_{229}H_{357}O_{100}NNa_3$	1596.753	1596.752	0.6
D/ +4	S1		$C_{386}H_{577}O_{156}NS_3Na_4$	1923.650	1923.686	18.7

[a] The molecular weight was calculated using the following equation: $m/z = (M_{[CTA]}+M_{[SKA]} * x + M_{[Na+]} * n)/n$ ($n=$ +1, +2 or +3) with x as the degree of polymerization

4.2.2 Synthesis of PDHPA-*b*-PNIPAAm
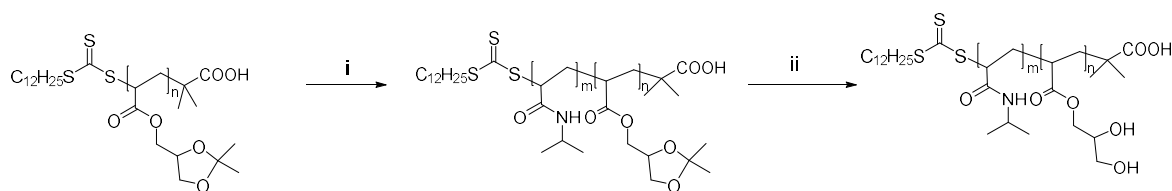
Figure 44. Synthesis of block copolymers by RAFT-Polymerization of SKA and NIPAAm: i) NIPAAm, 1,4-dioxane, AIBN, 70 °C; ii) HAc, H_2O, 6 h, 90 °C

The obtained PSKA homopolymer were used as macromolecular RAFT agent (macro-CTA) for the RAFT polymerization of NIPAAm to provide access to PSKA-*b*-PNIPAAm block copolymers. To prove the "living" or controlled feature of the RAFT polymerization using PSKA-based macro-CTA (M_n = 5000 g/mol, Đ = 1.19, PSKA 6, Table 11) the sequential block copolymerization with NIPAAm was performed. The RAFT polymerization of NIPAAm was performed using AIBN as radical source in 1,4-dioxane at 70 °C ([NIPAAm]$_0$/[PSKA macro-CTA]$_0$/[AIBN]$_0$ = 50/1/0.15). The molar masses and dispersity values of the resulting copolymers were determined by SEC (Table 11). Under this condition, excellent blocking efficiency with over 90 % monomer conversion was observed. Moreover, as shown by SEC analysis (Figure 45), block copolymer formation led to a shift in the molar mass distribution towards higher molar masses with no observable homopolymer traces. A well-defined block copolymer PSKA-*b*-PNIPAAm 6 with a low Đ as well as a unimodal molar mass distribution (M_n = 10,800 g/mol, Đ = 1.21, Table 12) was obtained verifying the "living" feature of RAFT block copolymerization.

Table 11. Macromolecular characteristics of PSKA before and after chain extension with NIPAAm and subsequent hydrolysis.

Polymer	Conv[a] (%)	M_n[b] (g/mol)	Đ[b]
PSKA 6	95	5,000	1.19
PSKA-*b*-PNIPAAm	97	10,800	1.21
PDHPA-*b*-PNIPAAm	99	13,000	1.22

[a] Determined using ^{1}H-NMR spectroscopy

[b] Determined by SEC in DMAc at 50 °C with PMMA standard calibration
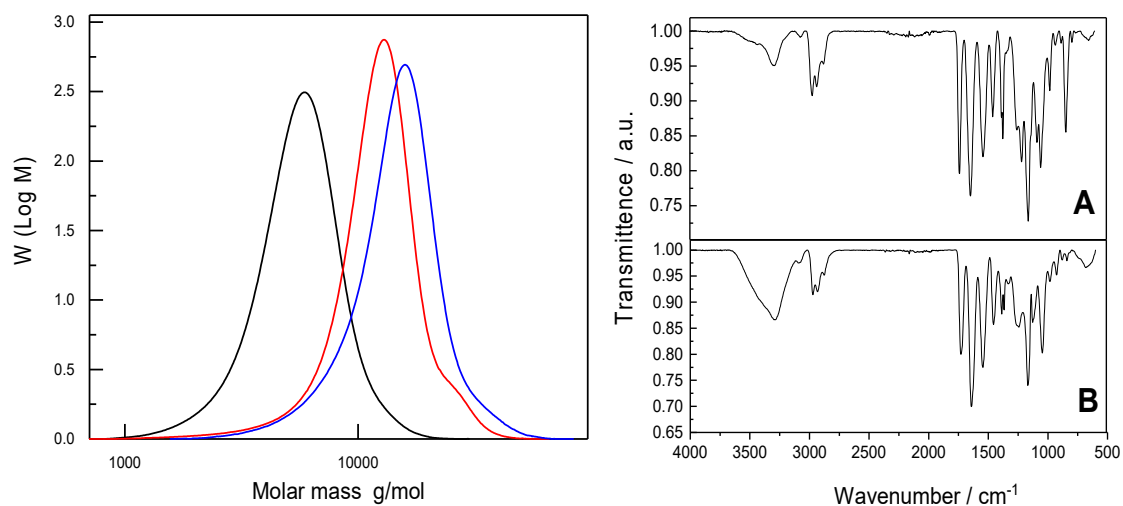
Figure 45. Left: overlaid SEC traces of PSKA 6 (-), PSKA-*b*-PNIPAAm (-) and the deprotected amphiphilic PDHPA-*b*-PNIPAAm block copolymer (-); right: superposition of FTIR spectra of (A) PSKA-*b*-PNIPAAm and (B) PDHPA-*b*-NIPAAm block copolymers. (Reprinted from [186] with permission from John Wiley and Sons (2018))
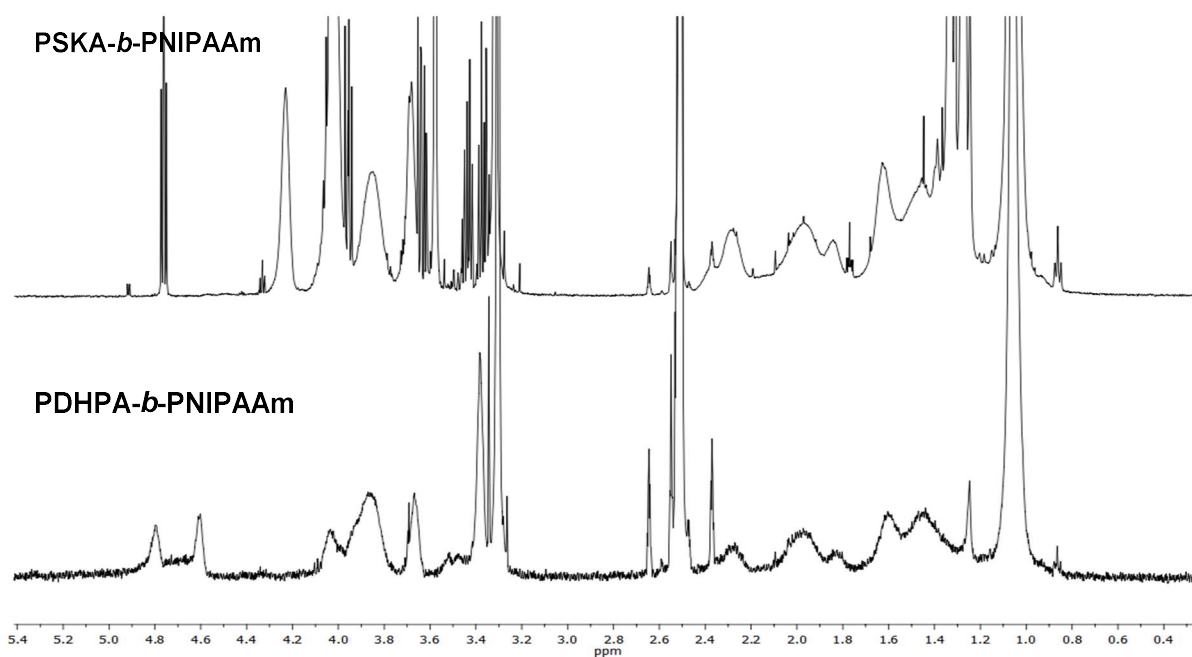
Figure 46. ^{1}H-NMR spectra of the copolymer: PSKA-*b*-PNIPAAm (upper) and PDHPA-*b*-PNIPAAm (lower) after hydrolysis (Reprinted from [186] with permission from John Wiley and Sons (2018))

The regeneration of the diol group was achieved by treating the PSKA-*b*-PNIPAAm copolymer with glacial acetic acid and water in THF solution under reflux for 6 h. The deprotection of the 1,2-diol was studied by NMR and IR spectroscopy. Figure 46 shows the ^{1}H-NMR spectra of the block copolymers before and after deprotection. The characteristic signals of the diol group at

4.61 and 4.79 ppm and at the same time the absence of the characteristic signals of the acetal-protecting group at 1.27 and 1.33 ppm can be observed. Signals corresponding to the methyl group from dodecyltrithiocarbonate and to the methyl protons of PNIPAAm units appear at 0.86 ppm and at 1.06 ppm, respectively. No change in the integral ratio of those two peaks was seen before and after the hydrolysis reaction. It is worth noting that the functional groups of the RAFT agent (Z-group) were also stable to this hydrolysis condition.

Figure 45 right shows the superposition of FTIR spectra before and after deprotection of the PSKA-*b*-PNIPAAm block copolymer. The apparent deformation band at 3300 cm^{-1} arises from hydrogen bonding of the carbonyl group with diol groups in the deprotected copolymer. The peak at 1380 cm^{-1} reforming to the stretching absorption of the methyl groups of the dioxolane ring diminished after deprotection. Moreover, the presence of trithiocarbonate (Z-group) as an end group was also shown by FT-IR spectra. Strong absorption peaks at around 1050 cm^{-1} due to C=S stretching were detected. Based on the results from NMR and FTIR spectra, complete hydrolysis of the block copolymer was achieved without loss of the end groups, thus obtaining the temperature sensitive amphiphilic block copolymer PDHPA-*b*-PNIPAAm.

With this method, the relative block length ratio between the hydrophilic PDHPA and the hydrophobic PNIPAAm block could be varied from 1:1 to 1: 6.5. Dispersity values of the block copolymers differ between 1.3 and 1.6 with number average molar masses between 10,000 and 40,000 g/mol (shown in Table 12).

Table 12. Macromolecular characteristics of the synthesized PDHPA-*b*-PNIPAAm block copolymers.

Polymer	Targeted block lengths	Relative block length ratio (PDHPA/PNIPAAm)[a]	Đ$_{GPC}$ [b]	M$_{n,GPC}$ (g/mol) [b]
PDH-PN-1	PDHPA$_{50}$-*b*-PNIPAAm$_{50}$	1: 1.30	1.25	15,000
PDH-PN-2	PDHPA$_{50}$- *b*-PNIPAAm$_{100}$	1: 1.82	1.58	15,300
PDH-PN-3	PDHPA$_{50}$- *b*-PNIPAAm$_{200}$	1: 3.28	1.40	30,000
PDH-PN-4	PDHPA$_{50}$- *b*-PNIPAAm$_{300}$	1: 3.96	1.66	29,200
PDH-PN-5	PDHPA$_{50}$- *b*-PNIPAAm$_{325}$	1: 5.90	1.38	39,600

[a] Determined using ^{1}H-NMR spectroscopy

[b] Determined by SEC in DMAc at 50 °C with PMMA standard calibration

In order to synthesize PDHPA-*b*-PNIPAAm block copolymers, 2,3-dihydroxypropyl acrylate (DHPA) was also used as a hydrophilic monomer for RAFT polymerization. The process was carried out using CDPA as RAFT-CTA in ethanol. After the polymerization, the crude polymer was subjected to dialysis against pure water and subsequent freeze-drying. SEC analysis revealed a much higher molar mass (M_n= 13,000 g/mol, Đ = 9) than expected from theoretical values based on monomer to CTA ratio (40/1). Compared to the kinetic studies on the RAFT polymerization of SKA, polymerization of DHPA via RAFT shows a poor control of the polymerization and the apparent deviation from an ideal RAFT process is attributed to the free hydroxyl groups in the DHPA monomer: a crosslinking process may occur during the polymerization in polar media accompanied by irreversible intra- and intermolecular radical recombination. Due to the poor control of the polymerization, DHPA is not a suitable monomer to synthesize amphiphilic block copolymers.

4.2.3 Synthesis of PHIPAAm homopolymers and PHIPAAm-*b*-PNIPAAm block copolymers
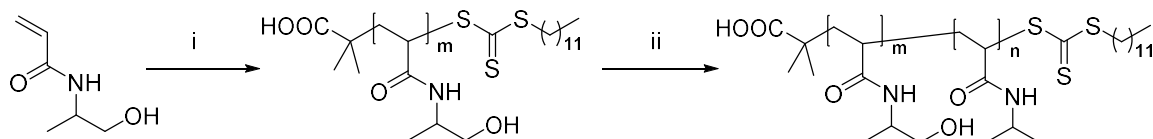
Figure 47. Synthesis of block copolymers by RAFT-Polymerization of HIPAAm and NIPAAm: i) DMP, DMF, AIBN, 70 °C; ii) NIPAAm, DMF, AIBN, 70 °C.

For the synthesis of the second amphiphilic block copolymer, *N*-(2-hydroxyisopropyl) acrylamide was employed as monomer. *N*-(2-hydroxyisopropyl) acrylamide was firstly reported by a Japanese group in 2005 for the preparation of a novel functional temperature-responsive copolymer by random copolymerization with NIPAAm.[153] In this study, the obtained polymer exhibited a phase transition in response to temperature changes in aqueous solution. Their thermoresponsive behavior was not affected by the pH-value, even with a higher content of hydrophilic comonomer. Due to their similar chemical structure, the two monomers showed a similar reactivity in the copolymerization, making it possible to introduce the HIPAAm

comonomers into the NIPAAm-based copolymer without losing the interesting features of both monomers: hydrophilic effect and thermoresponsive behavior.[171,172] Based on these chemical and physical characteristics, the HIPAAm has attracted great interest as a hydrophilic comonomer for acrylamide-type thermoresponsive block copolymers.[171]

In the present work, the synthesis of PHIPAAm-*b*-PNIPAAm block copolymers was carried out using RAFT polymerization. Crucial for the control of the RAFT polymerization is the selection of a suitable RAFT-CTA for the monomers and finding the proper reaction conditions.[82] For the RAFT-polymerization, the acrylamide-type monomer NIPAAm belongs to the more activated monomers (MAM) which can be polymerized in a controlled fashion trithiocarbonates such as DMP.[81,173] Compared to NIPAAm, HIPAAm has a similar chemical structure with an increased hydrophilicity attributed to the presence of the hydroxyl group. Therefore, a homopolymer of PHIPAAm was firstly prepared using DMP as RAFT-CTA at 70 °C. Due to the solubility of both monomer and polymer, DMF was used as solvent instead of 1,4-dioxane. PHIPAAm was obtained after freeze-drying as a white powder and used as macro-CTA for the subsequent block copolymerization under the same reaction conditions. In size exclusion chromatography (SEC) analysis, the PHIPAAm homopolymer showed a number average molar mass M_n = 7,500 g/mol and a dispersity of 1.94, based on polystyrene calibration. By analogy to the polymerization of DHPA. the moderate dispersity of PHIPAAm may be explained with the branching of the polymer chain based on the interaction between free hydroxy groups of monomers and the carbonyl acid end group of RAFT-CTA. After adding the second monomer NIPAAm, a significant increase of the number average molar mass to M_n = 47,000 g/mol could be observed, resulting in a chain extension by a factor of approximately 5 according to the PHIPAAm block. The block copolymer exhibited a higher dispersity of Đ = 3.58, which is not consistent with the features of a controlled polymerization. The SEC trace of the block copolymer shows a slight shoulder appearing at a molar mass around 10,000 g/mol attributed to dead chains from inactive macro-RAFT agent (Figure 48). A partial inactivation of the PHIPAAm-CTA cannot be neglected, which might be the reason for the significant increase in dispersity of the block copolymer.
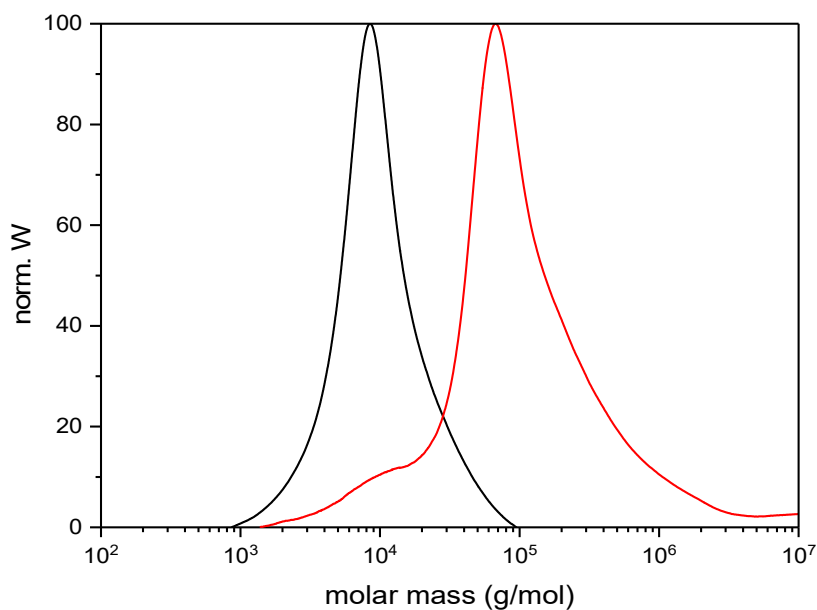
Figure 48. overlaid molar mass distributions of PHIPAAm (**-**) and PHIPAAm-*b*-PNIPAAm (**-**), determined by SEC in DMAc at 50 °C with PMMA standard calibration.

4.2.4 Synthesis of PDMAA homopolymer and PDMAA-*b*-PNIPAAm block copolymers
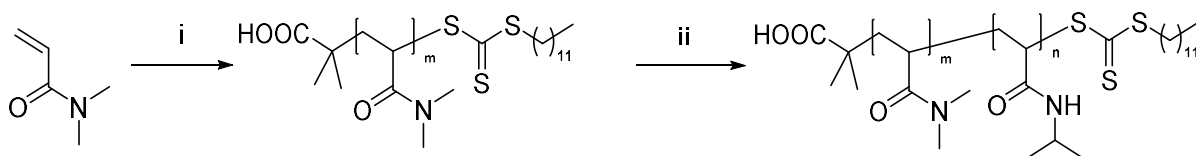
Figure 49. Synthesis of block copolymers by RAFT-Polymerization of DMAA and NIPAAm: i) DMP, 1,4-dioxane, AIBN, 70 °C; ii) NIPAAm, 1,4-dioxane, AIBN, 70 °C.

In this work, poly (*N,N*-dimethylacrylamide) (PDMAA) was also applied as another water-soluble polymer. PDMAA was extensively studied in the context of interpolymer complexations by cooperative hydrogen bonding,[174–176] and the synthesis of stimuli-responsive polymer networks[177] and hydrogel.[178] Furthermore, several scientific and practical applications based on PDMAA were investigated, including polymeric catalysts for two phase reactions[179] and the design of drug release systems.[180] In comparison to NIPAAm, DMAA is a disubstituted acrylamide with one methylene group less than NIPAAm. Consequently, PDMAA shows a

higher hydrophilicity than PNIPAAm, so that no LCST behavior could be observed for PDMAA in water below 100 °C.[181] In designing homo- and copolymers of PDMAA serval methods were employed to obtain the different kinds of polymers. Well-defined PDMAA homo polymers with high molar masses and low dispersities were synthesized by ATRP using methyl 2-chloropionate as initiator and a CuCl/Me$_6$tren complex as catalyst.[182] Moreover, PDMAA homo polymers were successfully employed as macroinitiators for block copolymer synthesis. A comparative study of RAFT polymerization of DMAA utilizing various chain transfer agents was published by Donovan et al.[183] By adjusting the initial ratio CTA/I a good control of the DMAA polymerization could be demonstrated. The kinetic data exhibited a first-order relationship for monomer conversion with time. The synthesis of nanostructured hydrogels was reported by An et al. using facile RAFT precipitation polymerization.[184] For this purpose, cross-linked nanoparticles were produced using amphiphilic macro-CTAs. Spontaneous self-assembly yielded core-shell structures with excellent control over the RAFT precipitation polymerization process.

For the synthesis of linear PDMAA-*b*-PNIPAAm block copolymers in the present work, RAFT polymerization was employed using DMP in dioxane at 70 °C. PDMAA homopolymer was obtained as a light-yellow powder after precipitation. It was used as macro-CTA for chain extension with NIPAAm to form the amphiphilic block copolymers. SEC analysis showed two PDMAA homopolymers with targeted degrees of polymerization of PD = 50 and PD = 80. The SEC traces were monomodal with narrow dispersities (Đ = 1.14 – 1.15, as shown in Table 13), indicating good control over the DMAA polymerization. Moreover, the number average molar mass increased with higher monomer/CTA ratios, which is also in good agreement with the features of RDRP. In order to further evaluate the ability of copolymerization, PDMAA homopolymers were used as macro-RAFT agents for chain extension with NIPAAm to produce block copolymers of different block length ratios. As shown in Table 13, after chain extension the dispersity increased from Đ = 1.14 – 1.15 to Đ = 1.53 – 1.62. In the SEC traces (Figure 50), a significant shoulder appeared in the lower molar mass range. This shoulder can be clearly attributed to unreacted homopolymer chains. The relative block length ratios are consistent

with the targeted block lengths, further proving good control over block copolymerization. The partial inactivation of PDMAA chains by the undesired termination reactions (recombination or disproportionation) cannot be neglected (approximately 10 %).

Table 13. Macromolecular characteristics of PDMAA homopolymers and PDMAA-*b*-PNIPAAm block copolymer

Polymer	Targeted block lengths	Relative block length ratio [a] (PDMAA/ PNIPAAm)	$Đ_{GPC}$ [b]	$M_{n,GPC}$ (g/mol) [b]
PD-1	PDMAA$_{50}$	1: -	1.14	5,000
PD-2	PDMAA$_{80}$	1: -	1.15	6,700
PD-PN-1	PDMAA$_{50}$-*b*-NIPAAm$_{100}$	1: 1.84	1.53	12,800
PD-PN-2	PDMAA$_{50}$- *b*-NIPAAm$_{200}$	1: 2.64	1.59	16,100
PD-PN-3	PDMAA$_{80}$- *b*-NIPAAm$_{320}$	1: 4.97	1.62	28,600
PD-PN-4	PDMAA$_{50}$-*b*-NIPAAm$_{50}$	1.84: 1	1.24	8,000
PD-PN-6	PDMAA$_{50}$-*b*-NIPAAm$_{50}$	2.09: 1	1.18	6,500

[a] Determined using ^{1}H-NMR spectroscopy

[b] Determined by SEC in DMAc at 50 °C with PMMA standard calibration
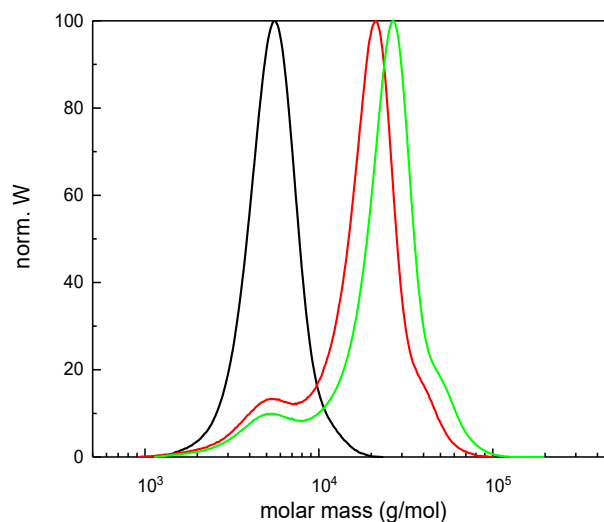
Figure 50. Overlaid molar mass distributions traces of PDMAA$_{50}$(-), PDMAA$_{50}$-*b*-PNIPAAm$_{100}$ (-), PDMAA$_{50}$-*b*-NIPAAm$_{200}$ (-), determined by SEC in DMAc at 50 °C with PMMA standard calibration

4.2.5 Synthesis of PEG-CDPA macroinitiator and PEG-*b*-PNIPAAm
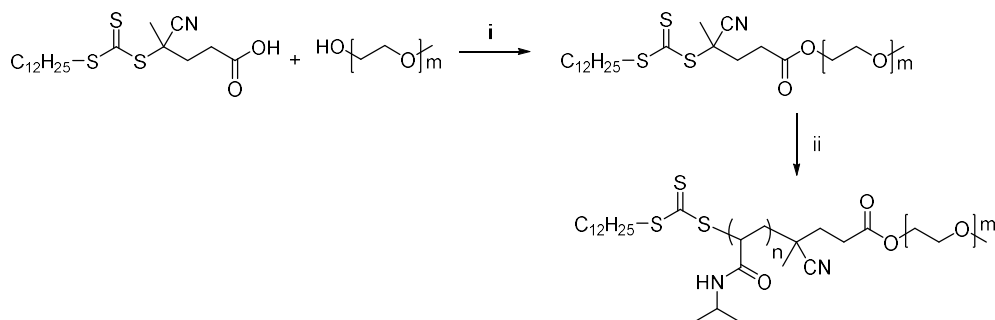
Figure 51. Synthesis of a PEG-based macro-RAFT for block copolymerization with NIPAAm: i) DIC, DMAP, chloroform, r. t.; ii) NIPAAm, 1,4-dioxane, AIBN, 70 °C.

As the third series of thermo-responsive amphiphilic block copolymers block copolymers from PEG and PNIPAAm were prepared by RAFT polymerization. Poly(ethylene glycol) (PEG)-containing copolymers are widely used in the field of nanopharmaceuticals, because of their biocompatibility.[32] The combination of PEG together with thermo-responsive polymers recently attracted a lot of attention as drug delivery systems.[185–187]

Block copolymers of PEG and PNIPAAm were synthesized according to the route shown in Figure 51. A Steglich esterification reaction was applied to obtain a PEG-based macro-CTA. The free hydroxyl group from PEG monomethyl ether (M_n = 5,000 g/mol) can be reacted with an excess of 4-cyano-4-[(dodecylsulfanylthiocarbonyl)sulfanyl]pentanoic acid (CDPA).[188] By precipitation, the excess of CDPA can be readily removed. After drying under vacuum the PEG-modified CDPA was analyzed by ^{1}H-NMR spectroscopy and SEC in order to evaluate the end group functionality of the PEG. A triplett at δ = 0.88 ppm corresponds to methyl protons at the chain end of the dodecylsulfanylthiocarbonyl moiety and the singulett peak at δ = 3.37 ppm corresponds to the methyl protons of the ethylene oxide methyl ether (three protons in Figure 53). From the integrated areas under these two peaks, the modification efficiency of PEG and CDPA was calculated to be 91 % and the PEG chain consisted of 100 ethylene oxide units. The 9 % unreacted PEG chains may attribute a broad molar mass distribution by the copolymerization.

Moreover, the SEC chromatogram showed a unimodal molar mass distribution as well as a low

Đ with a number average molar mass of M_n = 8,900 g/mol. This value is higher than expected, which was due to the SEC PMMA standard calibration in the SEC analysis (Figure 53).
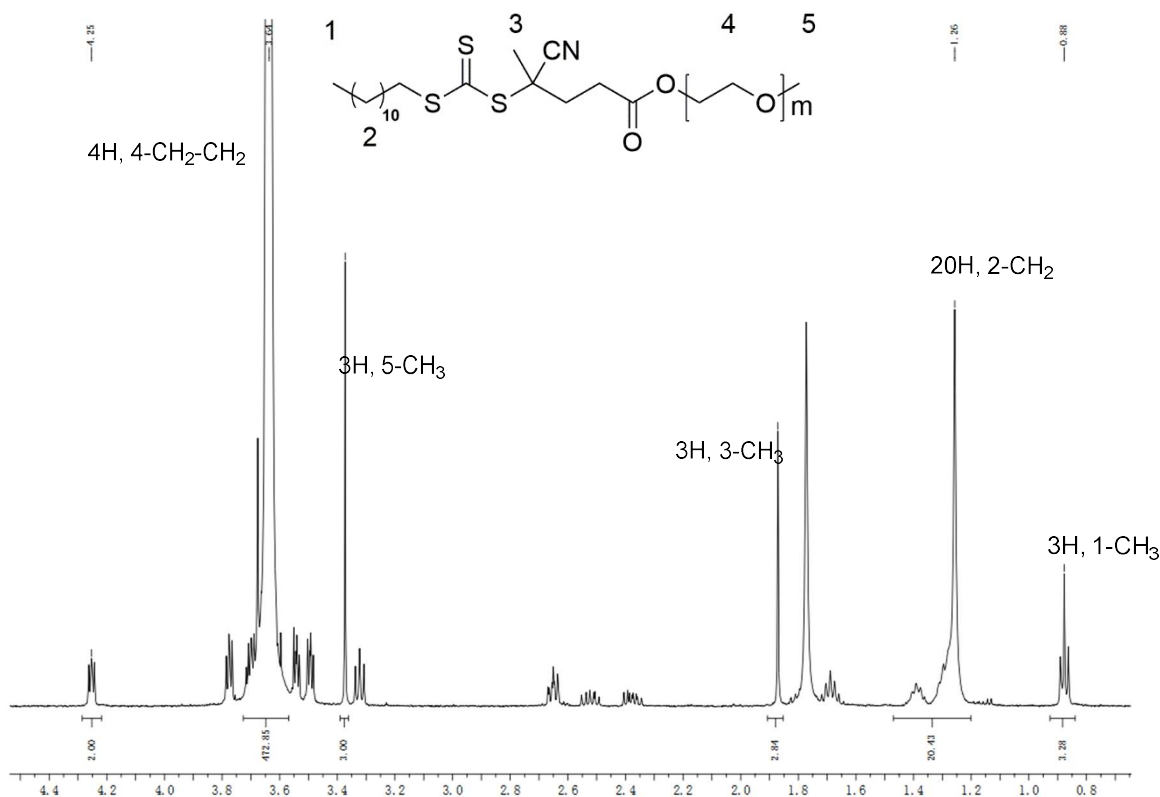
Figure 52: ^{1}H-NMR spectra of the PEG-based macro-CTA.

Three PEG-*b*-PNIPAAm block copolymers were prepared with targeted PEG-*b*-PNIPAAm block length ratios of 1:2, 1:4 and 1:6. The block copolymer characteristic are shown in Table 14. The number average molar mass of the block copolymers rises significantly with the increasing PNIPAAm block length. A well-defined block copolymer was observed with a relative short PNIPAAm block, verifying the successful control of the copolymerization (M_n = 25,800 g/mol, Đ = 1.31, Table 14). With further increasing PNIPAAm block length, the control over the number average molar mass and the molar mass distribution during the polymerization diminishes. Copolymer samples PEG-*b*-PNIPAAm$_{400}$ (PEG-PN-2) and PEG-*b*-PNIPAAm$_{600}$ (PEG-PN-3) show a less increase in number average molar mass but tend to give higher dispersities of Đ = 1.47 to Đ = 1.70 under the same polymerization conditions. Due to the undesired termination reactions by recombination or disproportionation, the general RAFT polymerization process may not be suitable for the synthesis of linear PEG block copolymer with high molecular

weight.[188] The shoulder in molar mass distribution at the low molar mass area can be attributed by the unreacted homopolymer chains.

Table 14. Macromolecular characteristics of PEG-based macro-CTA and PEG-*b*-PNIPAAm block copolymer.

Polymer	Targeted block lengths	Relative block length ratio[a] PEG/PNIPAAm	Đ$_{GPC}$ [b]	M$_{n,GPC}$ (g/mol) [b]
PEG-CDPA	PEG-CDPA	1: -	1.05	8,900
PEG-PN-1	PEG-*b*-PNIPAAm$_{200}$	1: 1.32	1.31	25,800
PEG-PN-2	PEG-*b*-PNIPAAm$_{400}$	1: 1.71	1.47	30,700
PEG-PN-3	PEG-*b*-PNIPAAm$_{600}$	1: 1.94	1.70	33,800

[a] Determined using ^{1}H-NMR spectroscopy

[b] Determined by SEC in DMAc at 50 °C with PMMA standard calibration
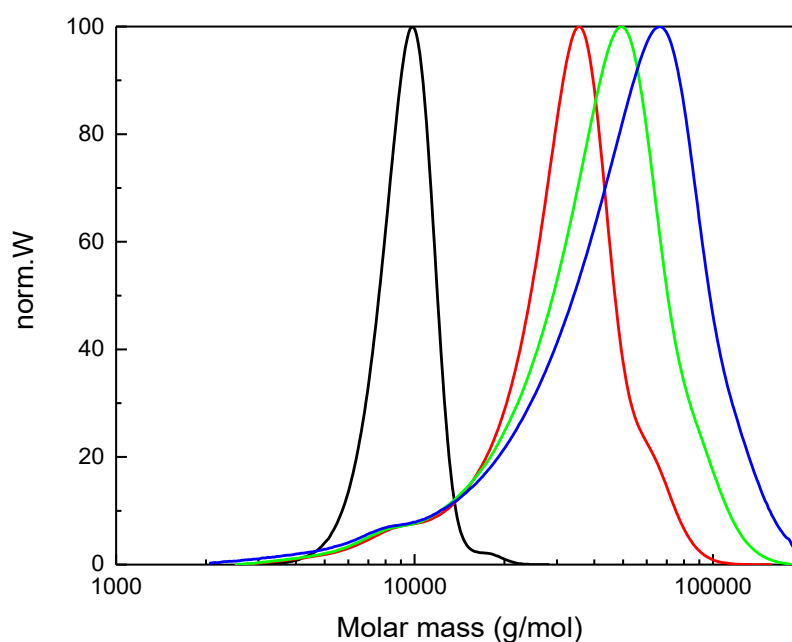
Figure 53. Overlaid SEC traces of PEG-CDPA (-), PEG-*b*-PNIPAAm$_{200}$ (-), PEG-*b*-PNIPAAm$_{400}$ (-), PEG-*b*-PNIPAAm$_{400}$ (-), determined by SEC in DMAc at 50 °C with PMMA standard calibration.

4.2.6 Post-polymerization attachment of L-proline and L-prolinamide organocatalysts

A new class of azlactone-functionalized amphiphilic block copolymers was synthesized via RAFT polymerization and characterized by ^{1}H-NMR spectroscopy and SEC. Such polymers

comprise a permanently hydrophilic block (PDHPA, PDMAA or PEG) and a thermo-sensitive PNIPAAm block with copolymerized 2-vinyl-4,4-dimethylazlactone (VDMA) units. The high reactivity of the azlactone moiety is well documented, undergoing a ring-opening reaction in presence of nucleophilic species.[111] Therefore, the resulting amphiphilic VDMA-containing block copolymers can be modified with nucleophilic organocatalysts.

Synthesis of P(NIPAAm-*co*-VDMA)
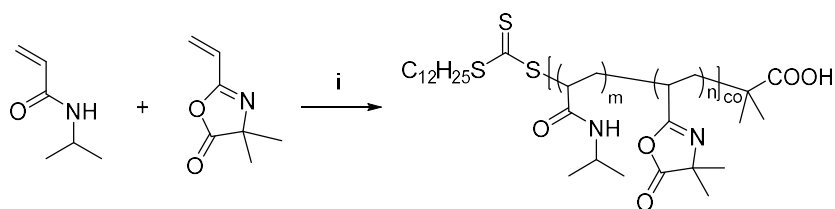
Figure 54. Synthesis of copolymers containing NIPAAm and VDMA via RAFT polymerization: i) DMP, 1,4-dioxane, AIBN, 70 °C.

In order to check the compatibility of NIPAAm and VDMA, copolymerization of both monomers via RAFT was conducted. 2-(2-Cyanopropyl) dithiobenzoate (CPDB) and DMP were shown to mediate the RAFT polymerization of the reactive monomer VDMA.[154] In the present work, the synthesis of P(NIPAAm-*co*-VDMA) was carried out with NIPAAm/VDM/DMP/AIBN at a molar ratio of 95/5/1/0.1. A content of 5 mol% VDMA seemed to be reasonable in order to achieve a high catalyst loading and still providing thermo-responsive behavior. After precipitation in *n*-hexane, the polymer was obtained as a light-yellow powder. The molar mass distribution of the obtained copolymer is shown in Figure 56. A well-defined copolymer with low dispersity as well as unimodal molar mass distribution (M_n = 11,400 g/mol, $Đ$ = 1.14) was obtained verifying the controlled proceeding of RAFT copolymerization. Thus, this copolymer can be used to build a functional thermo-responsive block copolymer in the next step. Due to the low content of VDMA (5 mol%) and signal overlapping with the backbone protons, it is not directly possible to determine the copolymer composition by ^{1}H-NMR spectroscopy. However, post-polymerization modification of the azlactone groups will introduce new signals in the ^{1}H-NMR spectrum, making it possible to indirectly determine the former VDMA content.
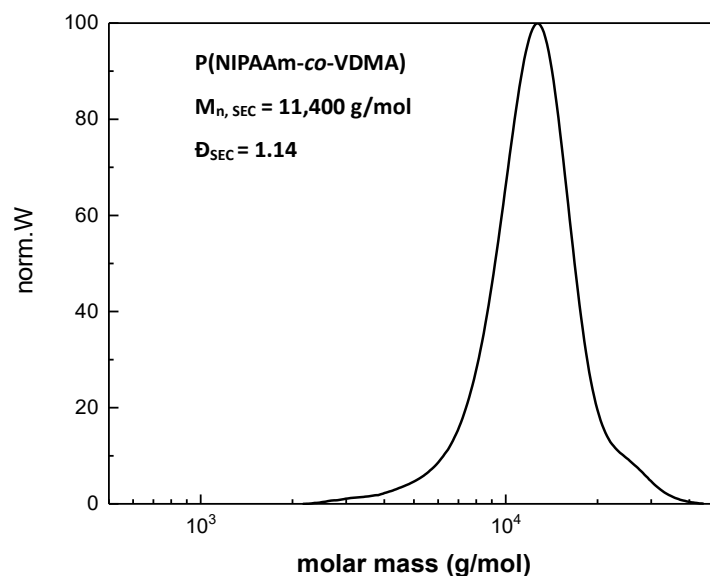
Figure 55. Molar mass distribution of P(NIPAAm-*co*-VDMA) with 95 mol% NIPAAm and 5 mol% VDMA, determined by SEC in THF at 50 °C with PMMA standard calibration.

Synthesis of amphiphilic VDMA-containing block copolymers

With the RAFT polymerization, a series of amphiphilic VDMA-containing block copolymers with the following structure were synthesized PSKA-*b*-P(NIPAAm-*co*-VDMA), PDMAA-*b*-P(NIPAAm-*co*-VDMA) and PEG-*b*-P(NIPAAm-*co*-VDMA).

According to the RAFT mechanism, the hydrophobic Z-group will be located at the end of the lastly polymerized block. For the latter self-assembly of the block copolymers, it would be reasonable if the Z-group sticks to the temperature-sensitive block. Therefore, the block copolymers synthesis starts with the permanently hydrophilic block producing PEG-based, and PSKA-based macro-RAFT agents. In the second step, these macro-RAFT agents will be used to copolymerize NIPAAm and VDMA.
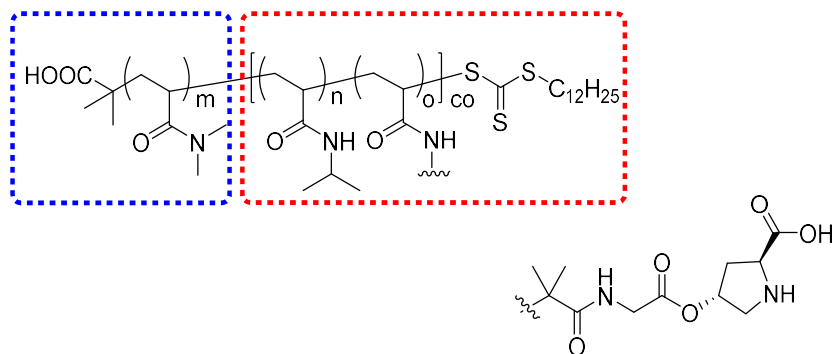
Figure 56. Designed amphiphilic block copolymer with end group from chain transfer agent: hydrophilic block (blue) and hydrophilic block above LCST (red).

In order to stabilize temperature-induced aggregates VDMA containing block copolymers were synthesized consisting of a relatively long thermos-responsive P(NIPAAm-*co*-VDMA) block and a short hydrophilic block. In brief, the monomers NIPAAm (95 mol%) and VDMA (5 mol%) were polymerized to conversions over 90 %, targeting a relative block length ratio of 1/7. The relative block length ratio of the hydrophilic block and the PNIPAAm block can be estimated by ^{1}H-NMR spectroscopy. As shown in Table 15, the relative block length ratio depends on the nature of the hydrophilic macro-CTA. Using PSKA-based and PDMAA-based macro-RAFT-agents, block copolymers exhibited a rather broad molar mass distribution with dispersities of 1.49 and 1.91 respectively. For the PEG-based macro-RAFT agent, a block copolymer with a relatively short thermos-responsive block was obtained yet showing a lower dispersity of 1.43.

Table 15. Macromolecular characteristics of functional amphiphilic block copolymers.

Sample	m/n [a] (NMR)	Đ$_{GPC}$ [b]	M$_{n,GPC}$ [b] (g/mol)	M$_{n,th}$ (g/mol) [c]
PSKA$_m$-*b*-P(NIPAAm-*co*-VDMA)$_n$	1: 10.0	1.49	46,800	49,700
PDMAA$_m$-*b*-P(NIPAAm-*co*-VDMA)$_n$	1: 6.37	1.91	55,900	85,800
PEG$_m$-*b*-P(NIPAAm-*co*-VDMA)$_n$	1: 3.13	1.43	39,700	74,100

[a] Determined using ^{1}H-NMR spectroscopy

[b] Determined by SEC in THF with PMMA standard calibration

[c] The molecular weight was calculated from ^{1}H-NMR data using the following equation: $M_{n,th} = m* M_{SKA} + (M_{NIPAAm}* 95 \% + M_{VDMA} * 5 \%)*n + M_{CTA}$

The number-average molar mass of the synthesized copolymers was determined by THF-SEC with PMMA calibration. The resulting polymers showed a relative large molecular weight (over

40,000 g/mol), which is unusual for the synthesis of linear block copolymers by normal RAFT polymerization. All of the three copolymers exhibited a distinctly monomodal molar mass distribution. In contrast to the block copolymers without VDMA, SEC traces of the VDMA containing block copolymers reveals no shoulders on lower molecular weight side, showing no signs of residual unreacted homopolymer chains (Figure 57). However, molar mass distributions were rather broad with dispersities between Đ = 1.43 – 1.91. It can be attributed to undesired side reactions by radical-radical coupling and long reaction time. For the PSKA-*b*-P(NIPAAm-*co*-VDMA) and PEG-*b*-P(NIPAAm-*co*-VDMA) block copolymers relative low dispersities (< 1.5) can still be achieved. These results suggest that the strategy of RAFT copolymerization was successfully applied to the synthesis of different kinds of functional amphiphilic VDMA-containing block copolymers. Thus, three amphiphilic block copolymers were available as supporting materials for the immobilization of L-proline and L-prolinamide derivate.
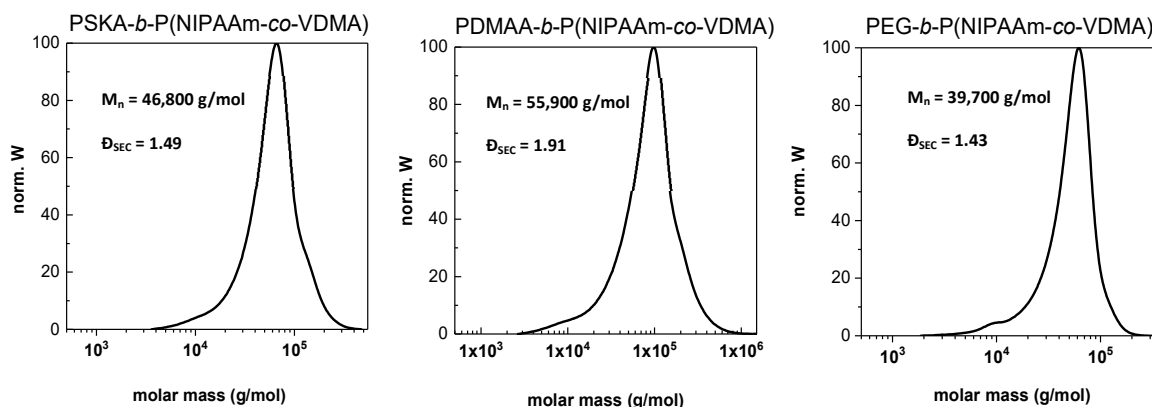
Figure 57. Molar mass distribution of PSKA-*b*-P(NIPAAm-*co*-VDMA) (left), PDMAA-*b*-P(NIPAAm-*co*-VDMA) (middle) and PEG-*b*-P(NIPAAm-*co*-VDMA) (right), determined by SEC in THF with PMMA standard calibration.

Post polymerization attachment of amino-functionalized L-proline and L-prolinamide derivatives

Post-polymerization modification is attracting more and more attention and becoming an important synthetic approach to design new classes of materials.[189] The azlactone functionality is capable of undergoing a ring opening reaction in the presence of nucleophiles. Due to its high efficiency, this reaction is regarded as a practical route for the synthesis of side-

chain functionalized polymers.[112] The chemical reactivity of the azlactone group is determined by the presence of multiple electrophilic functional groups (C=O, C=C and C=N). The slightly exothermic ring opening reaction will take place with primary amines and thiolates in the absence of any catalyst. If alcohols are employed as nucleophiles, a catalysis (either acid or base) is required. Under strong acidic conditions, an undesired side reaction involving Michael addition to the carbon-carbon double bond is observed. Therefore, cyclic amines such as 1,8-diazabicyclo[5.4.0]undec-7-ene (DBU) are usually applied as catalyst for the reaction with alcohols.[190] An example of the reaction of PVDMA with alcohols using of DBU at 50 °C was reported by Sun et al. to develop a new classes of cationic polyelectrolytes.[191]
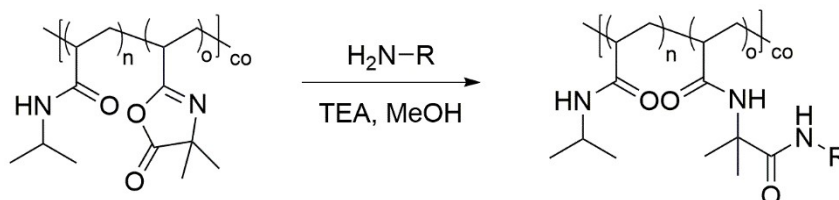
Figure 58. Post-polymerization attachment of a primary amine to a VDMA-containing PNIPAAm copolymer.[111]

In the present work, the post-polymerization modification of PVDMA was carried out using a variety of different amino-functionalized L-proline and L-prolineamide derivatives (shown in Figure 58). According to the synthetic route, final deprotection afforded the amino-functionalized organocatalysts as hydrochloric acid adducts. To restore the nucleophilicity of the amino group, the hydrochloric acid was neutralized by stoichiometric amounts of triethylamine (TEA). The resulting triethylamine hydrochloride salt can be easily removed by dialysis against water. Moreover, the hydrochloric adducts of the organocatalyst showed low solubility in most organic solvent, which slows down the reaction rate of the ring opening. Different solvents such as DMSO, dioxane, DMF and methanol were tested for the solubility of both functional polymers and the hydrochloric adducts of the organocatalysts to find out a suitable media of the ring opening reaction. Methanol shows a good compatibility. In order to reduce the competitive reaction between PVDMA and methanol, the post-polymerization modification was carried out at room temperature in presence of an excess of organocatalyst hydrochloric adducts and the stoichiometric amount of TEA.
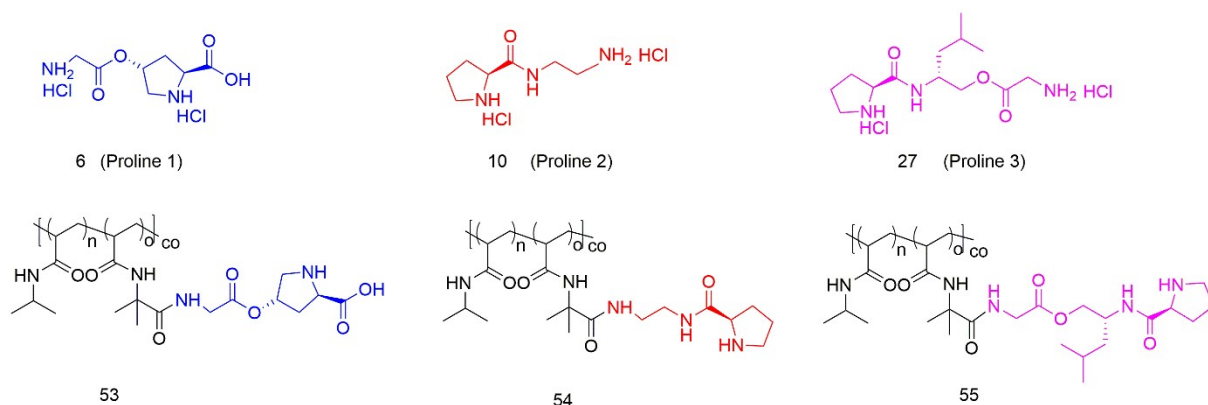
Figure 59. Designed L-proline and L-prolineamide with primary amine for the post-polymerization modification.

After the post-polymerization modification, solvent was removed under vacuum and the resulting polymers (PDMAA-*b*-P(NIPAAm-*co*-VDMA-proline) and PEG-*b*-P(NIPAAm-*co*-VDMA-proline) were purified by dialysis against water. For the polymer PSKA-*b*-P(NIPAAm-*co*-VDMA-proline), the regeneration of the diol group was obtained by treating the copolymer with glacial acetic acid and water in THF solution under reflux for 6 h.

As the most important feature of the modified block copolymers, the catalyst loading of the copolymers was analyzed by ^{1}H-NMR spectroscopy. Figure 60 and Figure 61 show the ^{1}H-NMR spectra of the different block copolymers after post-polymerization immobilization of the organocatalysts. In Figure 60, the copolymer compositions of PEG-*b*-P(NIPAAm-*co*-VDMA-proline (1-3)) with different contents of organocatalyst was calculated by comparing the characteristic signals corresponding to CH of PNIPAAm (labeled as signal 3 in Figure 60, at 3.84 ppm), the CH$_2$-CH$_2$ of PEG (labeled as signal 2, at 3.51 ppm) and the CH$_2$ of the proline-moiety (labeled as signal 1, at 2.75 ppm). In this case, the same PEG-*b*-P(NIPAAm-*co*-VDMA) block copolymer was used as the supporting material for the three different organocatalysts in order to keep the block length ratio PEG/PNIPAAm= 1/3 as constant. For investigation of the influence of copolymer structure on the catalyst, the prolinamide catalyst 2 was attached to all of the three different block copolymers. The molar copolymer compositions of PDHPA-*b*-P(NIPAAm-*co*-VDMA-proline) was calculated by comparing the characteristic signals corresponding to CH of PNIPAAm (Figure 60, at 3.84 ppm), the OH of PDHPA (at 4.59 and 4.78 ppm) and the CH$_2$ of the proline-moiety (at 2.87 ppm). For the modified block copolymer

PDMAA-*b*-P(NIPAAm-*co*-VDMA-proline), the molar compositions were determined by comparing the integral under the peaks attributed to the CH of PNIPAAm (at 3.84 ppm), the CH_3 of PDMAA (at 2.79 ppm) and the CH of proline-moiety (at 3.51 ppm). The thermos-responsive block copolymers bearing the immobilized organocatalyst were obtained with an effective catalyst loading of appr. 4-5 mol%. The molar and the mass-relative copolymer compositions including the catalyst loading are summarized in detail in Table 16. It is noteworthy, that the peaks at 0.86 ppm corresponding to methyl group from dodecyltrithiocarbonate usually disappeared after post-polymerization immobilization of the organocatalysts. The reaction of thiocarbonylthio compounds with nucleophiles is one of the most widely reported methods to convert RAFT end groups. The free primary amine attacks the thiocarbonylthio groups in an amidation reaction, thereby releasing the thiol end group in the polymer. Therefore, the RAFT end group are not stable under post-polymerization modification conditions. In this way, the hydrophobic dodecyl group, which might have an influence on the self-assembly process, could be removed.

Table 16. Polymer composition after immobilization with proline 1-proline 3

Sample	Polymer composition
POC 1	PEG-*b*-P(NIPAAm-*co*-VDMA-Proline 1)
POC 2	PEG-*b*-P(NIPAAm-*co*-VDMA-Proline 2)
POC 3	PEG-*b*-P(NIPAAm-*co*-VDMA-Proline 3)
POC 4	PDHPA-*b*-P(NIPAAm-*co*-VDMA-Proline 2)
POC 5	PDHPA-*b*-P(NIPAAm-*co*-VDMA-Proline 3)
POC 6	PDMAA-*b*-P(NIPAAm-*co*-VDMA-Proline 2)
POC 7	PDMAA-*b*-P(NIPAAm-*co*-VDMA-Proline 3)

4. Results and discussion
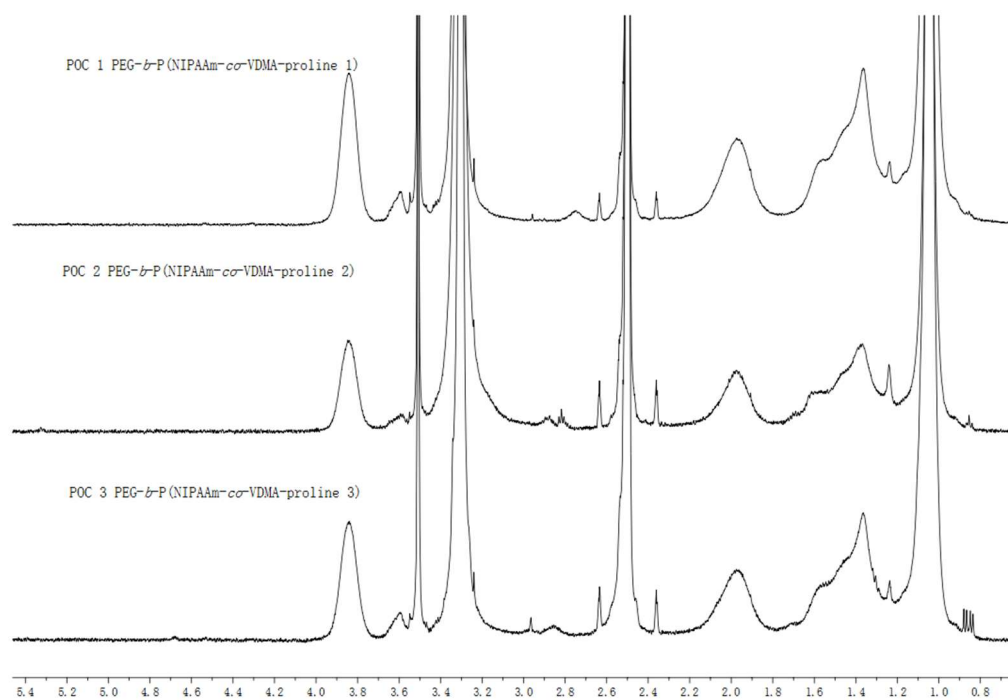
Figure 60. ^{1}H-NMR spectra of the PEG-*b*-P(NIPAAm-*co*-VDMA) after immobilization with Proline 1(upper), Proline 2 (middle) and Proline 3 (lower).
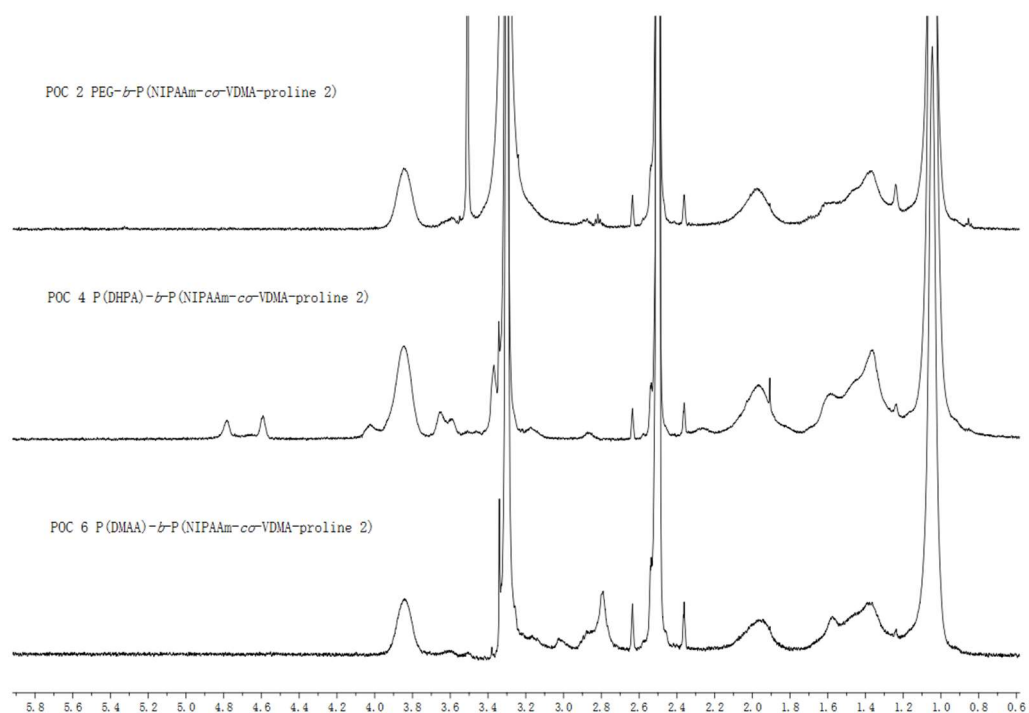
Figure 61. ^{1}H-NMR spectra of the different amphiphilic block copolymers after immobilization with Proline 2: PDHPA-*b*-P(NIPAAm-*co*-VDMA-Proline 2)(upper), PEG-*b*-P(NIPAAm-*co*-VDMA-Proline 2) (middle) and PDMAA-*b*-P(NIPAAm-*co*-VDMA-Proline 2) (lower).

Table 17. Copolymer composition and catalyst loading of the amphiphilic block copolymers veering the immobilized organocatalyst.

Sample	m/n/p (molar)[a]	Proline-content[b] (mol%)	m*/n*/p* (mass)[c]	Proline-content[d] (% w/w)
POC 1	1/3.21/0.17	4	44/362/49	11
POC 2	1/3.09/0.13	3	44/349/42	10
POC 3	1/3.13/0.13	4	44/354/53	12
POC 4	1/10.0/0.53	5	140/1130/157	12
POC 5	1/11.19/0.28	2	140/1254/114	8
POC 6	1/6.4/0.26	3	99/712/80	9
POC 7	1/5.9/0.23	3	99/667/94	11

[a] calculated from ^{1}H-NMR spectroscopy hydrophilic/PNIPAAm/Proline-mioety ratio in molar

[b] Proline loading (in molar) was calculated by $p/(m+n+p) \times 100$ %

[c] mass-related copolymer composition calculated by $m \times M_{hydrophilic}/n \times M_{NIPAAm}/ p \times M_{VDMA-Proline}$

[d] mass-related proline-content calculated by $p*/(m*+n*+p*) \times 100$ %

4.3 Temperature-dependent aggregation of the block copolymers

Block copolymers are well known as an important class of materials capable of self-assembling in a selective solvent, adapting different morphologies.[47,192] Thermodynamic and kinetic parameters control the formation of nanometer-scale structures such as micelles and vesicles in dilute solution. Dynamic light scattering (DLS) is an important method to characterize particles in colloidal systems. Analysis of the diffusion properties afford the hydrodynamic radius of the particles of amphiphilic block copolymers in the present work comprise a thermo-responsive block based on PNIPAAm, showing a critical phase transition temperature (T_{cr}) at about 32 °C in water.[193–195] When the solution temperature exceeds the critical phase transition temperature the macromolecules become amphiphilic, thus forming stable self-assembled aggregates in terms of micellar or vesicles.[196,197] For hard spherical particles in a dilute solution, the relation of self-diffusion coefficient D to the particle radius R is given by the Stokes-Einstein equation (equation 1) with k_B as Boltzmann's constant, T as the

absolute temperature and η as the viscosity of the medium. Under normal circumstances, the particles are neither spherical, hard nor monodisperse. That is why the calculated radius is called "hydrodynamic radius", which represents the radius of a hard sphere showing the same diffusion properties as the colloidal particle.

$$D = k_B T / 6\pi\eta R \qquad\qquad \text{equation 1}$$

Figure 62 show the results of the temperature-dependent DLS measurement of an aqueous solution of a PDMAA-*b*-P(NIPAAm-*co*-VDMA-proline 2) with short PNIPAAm. Each data point represents the mean value of 3 consecutive DLS measurements plotted against solution temperature. As seen, the z-average of the apparent hydrodynamic diameter shows a small decrease from 140 nm to 110 nm at a temperature of appr. 40 °C. According to the block copolymer self-assembly an increase in particle diameter is expected exceeding the critical volume phase transition temperature. In the same diagram, the second y-axis displays the polydispersity index (PDI) as a function of temperature. This index is a dimensionless number calculated from the correlation function (the cumulants analysis). In contrast to the definition of Đ, the PDI in the DLS experiment would be 0.0 for a perfectly uniform sample. A highly monodisperse sample corresponds to a PDI between 0.0 – 0.1. However, the PDI values shown in Figure 62 are in the range between 0.5 - 0.7, indicating that the sample has a very broad size distribution. In summary, the DLS results for the PDMAA-*b*-P(NIPAAm-*co*-VDMA-proline 2) are not in agreement with the expected trend for the self-assembly of LCST-type block copolymers.
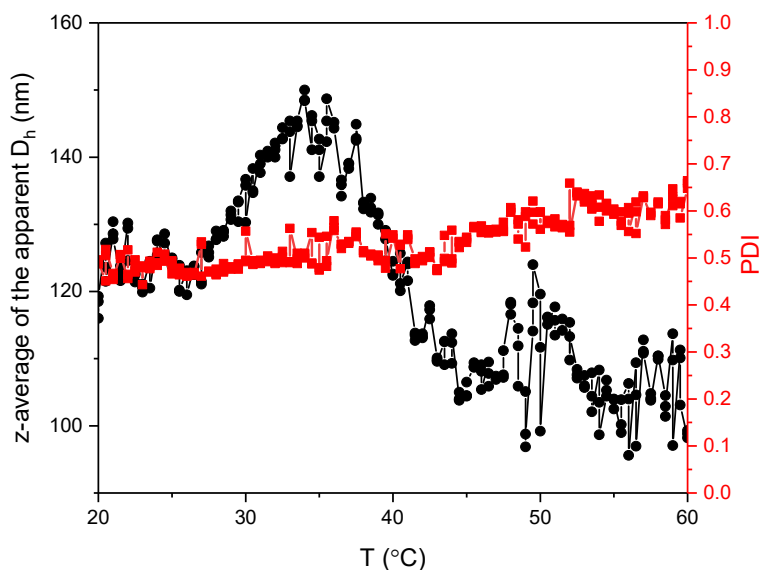
Figure 62. Z-average of the apparent hydrodynamic diameter and the PDI as function of temperature for the DLS measurement of an aqueous solution of the sample PDMAA-*b*-P(NIPAAm-*co*-VDMA-proline 2) with relative copolymer composition DMAA/NIPAAm/VDMA = 2/1/0.1.

4.3.1 Influence of end groups

Since, the above-mentioned DLS results of an aqueous PDMAA-*b*-PNIPAAm polymer solution show a clearly unexpected behavior, the effect of polymer end groups originating from RAFT-CTA was firstly investigated. Thus, two further PDMAA-*b*-PNIPAAm block copolymer samples were synthesized using 2-cyano-2-propyl dodecyl trithiocarbonate (CPDT) and 2-(Dodecylthiocarbonothioylthio)-2-methylpropionic acid (DMP). The targeted relative molar block length ratio of the PDMAA and PNIPAAm block was 2:1. The macromolecular characteristics of the two block copolymers are summarized in Table 18.

Table 18. Macromolecular characteristics of the PDMAA-*b*-PNIPAAm block copolymers

CTA	PDMAA		PDMAA-*b*-PNIPAAm	
	$M_{n, GPC}$ (g/mol)	$Đ_{GPC}$	$M_{n, GPC}$ (g/mol)	$Đ_{GPC}$
CPDT	5,000	1.18	8,000	1.24
DMP	3,800	1.16	6,500	1.18

determined by SEC in THF with PMMA standard calibration

121

The physical properties of the applied chain transfer agent should be considered in detail in terms of α- or ω-end group of the polymer. Both chain transfer agent DMP and CDPA consist of a hydrophobic trithiocarbonate Z-group and a hydrophilic tertiary R-group, which possibly influence the formation of the aggregates in water above the LCST. The established mechanism for RAFT polymerization involving fragmentation and addition process is proposed that the hydrophilic block should be first performed and the hydrophilic homopolymer (PSKA, PDMAA and PEG-CDPA) were used as macroinitiator for the chain extension with NIPAAm and VDMA. As shown in Figure 63, below the critical phase transition temperature, both block of the desired polymer is water soluble and the hydrophobic contribution of trithiocarbonate Z-group can be neglected. Above the critical phase transition temperature, PNIPAAm block become hydrophobic in water as desired and generate self-assembly nano structures.

Table 19. α- or ω-end groups of the PDMAA-*b*-PNIPAAm block copolymer

Sample	α-end group	ω-end group
PD-PN 4	trithiocarbonates ($C_{12}H_{25}CS_2$)	isobutyronitrile (-$C(CH_3)_2CN$)
PD-PN 5	SH	isobutyronitrile (-$C(CH_3)_2CN$)
PD-PN 6	trithiocarbonates ($C_{12}H_{25}CS_2$)	isobutyric acid (-$C(CH_3)_2COOH$)
PD-PN 7	SH	isobutyric acid (-$C(CH_3)_2COOH$)

The designed block copolymers consist of a dodecyl thiocarbonyl thio group on the ω-end and an isobutyronitrile (-$C(CH_3)_2CN$, PD-PN-4) or an isobutyric acid (-$C(CH_3)_2COOH$, PD-PN-6) at the α-end of the polymer chain. In order to investigate the influence of the ω-end group, a part of the block copolymers PD-PN-4 and PD-PN-6 were subjected to aminolysis to remove the trithio carbonate end group, as reported in literature.[198,199] After the aminolysis, the resulting polymers exhibit an isobutyronitrile (-$C(CH_3)_2CN$, PD-PN-5) or isobutyric acid(-$C(CH_3)_2COOH$, PD-PN-7) group at the α- end, as well as a thio group at the ω-end.(Table 19) The temperature-dependent aggregation of all four block copolymers in aqueous solution was analyzed by DLS (Figure 63).
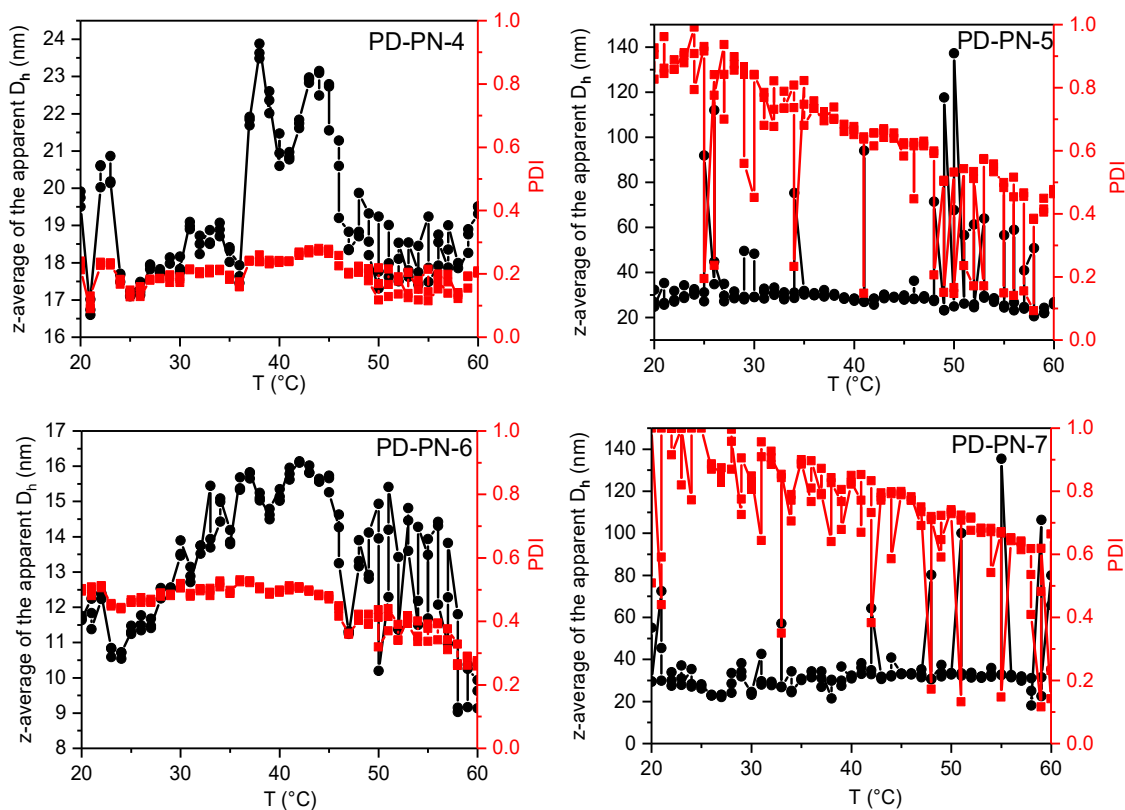
Figure 63 Results of the temperature-dependent DLS analysis of the PDMAA-*b*-PNIPAAm block copolymer with different end groups in aqueous solution.

None of the four block copolymer samples exhibit a phase transition characterized by a jump in particle size at a critical temperature. The sample PD-PN-4 and PD-PN-6, whose end groups are determined by the respective RAFT-CTA tend to form smaller aggregates ($D_h < 25$ nm) with a more uniform particle size distribution (PDI = 0.2 - 0.4). PD-PN-5 and PD-PN-7 are the block copolymer samples after the aminolysis, where the hydrophobic dodecyl thio carbonyl group was cleaved off. Those block copolymers form large aggregates with a hydrodynamic diameter of about $D_h = 30$ nm. In contrast, the sample PD-PN-5 and PD-PN-7 exhibited broader particle size distribution (PDI = 0.5 – 1.0) and the PDI values slightly decreased upon heating 60 °C. Under this condition, the PNIPAAm block becomes hydrophobic, which may make the contribution of the reduce of the PDI. At all temperatures particles do not aggregate, which was not because of end groups. While the slight change might still occur to some extent in the PDI. As noted above, block copolymers PD-PN-4 with more hydrophilic components demonstrate a better aggregation behavior in respect of PDI. Since the end groups do not

123

significantly influence the aggregation behavior of the block copolymers, the relative block length ratio will be further investigated in the next chapter.

4.3.2 Influence of block length ratio

PDMAA-*b*-PNIPAAm block copolymers

The balance between hydrophilic and hydrophobic domains is known to be crucial for the self-assembly of amphiphilic molecules. For amphiphilic block copolymers, the relative and absolute block length ratio is critical for the stability and morphology of the aggregates formed.[200] Therefore, three PDMAA-*b*-PNIPAAm samples with varying block lengths were synthesized. (Table 20). The block length ratio of PDMAA to PNIPAAm varied from 1:1.8 and 1:2.6 to 1:5. With increasing length of the PNIPAAm block the number average molar mass increased from 12,800 g/mol and 28,600 g/mol. All of these block copolymers were analyzed in aqueous solution by temperature-dependent DLS measurements (Figure 64). The sample with the shortest PNIPAAm block (PD-PN-1) exhibited no visible phase transition although the PDI values drop down to 0.2 at a temperature of 35 °C, which is close to the LCST of PNIPAAm. In contrast, the block copolymers PD-PN-2 and PD-PN-3 show the expected jump in particle size at a temperature of 33 °C. Particle with a hydrodynamic radius of 60-65 nm were formed above the critical phase transition temperature. The PDI dropped to 0.06, indicating the formation of nearly uniform particles. The samples PD-PN-1 and PD-PN-2 were prepared using the same PDMAA$_{50}$-macro-CTA, which means that both copolymers have the identical chain length of the hydrophilic block. It can be considered that the extended PNIPAAm block has contributed more hydrophobic core to the self-assembly at higher temperature. Sample PD-PN-3 with the longest PNIPAAm block shows the smallest aggregates below the critical phase transition temperature. This behavior can be easily explained by the feature of the PNIPAAm block. At temperature below T$_{cr}$, PNIPAAm is hydrophilic, which leads to a good solubility of the whole polymer. When the temperature exceeds T$_{cr}$, PNIPAAm becomes hydrophobic, which represents the driving force for the self-assembly forming aggregates with a stable

PNIPAAm core.
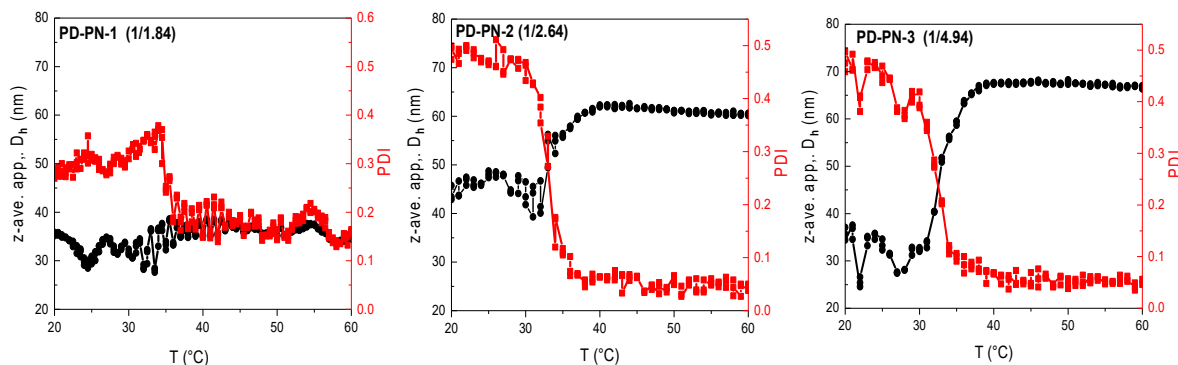
Figure 64. Results of the temperature-dependent DLS analysis of the PDMAA-*b*-PNIPAAm block copolymer with different block length ratios in aqueous solution

Table 20. Macromolecular characteristics of the PDMAA-*b*-PNIPAAm block copolymers and the results of the temperature-dependent DLS analysis at a temperature of 25 °C and 40 °C.

Sample[a]	Đ$_{SEC}$[b]	M$_{n, SEC}$[b] (g/mol)	T$_{cr}$[c] (°C)	25 °C			40 °C		
				PDI	Intensity (d.nm)	Number (d.nm)	PDI	Intensity (d.nm)	Number (d.nm)
PD-PN-1 (1/1.84)	1.53	12,800	-	0.307	164	8	0.151	39	22
PD-PN-2 (1/2.64)	1.59	16,100	34	0.469	136	12	0.063	66	49
PD-PN-3 (1/4.97)	1.62	28,600	33	0.450	111	9	0.067	71	54

[a] the relative block length ratio was calculated from ^{1}H-NMR spectroscopy

[b] determined by SEC in THF with PMMA standard calibration

[c] phase transition temperature determined by DLS

Beside the z-average hydrodynamic diameter, the Zetasizer software can also report the intensity, volume, or number-based size distributions. By comparing the particle size data for the same sample with different distribution index, there is a possibility that the values can be very different from the number weighted size distribution to intensity weighted size distribution (as shown in Table 20). It is a pragmatic decision which size distribution should be reported in the data analysis of the DLS measurement. The most common view is that the intensity-dependent size distribution is always correct and those data are obtained without any assumptions about the Mie scattering function. To convert the intensity-based size distribution into the volume and number-based distribution, Mie theory is used in the Zetasizer software.[201] According to the quality of the cumulant fit error, volume and the

number size distributions display more details about the sample.[201] The effect of different distribution were investigated by Malvern Instrument.[202] For a sample consisting of an equal number of particles with a diameter of 5 nm and 50 nm, respectively. The peaks ratio in the volume weighted distribution is thousand times higher for the 50 nm particles and in the intensity weighted distribution diagram, the peak ratio is even larger up to one million times.
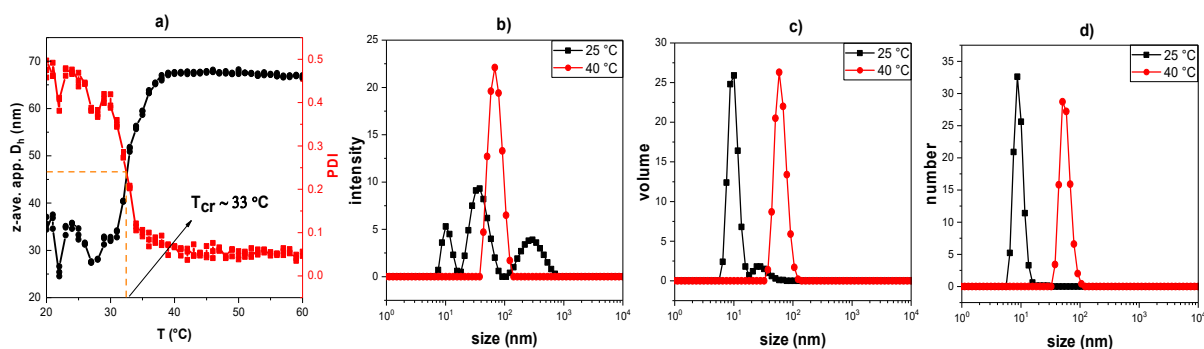
Figure 65. DLS results of the temperature-dependent of the sample PD-PN-3: b) intensity-, c) volume- and d) number particle size distributions at two temperatures (25 °C and 40 °C).

The difference between differently weighted particle size distributions is shown in Figure 65 for the DLS analysis of sample PD-PN-3. The plot of the z-average hydrodynamic diameter as a function of temperature reveals a jump in particle size at a critical temperature of 33 °C. The intensity-based particle size distribution (PSD) shows multimodal broadly distributed sizes below the critical temperature. At a temperature of 40 °C, PSD becomes monomodal and narrowly distributed with a mean size of 71 nm. These results correspond to the drop of the PDI if the solution temperature exceeds T_{cr}. Multimodality of the intensity-based PSD below T_{cr} makes it difficult to visualize the phase transition. However, the larger species in the intensity-based PSD are over emphasized due to their higher scattering intensity. In the volume- and number-based PSD these differences in scattering intensity are corrected, resulting in an almost monomodal PSD.[201] Therefore, the number-based PSD can be used to clearly visualize the volume phase transition, accompanied by an increase in particle size from 9 nm (below T_c) to 54 nm (above T_c).

PDHPA-*b*-PNIPAAm block copolymers

To investigate the influence of the chemical structure of the hydrophilic block, three block copolymers with PDHPA as hydrophilic block were synthesized. Thereby, the block length ratio between PDHPA and PNIPAAm was varied in the range of 1:1.84, and 1:3.28 up to 1:5.9 (Table 21). These three PDHPA-*b*-PNIPAAm samples were subjected to temperature-dependent DLS analysis in aqueous solution. The results are summarized in Figure 66.
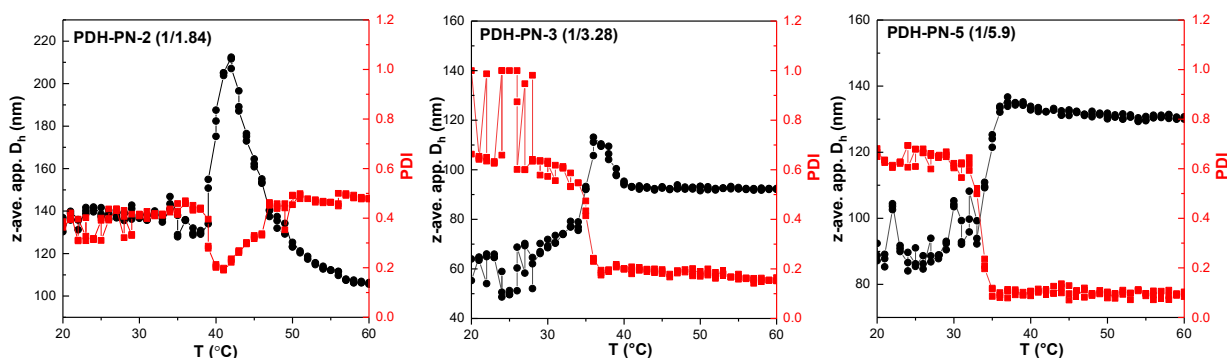
Figure 66. DLS results of the temperature-dependent of the sample PDHPA-*b*-PNIPAAm block copolymer with different block length ratios in aqueous solution.

Figure 66 display the z-average of the apparent hydrodynamic radius as a function of temperature for relative block length ratio of PDHPA and PNIPAAm varying from 1/1.82 up to 1/5.90. The observed diagrams for PDHPA-*b*-PNIPAAm block copolymers display a similar trend as for the PDMAA-*b*-PNIPAAm block copolymers. With increasing length of the PNIPAAm block the critical phase transition temperature became more pronounced. Moreover, with increasing length of the PNIPAAm block the aggregates formed above T_{cr} exhibit lower PDI values. Consequently, the block copolymers with larger PNIPAAm block length tend to form stable aggregates in water. Additionally, for the sample PDH-PN-5 with PDHPA/PNIPAAm ratio of 1/5.9 larger particle sizes (z-average, D_h= 135 nm) was observed at 40 °C. The particle sizes for sample PDH-PN-3 are smaller than 100 nm, showing that, the PNIPAAm block acts as a hydrophobic group to form the core of the aggregates at higher temperatures. Thus, its chain length has a considerable influence on the size of the self-assembly nanostructures in water.

Taking a view at the intensity- and number-based size distributions, the focus is laid on the change in particle size. The respective size distributions at different temperatures are

127

presented in Table 21. Apart from the sample PDH-PN-2, the other two block copolymers exhibited a phase transition temperature at 34 °C, which is close to the LCST of PNIPAAm. Sample PDH-PN-2 with a relative block length ratio of PDHPA and PNIPAAm smaller than 1/2, shows a slight increase in particle size upon heating above T_{cr}. In contrast, the number-based size distribution revealed a slight decrease in particle size from 53.2 to 40.4 nm for the same sample. The samples PDH-PN-3 as well as PDH-PN-5 with an extended PNIPAAm block show expected self-assembly behavior of the temperature sensitive amphiphilic block copolymer: For sample PDH-PN-3, a shifting of the number-based distribution peak was observed from 7 nm to 57 nm and for the sample PDH_{50}-$PNIPAAm_{325}$ the temperature-induced aggregation afforded particles of about 100 nm in size. As already observed for the PDMAA-*b*-PNIPAAm block copolymers, the PDHPA-*b*-PNIPAAm block copolymers with a longer PNIPAAm block showed a better temperature-induced aggregation behavior in water. However, the size of the formed aggregates was bigger for the PDHPA-*b*-PNIPAAm samples compared to the PDMAA-containing block copolymers.
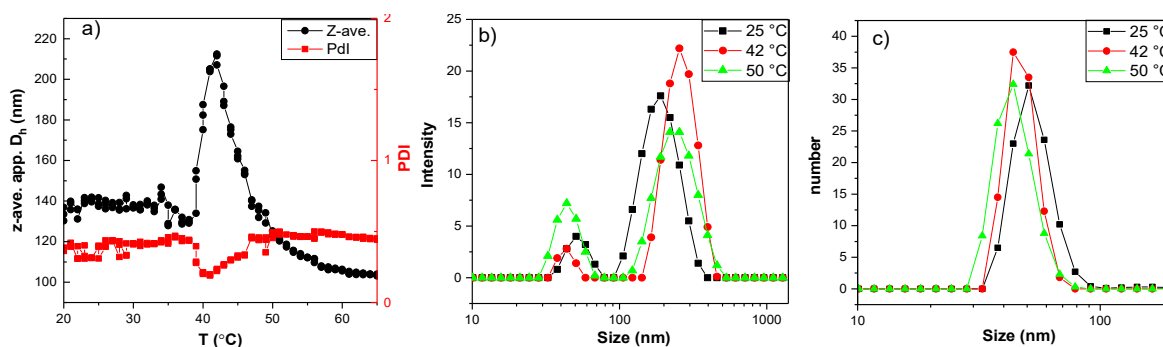
Figure 67. The DLS results of a temperature-dependent measurement of the sample PDH-PN-2. a) Intensity-, b) volume-, c) number-based particle size distributions at different temperature at 25 °C, 42 °C and 50 °C.

4. Results and discussion

Table 21. Macromolecular characteristics of the PDHPA-*b*-PNIPAAm block copolymers and the results of the PSD at 25 °C and 50 °C.

Sample[a]	Đ$_{GPC}$[b]	M$_{n,GPC}$[b] (g/mol)	T$_{cr}$ [c]	25 °C			40 °C		
				PDI	Intensity (d.nm)	Number (d.nm)	PDI	Intensity (d.nm)	Number (d.nm)
PDH-PN-2 (1:1.84)	1.58	15,300	40	0.39	183	53	0.21	211	40
PDH-PN-3 (1:3.28)	1.40	30,000	34	1.0	180	7	0.20	118	57
PDH-PN-5 (1:5.90)	1.38	39,600	34	0.67	273	12	0.10	148	95

[a] the relative block length ratio was calculated from ^{1}H spectroscopy

[b] determined by SEC in THF with PMMA standard calibration

[c] phase transition temperature determined by DLS

PEG-*b*-PNIPAAm block copolymers

For the third series of block copolymers, PEG was used as hydrophilic block. The relative block copolymer length ratio of PEG and PNIPAAm varied between 1:1.32 and 1.94 (Table 22). According to limitation in the synthesis, the relative PNIPAAm block length is much smaller compared to the PDMAA-*b*-PNIPAAm and PDHPA-*b*-PNIPAAm block copolymers. However, for the PEG-based samples, even the block copolymer with the shortest PNIPAAm segment (1/1.32) shows a self-assembly process at a temperature of 33 °C, whereas for the previously discussed block copolymers with PDMAA and PDHPA as hydrophilic block the PNIPAAm segment had to be at least twice as long as the hydrophilic segment to show temperature-induced self-assembly. Nevertheless, also for the PEG-based block copolymers the phase transition is more pronounced with increasing PNIPAAm block length. During the self-assembly process a jump in the hydrodynamic diameter from 30 nm at 25 °C to 110 nm above 33 °C could be observed. In case of the shortest PNIPAAm segment aggregates of 50 nm in size were formed. As already seen for the previously discussed block copolymers, there is a drop of the PDI from over 0.5 to values less than 0.1 during the self-assembly. Below T$_{cr}$ a broad multimodal intensity-based PSD is observed. By heating the sample solution to 40 °C the PSD becomes almost uniform (PDI<0.05). The intensity-mean size (51 nm) and the number mean size (46 nm) are similar, due to the low PDI of the sample PEG-PN-1. As the PDI increases, the

deviation between intensity mean and the number mean size becomes more pronounced.
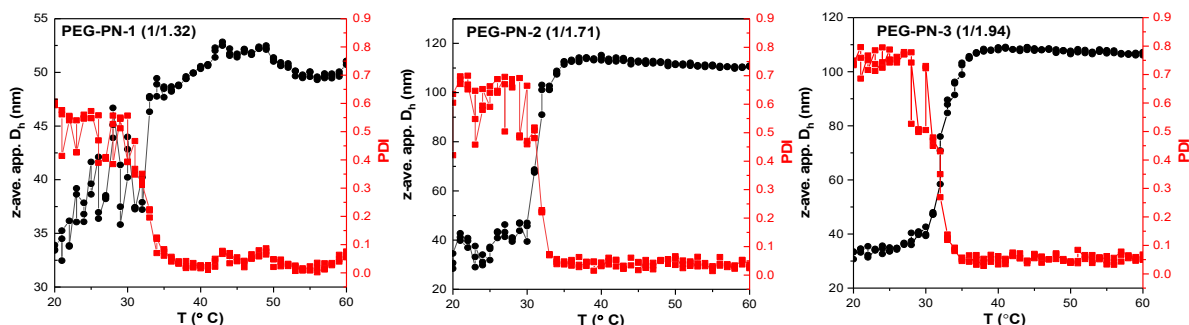
Figure 68. Results of the temperature-dependent DLS analysis of the PEG-b-PNIPAAm block copolymers with varying block length ratios in aqueous solution.

Table 22. Macromolecular characteristics of the PEG-*b*-PNIPAAm block copolymers and the results of the DLS at 25 °C and 40 °C.

Sample[a]	$Đ_{GPC}$[b]	$M_{n,GPC}$[b] (g/mol)	T_{cr}[c]	25 °C			40 °C		
				PDI	Intensity (d.nm)	Number (d.nm)	PDI	Intensity (d.nm)	Number (d.nm)
PEG-PN-1 (1: 1.32)	1.31	25, 800	33	0.55	165.9	12.9	0.01	51.4	45.9
PEG-PN-2 (1: 1.71)	1.47	30, 700	32	0.64	129.6	11.6	0.03	116.3	100.7
PEG-PN-3 (1: 1.94)	1.70	33, 800	32	0.75	126.0	11.6	0.05	115.4	87.0

[a] the relative block length ratio was calculated from ^{1}H-NMR spectroscopy

[b] determined by SEC in THF with PMMA standard calibration

[c] phase transition temperature determined by DLS

4.3.3 Influence of immobilized organocatalyst
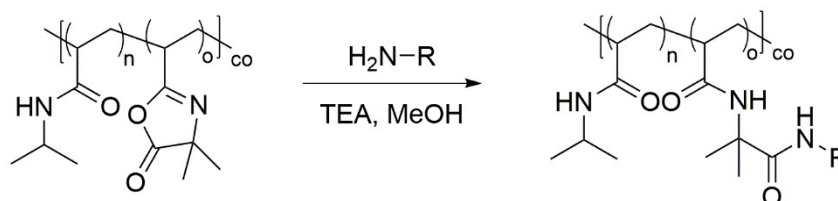
Figure 69. Schematic showing the post-polymerization reaction of P(NIPAAm-*co*-VDMA) with nucleophilic.

Based on previous DLS results of the three different amphiphilic block copolymers, it has been concluded that the extended PNIPAAm block showed the best results for the temperature-induced nanostructures. At this point, it would be interesting to see whether the aggregation behavior of the block copolymer would change after the immobilization of the organocatalyst.

As shown in Table 23, organocatalyst proline 2 was successfully attached to VDMA-containing block copolymers with PDMAA, PDHPA and PEG as hydrophilic block. The proline content was determined to be in the range of 2-5 mol% according to ^{1}H-NMR-spectroscopy. Those block copolymers bearing the organocatalyst were also subjected to temperature-dependent DLS analysis. The results are summarized in Figure 70 and Table 23. For all of the three functionalized block copolymers, a jump in particles size can be observed at a temperature of 34 °C. After passing a maximum, the particle size for all three samples converged to a fix value upon further heating. The sample PDHPA-*b*-P(NIPAAm-*co*-VDMA-proline 2) (POC 4) formed the smallest aggregates with D_h= 80 nm, meanwhile the aggregations of PDMAA-*b*-P(NIPAAm-*co*-VDMA-proline 2) (POC 6) (D_h= 110 nm) and PEG-*b*-P(NIPAAm-*co*-VDMA-proline 2) (POC 2) (D_h= 140 nm) were significantly larger. Above T_{cr}, the PDI values for all samples were in the range of 0.15-0.25 indicating a relatively narrow PSD. Since there is no significant change in T_{cr} compared to the block copolymers without organocatalyst, the immobilization of the organocatalyst does not significantly alter the hydrophilic/hydrophobic balance of the block copolymer.
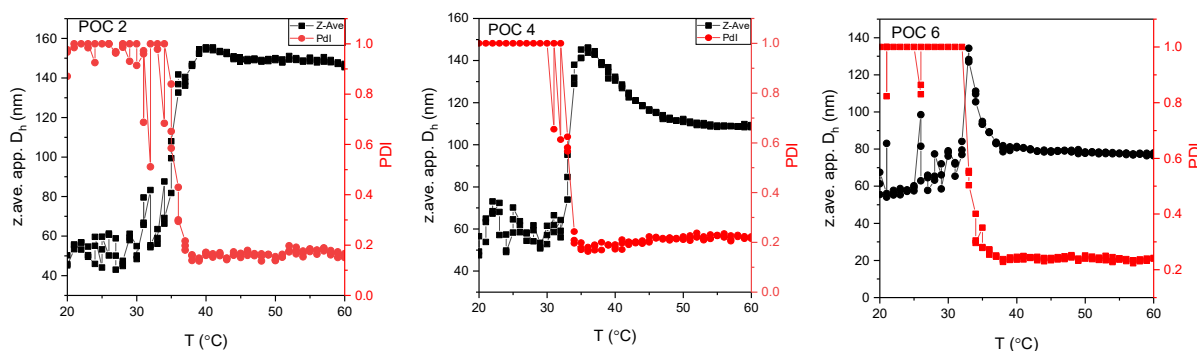
Figure 70. Results of the temperature-dependent DLS analysis of different immobilized organocatalysts.

Table 23. Result of the DLS analysis of different immobilized organocatalysts. at 25 °C and 50 °C.

Sample	T_{cr} (°C)	25 °C		40 °C	
		PDI	Number (d.nm)	PDI	Number (d.nm)
POC 2	35	1	11	0.17	124
POC 4	32	1	7	0.24	55
POC 6	33	1	10	0.18	40

phase transition temperature measurement by DLS

Finally, the temperature-dependent self-assembly was investigated in the presence of the reagents (CH, *p*-NBA). Thus, the composition of the analyst matches the reaction mixture for the micellar catalysis experiment. First of all, all the three reaction systems exhibited a sharp phase transition at a temperature of about 32 °C – 35 °C, which is in good agreement with the measurement of the T_{cr} for the functionalized block copolymers in water. The reaction mixtures with the PDHPA- and PDMAA-based block copolymers show a similar trend as in pure aqueous solution. At temperature below T_{cr}, particles of more than 800 nm in size are visible due to the bad solubility of the reagents in water. However, with the increase of the temperature above T_{cr} the hydrodynamic diameter dramatically decreases to 100 nm and remains constant. These results indicate that the organic components are solubilized in the micelles to form stable nano-scale reactors in water at a higher temperature. The mixture containing the PEG-based functionalized block copolymer shows a completely reverse trend. No aggregation was observed at low temperatures and above the phase transition temperature, the aggregation afforded particles with a hydrodynamic diameter of about 1300 nm in size. The PEG-based functionalized block copolymers are not able to solubilize the reagents within micelles. The large particle size suggests the formation of vesicular systems. The reason could be the relatively short PNIPAAm block compared to the other functionalized block copolymers, since the PNIPAAm block is mainly responsible for the aggregation process. However, the different capability solubilizing the reagents might have a significant influence on the micellar catalysis using the three functionalized block copolymers.
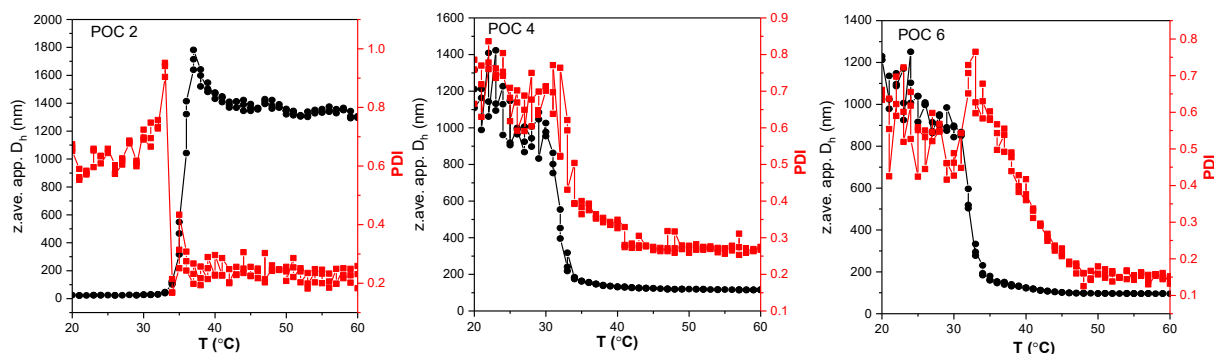
Figure 71. Results of the temperature-dependent DLS analysis of different immobilized organocatalysts in reaction mixture.

Table 24. The DLS measurement of the different amphiphilic block copolymer with supported Proline 2 in reaction mixture.

Sample	T_{cr} (°C)	25 °C		40 °C	
		PDI	Number (d.nm)	PDI	Number (d.nm)
POC 2 + educts	35	0.66	10	0.23	625
POC 4 + educts	32	0.68	448	0.32	73
POC 6 + educts	32	0.56	572	0.38	82

Phase transition temperature measurement by DLS

4.4 Micellar catalysis

In the last step of the present work, the thermos-responsive block copolymers bearing the immobilized organocatalyst are applied in micellar catalysis experiments. Based on their thermos-responsive block micelles are formed with the immobilized catalyst located in the hydrophobic core domain. In these nanoreactors a stereoselective Aldol reaction of CH and *p*-*p*-NBA are carried out (as shown Figure 72). With control of the temperature below the LCST PNIPAAm segment will be water soluble, to switch off the catalytic process. This system was particularly interesting due to its easy recycling by extraction. The product was characterized with both NMR and HPLC to determine the conversion as well as the stereoselectivity of the aldol reaction.
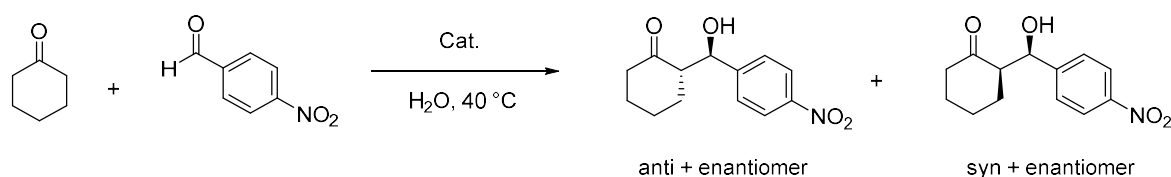
Figure 72. Asymmetric Aldol reaction between *p*-NBA and CH in water catalyzed by the supported organocatalyst.
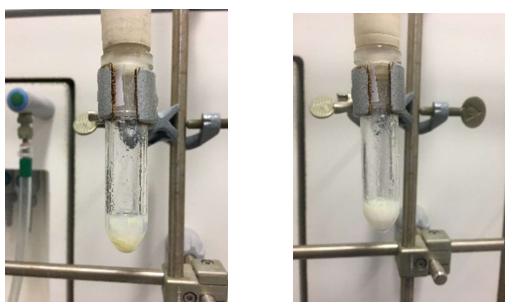
Figure 73. Photos of the submitted *p*-NBA and CH in the absence of in water before (left) and after (right) the reaction.

133

4.4.1 Asymmetric reaction using different polymer-supported organocatalysts

At first, the functionalized block copolymer PEG-*b*-P(NIPAAm-*co*-VDMA-proline 2) (POC 2) was used to catalyze the reaction between *p*-NBA and CH in water. To study the effect of organocatalyst immobilization a reference system containing the free organocatalyst and the block copolymer was chosen. For all the reactions an excess of CH was employed and the conversion of *p*-NBA obtained from the ratio of the signals for the aromatic protons in the educts at 8.14 ppm and product at 7.58 ppm in DMSO was used to calculated *p*-NBA conversion. The diastereomeric ratio can be determined from the signals of the protons in the hydroxy (*syn*: 5.44 ppm, *anti*: 5.50 ppm) group or the methine proton (*syn*: 5.22 ppm, *anti*: 5.08 ppm) in DMSO (as shown in Figure 74). The enantioselectivity (ee) was determined by chiral HPLC analysis.
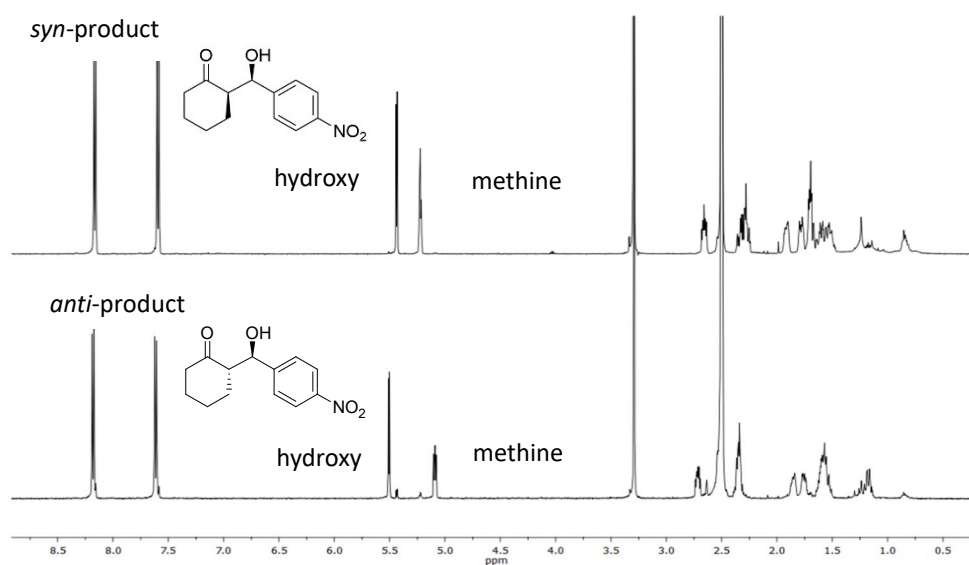
Figure 74. ^{1}H-NMR spectra of the syn- and anti product for the asymmetric aldol reaction between *p*-NBA and CH.

As shown in Table 25, the reaction with the PEG-*b*-PNIPAAm (PEG-PN-1) amphiphilic block copolymer and the free proline 2 organocatalyst achieved 0 % conversion at both lower and higher temperatures. This result can be explained by the solubility of both reagents and catalyst. At lower temperature both the organocatalyst proline 2 and the amphiphilic block

copolymer show a good water solubility. However, the reagents CH and *p*-NBA are almost insoluble in water. Thus, the phase separation between catalyst and reagents prevents a reaction. At high temperatures the block copolymer become amphiphilic and helps to stabilize the reagents in the aqueous media. But the organocatalyst still remains water-soluble, not capable of promoting the reaction. On the other hand, due to the deprotection process residues of HCl in the reaction products may also interfere with the aldol reaction. Therefore, triethylamine TEA was added to the reaction system to neutralize the HCl in order to counteract the effect of residual HCl on the aldol reaction. TEA is often reported as an additive in various enantioselective reaction.[203] Upon TEA addition, self-assembly does not affect the organocatalytic reaction. A possible explanation would be the increased hydrophobicity of the organocatalyst under basic conditions. As a result of the HPLC and NMR analysis, the catalyst stereoselectivity was also independent from temperature resulting in moderate anti/syn ratio (< 70 % anti) and the poor ee values (< 3%). When using the polymer-supported proline 2 organocatalyst, the rate of aldol reaction was directly related to temperature. The reaction reached 10 % conversion after 24 h stirring below the phase transition temperature and the catalyst system gave an enhanced rate of aldol formation when the temperature increased from 25 °C to 40 °C. In contrast to the free organocatalyst, the immobilized proline 2 resulted in an increased anti/syn ratio of > 75 % anti and a slight improvement of the ee selectivity. This phenomenon illustrates that the temperature-induced phase transition can be utilized to control the reaction rate and to improve catalyst reactivity by forming nanoreactors. In the next step, the influence of the concentration and the structure of the hydrophilic block on the organocatalytic reaction is investigated.

Table 25. Data for the aldol reaction of CH and *p*-NBA using free proline 2 **(10)** in water (3 mL) at different reaction conditions.

Cat.	T (°C)	$\frac{n(catalyst)}{n(educt)}$ (%)	conv. [a] (%)	dr [a, b](anti/syn) NMR; HPLC	ee (%)[b] (anti; syn)
PEG-PN-1 + **(10)**	25	7.4	0	-	-
	40	7.4	0	-	-
PEG-PN-1 + **(10)** + TEA	25	7.4	100	66/34; 70/30	1; 3
	40	7.4	100	67/33; 69/31	2; 2
POC 2	25	8.1	10	75/25; 75/25	14; 23
	40	8.1	57	83/17; 77/23	20; 6

[a] from ^{1}H-NMR spectroscopy calculated

[b] determined by HPLC, AD-H, isopropanol/n-hexan (1/9)

Table 26. Data for the aldol reaction of CH and *p*-NBA using polymer-supported proline 2 by different reaction conditions after 24 h.

Cat.	T °C	$V_{(H2O)}$ (mL)	$\frac{n(catalyst)}{n(educt)}$ (%)	Conv. (%)	dr [a, b](anti/syn) NMR; HPLC	ee (%) (anti; syn)
POC 2	25	3	8.1	10	75/25; 75/25	14; 23
	40	1	8.1	74	77/23; 79/21	33; 1
	40	3	8.1	58	83/17; 77/23	20; 6
	40	6	8.1	80	77/23; 68/32	27; 4
POC 4	25	3	8.0	6	85/15; 80/20	43; 22
	40	1	8.0	83	81/19; 65/35	82; 40
	40	3	8.0	55	80/20; 75/25	60; 23
	40	6	8.2	14	80/20; 81/19	33; 9
POC 6	25	3	8.0	10	85/15; 80/20	23; 25
	40	1	8.0	83	80/20; 59/41	61; 64
	40	3	8.0	39	82/18; 77/23	45; 2
	40	6	7.6	16	84/16; 80/20	34; 7

[a] calculated from ^{1}H-NMR spectroscopy

[b] determined by HPLC, AD-H, isopropanol/n-hexane (1/9)

To study the effect of different structures of the hydrophilic block on the catalytic reaction proline 2 moiety was immobilized on the different amphiphilic block copolymers (PDHPA-*b*-P(NIPAAm-*co*-VDMA-proline 2) (POC 4), PDMAA-*b*-P(NIPAAm-*co*-VDMA-proline 2) (POC 6) and PEG-*b*-P(NIPAAm-*co*-VDMA-proline 2) (POC 2) by post polymerization modification with 4 - 5 mol% loading of the catalyst on the polymer chain. In these reactions 7.6 – 8.1 % of the proline moiety relative to the amount of *p*-NBA was used. Beside the structure of the hydrophilic block, the reagents concentration was varied by altering the amount of water. The reactions reached a maximal of 10 % conversion after 24 h, when the reaction mixture was stirred at 25 °C, so that no temperature-induced aggregation occurred. When the reaction temperature increased from 25 °C to 40 °C, all the three catalyst systems exhibited an enhanced reaction rate.

As shown in Table 26, the structure of the different supporting polymers as well as the reagent concentration had a significant influence on the aldol reaction. The use of PEG-*b*-P(NIPAAm-*co*-VDMA-proline 2) (POC 2) in different volumes of the water (1 mL, 3 mL and 6 mL), led to *p*-NBA conversions from 58 % to 80 %. However, the catalyst stereoselectivity was maintained at a low level with respect to the anti/syn ratio (< 80% anti-product) and the ee values (< 33 %). The reaction systems involving the PDHPA- or PDMAA-based block copolymers were more sensitive to changes in concentration. As the reaction mixture was diluted to 6 mL, the reaction rates were almost 6 times lower. Simultaneously the ee selectivity for PDHPA-*b*-P(NIPAAm-*co*-VDMA-proline 2) dropped from 82 % to 33 %. For surface-catalyzed bimolecular reactions in thermos-responsive nanoreactors, there are two factors influencing the catalyst activity: the reactant diffusion and surface reaction rates.[204] Firstly, for the catalytic reactions using PDHPA- or PDMAA-containing block copolymers in dilute reaction conditions, the lower concentration gradient of reactants in the system, slows down the substance diffuse rate from bulk aqueous dispersion to the core of the micelles. Secondly, for the aldol reactions under concentrated conditions with different polymer-supported catalysts the results indicate a drastic increasing of the ee selectivity with increasing PNIPAAm content: PEG-*b*-P(NIPAAm-*co*-VDMA-proline 2) with 73.2 mol% of PNIPAAm, PDMAA-*b*-P(NIPAAm-*co*-VDMA-proline 2) with 83.6 mol% of PNIPAAm and PDHPA-*b*-P(NIPAAm-*co*-VDMA-proline 2) with 86.7 mol% of PNIPAAm. At higher

temperatures, the collapsed PNIPAAm block formed a more hydrophobic environment for the formation of enamine species, which shifted the reaction equilibrium rapidly to the product with higher enantiomer selectivity.

These results agree with previous studies by Zotova et al. suggesting that by addition of water to the proline-mediated aldol reaction with aromatic aldehydes the intrinsic rate per active catalyst species within the cycle is suppressed. The generally accepted catalytic cycle for aldol reactions shown in Figure 75.[126] Two conflicting effects of water were investigated for solution reactions and has been kinetically validated. In the absence of water, an irreversible deactivation of proline occurs in the presence of aromatic aldehydes such as p-NBA (Figure 77). With the addition of water, the formation of the iminium species **9** as well as the key intermediate **5** are suppressed (Figure 75). Therefore, the selectivity of the reaction can be obviously improved by reducing the amount of water in the reaction system, e.g. by performing the reaction in a more hydrophobic environment, such as the core of nanoreactors.
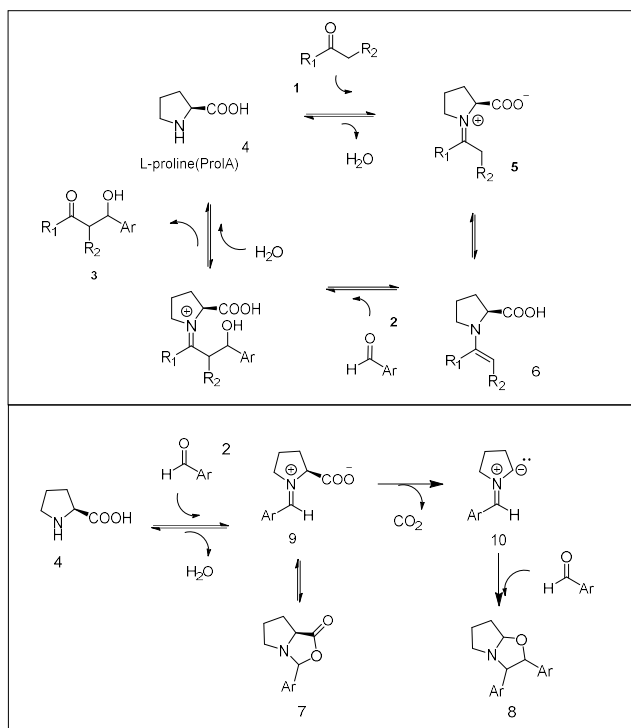
Figure 75. Proposed mechanism for the proline-mediated intermolecular aldol reaction cycle and side reactions of aromatic aldehydes with proline.[126] (Adapt with permission from (Zotova, N.; Franzke, A.; Armstrong, A.; Blackmond, D. G. Clarification of the role of water in proline-mediated aldol reactions. *J. Am. Chem. Soc.* **2007**, 129, 15100–15101). Copyright (2018) American Chemical Society)

4.4.2 Reaction kinetics studies

The results of the organocatalytic reaction using polymer-supported L-proline containing nanoreactors suggested, that the formation of the hydrophobic environment within the nanoreactor controlled the reaction rate and enhanced the selectivity of the asymmetric aldol reaction in water. At this point, it has to be investigated whether the increased reaction rate at higher temperatures is related to block copolymer aggregation, or if it is just an Arrhenius-type behavior. For the kinetic research the asymmetric Aldol reaction was carried out at 5 different temperatures (25 °C, 30 °C, 35 °C, 40 °C and 45 °C) using the polymer-supported catalysts in 6 mL water. After certain time intervals, 0.1 mL of the reaction mixture was withdrawn to determine the *p*-NBA conversion via ^{1}H-NMR spectroscopy. By comparing the reaction rate constant at different temperatures, the performance of the temperature-induced nanoreactors was evaluated. The calculation of reaction rate constant k was performed using eq.2 and eq.3, where k is the reaction rate constant (L·s/mol), $[A]_0$ is the concentration of *p*-NBA at t = 0 s and $[A]_t$ is the concentration of *p*-NBA at a time t. $[B]_0$ is the concentration of CH at t = 0 s and $[B]_t$ is the concentration of CH at a time t. Most of the kinetic studies in literature assume to be dealing with pseudo unimolecular reactions, when CH in large excess ($[B]_t \approx [B]_0$ and $[B]_0 = 5.83[A]_0$ = constant).

For the rate laws of a pseudo unimolecular reaction, the differential form is shown in eq. 2.

$$\upsilon = -\frac{d[A]}{dt} = -\frac{d[B]}{dt} = k[A][B] \approx k'[A] \qquad \text{eq. 2}$$

And the integrated form is given below in eq. 3:

$$\ln\frac{[A]_0}{[A]_t} = k't \qquad \text{eq. 3}$$

Hence, the reaction rate constant can be calculated with a plot of ln ($[A]_0/[A]_t$) versus t and summaries in Table 27.

Table 27. Reaction rate constant and standard error of the different immobilized organocatalysts.

T (°C)	POC 2		POC 4		POC 6	
	k'[L·s/mol][a]	standard error	k' [L·s/mol][a]	standard error	k' [L·s/mol] [a]	standard error
25	$1.94*10^{-6}$	$5.94*10^{-7}$	$2.22*10^{-7}$	$1.05*10^{-7}$	$9.28*10^{-7}$	$2.64*10^{-7}$
30	$6.12*10^{-6}$	$1.53*10^{-6}$	$5.99*10^{-7}$	$1.62*10^{-7}$	$9.53*10^{-7}$	$1.18*10^{-7}$
35	$2.50*10^{-5}$	$1.85*10^{-6}$	$1.78*10^{-6}$	$2.16*10^{-7}$	$1.96*10^{-6}$	$1.89*10^{-7}$
40	$2.63*10^{-5}$	$8.11*10^{-7}$	$4.23*10^{-6}$	$3.24*10^{-7}$	$3.59*10^{-6}$	$2.54*10^{-7}$
45	$2.48*10^{-5}$	$2.88*10^{-6}$	$6.37*10^{-6}$	$8.11*10^{-7}$	$7.44*10^{-6}$	$1.47*10^{-6}$

[a] calculated from the ^{1}H-NMR spectra

As known, the majority of temperature activated reactions is following the Arrhenius-type behavior, which is shown in eq. 3, where T is the absolute temperature in Kelvin, A is the pre-exponential factor, E_a is the activation energy for the reaction and R is the universal gas constant. In the logarithmizied of Arrhenius' equation, a plot of ln(k) versus 1/T shows a linear behavior.

$$k = A\, e^{\frac{-E_a}{RT}} \quad \text{and} \quad \ln(k) = \frac{-E_a}{R}\left(\frac{1}{T}\right) + \ln(A) \qquad \text{eq. 4/5}$$
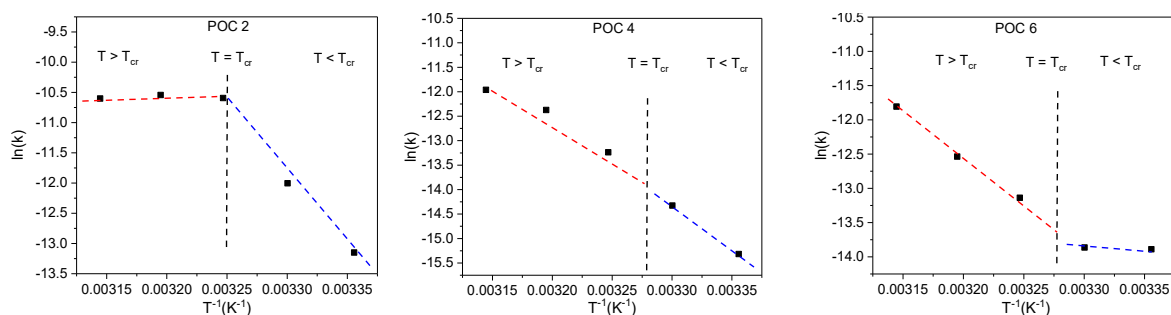
Figure 76. Arrhenius plot of reaction rate constants vs inverse temperature of different immobilized organocatalyst systems.

Figure 76 shows the conversion-time diagram as well as the Arrhenius-plot of the asymmetric aldol reaction catalyzed by different block copolymers bearing the proline 2 organocatalyst. As already mentioned, the reaction using PDMAA-*b*-P(NIPAAm-*co*-VDMA-proline 2) (POC 6) and PDHPA-*b*-P(NIPAAm-*co*-VDMA-proline 2) (POC 4) in dilute water medium (6 mL) exhibited a significant reduction of the reaction rate, due to the slowing down of the reagent mass transport from bulk aqueous dispersion to the core of the micelles. However, studying the

change of the reaction rate below and above the phase transition temperature is of high importance. As reported by Khokhlov et al. and Liu et al. the catalyzed reaction using a copolymers-supported catalyst did not follow the Arrhenius-type behavior. The Arrhenius plot showed a pronounced upward curvature above the critical micellization temperature, resulting in higher reaction rates than predicted by the Arrhenius law.[205,206] Thus, a deviation from the linear Arrhenius plot can be used to confirm, that the temperature-induced aggregation has an effect on the reaction rate. The reaction systems involving the three different functionalized block copolymers exhibit distinctly different behavior in the Arrhenius plot (Figure 76). PEG-*b*-P(NIPAAm-*co*-VDMA-proline 2) (POC 2) showed a phase transition temperature of about 35 °C, which was determined by DLS measurement. The Arrhenius-plot shows that, the reaction rate constant slows down upon exceeding the phase transition temperature. Consequently, the formation of micelles seemed to inhibit the reaction rate. In contrast, the PDMAA-*b*-P(NIPAAm-*co*-VDMA-proline 2) (POC 6) system exhibit a prominent upward curvature for temperatures higher than T_{cr}. This is in good agreement with the principle of micellar catalysis. It can be calculated that for the aldol reaction using PDMAA-*b*-P(NIPAAm-*co*-VDMA-proline 2) (POC 6), the slope of ln(k) vs 1/T increased almost 40 times above the critical transition temperature. However, the catalytic process using PDHPA-*b*-P(NIPAAm-*co*-VDMA-proline 2) (POC 4) appears to be less influenced by the critical transition temperature. There is just a slight upward curvature above 33 °C. This slope is only 1.16 times higher than below the critical transition temperature. In summary, the effect of block copolymer aggregation on the reaction rate seems to be affected by the block copolymer structure.
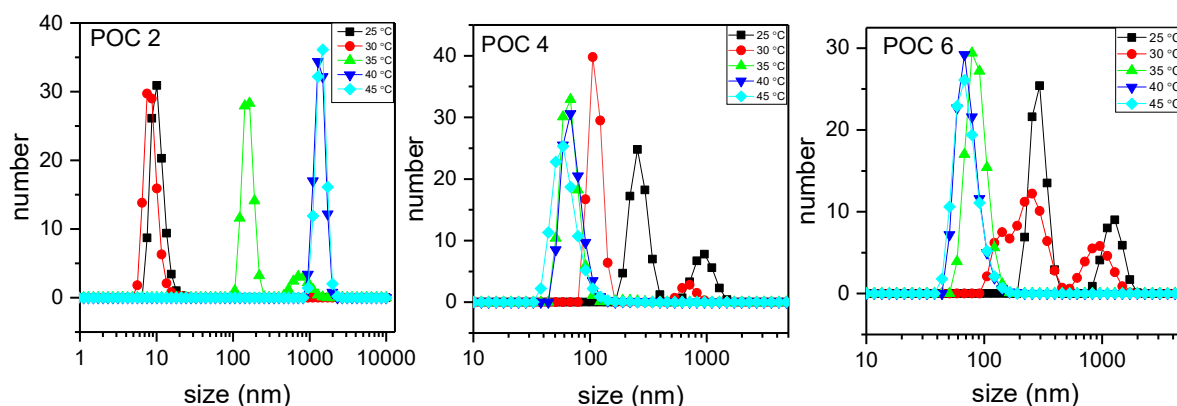
Figure 77. Number distribution of hydrodynamic diameter for polymer-supported catalysts with *p*-NBA and CH in dilute aqueous solution.

To explain the different aggregation dependence of the reaction rate constant the DLS data from chapter 4.3 are discussed in detail with respect to the number-based size distribution of the different block copolymers in aqueous media at different temperature. Due to the heterogenicity of the reaction mixture, 1 mL of the reaction solutions was further diluted with 9 mL deionized water and stirred overnight. Figure 77 displays the number-based size distribution of the apparent hydrodynamic diameter for the different proline 2 bearing block copolymers in the dilute reaction mixture at different temperatures. For the samples PDMAA-*b*-P(NIPAAm-*co*-VDMA-proline 2) (POC 6) and PDHPA-*b*-P(NIPAAm-*co*-VDMA-proline 2) (POC 4) the hydrodynamic diameter decreased from several hundred nm to almost 70 nm, when the temperature was raised from 25 °C to 45 °C. Vasilevskaya et al. proposed a theoretical analysis of a catalytic reaction in miniemusions.[207] They suggested that, the acceleration effect of the reaction rate in micellar solutions resulted from a large local concentration of reagents at the interface of the aggregates. Thus, the reaction rate significantly depended on the emulsion droplet size. For the reaction using low-molecular weight surfactants the effect was stronger than in the case of amphiphilic macromolecular surfactants. Therefore, for the PEG-*b*-P(NIPAAm-*co*-VDMA-proline 2) above the critical transition temperature, aggregates growth of more than 1000 nm in size was observed, which causes the dramatic reduction of the local catalyst concentration at the interface of the aggregate, leading to a reduction of the reaction rate constant. As mentioned above, for PDHPA-*b*-P(NIPAAm-*co*-VDMA-proline 2) (POC 4) and

PDMAA-*b*-P(NIPAAm-*co*-VDMA-proline 2) (POC 6) the aggregates smaller than 100 nm were observed above the phase transition temperature, leading to an enhancement of the catalytic activity upon self-assembly.

4.4.3 Comparison of supported L-prolines and L-prolinamides

In this chapter, the catalytic activity of the different L-proline and L-prolinamide derivatives supported on PEG-based block copolymers is compared. According to the chemical structure, the immobilized proline moiety may be divided into two major categories: Proline 1 was synthesized using 4-hydroxyl-L-proline, which belongs to the original class of L-proline organocatalysts. The proline 2 and proline 3 belongs to prolinamide analogues, well known to act as organocatalyst for asymmetric organic transformations, providing the products in high yields and good stereoselectivities.[208,209] However, there are a lot of prolinamide analogues, which were successfully employed in enantioselective asymmetric organic transformations, but which are not suitable for immobilization in the present work.[210] Due to the large steric hindrance of some prolinamide analogies, it is difficult to introduce NH_2 groups for further post-polymerization modification.
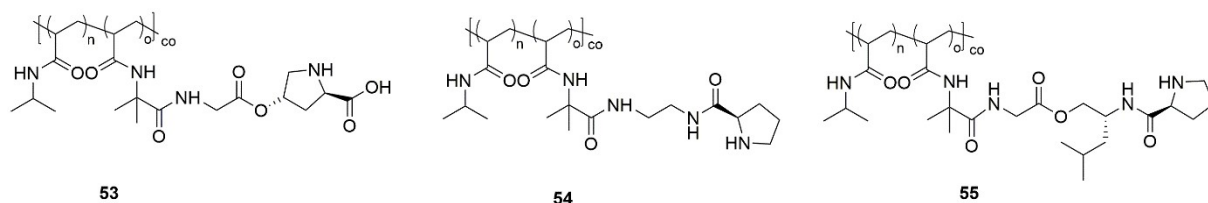
Figure 78. Chemical structures of the immobilized L-proline and prolinamide analogues (53)-(55).

Table 28. Data for the aldol reaction of CH and 4-nitrobenzaldeyde using different polymer-supported L-proline and L-prolinamide analogies.

Cat.	T (°C)	H₂O (mL)	$\frac{n(catalyst)}{n(educt)}$ (%)	Conv. (%)[a]	dr [a, b](anti/syn) NMR; HPLC	ee (%)[b] (anti; syn)
POC 1	25	3	8.3	0	-	-
	40	3	8.3	13	67/33; -/-	-
POC 2	25	3	8.1	10	75/25; 75/25	14; 23
	40	3	8.1	58	83/17; 77/23	20; 6
	40	1	8.1	74	77/23; 79/21	33; 1
POC 3	25	3	7.3	0	-	-
	40	3	8.0	41	76/24; -/-	-
	40	3	12.6	76	80/20; 72/28	76; 29
	40	1	11.0	100	84/16; 76/24	86; 29

[a] calculate from ¹H-NMR spectra

[b] determined by HPLC, AD-H colume, isopropanol/n-hexane (1/9)

Table 28 summarizes the results of the micellar organocatalyst reactions using different proline and prolinamide analogies. Firstly, for the aldol reaction using PEG-*b*-P(NIPAAm-*co*-VDMA-proline 1) (POC 1), the *p*-NBA conversion was observed to be lower than 15 % after 24 h reaction time at 40 °C and in the HPLC measurement no available information was detected about the dr and ee selectivity of the product due to the too low concentration of the product. The unexpectedly low reaction rate may be attributed to the functionalized L-proline moiety. After immobilization of the organocatalyst, the PNIPAAm block became more hydrophilic, thereby reducing the hydrophobic character of the aggregate core. This reduced hydrophobicity directly affected the catalyst activity. In contrast, for the reactions using PEG-*b*-P(NIPAAm-*co*-VDMA-proline 2) (POC 2) and PEG-*b*-P(NIPAAm-*co*-VDMA-proline 3) (POC 3) a temperature-dependent switch of catalyst activity could be observed. Using PEG-*b*-P(NIPAAm-*co*-VDMA-proline 2) (POC 2) as catalyst, the conversion increased from 10 % to 58 % by raising the temperature from 25 °C to 40 °C. However, there is no obvious change in the stereoselectivity. Moreover, a significant increase of the reaction rate was found for higher

reagent and block copolymer concentrations. In comparison to PEG-*b*-P(NIPAAm-*co*-VDMA-proline 2) (POC 2), the use of PEG-*b*-P(NIPAAm-*co*-VDMA-proline 3) (POC 3) led to similar results according to both *p*-NBA conversions and diastereomeric ratio. However, all the reactions using PEG-*b*-P(NIPAAm-*co*-VDMA-proline 3) (POC 3) exhibited a significantly higher enantioselectivity with ee values of up to 86 % for the anti-enantiomer, which are almost three times higher than for the PEG-*b*-P(NIPAAm-*co*-VDMA-proline 2) (POC 2) catalyst. In addition, *p*-NBA conversion could be increased to a quantitative level by increasing the catalyst loading to 12 mol% and simultaneously reducing the amount of water. These results suggest that the organocatalytic reaction can be efficiently conducted at higher temperature due to the formation of nanoreactors containing the immobilized organocatalyst within the hydrophobic core. Similar to the reactions in organic solvents the higher local concentration of catalyst improves the reaction. Beside the reaction conditions such as temperature and catalyst loading, the chemical structure of block copolymer support is an important prerequisite for an optimal reactor performance. The results of the aldol reaction using the proline 3 organocatalyst immobilized on different block copolymers is shown in Tabel 29. High *p*-NBA conversions and good stereoselectivity could be achieved. For the PDHPA- and PDMAA-based block copolymers (POC 3 and POC 7) the catalyst loading could be reduced to 5 and 7% respectively, without loss of catalytic efficiency.

Table 29. Data for the aldol reaction of CH and *p*-NBA using polymer-supported proline 3 in 1 mL water (1 mL) after 24 h reaction time.

Cat.	$\frac{n(catalyst)}{n(educt)}$ (%)	Conv.[a] (%)	dr [a, b](anti/syn) NMR; HPLC	ee (%) (anti; syn)[b]
POC 3	11.0	100	84/16; 76/24	86; 29
POC 5	4.6	100	86/14; 80/20	86; 24
POC 7	7.3	100	81/19; 75/25	85; 19

[a] calculated from ^{1}H-NMR spectroscopy

[b] determined by HPLC, AD-H column, isopropanol/n-hexane (1/9)

4.4.4 Recycling and reuse of supported organocatalysts, application to other substrates

The catalyst recycling was studied using the same aldol reaction between *p*-NBA and CH with PEG-*b*-P(NIPAAm-*co*-VDMA-proline 2) (POC 2) as catalyst at 40 °C. After 24 h reaction products were obtained by extraction with diethyl ether and the polymer-supported catalyst was recovered from the aqueous phase by freeze-drying. The resulting dry polymer was reused in consecutive reaction cycles under the same reaction conditions. The immobilized organocatalyst was used for five cycles showing a high recovery rate with only 4 - 8% w/w weight loss per each cycle (Table 30). The *p*-NBA conversions and the diastereoselectivity remained practically unchanged. However, a steady reduction of enantioselectivity was observed especially after the 4th and 5th cycle.[211]

Table 30. Results for catalyst recycling using POC 2 in water (6 mL) at 40 °C for 24 h.

Cycle	Amount of the polymer	Conversion (%)[a]	dr [a, b](anti/syn) NMR; HPLC	ee[b] (%)
1	50 mg	100	57/43; 67/33	54
2	47 mg	100	61/39; 61/39	61
3	45 mg	88	65/35; 65/35	40
4	41 mg	100	60/40; 60/40	27
5	39 mg	100	55/45; 55/45	1

[a] calculated from ^{1}H-NMR spectroscopy

[b] determined by HPLC, AD-H column, isopropanol/n-hexane (1/9)

Finally, the applicability of the immobilized catalyst to a variety of aromatic aldehyde was studied. Therefore, the immobilized organocatalyst PEG-*b*-P(NIPAAm-*co*-VDMA-proline 2) was applied to the aldol reaction of *p*-NBA, benzaldehyde and *p*-benzyloxy benzaldehyde with CH (Table 31). Reaction conditions were equal to the previously discussed experiments. Aldehyde conversions varied from 35 % to 57 % depending on the electrophilicity of the aldehyde. By comparison of peaks at 4.9- 5.1 ppm a relative ratio of diastereomers was calculated from [1]H-

NMR spectra with a value varying from 79/21 to 83/17. An elaborate determination of the dr and ee values were not possible due to peak overlapping in the chromatograms of the HPLC measurement. As mentioned in chapter 4.4.1, the PEG-*b*-P(NIPAAm-*co*-VDMA-proline 2) as polymer-supported organocatalyst showed a relatively low selectivity. Therefore, a better reactivity and selectivity may be achieved by using the immobilized proline 3 catalyst under optimized reaction conditions.

Table 31. Extension aldol reaction with benzaldehyde and 4-(Benzyloxy) benzaldehyde.

R_1 = OBn
R_2 = H
R_3 = NO$_2$

R_1 = OBn
R_2 = H
R_3 = NO$_2$
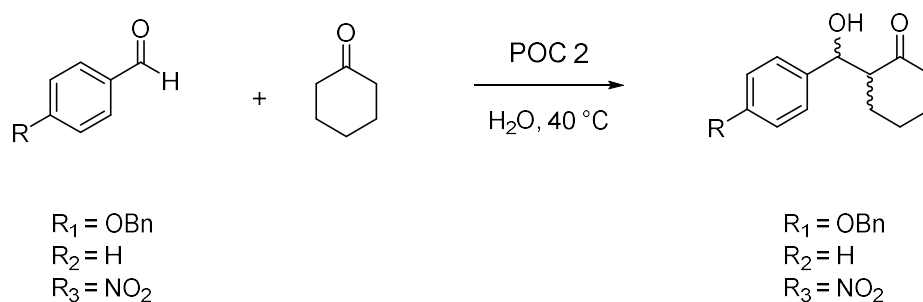
Sample	R	$\frac{n(catalyst)}{n(educt)}$ (%)	Conv.[a] (%)	dr[a]
entry 1	OBn	7.8	36	80/20
entry 2	H	7.8	44	79/21
entry 3	NO$_2$	8.1	58	83/17

[a] calculated from ^{1}H-NMR spectra

5. Conclusion

In this present work a series of thermo-responsive polymer-supported organocatalysts were successfully prepared and employed in the direct asymmetric aldol reaction between *p*-NBA and CH in water. An optimization of RAFT polymerization conditions (e.g. selection of CTA and CTA/initiator ratio) was conducted for synthesis of PSKA in particles. The investigation of SKA polymerization kinetics revealed a constant radical concentration as well as a consistent growth of the polymer chains. Thus, the average molecular weight could be adjusted, leading to polymers with narrow molar mass distributions. End group functionality was analyzed using ESI-IMS-ToF mass spectra showing that the majority of polymer chains carried the expected end groups depended on by the applied RAFT agent and initiator. Chain extension with NIPAAm was successfully performed by using PSKA-based macro-CTAs. Amphiphilic block copolymers of PDHPA-*b*-PNIPAAm were successfully obtained after hydrolysis of the SKA. Using this method, well-defined amphiphilic block copolymers of PDHPA-*b*-PNIPAAm, PDMAA-*b*-PNIPAAm, PEG-*b*-NIPAAm with varying chain length (up to a ratio 1/6 of hydrophilic block PNIPAAm were synthesized by sequential RAFT polymerization using different macro-CTAs. Temperature-induced self-assembly of these block copolymers in aqueous solution was studied by dynamic light scattering (DLS). The critical solution temperatures for the synthesized block copolymers were determined to be in the range of 32 - 35 °C. Block copolymers with longer PNIPAAm blocks exhibited a more pronounced phase transition, forming more stable nano-structures with an apparent hydrodynamic diameter ranging from 50–100 nm above the critical phase transition temperature (T_{cr}). As supporting materials for the organocatalyst immobilization, azlactone-functionalized amphiphilic block copolymers were synthesized via RAFT copolymerization of NIPAAm and VDMA, starting from poly(ethylene glycol) (PEG), poly(*N*,*N*-dimethylacrylamide) (PDMAA) or poly(solketal acrylate) (PSKA) based macro-CTAs. The resulting block copolymers comprised a hydrophilic block (PEG, PDMAA, PDHPA) and a thermo-responsive PNIPAAm block with VDMA moieties for the attachment of the organocatalyst. For the immobilization, different amino-functionalized L-

5. Conclusion

proline and L-prolineamide derivatives were successfully synthesized. Post-polymerization attachment of the organocatalyst was achieved by the nucleophilic ring opening reaction of the amino-functionalized organocatalyst with the azlactone functional group, yielding polymer chains with 2 – 5 mol% immobilized organocatalyst. DLS results showed, that after the organocatalyst immobilization, there was no significant increase or decrease of the critical phase transition temperature compared to the amphiphilic block copolymers without the immobilized organocatalyst. The asymmetric aldol reaction between *p*-NBA and CH in aqueous medium was used as model reaction to evaluate the activity and selectivity of the immobilized organocatalysts. Compared to the free organocatalyst the polymer-supported organocatalysts displays a higher catalyst activity for the asymmetric aldol reaction in aqueous media. For the organocatalytic process, both the selection of the supporting materials as well as the chemical structure of the immobilized organocatalyst play a key role: The chemical structure of the temperature-responsive amphiphilic block copolymers influenced the formation of the micellar aggregates above T_{cr}, thereby providing a hydrophilic environment for solubilizing the regents and a high interfacial area for the contact with catalyst and water. As a result of the kinetic studies the aldol reaction involving the organocatalyst immobilized on a PDMAA-based thermo-sensitive block copolymer exhibited a significant acceleration upon block copolymer self-assembly. In contrast, the PEG-based thermo-responsive block copolymers carrying the organocatalyst self-assembled into large aggregates of several hundred nm in size. Therefore, a substantial slowdown of the aldol reaction upon self-assembly could be observed. Variations in the chemical structure of the immobilized catalyst mainly affected the stereoselectivity of the reaction. The use of prolinamide afforded aldol products with higher diastereomeric and enantiomeric selectivity. In addition, the recovery of the polymer-supported organocatalyst was successfully achieved by extraction and freeze-drying. Reuse of the immobilized organocatalyst showed no loss in catalyst activity, even after five cycles. However, the diastereoselectivity as well as the enantioselectivity declined steadily with each cycle. In the last part of this work, the immobilized organocatalyst was successfully applied in the aldol reaction of different aldehydes with CH.

6. Outlook

There are several issues in this work, which can be further investigated and optimized in various directions. Firstly, the asymmetric proline-catalyzed aldol reaction requires a low water content. Therefore, the formation of a stable hydrophobic environment is a key aspect to further improve the nanoreactor. Beside the extension of the PNIPAAm block, the addition of hydrophobic monomers e.g. styrene, butyl acrylate in the PNIPAAm block would also enhance hydrophobic properties within the micellar core. Due to the similar reactivity of the monomers P(NIPAAm-co-styrene(butyl acrylate)-*co*-VDMA) block can be prepared by copolymerization via RAFT under optimized conditions. In a second strategy, post polymerization modification can serve as a tool not only for the catalyst immobilization but also for the introduction of hydrophobic components e.g. benzylamine or butylamine. In this way, the hydrophobicity within the micellar core could also be improved.

Another key issue concerns the organocatalyst structure. The present results clearly show that the prolineamide-derivates exhibit a better stereoselectivity in the asymmetric aldol reaction. In the further research, numerous proline-derivates including prolineamide and prolinamide-thiourea (1-3) can be employed as immobilized organocatalyst. As reported, the chiral centers of the diamine unit and the thiourea moiety are required for high catalytic activity, while the contributions from the designed thiourea hydrogen and the amide hydrogen are considered as the predominant source of the hydrogen bonding.[208] In terms of „green chemistry ", the catalyst recovery and re-use can be optimized by taking advantage of the stimuli-sensitive behavior.
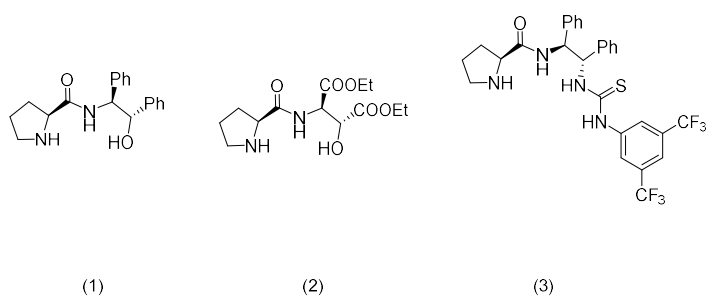
(1) (2) (3)

7. Acknowledgment

Anerkennung der Promotionsordnung

Hiermit erkenne ich die Promotionsordnung der Fakultät für Naturwissenschaften der Universität Paderborn vom 12. November 2012 an. Erlassen von der Universität Paderborn aufgrund des § 2 Abs. 4 und des § 67 Abs. 3 des Gesetzes über die Hochschulen des Landes Nordrhein-Westfalen (Hochschulgesetz – HG) vom 31. Oktober 2006 (GV.NRW. 2006 S. 474), zuletzt geändert durch Art. 1 des Gesetzes zur Änderung des Hochschulgesetzes, des Kunsthochschulgesetzes und weiterer Vorschriften vom 31. Januar 2012 (GV.NRW. 2012 S. 90).

_____

Xiaoqian Yu

Eidesstattliche Erklärung

Hiermit versichere ich, dass ich die vorliegende Arbeit ohne unzulässige Hilfe Dritter und ohne Benutzung anderer als der angegebenen Hilfsmittel angefertigt habe; die aus fremden Quellen direkt oder indirekt übernommenen Gedanken sind als solche kenntlich gemacht. Die Arbeit wurde bisher weder im Inland noch im Ausland in gleicher oder ähnlicher Form einer anderen Prüfungsbehörde vorgelegt.

Die Dissertation wurde an der Professur für Organische und Makromolekulare Chemie der Universität Paderborn fortgeführt und unter wissenschaftlicher Betreuung durch Prof. Dr. rer. nat. habil. Dirk Kuckling angefertigt.

_____

Xiaoqian Yu

Danksagung

8. Abbreviations

^{13}C-NMR	Carbon-13 nuclear magnetic resonance
^{1}H-NMR	Proton nuclear magnetic resonance
2. 2'-bpy	2,2'-Bipyridine
ACVA	4,4'-Azobis(4-cyanovaleric acid)
AIBN	2,2'-Azobis(2-methylpropionitrile)
AM	Acrylamide
AN	Acrylonitrile
ATR-IR	Attenuated total reflection infrared spectroscopy
ATRP	Atom transfer radical polymerization
BHT	2,6-di-*tert*-butyl-*p*-cresol
Boc	*tert*-Butoxycarbonyl protecting group
Boc$_2$O	di-*tert*-Butyl dicarbonate
Cbz	Benzyl carbamates protecting group
CCS	Coillision cross section
CDCl$_3$-*d*	Deuterated chloroform
CDPA	4-Cyano-4-[(dodecylsulfanylthiocarbonyl)sulfanyl]pentanoic acid
CH	Cyclohexanone
CHCl$_3$	Chloroform
CSIRO	Commonwealth Scientific and Research Organization
CTA	Chain transfer agent
d	Doublet
DCM	Dichloromethane
dd	Double doublet
D$_h$	Hydrodynamic diameter

DHPA	2,3-dihydroxypropyl acrylate
DIC	Diisopropylcarbodiimide
DIPEA	*N,N*-Diisopropylethylamine
DLS	Dynamic light scattering
DMAA	*N,N*-Dimethylacrylamide
DMAc	*N,N*-Dimethylacetamide
DMP	2-(Dodecylthiocarbonothioylthio)-2-methylpropionic acid
DMSO	Dimethyl sulfoxide
DMSO-d$_6$	Deuterated dimethyl sulfoxide
dr	Diastereomeric ratio
Đ	Dispersity
EBriB	Ethyl-2-bromoisobutyrat
EDC HCl	*N*-(3-Dimethylaminopropyl)-N'-ethylcarbodiimide hydrochloride
ee	Enantiomeric excess
ESI-TOF-MS	Electrospray ionisation time-of-flight mass spectrometry
EtOAc	Ethyl acetate
EtOH	Ethanol
Fmoc	9-Fluorenylmethoxycarbonyl protecting group
HIPAAm	*N*-(2-hydroxyisopropyl) acrylamide
HPLC	High performance liquid chromatography
HPMA	*N*-(2-Hydroxypropyl)-methacrylamide
k$_{act}$	Rate constant of activation
k$_{deact}$	Rate constant of deactivation
k$_{exch}$	Rate constant of chain exchange
k$_p$	Rate constant of propagation
k$_t$	Rate constant of termination
LAM	Low active monomer

LCST	Lower critical solution temperature
MA	Methacrylate
MAM	More active monomer
MBrAc	Methyl bromoacetate
MBrP	methyl D,L-2-bromopropionate
Me$_6$Tren	Tris[2-(dimethylamino)ethyl] amine
MeOH	Methanol
MgSO$_4$	Magnesium sulfate
MMA	Methyl methacrylate
NIPAAm	*N*-Isopropyl acrylamide
NMRP	Nitroxide mediated radical polymerization
NVC	*N*-Vinyl-caprolactam
NVP	1-Vinyl-2-pyrrolidinone
PDHPA	Poly (2,3-dihydroxypropyl acrylate)
PDMAA	Poly (*N,N*-dimethylacrylamide)
PEBr	1-(bromoethyl)benzene
PEG	Poly (ethylene oxide)
PHIPAAm	Poly (*N*-(2-hydroxyisopropyl) acrylamide)
PMDETA	*N, N, N', N'', N''*-Pentamethyldiethylenetriamine
p-NBA	4-Nitrobenzaldehyde
PNCPAm	Poly (*N*-cyclopropyl acrylamide)
PNIPAAm	Poly (*N*-isopropyl acrylamide)
PNNPAAm	Poly (*N,N*-propyl acrylamide)
PNVBA	Poly (*N*-vinyl-*n*-butylamide)
ppm	Chemical shift
PSD	Particle size distribution
PSKA	Poly (solketal acrylate)
PVCL	Poly (*N*-vinylcaprolactam)

PVDMA	Poly (2-Vinyl-4,4-dimethylazlacton)
RAFT	Reversible addition fragmentation chain transfer
RDRP	Reversible degeneration radical polymerization
R_f	Retention factor
S	Singulett
SEC	Size exclusion chromatography
SKA	Solketal acrylate
ß	Concentration in mass
St	Styrene
T	Temperature
T_{cr}	Critical solution temperature
TEA	Triethylamine
TEMPO	2,2,6,6- (tetramethylpiperidiny-1-yl)oxyl
TFA	Trifluoroacetic acid
THF	Tetrahydrofuran
TIPNO	2,2,5-Trimethyl-4-phen- yl-3-azahexane 3-nitroxide
TLC	Thin layer chromatography
UCST	Upper critical solution temperature
UV-VIS	Ultraviolet–visible light spectroscopy
VAc	Vinyl acetate
VDMA	2-Vinyl-4,4-dimethylazlacton

9. References

(1) MacMillan, D. W. C. The advent and development of organocatalysis. *Nature* **2008**, *455*, 304–308.

(2) List, B.; Lerner, R. A.; Barbas III, Carlos F. Proline-Catalyzed Direct Asymmetric Aldol Reactions. *J. Am. Chem. Soc.* **2000**, *122*, 2395–2396.

(3) Córdova, A.; Notz, W.; Zhong, G.; Betancort, J. M.; Barbas III, Carlos F. A Highly Enantioselective Amino Acid-Catalyzed Route to Functionalized α-Amino Acids. *J. Am. Chem. Soc.* **2002**, *124*, 1842–1843.

(4) Dalko, P. I.; Moisan, L. In the golden age of organocatalysis. *Angew. Chem. Int. Ed.* **2004**, *43*, 5138–5175.

(5) Gruttadauria, M.; Giacalone, F.; Noto, R. Supported proline and proline-derivatives as recyclable organocatalysts. *Chem. Soc. Rev.* **2008**, *37*, 1666–1688.

(6) Diaz Diaz, D.; Kuhbeck, D.; Koopmans, R. J. Stimuli-responsive gels as reaction vessels and reusable catalysts. *Chem. Soc. Rev.* **2011**, *40*, 427–448.

(7) Fendler, E. J.; Fendler, J. H. Micellar Catalysis in Organic Reactions: Kinetic and Mechanistic Implications. *Adv. Phys. Org. Chem.* **1970**, *8*, 271–406.

(8) Riepe, A.; Beier, H.; Gross, H. J. Enhancement of RNA self-cleavage by micellar catalysis. *FEBS Letters* **1999**, *457*, 193–199.

(9) *Polymeric materials in organic synthesis and catalysis;* Buchmeiser, M. R., Ed.; Wiley-VCH: Weinheim, 2003.

(10) Shield, J. W.; Ferguson, H. D.; Bommarius, A. S.; Hatton, T. A. Enzymes in reversed micelles as catalysts for organic-phase synthesis reactions. *Ind. Eng. Chem. Fund.* **1986**, *25*, 603–612.

(11) La Sorella, G.; Strukul, G.; Scarso, A. Recent advances in catalysis in micellar media. *Green Chem.* **2015**, *17*, 644–683.

(12) Guo, G.; Wu, Y.; Zhao, X.; Wang, J.; Zhang, L.; Cui, Y. Polymerization of l-proline functionalized styrene and its catalytic performance as a supported organocatalyst for direct enantioselective aldol reaction. *Tetrahedron: Asymmetry* **2016**, *27*, 740–746.

(13) Doyagüez, E. G.; Corrales, G.; Garrido, L.; Rodríguez-Hernández, J.; Gallardo, A.; Fernández-

9. References

Mayoralas, A. Linear Copolymers of Proline Methacrylate and Styrene as Catalysts for Aldol Reactions in Water: Effect of the Copolymer Aggregation on the Enantioselectivity. *Macromolecules* **2011**, *44*, 6268–6276.

(14) Zayas, H. A.; Lu, A.; Valade, D.; Amir, F.; Jia, Z.; O'Reilly, R. K.; Monteiro, M. J. Thermoresponsive Polymer-Supported l -Proline Micelle Catalysts for the Direct Asymmetric Aldol Reaction in Water. *ACS Macro Lett.* **2013**, *2*, 327–331.

(15) Lendlein, A.; Shastri, V. P. Stimuli-sensitive polymers. *Adv. Mater. (Weinheim, Ger.)* **2010**, *22*, 3344–3347.

(16) Galaev, I. 'Smart' polymers and what they could do in biotechnology and medicine. *Trends Biotechnol.* **1999**, *17*, 335–340.

(17) Hoffman, A. S.; Stayton, P. S.; Bulmus, V.; Chen, G.; Chen, J.; Cheung, C.; Chilkoti, A.; Ding, Z.; Dong, L.; Fong, R. *et al.* Really smart bioconjugates of smart polymers and receptor proteins. *J. Biomed. Mater. Res.* **2000**, *52*, 577–586.

(18) Roy, D.; Cambre, J. N.; Sumerlin, B. S. Future perspectives and recent advances in stimuli-responsive materials. *Prog. Polym. Sci.* **2010**, *35*, 278–301.

(19) Stuart, M. A. C.; Huck, W. T. S.; Genzer, J.; Müller, M.; Ober, C.; Stamm, M.; Sukhorukov, G. B.; Szleifer, I.; Tsukruk, V. V.; Urban, M. *et al.* Emerging applications of stimuli-responsive polymer materials. *Nat. Mater.* **2010**, *9*, 101–113.

(20) Liu, F.; Urban, M. W. Recent advances and challenges in designing stimuli-responsive polymers. *Prog. Polym. Sci.* **2010**, *35*, 3–23.

(21) Scarpa, J. S.; Mueller, D. D.; Klotz, I. M. Slow hydrogen-deuterium exchange in a non-.alpha.-helical polyamide. *J. Am. Chem. Soc.* **1967**, *89*, 6024–6030.

(22) Roy, D.; Brooks, W. L. A.; Sumerlin, B. S. New directions in thermoresponsive polymers. *Chem. Soc. Rev.* **2013**, *42*, 7214–7243.

(23) Meewes, M.; Ricka, J.; Silva, M. de; Nyffenegger, R.; Binkert, T. Coil-globule transition of poly(N-isopropylacrylamide): A study of surfactant effects by light scattering. *Macromolecules* **1991**, *24*, 5811–5816.

(24) Maeda, Y.; Higuchi, T.; Ikeda, I. Change in Hydration State during the Coil–Globule Transition of

9. References

Aqueous Solutions of Poly(N -isopropylacrylamide) as Evidenced by FTIR Spectroscopy †. *Langmuir* **2000**, *16*, 7503–7509.

(25) Clark, E. A.; Lipson, J.E.G. LCST and UCST behavior in polymer solutions and blends. *Polymer* **2012**, *53*, 536–545.

(26) Ito, D.; Kubota, K. Solution Properties and Thermal Behavior of Poly(N - n -propylacrylamide) in Water. *Macromolecules* **1997**, *30*, 7828–7834.

(27) Maeda, Y.; Nakamura, T.; Ikeda, I. Changes in the Hydration States of Poly(N -alkylacrylamide)s during Their Phase Transitions in Water Observed by FTIR Spectroscopy †. *Macromolecules* **2001**, *34*, 1391–1399.

(28) Kunugi, S.; Tada, T.; Yamazaki, Y.; Yamamoto, K.; Akashi, M. Thermodynamic Studies on Coil−Globule Transitions of Poly(N -vinylisobutyramide- co -vinylamine) in Aqueous Solutions. *Langmuir* **2000**, *16*, 2042–2044.

(29) Lau, A. C. W.; Wu, C. Thermally Sensitive and Biocompatible Poly(N -vinylcaprolactam): Synthesis and Characterization of High Molar Mass Linear Chains. *Macromolecules* **1999**, *32*, 581–584.

(30) de Las Heras Alarcon, Carolina; Pennadam, S.; Alexander, C. Stimuli responsive polymers for biomedical applications. *Chem. Soc. Rev.* **2005**, *34*, 276–285.

(31) Donaruma, L. G. Synthetic biologically active polymers. *Prog. Polym. Sci.* **1975**, *4*, 1–25.

(32) Duncan, R. Polymer conjugates as anticancer nanomedicines. *Nat. Rev. Cancer* **2006**, *6*, 688–701.

(33) Harris, J. M.; Chess, R. B. Effect of pegylation on pharmaceuticals. *Nat. Rev. Drug Discovery* **2003**, *2*, 214–221.

(34) Masayuki, Y.; Mizue, M.; Noriko, Y.; Teruo, O.; Yasuhisa, S.; Kazunori, K.; Shohei, I. Polymer micelles as novel drug carrier: Adriamycin-conjugated poly(ethylene glycol)-poly(aspartic acid) block copolymer. *J. Controlled Release* **1990**, *11*, 269–278.

(35) Duncan, R. The dawning era of polymer therapeutics. *Nat. Rev. Drug Discovery* **2003**, *2*, 347–360.

(36) Wei, H.; Zhang, X.-Z.; Zhou, Y.; Cheng, S.-X.; Zhuo, R.-X. Self-assembled thermoresponsive micelles of poly(N-isopropylacrylamide-b-methyl methacrylate). *Biomaterials* **2006**, *27*, 2028–2034.

(37) Loh, X. J.; Zhang, Z.-X.; Wu, Y.-L.; Lee, T. S.; Li, J. Synthesis of Novel Biodegradable Thermoresponsive Triblock Copolymers Based on Poly[(R)-3-hydroxybutyrate] and Poly(N -isopropylacrylamide) and Their Formation of Thermoresponsive Micelles. *Macromolecules* **2009**, *42*, 194–202.

9. References

(38) Maeda, H.; Wu, J.; Sawa, T.; Matsumura, Y.; Hori, K. Tumor vascular permeability and the EPR effect in macromolecular therapeutics: A review. *J. Controlled Release* **2000**, *65*, 271–284.

(39) Fetters, L. J. Synthesis of block polymers by homogeneous anionic polymerization. *J. polym. sci., C Polym. symp.* **1969**, *26*, 1–35.

(40) Zhang, X.; Matyjaszewski, K. Synthesis of Well-Defined Amphiphilic Block Copolymers with 2-(Dimethylamino)ethyl Methacrylate by Controlled Radical Polymerization. *Macromolecules* **1999**, *32*, 1763–1766.

(41) Messerschmidt, M.; Millaruelo, M.; Komber, H.; Häussler, L.; Voit, B.; Krause, T.; Yin, M.; Habicher, W.-D. Synthesis of Partially Protected Block Copolymers Based on 4-Hydroxystyrene Using NMRP and a Sequence of Polymer Analogous Reactions. *Macromolecules* **2008**, *41*, 2821–2831.

(42) Keddie, D. J. A guide to the synthesis of block copolymers using reversible-addition fragmentation chain transfer (RAFT) polymerization. *Chemical Society reviews* **2014**, *43*, 496–505.

(43) Nomura, K.; Abdellatif, M. M. Precise synthesis of polymers containing functional end groups by living ring-opening metathesis polymerization (ROMP): Efficient tools for synthesis of block/graft copolymers. *Polymer* **2010**, *51*, 1861–1881.

(44) Feng, H.; Lu, X.; Wang, W.; Kang, N.-G.; Mays, J. Block Copolymers: Synthesis, Self-Assembly, and Applications. *Polymers* **2017**, *9*, 494.

(45) M. Szwarg. Some aspects of anionic polymerization. *Macromol. Chem. Phys.* **1959**, *35*, 132–158.

(46) Matyjaszewski, K.; Sigwalt, P. Unified approach to living and non-living cationic polymerization of alkenes. *Polym. Int.* **1994**, *35*, 1–26.

(47) Epps, I. T. H.I.I.; O'Reilly, R. K. Block copolymers: Controlling nanostructure to generate functional materials – synthesis, characterization, and engineering. *Chem. Sci.* **2016**, *7*, 1674–1689.

(48) Braunecker, W. A.; Matyjaszewski, K. Controlled/living radical polymerization: Features, developments, and perspectives. *Prog. Polym. Sci.* **2007**, *32*, 93–146.

(49) Wang, J.-S.; Matyjaszewski, K. Controlled/"Living" Radical Polymerization. Halogen Atom Transfer Radical Polymerization Promoted by a Cu(I)/Cu(II) Redox Process. *Macromolecules* **1995**, *28*, 7901–7910.

(50) Matyjaszewski, K.; Xia, J. Atom Transfer Radical Polymerization. *Chem. Rev.* **2001**, *101*, 2921–2990.

(51) Fischer, H. The Persistent Radical Effect: A Principle for Selective Radical Reactions and Living Radical

9. References

Polymerizations. *Chem. Rev.* **2001**, *101*, 3581–3610.

(52) Chong, Y. K.; Le, T. P. T.; Moad, G.; Rizzardo, E.; Thang, S. H. A More Versatile Route to Block Copolymers and Other Polymers of Complex Architecture by Living Radical Polymerization: The RAFT Process. *Macromolecules* **1999**, *32*, 2071–2074.

(53) Bednarek, M.; Biedroń, T.; Kubisa, P. Synthesis of block copolymers by atom transfer radical polymerization oftert-butyl acrylate with poly(oxyethylene) macroinitiators. *Macromol. Rapid Commun.* **1999**, *20*, 59–65.

(54) Bednarek, M.; Biedroń, T.; Kubisa, P. Studies of atom transfer radical polymerization (ATRP) of acrylates by MALDI TOF mass spectrometry. *Macromol. Chem. Phys.* **2000**, *201*, 58–66.

(55) Mendonça, P. V.; Averick, S. E.; Konkolewicz, D.; Serra, A. C.; Popov, A. V.; Guliashvili, T.; Matyjaszewski, K.; Coelho, J. F. J. Straightforward ARGET ATRP for the Synthesis of Primary Amine Polymethacrylate with Improved Chain-End Functionality under Mild Reaction Conditions. *Macromolecules* **2014**, *47*, 4615–4621.

(56) Dong, H.; Tang, W.; Matyjaszewski, K. Well-Defined High-Molecular-Weight Polyacrylonitrile via Activators Regenerated by Electron Transfer ATRP. *Macromolecules* **2007**, *40*, 2974–2977.

(57) Xiao, D.; Wirth, M. J. Kinetics of Surface-Initiated Atom Transfer Radical Polymerization of Acrylamide on Silica. *Macromolecules* **2002**, *35*, 2919–2925.

(58) Moineau, G.; Minet, M.; Dubois, P.; Teyssié, P.; Senninger, T.; Jérôme, R. Controlled Radical Polymerization of (Meth)acrylates by ATRP with NiBr 2 (PPh 3) 2 as Catalyst †. *Macromolecules* **1999**, *32*, 27–35.

(59) Qiu, J.; Matyjaszewski, K. Polymerization of Substituted Styrenes by Atom Transfer Radical Polymerization. *Macromolecules* **1997**, *30*, 5643–5648.

(60) Kotani, Y.; Kato, M.; Kamigaito, M.; Sawamoto, M. Living Radical Polymerization of Alkyl Methacrylates with Ruthenium Complex and Synthesis of Their Block Copolymers 1. *Macromolecules* **1996**, *29*, 6979–6982.

(61) Granel, C.; Dubois, P.; Jérôme, R.; Teyssié, P. Controlled Radical Polymerization of Methacrylic Monomers in the Presence of a Bis(ortho-chelated) Arylnickel(II) Complex and Different Activated Alkyl Halides. *Macromolecules* **1996**, *29*, 8576–8582.

9. References

(62) Zhang, X.; Matyjaszewski, K. Synthesis of Functional Polystyrenes by Atom Transfer Radical Polymerization Using Protected and Unprotected Carboxylic Acid Initiators. *Macromolecules* **1999**, *32*, 7349–7353.

(63) Haddleton, D. M.; Waterson, C.; Derrick, P. J.; Jasieczek, C. B.; Shooter, A. J. Monohydroxy terminally functionalised poly(methyl methacrylate) from atom transfer radical polymerisation. *Chem. Commun.* **1997**, 683–684.

(64) Percec, V.; Barboiu, B.; Kim, H.-J. Arenesulfonyl Halides: A Universal Class of Functional Initiators for Metal-Catalyzed "Living" Radical Polymerization of Styrene(s), Methacrylates, and Acrylates †. *J. Am. Chem. Soc.* **1998**, *120*, 305–316.

(65) Gaynor, S. G.; Wang, J.-S.; Matyjaszewski, K. Controlled Radical Polymerization by Degenerative Transfer: Effect of the Structure of the Transfer Agent. *Macromolecules* **1995**, *28*, 8051–8056.

(66) Brandts, J. A.M.; van de Geijn, P.; van Faassen, E. E.; Boersma, J.; van Koten, G. Controlled radical polymerization of styrene in the presence of lithium molybdate(V) complexes and benzylic halides. *J. Organomet. Chem.* **1999**, *584*, 246–253.

(67) Ando, T.; Kamigaito, M.; Sawamoto, M. Iron(II) Chloride Complex for Living Radical Polymerization of Methyl Methacrylate1. *Macromolecules* **1997**, *30*, 4507–4510.

(68) Kotani, Y.; Kamigaito, M.; Sawamoto, M. Re(V)-Mediated Living Radical Polymerization of Styrene: 1 ReO 2 I(PPh 3) 2 /R–I Initiating Systems. *Macromolecules* **1999**, *32*, 2420–2424.

(69) Tang, W.; Fukuda, T.; Matyjaszewski, K. Reevaluation of Persistent Radical Effect in NMP. *Macromolecules* **2006**, *39*, 4332–4337.

(70) Druliner, J. D. Living radical polymerization involving oxygen-centered species attached to propagating chain ends. *Macromolecules* **1991**, *24*, 6079–6082.

(71) Georges, M. K.; Veregin, R. P. N.; Kazmaier, P. M.; Hamer, G. K. Narrow molecular weight resins by a free-radical polymerization process. *Macromolecules* **1993**, *26*, 2987–2988.

(72) Malmström, E.; Miller, R. D.; Hawker, C. J. Development of a new class of rate-accelerating additives for nitroxide-mediated 'living' free radical polymerization. *Tetrahedron* **1997**, *53*, 15225–15236.

(73) Chang, C.-C.; Studer, A. Acceleration of the Styryl-TEMPO-Mediated Controlled Radical Styrene Polymerization by Addition of an Efficient Alkoxyamine. *Macromolecules* **2006**, *39*, 4062–4068.

9. References

(74) Cameron, N. R.; Lagrille, O.; Lovell, P. A.; Thongnuanchan, B. A Nitroxide for Effecting Controlled Nitroxide-Mediated Radical Polymerization at Temperatures ≤90 °C. *ACS Macro Lett.* **2012**, *1*, 1262–1265.

(75) *Nitroxide Mediated Polymerization: From Fundamentals to Applications in Materials Science;* Moad, G.; Rizzardo, E., Eds.; Royal Society of Chemistry, 2016.

(76) Tuinman, E.; McManus, N. T.; Roa-Luna, M.; Vivaldo-Lima †, E.; Lona, L. M. F.; Penlidis, A. Controlled Free-Radical Copolymerization Kinetics of Styrene and Divinylbenzene by Bimolecular NMRP using TEMPO and Dibenzoyl Peroxide. *J. Macromol. Sci., Pure Appl. Chem.* **2006**, *43*, 995–1011.

(77) Nabifar, A.; McManus, N. T.; Vivaldo-Lima, E.; Lona, L. M.F.; Penlidis, A. Thermal polymerization of styrene in the presence of TEMPO. *Chem. Eng. Sci.* **2009**, *64*, 304–312.

(78) *Nitroxide mediated polymerization: From fundamentals to applications in material science;* Gigmes, D., Ed.; RSC polymer chemistry series no. 19; Royal Society of Chemistry: Cambridge, UK, 2016.

(79) Hawker, C. J. Molecular Weight Control by a "Living" Free-Radical Polymerization Process. *J. Am. Chem. Soc.* **1994**, *116*, 11185–11186.

(80) Barton, D. H.R.; Crich, D.; Motherwell, W. B. The invention of new radical chain reactions. Part VIII. Radical chemistry of thiohydroxamic esters; A new method for the generation of carbon radicals from carboxylic acids. *Tetrahedron* **1985**, *41*, 3901–3924.

(81) Moad, G.; Rizzardo, E.; Thang, S. H. Toward living radical polymerization. *Acc. Chem. Res.* **2008**, *41*, 1133–1142.

(82) Keddie, D. J.; Moad, G.; Rizzardo, E.; Thang, S. H. RAFT Agent Design and Synthesis. *Macromolecules* **2012**, *45*, 5321–5342.

(83) Perrier, S. 50th Anniversary Perspective: RAFT Polymerization—A User Guide. *Macromolecules* **2017**, *50*, 7433–7447.

(84) Moad, G.; Chong, Y. K.; Postma, A.; Rizzardo, E.; Thang, S. H. Advances in RAFT polymerization: The synthesis of polymers with defined end-groups. *Polymer* **2005**, *46*, 8458–8468.

(85) *Block Copolymer Synthesis through the Use of Switchable RAFT Agents;* Moad, G.; Benaglia, M.; Chen, M.; Chiefari, J.; Chong, Y. K.; Keddie, D. J.; Rizzardo, E.; Thang, S. H., Eds. 1066; ACS Symposium Series,

9. References

2011.

(86) Keddie, D. J.; Guerrero-Sanchez, C.; Moad, G.; Rizzardo, E.; Thang, S. H. Switchable Reversible Addition–Fragmentation Chain Transfer (RAFT) Polymerization in Aqueous Solution, N , N - Dimethylacrylamide. *Macromolecules* **2011**, *44*, 6738–6745.

(87) Benaglia, M.; Chiefari, J.; Chong, Y. K.; Moad, G.; Rizzardo, E.; Thang, S. H. Universal (switchable) RAFT agents. *J. Am. Chem. Soc.* **2009**, *131*, 6914–6915.

(88) Willcock, H.; O'Reilly, R. K. End group removal and modification of RAFT polymers. *Polym. Chem.* **2010**, *1*, 149–157.

(89) Qiu, X.-P.; Winnik, F. M. Facile and Efficient One-Pot Transformation of RAFT Polymer End Groups via a Mild Aminolysis/Michael Addition Sequence. *Macromol. Rapid Commun.* **2006**, *27*, 1648–1653.

(90) Kim, B. J.; Given-Beck, S.; Bang, J.; Hawker, C. J.; Kramer, E. J. Importance of End-Group Structure in Controlling the Interfacial Activity of Polymer-Coated Nanoparticles. *Macromolecules* **2007**, *40*, 1796–1798.

(91) Bordwell, F. G.; Landis, P. S. Elimination Reactions. VIII. A trans Chugaev Elimination 1. *J. Am. Chem. Soc.* **1958**, *80*, 2450–2453.

(92) Postma, A.; Davis, T. P.; Moad, G.; O'Shea, M. S. Thermolysis of RAFT-Synthesized Polymers. A Convenient Method for Trithiocarbonate Group Elimination. *Macromolecules* **2005**, *38*, 5371–5374.

(93) Hu, Y. H.; Chen, C. Y.; Wang, C. C. Thermal degradation kinetics of poly(n-butyl acrylate) initiated by lactams and thiols. *Polym. Degrad. Stab.* **2004**, *84*, 505–514.

(94) Chong, Y. K.; Moad, G.; Rizzardo, E.; Thang, S. H. Thiocarbonylthio End Group Removal from RAFT-Synthesized Polymers by Radical-Induced Reduction. *Macromolecules* **2007**, *40*, 4446–4455.

(95) Chen, M.; Moad, G.; Rizzardo, E. Thiocarbonylthio end group removal from RAFT-synthesized polymers by a radical-induced process. *J. Polym. Sci. A Polym. Chem.* **2009**, *47*, 6704–6714.

(96) Inglis, A. J.; Sinnwell, S.; Davis, T. P.; Barner-Kowollik, C.; Stenzel, M. H. Reversible Addition Fragmentation Chain Transfer (RAFT) and Hetero-Diels–Alder Chemistry as a Convenient Conjugation Tool for Access to Complex Macromolecular Designs. *Macromolecules* **2008**, *41*, 4120–4126.

(97) Langer, M.; Brandt, J.; Lederer, A.; Goldmann, A. S.; Schacher, F. H.; Barner-Kowollik, C. Amphiphilic block copolymers featuring a reversible hetero Diels-Alder linkage. *Polym. Chem.* **2014**, *5*, 5330–5338.

9. References

(98) Nebhani, L.; Sinnwell, S.; Inglis, A. J.; Stenzel, M. H.; Barner-Kowollik, C.; Barner, L. Efficient Surface Modification of Divinylbenzene Microspheres via a Combination of RAFT and Hetero Diels-Alder Chemistry. *Macromol. Rapid Commun.* **2008**, *29*, 1431–1437.

(99) Convertine, A. J.; Ayres, N.; Scales, C. W.; Lowe, A. B.; McCormick, C. L. Facile, controlled, room-temperature RAFT polymerization of N-isopropylacrylamide. *Biomacromolecules* **2004**, *5*, 1177–1180.

(100) Schilli, C. M.; Zhang, M.; Rizzardo, E.; Thang, S. H.; Chong, Y. K.; Edwards, K.; Karlsson, G.; Müller, A. H. E. A New Double-Responsive Block Copolymer Synthesized via RAFT Polymerization: Poly(N -isopropylacrylamide)- block -poly(acrylic acid). *Macromolecules* **2004**, *37*, 7861–7866.

(101) Zhou, Y.; Jiang, K.; Song, Q.; Liu, S. Thermo-induced formation of unimolecular and multimolecular micelles from novel double hydrophilic multiblock copolymers of N,N-dimethylacrylamide and N-isopropylacrylamide. *Langmuir : the ACS journal of surfaces and colloids* **2007**, *23*, 13076–13084.

(102) Wang, X.; Li, S.; Su, Y.; Huo, F.; Zhang, W. Aqueous RAFT polymerization of N -isopropylacrylamide-mediated with hydrophilic macro-RAFT agent: Homogeneous or heterogeneous polymerization? *J. Polym. Sci. A Polym. Chem.* **2013**, *51*, 2188–2198.

(103) Theato, P.; Kim, J.-U.; Lee, J.-C. Controlled Radical Polymerization of Active Ester Monomers: Precursor Polymers for Highly Functionalized Materials. *Macromolecules* **2004**, *37*, 5475–5478.

(104) Gibson, M. I.; Fröhlich, E.; Klok, H.-A. Postpolymerization modification of poly(pentafluorophenyl methacrylate): Synthesis of a diverse water-soluble polymer library. *J. Polym. Sci. A Polym. Chem.* **2009**, *47*, 4332–4345.

(105) Zhu, Y.; Batchelor, R.; Lowe, A. B.; Roth, P. J. Design of Thermoresponsive Polymers with Aqueous LCST, UCST, or Both: Modification of a Reactive Poly(2-vinyl-4,4-dimethylazlactone) Scaffold. *Macromolecules* **2016**, *49*, 672–680.

(106) Xu, F. J.; Cai, Q. J.; Li, Y. L.; Kang, E. T.; Neoh, K. G. Covalent immobilization of glucose oxidase on well-defined poly(glycidyl methacrylate)-Si(111) hybrids from surface-initiated atom-transfer radical polymerization. *Biomacromolecules* **2005**, *6*, 1012–1020.

(107) Dörr, M.; Zentel, R.; Dietrich, R.; Meerholz, K.; Bräuchle, C.; Wichern, J.; Zippel, S.; Boldt, P. Reactions on Vinyl Isocyanate/Maleimide Copolymers: NLO-functionalized Polymers with High Glass Transitions for Nonlinear Optical Applications. *Macromolecules* **1998**, *31*, 1454–1465.

9. References

(108) D. Beyer, W. Paulus, M. Seitz, G. Maxein, H. Ringsdorf, M. Eich. Second harmonic generation in self-assembled alternating multilayers of hemicyanine containing polymers and polyvinylamine. *Thin Solid Films* **1995**, *271*, 73–83.

(109) Buck, M. E.; Schwartz, S. C.; Lynn, D. M. Superhydrophobic Thin Films Fabricated by Reactive Layer-by-Layer Assembly of Azlactone-Functionalized Polymers. *Chem. Mater.* **2010**, *22*, 6319–6327.

(110) Galvin, C. J.; Genzer, J. Applications of surface-grafted macromolecules derived from post-polymerization modification reactions. *Prog. Polym. Sci.* **2012**, *37*, 871–906.

(111) Buck, M. E.; Lynn, D. M. Azlactone-functionalized polymers as reactive platforms for the design of advanced materials: Progress in the last ten years. *Polym. Chem.* **2012**, *3*, 66–80.

(112) Heilmann, S. M.; Rasmussen, J. K.; Krepski, L. R. Chemistry and technology of 2-alkenyl azlactones. *J. Polym. Sci. A Polym. Chem.* **2001**, *39*, 3655–3677.

(113) Gauthier, M. A.; Gibson, M. I.; Klok, H.-A. Synthesis of functional polymers by post-polymerization modification. *Angew. Chem. Int. Ed.* **2009**, *48*, 48–58.

(114) Rasmussen, J. K.; Heilmann, S. M.; Krepski, L. R.; Jensen, K. M.; Mickelson, J.; Johnson, K.; Coleman, P. L.; Milbrath, D. S.; Walker, M. M. Crosslinked, hydrophilic, azlactone-functional polymeric beads: A two-step approach. *Reactive Polymers* **1992**, *16*, 199–212.

(115) Sun, B.; Liu, X.; Buck, M. E.; Lynn, D. M. Azlactone-functionalized polymers as reactive templates for parallel polymer synthesis: synthesis and screening of a small library of cationic polymers in the context of DNA delivery. *Chem. Commun. (Cambridge, U. K.)* **2010**, *46*, 2016–2018.

(116) Tully, D. C.; Roberts, M. J.; Geierstanger, B. H.; Grubbs, R. B. Synthesis of Reactive Poly(vinyl oxazolones) via Nitroxide-Mediated "Living" Free Radical Polymerization. *Macromolecules* **2003**, *36*, 4302–4308.

(117) Jones, M. W.; Richards, S.-J.; Haddleton, D. M.; Gibson, M. I. Poly(azlactone)s: versatile scaffolds for tandem post-polymerisation modification and glycopolymer synthesis. *Polym. Chem.* **2013**, *4*, 717–723.

(118) Fournier, D.; Pascual, S.; Fontaine, L. Copper-Mediated Living Radical Polymerization of 2-Vinyl-4,4-dimethyl-5-oxazolone. *Macromolecules* **2004**, *37*, 330–335.

(119) *RAFT Polymers: Novel Precursors for Polymer—Protein Conjugates;* Schilli, C. M.; Müller, A. H. E.; Rizzardo, E.; Thang, S. H.; Chong, Y. K., Eds. 854; ACS Symposium Series, 2003.

9. References

(120) Levere, M. E.; Ho, H. T.; Pascual, S.; Fontaine, L. Stable azlactone-functionalized nanoparticles prepared from thermoresponsive copolymers synthesized by RAFT polymerization. *Polym. Chem.* **2011**, *2*, 2878.

(121) Benaglia, M.; Puglisi, A.; Cozzi, F. Polymer-supported organic catalysts. *Chem. Rev.* **2003**, *103*, 3401–3429.

(122) Ahrendt, K. A.; Borths, C. J.; MacMillan, D. W. C. New Strategies for Organic Catalysis: The First Highly Enantioselective Organocatalytic Diels–Alder Reaction. *J. Am. Chem. Soc.* **2000**, *122*, 4243–4244.

(123) Peng, Y.; Ding, Q.; Li, Z.; Wang, P. G.; Cheng, J.-P. Proline catalyzed aldol reactions in aqueous micelles: An environmentally friendly reaction system. *Tetrahedron Lett.* **2003**, *44*, 3871–3875.

(124) Huerta, E.; Stals, P. J. M.; Meijer, E. W.; Palmans, A. R. A. Consequences of Folding a Water-Soluble Polymer Around an Organocatalyst. *Angew. Chem.* **2013**, *125*, 2978–2982.

(125) Zotova, N.; Broadbelt, L. J.; Armstrong, A.; Blackmond, D. G. Kinetic and mechanistic studies of proline-mediated direct intermolecular aldol reactions. *Bioorg. Med. Chem. Lett.* **2009**, *19*, 3934–3937.

(126) Zotova, N.; Franzke, A.; Armstrong, A.; Blackmond, D. G. Clarification of the role of water in proline-mediated aldol reactions. *J. Am. Chem. Soc.* **2007**, *129*, 15100–15101.

(127) Bui, T.; Barbas, C. F. A proline-catalyzed asymmetric Robinson annulation reaction. *Tetrahedron Letters* **2000**, *41*, 6951–6954.

(128) Mukherjee, S.; Yang, J. W.; Hoffmann, S.; List, B. Asymmetric enamine catalysis. *Chemical reviews* **2007**, *107*, 5471–5569.

(129) List, B.; Arseniyadis, S. *Asymmetric organocatalysis*; Topics in current chemistry 291; Springer: Heidelberg, New York, 2010.

(130) Koichi Kondo, Tom Yamano, Kiichi Takernoto*. Asymmetric robinson cyclization reaction catalyzed by polymer-bound L-proline. *makromol.chem* **1985**, *186*, 1781–1785.

(131) Zhao, B.; Jiang, X.; Li, D.; Jiang, X.; O'Lenick, T. G.; Li, B.; Li, C. Y. Hairy particle-supported 4-N,N-dialkylaminopyridine: An efficient and recyclable nucleophilic organocatalyst. *J. Polym. Sci. A Polym. Chem.* **2008**, *46*, 3438–3446.

(132) Kong, Y.; Tan, R.; Zhao, L.; Yin, D. l-Proline supported on ionic liquid-modified magnetic nanoparticles as a highly efficient and reusable organocatalyst for direct asymmetric aldol reaction in

9. References

water. *Green Chem.* **2013**, *15*, 2422.

(133) Mitsudome, T.; Kaneda, K. Advanced Core-Shell Nanoparticle Catalysts for Efficient Organic Transformations. *ChemCatChem* **2013**, *5*, 1681–1691.

(134) Akagawa, K.; Sakamoto, S.; Kudo, K. Direct asymmetric aldol reaction in aqueous media using polymer-supported peptide. *Tetrahedron Lett.* **2005**, *46*, 8185–8187.

(135) Liu, Y.-X.; Sun, Y.-N.; Tan, H.-H.; Liu, W.; Tao, J.-C. Linear polystyrene anchored l-proline, new recyclable organocatalysts for the aldol reaction in the presence of water. *Tetrahedron: Asymmetry* **2007**, *18*, 2649–2656.

(136) Kristensen, T. E.; Hansen, T. Polymer-Supported Chiral Organocatalysts: Synthetic Strategies for the Road Towards Affordable Polymeric Immobilization. *Eur. J. Org. Chem.* **2010**, *2010*, 3179–3204.

(137) Lu, A.; Smart, T. P.; Epps, T. H. 3.; Longbottom, D. A.; O'Reilly, R. K. L-Proline Functionalized Polymers Prepared by RAFT Polymerization and Their Assemblies as Supported Organocatalysts. *Macromolecules* **2011**, *44*, 7233–7241.

(138) Huerta, E.; van Genabeek, B.; Lamers, B. A. G.; Koenigs, M. M. E.; Meijer, E. W.; Palmans, A. R. A. Triggering activity of catalytic rod-like supramolecular polymers. *Chem.--Eur. J.* **2015**, *21*, 3682–3690.

(139) Pedrosa, R.; Andrés, J. M.; Gamarra, A.; Manzano, R.; Pérez-López, C. Novel sulfonylpolystyrene-supported prolinamides as catalysts for enantioselective aldol reaction in water. *Tetrahedron* **2013**, *69*, 10811–10819.

(140) Cotanda, P.; O'Reilly, R. K. Molecular recognition driven catalysis using polymeric nanoreactors. *Chem. Commun. (Cambridge, U. K.)* **2012**, *48*, 10280–10282.

(141) Garg, D.; Ahn, J.-H.; Chauhan, G. S. Proline-based polymeric monoliths: Synthesis, characterization, and applications as organocatalysts in aldol reaction. *J. Polym. Sci. A Polym. Chem.* **2010**, *48*, 1007–1015.

(142) Lu, A.; Moatsou, D.; Hands-Portman, I.; Longbottom, D. A.; O'Reilly, R. K. Recyclable l -Proline Functional Nanoreactors with Temperature-Tuned Activity Based on Core–Shell Nanogels. *ACS Macro Lett.* **2014**, *3*, 1235–1239.

(143) Picha, J.; Vanek, V.; Budesinsky, M.; Mladkova, J.; Garrow, T. A.; Jiracek, J. The development of a new class of inhibitors for betaine-homocysteine S-methyltransferase. *Eur. J. Med. Chem.* **2013**, *65*, 256–275.

(144) Neises, B.; Steglich, W. Simple Method for the Esterification of Carboxylic Acids. *Angew. Chem. Int.*

9. References

Ed. Engl. **1978**, *17*, 522–524.

(145) Mandal, P. K.; McMurray, J. S. Pd-C-induced catalytic transfer hydrogenation with triethylsilane. *J. Org. Chem.* **2007**, *72*, 6599–6601.

(146) Ben-Ishai, D.; Berger, A. Cleavage of N-Carbobenzoxy Groups by dry Hydrogen Bromide and Hydrogen Chloride. *J. Org. Chem.* **1952**, *17*, 1564–1570.

(147) Artjom Döring. *Synthese von smarten Blockcopolymeren für die mizellare Organokatalyse*; Dissertation: Uni Paderborn, 2012.

(148) Han, G.; Tamaki, M.; Hruby, V. J. Fast, efficient and selective deprotection of the tert-butoxycarbonyl (Boc) group using HCl/dioxane (4 m). *J Pept Res* **2001**, *58*, 338–341.

(149) Lai, J. T.; Filla, D.; Shea, R. Functional Polymers from Novel Carboxyl-Terminated Trithiocarbonates as Highly Efficient RAFT Agents. *Macromolecules* **2002**, *35*, 6754–6756.

(150) Chong, Y. K.; Moad, G.; Rizzardo, E.; Thang, S. H. Thiocarbonylthio End Group Removal from RAFT-Synthesized Polymers by Radical-Induced Reduction. *Macromolecules* **2007**, *40*, 4446–4455.

(151) Yu, C. C.; Lee, Y.-S.; Cheon, B. S.; Lee, S. H. Synthesis of Glycerol Monostearate with High Purity. *Bull. Korean Chem. Soc.* **2003**, *24*, 1229–1231.

(152) Feng, X.-S.; Pan, C.-Y.; Wang, J. Synthesis of 6-Armed Amphiphilic Block Copolymers with Styrene and 2,3-Dihydroxypropyl Acrylate by Atom Transfer Radical Polymerization. *Macromol. Chem. Phys.* **2001**, *202*, 3403–3409.

(153) Maeda, T.; Kanda, T.; Yonekura, Y.; Yamamoto, K.; Aoyagi, T. Hydroxylated poly(N-isopropylacrylamide) as functional thermoresponsive materials. *Biomacromolecules* **2006**, *7*, 545–549.

(154) Lokitz, B. S.; Messman, J. M.; Hinestrosa, J. P.; Alonzo, J.; Verduzco, R.; Brown, R. H.; Osa, M.; Ankner, J. F.; Kilbey, S. M. Dilute Solution Properties and Surface Attachment of RAFT Polymerized 2-Vinyl-4,4-dimethyl Azlactone (VDMA). *Macromolecules* **2009**, *42*, 9018–9026.

(155) Isidro-Llobet, A.; Alvarez, M.; Albericio, F. Amino acid-protecting groups. *Chem. Rev.* **2009**, *109*, 2455–2504.

(156) Li, J.; Yang, G.; Qin, Y.; Yang, X.; Cui, Y. Recyclable Merrifield resin-supported thiourea organocatalysts derived from l-proline for direct asymmetric aldol reaction. *Tetrahedron: Asymmetry* **2011**, *22*, 613–618.

9. References

(157) Putnam, D.; Langer, R. Poly(4-hydroxy- l -proline ester): Low-Temperature Polycondensation and Plasmid DNA Complexation. *Macromolecules* **1999**, *32*, 3658–3662.

(158) Lai, J. T. Ketoform reaction. Synthesis of hindered imines from 2,6-dialkylanilines and ketones. *Tetrahedron Lett.* **2002**, *43*, 1965–1967.

(159) Chong, Y. K.; Moad, G.; Rizzardo, E.; Thang, S. H. Thiocarbonylthio End Group Removal from RAFT-Synthesized Polymers by Radical-Induced Reduction. *Macromolecules* **2007**, *40*, 4446–4455.

(160) Zhang, Z.; Liu, G.; Bell, S. Synthesis of Poly(solketal methacrylate)- block -poly(2-(dimethylamino)ethyl methacrylate) and Preparation of Nanospheres with Cross-Linked Shells. *Macromolecules* **2000**, *33*, 7877–7883.

(161) Mapas, J. K. D.; Thomay, T.; Cartwright, A. N.; Ilavsky, J.; Rzayev, J. Ultrahigh Molecular Weight Linear Block Copolymers: Rapid Access by Reversible-Deactivation Radical Polymerization and Self-Assembly into Large Domain Nanostructures. *Macromolecules* **2016**, *49*, 3733–3738.

(162) Rossi, N. A. A.; Zou, Y.; Scott, M. D.; Kizhakkedathu, J. N. RAFT Synthesis of Acrylic Copolymers Containing Poly(ethylene glycol) and Dioxolane Functional Groups: Toward Well-Defined Aldehyde Containing Copolymers for Bioconjugation. *Macromolecules* **2008**, *41*, 5272–5282.

(163) Zhang, Q.; Hou, Z.; Louage, B.; Zhou, D.; Vanparijs, N.; De Geest, B. G.; Hoogenboom, R. Acid-Labile Thermoresponsive Copolymers That Combine Fast pH-Triggered Hydrolysis and High Stability under Neutral Conditions. *Angew. Chem.* **2015**, *127*, 11029–11033.

(164) Zhang, Q.; Vanparijs, N.; Louage, B.; Geest, B. G. de; Hoogenboom, R. Dual pH- and temperature-responsive RAFT-based block co-polymer micelles and polymer–protein conjugates with transient solubility. *Polym. Chem.* **2014**, *5*, 1140–1144.

(165) Louage, B.; Zhang, Q.; Vanparijs, N.; Voorhaar, L.; Vande Casteele, S.; Shi, Y.; Hennink, W. E.; van Bocxlaer, J.; Hoogenboom, R.; Geest, B. G. de. Degradable ketal-based block copolymer nanoparticles for anticancer drug delivery: A systematic evaluation. *Biomacromolecules* **2015**, *16*, 336–350.

(166) Zhen, Y.; Wan, S.; Liu, Y.; Yan, H.; Shi, R.; Wang, C. Atom Transfer Radical Polymerization of Solketal Acrylate Using Cyclohexanone as the Solvent. *Macromol. Chem. Phys.* **2005**, *206*, 607–612.

(167) Yu, X.; Picker, M.-T.; Schneider, M.; Herberg, A.; Pascual, S.; Fontaine, L.; Kuckling, D. Synthesis of Amphiphilic Block Copolymers Based on SKA by RAFT Polymerization. *Macromol. Chem. Phys.* **2017**, *29*,

9. References

1700506.

(168) Song, J.; Grün, C. H.; Heeren, R. M. A.; Janssen, H.-G.; van den Brink, Oscar F. High-resolution ion mobility spectrometry-mass spectrometry on poly(methyl methacrylate). *Angew. Chem. Int. Ed.* **2010**, *49*, 10168–10171.

(169) Katharina Reitz, A.; Sun, Q.; Wilhelm, R.; Kuckling, D. The use of stable carbene-CO 2 adducts for the polymerization of trimethylene carbonate. *J. Polym. Sci. Part A: Polym. Chem.* **2017**, *55*, 820–829.

(170) Kanu, A. B.; Dwivedi, P.; Tam, M.; Matz, L.; Hill, H. H. Ion mobility-mass spectrometry. *J. Mass Spectrom.* **2008**, *43*, 1–22.

(171) Maeda, T.; Takenouchi, M.; Yamamoto, K.; Aoyagi, T. Analysis of the formation mechanism for thermoresponsive-type coacervate with functional copolymers consisting of N-isopropylacrylamide and 2-hydroxyisopropylacrylamide. *Biomacromolecules* **2006**, *7*, 2230–2236.

(172) Maeda, T.; Yamamoto, K.; Aoyagi, T. Importance of bound water in hydration-dehydration behavior of hydroxylated poly(N-isopropylacrylamide). *J. Colloid Interface Sci.* **2006**, *302*, 467–474.

(173) Nash, M. A.; Yager, P.; Hoffman, A. S.; Stayton, P. S. Mixed stimuli-responsive magnetic and gold nanoparticle system for rapid purification, enrichment, and detection of biomarkers. *Bioconjugate Chem.* **2010**, *21*, 2197–2204.

(174) Wang, Y.; Morawetz, H. Fluorescence study of the complexation of poly(acrylic acid) with poly(N,N-dimethylacrylamide-co-acrylamide). *Macromolecules* **1989**, *22*, 164–167.

(175) Jie Dai, S. H. GOH, S. Y. LEE, and K. S. SIOW. Interpolymer Complexation between Poly(p-vinylphenol) and Pyridine-containing Polymers. *polymer jounal* **1994**, *26*, 905–911.

(176) Shibanuma, T.; Aoki, T.; Sanui, K.; Ogata, N.; Kikuchi, A.; Sakurai, Y.; Okano, T. Thermosensitive Phase-Separation Behavior of Poly(acrylic acid)- graft -poly(N,N -dimethylacrylamide) Aqueous Solution. *Macromolecules* **2000**, *33*, 444–450.

(177) Aoki, T.; Kawashima, M.; Katono, H.; Sanui, K.; Ogata, N.; Okano, T.; Sakurai, Y. Temperature-Responsive Interpenetrating Polymer Networks Constructed with Poly(acrylic acid) and Poly(N,N-dimethylacrylamide). *Macromolecules* **1994**, *27*, 947–952.

(178) Yeh, P.-Y.; Kopečková, P.; Kopeček, J. Biodegradable and pH-sensitive hydrogels: Synthesis by crosslinking of N,N-dimethylacrylamide copolymer precursors. *J. Polym. Sci. A Polym. Chem.* **1994**, *32*,

9. References

1627–1637.

(179) Kondo, S.; Nakashima, N.; Hado, H.; Tsuoa, K. Poly(N,N-dimethylacrylamide-co-styrene)s as highly efficient catalysts for two-phase reactions. *J. Polym. Sci. A Polym. Chem.* **1990**, *28*, 2229–2232.

(180) Xu, J.; Li, X.; Sun, F. In vitro and in vivo evaluation of ketotifen fumarate-loaded silicone hydrogel contact lenses for ocular drug delivery. *Drug delivery* **2011**, *18*, 150–158.

(181) Pagonis, K.; Bokias, G. Upper critical solution temperature—type cononsolvency of poly(N,N-dimethylacrylamide) in water—organic solvent mixtures. *Polymer* **2004**, *45*, 2149–2153.

(182) Neugebauer, D.; Matyjaszewski, K. Copolymerization of N , N -Dimethylacrylamide with n -Butyl Acrylate via Atom Transfer Radical Polymerization. *Macromolecules* **2003**, *36*, 2598–2603.

(183) Donovan, M. S.; Lowe, A. B.; Sumerlin, B. S.; McCormick, C. L. Raft Polymerization of N , N - Dimethylacrylamide Utilizing Novel Chain Transfer Agents Tailored for High Reinitiation Efficiency and Structural Control †. *Macromolecules* **2002**, *35*, 4123–4132.

(184) An, Z.; Shi, Q.; Tang, W.; Tsung, C.-K.; Hawker, C. J.; Stucky, G. D. Facile RAFT Precipitation Polymerization for the Microwave-Assisted Synthesis of Well-Defined, Double Hydrophilic Block Copolymers and Nanostructured Hydrogels. *J. Am. Chem. Soc.* **2007**, *129*, 14493–14499.

(185) Alexander, A.; Ajazuddin; Khan, J.; Saraf, S.; Saraf, S. Polyethylene glycol (PEG)-Poly(N-isopropylacrylamide) (PNIPAAm) based thermosensitive injectable hydrogels for biomedical applications. *European journal of pharmaceutics and biopharmaceutics* **2014**, *88*, 575–585.

(186) Lin, H.-H.; Cheng, Y.-L. In-Situ Thermoreversible Gelation of Block and Star Copolymers of Poly(ethylene glycol) and Poly(N -isopropylacrylamide) of Varying Architectures. *Macromolecules* **2001**, *34*, 3710–3715.

(187) Quan, Z.; Zhu, K.; Knudsen, K. D.; Nyström, B.; Lund, R. Tailoring the amphiphilicity and self-assembly of thermosensitive polymers: End-capped PEG-PNIPAAM block copolymers. *Soft Matter* **2013**, *9*, 10768–10778.

(188) Xu, X.; Liu, T.; Feng, E.; Zhang, W.; Li, Y.; Zheng, J. Study of PNIPAAm-PEG thermo-sensitive copolymer micelle and Application as drug carrier for icariin. In *ICME International Conference on Complex Medical Engineering (CME), 2013*, 25 - 28 May 2013, Beijing, China; IEEE: Piscataway, NJ, 2013; pp 523–527.

9. References

(189) Theato, P.; Klok, H.-A. *Functional Polymers by Post-Polymerization Modification*; Wiley-VCH Verlag GmbH & Co. KGaA: Weinheim, Germany, 2012.

(190) Heilmann, S. M.; Moren, D. M.; Krepski, L. R.; Pathre, S. V.; Rasmussen, J. K.; Stevens, J. The chemistry of 2-alkenyl-5(4H)-oxazolones. VIII acid-catalyzed reaction with alcohols. *Tetrahedron* **1998**, *54*, 12151–12160.

(191) Sun, B.; Lynn, D. M. Release of DNA from polyelectrolyte multilayers fabricated using 'charge-shifting' cationic polymers: Tunable temporal control and sequential, multi-agent release. *J. Controlled Release* **2010**, *148*, 91–100.

(192) Zhang, L.; Eisenberg, A. Multiple Morphologies of "Crew-Cut" Aggregates of Polystyrene-b-poly(acrylic acid) Block Copolymers. *SCIENCE* **1995**, *268*.

(193) Okabe, S.; Seno, K.-i.; Kanaoka, S.; Aoshima, S.; Shibayama, M. Micellization Study on Block and Gradient Copolymer Aqueous Solutions by DLS and SANS. *Macromolecules* **2006**, *39*, 1592–1597.

(194) Wagner, J. Teilchengrößen-Bestimmung mittels dynamischer Lichtstreuung. *Chem. Ing. Tech.* **1986**, *58*, 578–583.

(195) Heskins, M.; Guillet, J. E. Solution Properties of Poly(N-isopropylacrylamide). *J. Polym. Sci. A Polym. Chem.* **1968**, *2*, 1441–1455.

(196) Blackman, L. D.; Wright, D. B.; Robin, M. P.; Gibson, M. I.; O'Reilly, R. K. Effect of Micellization on the Thermoresponsive Behavior of Polymeric Assemblies. *ACS Macro Lett.* **2015**, *4*, 1210–1214.

(197) Hua, Z.; Pitto-Barry, A.; Kang, Y.; Kirby, N.; Wilks, T. R.; O'Reilly, R. K. Micellar nanoparticles with tuneable morphologies through interactions between nucleobase-containing synthetic polymers in aqueous solution. *Polym. Chem.* **2016**, *7*, 4254–4262.

(198) Scales, C. W.; Convertine, A. J.; McCormick, C. L. Fluorescent labeling of RAFT-generated poly(N-isopropylacrylamide) via a facile maleimide-thiol coupling reaction. *Biomacromolecules* **2006**, *7*, 1389–1392.

(199) Xu, J.; He, J.; Fan, D.; Wang, X.; Yang, Y. Aminolysis of Polymers with Thiocarbonylthio Termini Prepared by RAFT Polymerization: The Difference between Polystyrene and Polymethacrylates. *Macromolecules* **2006**, *39*, 8616–8624.

(200) Smart, T.; Lomas, H.; Massignani, M.; Flores-Merino, M. V.; Perez, L. R.; Battaglia, G. Block

copolymer nanostructures. *Nano Today* **2008**, *3*, 38–46.

(201) Malvern instruments. DLS technical note: Dynamic Light Scattering: Dynamic Light Scattering: An Introduction in 30 Minutes.

(202) Malvern Instruments Limited. A basic guide to particle characterization: Easy to read guide for understanding particle characterization techniques with a focus on particle size and particle shape analysis. https://www.malvernpanalytical.com/en/learn/knowledge-center/whitepapers/ WP120620BasicGuidePartChar.

(203) Xue, F.; Zhang, S.; Duan, W.; Wang, W. A Novel Bifunctional Sulfonamide Primary Amine-Catalyzed Enantioselective Conjugate Addition of Ketones to Nitroolefins. *Adv. Synth. Catal.* **2008**, *350*, 2194–2198.

(204) Roa, R.; Kim, W. K.; Kanduč, M.; Dzubiella, J.; Angioletti-Uberti, S. Catalyzed Bimolecular Reactions in Responsive Nanoreactors. *ACS catalysis* **2017**, *7*, 5604–5611.

(205) Ge, Z.; Xie, D.; Chen, D.; Jiang, X.; Zhang, Y.; Liu, H.; Liu, S. Stimuli-Responsive Double Hydrophilic Block Copolymer Micelles with Switchable Catalytic Activity. *Macromolecules* **2007**, *40*, 3538–3546.

(206) Okhapkin, I. M.; Bronstein, L. M.; Makhaeva, E. E.; Matveeva, V. G.; Sulman, E. M.; Sulman, M. G.; Khokhlov, A. R. Thermosensitive Imidazole-Containing Polymers as Catalysts in Hydrolytic Decomposition of p -Nitrophenyl Acetate. *Macromolecules* **2004**, *37*, 7879–7883.

(207) Vasilevskaya, V. V.; Aerov, A. A.; Khokhlov, A. R. Control of reactions between surfactant reagents in miniemulsions. Surface nanoreactors. *Colloid Polym Sci* **2006**, *284*, 459–467.

(208) Fotaras, S.; Kokotos, C. G.; Kokotos, G. A tripeptide-like prolinamide-thiourea as an aldol reaction catalyst. *Org. Biomol. Chem.* **2012**, *10*, 5613–5619.

(209) Qu, C.; Zhao, W.; Zhang, L.; Cui, Y. Preparation of immobilized L-prolinamide via enzymatic polymerization of phenolic L-prolinamide and evaluation of its catalytic performance for direct asymmetric aldol reaction. *Chirality* **2014**, *26*, 209–213.

(210) Zhao, J.-F.; He, L.; Jiang, J.; Tang, Z.; Cun, L.-F.; Gong, L.-Z. Organo-catalyzed highly diastereo- and enantio-selective direct aldol reactions in water. *Tetrahedron Lett.* **2008**, *49*, 3372–3375.

(211) Cotanda, P.; Lu, A.; Patterson, J. P.; Petzetakis, N.; O'Reilly, R. K. Functionalized Organocatalytic Nanoreactors: Hydrophobic Pockets for Acylation Reactions in Water. *Macromolecules* **2012**, *45*, 2377–2384.